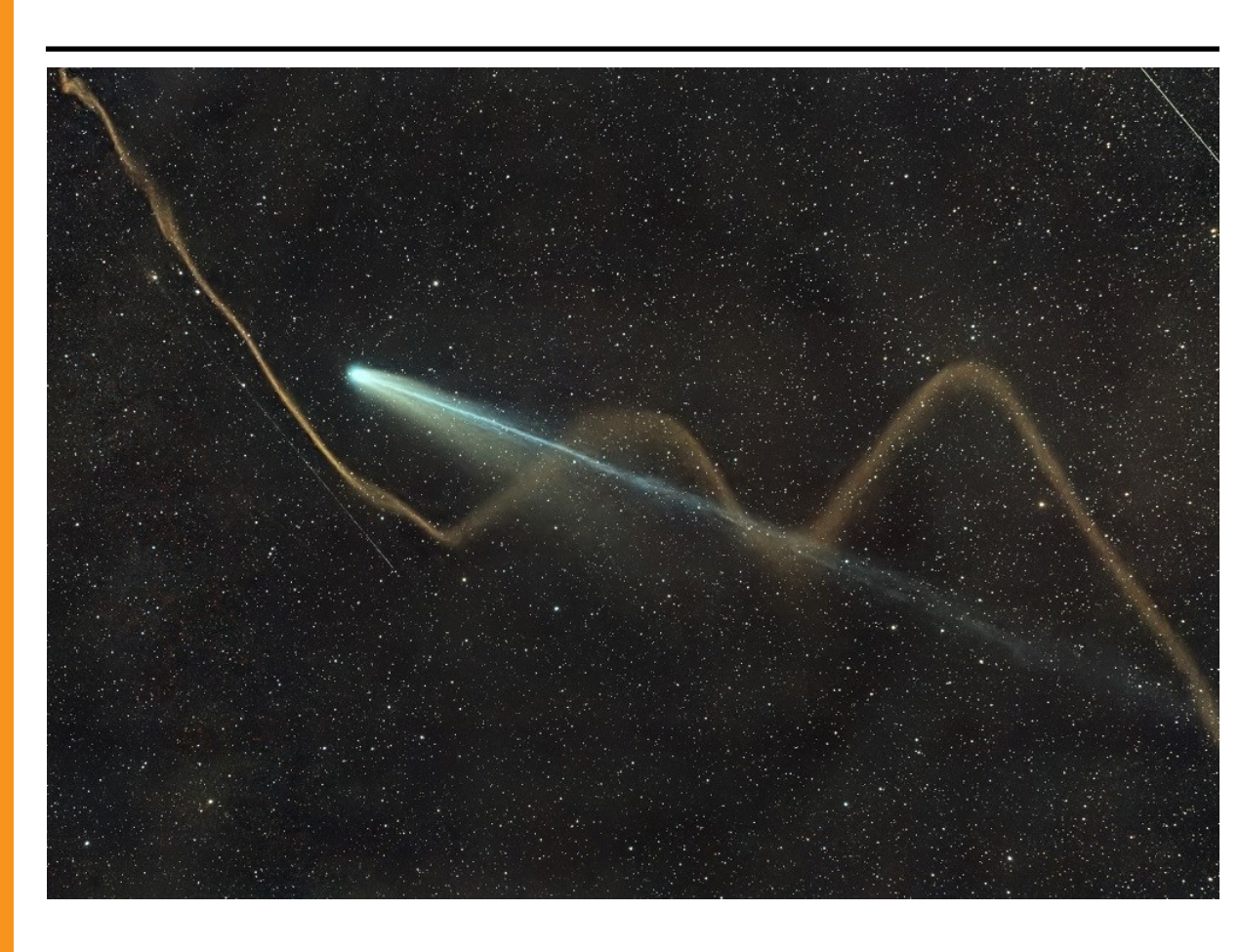


# eJournal for meteor observers

# www.emetn.net



Comet C/2025 A6 (Lemmon) photographed on 24 October 2025 when a bright meteor crossed the camera field and left a persistent trail that lasted several minutes. A sequence of images shows the distortion of the trail. 200mm telephoto lens with a focal length of f/2.0 @ f/2.8 - Canon DSLR camera. 20-second exposure - Location: Manciano (Grosseto), Italy - Author: Massimo Penna.

Jovian-resonance meteor showers

Delta-Horologiids

New meteor shower in Delphinus

CARMELO reports

New meteor shower in Hydrus

Radio observations

■ Epsilon-Ursae Minorids outburst

Fireballs

# **Contents**

Jovian-resonance meteor showers	
Shiba Y	335
New meteor shower in Delphinus (M2025-S1)	
	240
Šegon D., Vida D. and Roggemans P.	348
M2024-S1 activity confirmed in 2025	
Roggemans P., Vida D. and Šegon D	353
Epsilon-Ursae Minorids (EPU#1044) enhanced activity in 2025	
Roggemans P., Vida D. and Šegon D.	360
New meteor shower in Hydrus (M2025-S2)	
	260
Šegon D., Vida D., Roggemans P., Scott J.M. and Wood J	368
Delta-Horologiids (DHO#1146) in 2025	
Roggemans P., Šegon D., Vida D., Scott J.M. and Wood J	378
Roggemans I., segon D., Fraa D., seon v.n. and Frood v.	570
August 2025 CARMELO report	
Maglione M. and Barbieri L	384
September 2025 CARMELO report	
Maglione M. and Barbieri L	388
Radio meteors August 2025	
Verbelen F	202
verbeien F.	392
Radio meteors September 2025	
Verbelen F.	404
Remarkable fireballs spotted in the framework of the Southwestern Europe Meteor Network from February	
to April 2025	
Madiedo J.M., Ortiz J.L., Aceituno F., Aceituno J., de Guindos E., Ávila D., Gómez-Hernández A.,	
Gómez-Martínez J. García A and Aimee A I	412

# Jovian-resonance meteor showers

#### Yasuo Shiba

#### SonotaCo Network, Japan

kqc43540@biglobe.ne.jp

This study focuses on the investigation of six Jupiter-family meteor showers using 2007–2024 data obtained from the Japanese automatic-TV meteor-observation SonotaCo Network. These meteor showers exhibit periodic activity enhancements that seem to result from resonances with Jupiter. The orbital periods of these meteor showers are in ratios of whole numbers to Jupiter's orbital period, demonstrating that the meteoroids are concentrated into a distinct "swarm" in a special mean anomaly's part of its orbit owing to the resonance. The observed position of the mean anomaly of the swarm center was compared with the position resulting of a simple geometric model. The model's principle is that if Jupiter is located at a specific angle from the aphelion direction of the major axis of the meteoroid orbit, then individual meteoroids form a cluster at the aphelion point. The particular angle is derived from the whole-number ratio between the orbital periods of the meteoroid and Jupiter. The predictions of this model agree, to within less than a half-year error, with the years of enhanced activity for four meteor showers. However, the result for the  $\kappa$  Cygnids (KCG, #12) may indicate that the path of the swarm center is beyond the Earth's orbit. Although the observational result for the h Virginids (HVI, #343) also does not agree with the calculated value according to this theory, it is expected that the result can be improved when more observational data can be collected in the future.

Keywords: Planetary systems - meteor: Planetary systems-physical evolution

#### 1 Introduction

Investigations of asteroidal resonances progressed faster because accurate data for individual orbital elements were obtained over many years of astrometric observations. However, meteor-resonance research had been delayed because it had been based on too few meteor registrations, which resulted in large orbital errors. In one such investigation, Scholl and Froeschlé (1988) studied seven known meteor showers that had been thought to be resonance meteor showers, and they concluded that the observed arc of the meteoroids' orbit was not consistent with the orbital-resonance evolution of the meteoroids.

In the first study based on visual observations, Asher and Izumi (1998) concluded that the enhancement of Taurid-fireball activity can be explained as being caused by a resonance with Jupiter. However, radio observations of the Taurids by Egal et al. (2022) indicated no enhanced activity like for the visual observations. These results show either that the influence of the resonance had affected mainly large meteoroids or else that fine-grain meteoroids were removed by the resonance effect.

An amateur meteor-observation TV network, the SonotaCo Network (SonotaCo, 2009) became operational in 2007 in Japan to provide statistical research data on distributions of meteoroids around Earth orbit over long periods. In this study, SonotaCo Network's data, accumulated for 18 years, were used to evaluate the periodic activity detected in six Jovian-resonance meteor showers. I compared the observed meteor showers' active years with a simple geometric model and evaluated this against the calculated years.

## 2 Observational Results

Six meteor showers exhibited years with periodic activity enhancements in the SonotaCo network's 18-year results, which seem to be caused by Jovian resonance. The observed properties of these meteor showers, shown in *Table 1*, have been calculated using the data from the years when enhanced activity has been observed.

The data labels in Table 1 from left are: the meteor shower name with the IAU MDC meteor shower code and number,  $\lambda_{O}$ : mean solar longitude,  $\lambda_{OB}$ : solar longitude of the earliest meteor,  $\lambda_{OE}$ : solar longitude of the last meteor,  $\alpha$ : mean corrected radiant position in Right Ascension,  $\delta$ : mean corrected radiant position in Declination,  $\Delta \alpha$ : radiant drift in Right Ascension per degree in solar longitude,  $\Delta\delta$ : radiant drift in declination per degree in solar longitude,  $v_g$ : mean geocentric meteor velocity in km/s,  $\Delta v_g$ : geocentric velocity variation per degree in solar longitude, a: semimajor axis in AU, q: perihelion distance in AU, e: eccentricity, P: orbital period in years,  $\omega$ : argument of perihelion,  $\Omega$ : ascending node, i: inclination, N: observed number of meteors number, mag: mean luminous magnitude, Luminous Index: luminosity index,  $H_b$ : mean beginning height in km,  $H_e$ : mean ending height in km.

Calculating a precise meteor orbit is challenging because the velocity of the meteor is decelerated by the atmospheric drag, mainly leading to underestimations. The SonotaCo Network's meteor-orbit calculation software, UFOOrbit, provides the opportunity to insert an input value, labeled  $vi\theta$ , to help reducing the influence of this underestimate.

Table 1 – Jovian-resonance meteor showers' orbital elements, all J2000.0.

Meteor Shower	$\lambda_{O}$	$\lambda_{OB}$	$\lambda_{OE}$	α	δ	Δα	$\Delta\delta$	$v_g$	$\Delta v_g$	N	mag	Lum.	$H_b$	$H_e$
MDC Code	J	2000.0 (°	)	(°)	(°)	(°)	(°)	Km/s	Km/s			Index	km	km
Southern Taurids (STA#2)	225.1	210	247	55.2	14.7	0.53	0.03	28.0	-0.31	2014	-1.1	3.0	96.4	74.3
η Virginids (EVI#11)	357.1	348	8	185.6	3.3	0.70	-0.23	27.2	-0.17	227	-0.5	3.2	91.2	75.8
к Cygnids (KCG#12)	138.9	114	157	284.9	47.8	0.54	0.90	22.4	0.19	499	-1.2	2.8	94.3	81.0
h Virginids (HVI#343)	39.2	32	45	203.2	-11.1	0.23	-0.21	18.7	-0.27	99	-0.6	2.7	93.3	81.9
68 Virginids (OAV#651)	19.1	10	28	203.6	-14.9	0.57	-0.27	28.0	-0.16	111	-0.7	4.0	92.8	77.3
χ Cygnids (CCY#757)	169.4	162	178	302.0	29.3	-1.62	0.79	15.2	-1.64	49	-0.3	3.2	89.4	77.1

Meteor Shower	a (AU)	q (AU)	e	P (years)	ω (°)	$\mathcal{Q}\left(^{\circ}\right)$	i (°)
Southern Taurids (STA#2)	2.154	0.369	0.829	3.16	112.8	45.1	5.4
2015 TX24 <sup>1</sup>	2.262	0.285	0.874	3.40	127.8	32.3	6.1
2019 UN12 <sup>1</sup>	2.257	0.348	0.846	3.39	301.7	222.6	5.2
η Virginids (EVI#11)	2.450	0.442	0.819	3.83	283.6	357.1	5.3
$2003 \; \mathrm{FB5^1}$	2.517	0.532	0.789	3.99	288.3	358.4	5.4
κ Cygnids (KCG#12)	3.589	0.966	0.731	6.80	206.7	138.9	33.3
h Virginids (HVI#343)	3.061	0.754	0.754	5.36	65.5	219.2	0.7
$2017~\mathrm{GM^1}$	3.295	0.821	0.751	5.98	55.9	195.3	0.2
68 Virginids (OAV#651)	2.412	0.414	0.828	3.75	107.2	199.1	5.1
2017 FY64 <sup>1</sup>	2.499	0.439	0.824	3.95	82.0	208.6	2.7
χ Cygnids (CCY#757)	2.888	0.939	0.675	4.91	213.0	169.4	17.6
2021 QP2 <sup>1</sup>	2.942	1.148	0.610	5.05	200.6	213.3	38.6
2006 TA81	2.596	1.008	0.612	4.18	204.6	175.6	18.3

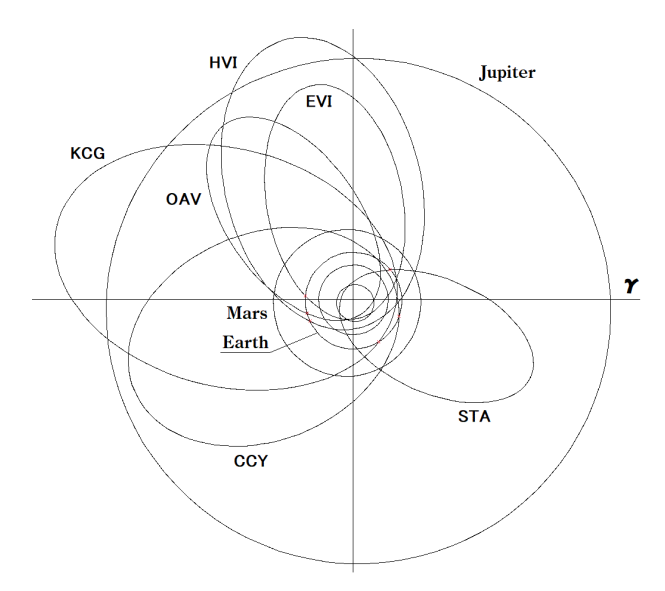


Figure 1 – Resonance meteor showers' mean orbits.

In the present study, the following condition is set:

$$vi0 = 0.5 \frac{km}{s} \tag{1}$$

The plot of the orbits for the six meteor showers investigated in this study is shown in *Figure 1*.

The observed number of individual shower meteors for each year is shown in Figure 2. Meteor shower associations were defined by using the D criterion (Drummond, 1981) using the orbital elements given in Table 1, but using a strict threshold ( $D_D < 0.0525$ ), half of the commonly used value. The inverted filled triangles mark the meteor shower activity which could be identified visibly in the radiant distribution diagrams for the year. The empty inverted triangles were not unusual but confirmed each meteor shower's existence. The red empty circles did not allow to detect the meteor shower existence in SonotaCo data but in EDMOND data (Kornos et al., 2013). The Southern Taurids' marks were established by the orbital elements' statistical distribution characteristics because the resonance meteor components activity overlapped with the annual component activity.

This value is empirically suitable for reducing the statistical influence of the velocity underestimates for the Jupiterfamily meteor showers (Shiba, 2022).

<sup>&</sup>lt;sup>1</sup>https://ssd.jpl.nasa.gov/

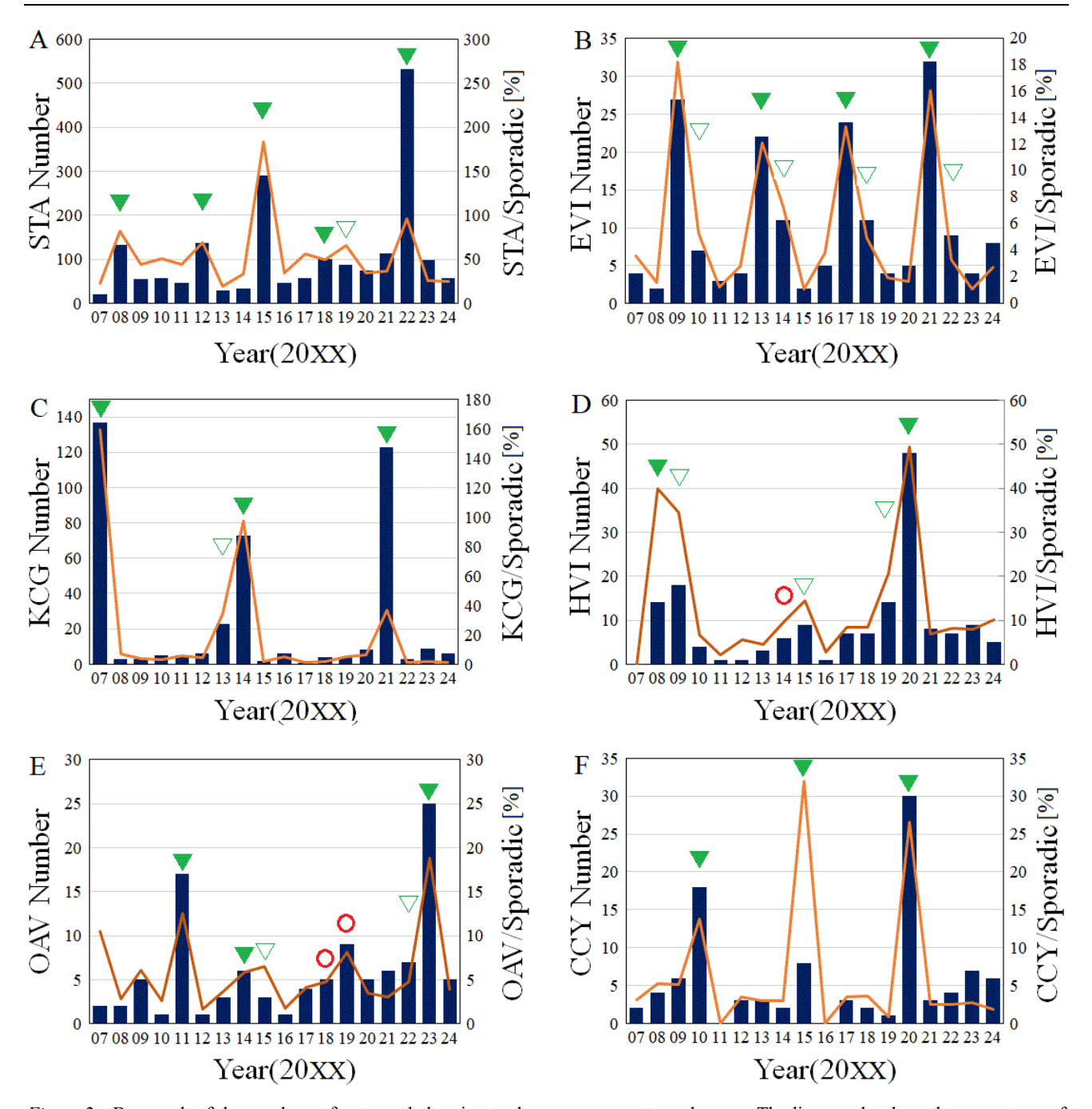


Figure 2 – Bar graph of the numbers of meteors belonging to the resonance meteor showers. The line graphs show the percentage of shower meteors relative to the number of sporadics.

# 3 Individual meteor showers

#### 3.1 Southern Taurids (STA, #2)

The first Jovian-resonance meteor shower to be identified was the Taurid meteor shower (Asher and Izumi, 1998). This result has meanwhile been confirmed by other researchers (Beech et al., 2004; Johannink and Miskotte, 2006; Dubietis and Arlt, 2007). The enhancement in the Taurid meteor-shower activity was identified as a "swarm" that can be observed in the mean-anomaly range of  $30^{\circ}-40^{\circ}$  (Asher and Izumi, 1998).

The Taurid meteor shower consists of two individual showers, Northern and Southern, which have opposite inclinations. Only the Southern Taurids (STA) include resonance components; the Northern Taurids (NTA, #17)

don' have these (Shiba, 2016) as confirmed by Spurny et al. (2017). Moreover, the Southern Taurids consist of both annual and swarm components. The observational data on the STA, acquired in the 20<sup>th</sup> century, did not clearly distinguish both components. The swarm component is thought to be the same as the s-Taurids (STS, #628) identified by Jenniskens et al. (2016a). The orbital elements of both components indicate another drifting in function of the solar longitude, as shown in *Figure 3*. Note that annual components overlap in the swarm-component figure (the left-hand panels in *Figure 3*). The left side in *Figure 3* is the swarm component activity observed in the years 2008, 2012, 2015, 2018, and 2022 superposed. On the right side are eleven years superposed when the swarm component was absent with only the annual component distribution.

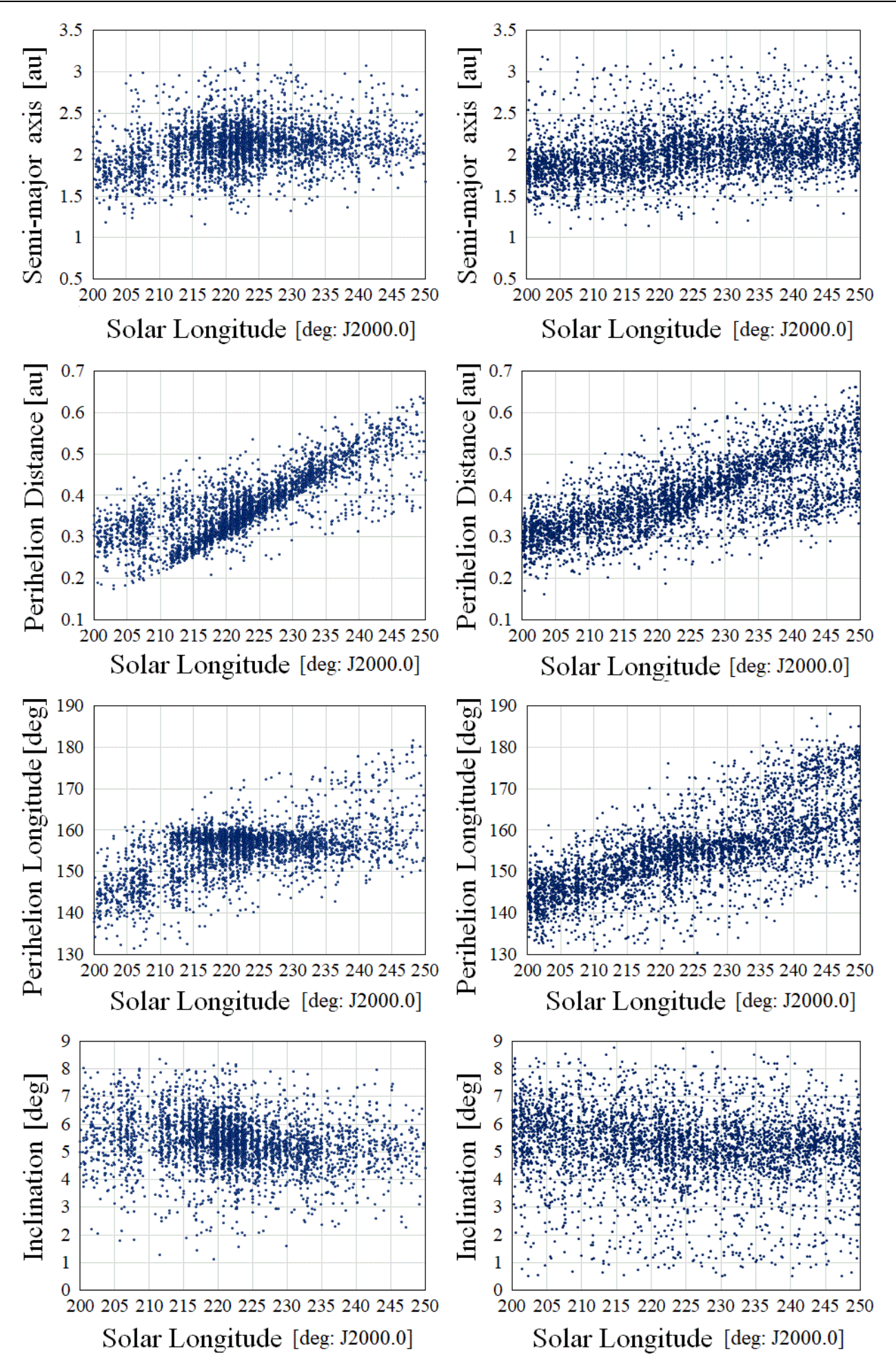


Figure 3 – Southern Taurids orbital elements versus solar longitude.

The semimajor axis a of the swarm component is, on average, 0.14 AU larger than that of the annual component. The perihelion distance q of the swarm components increases in function of the solar longitude, but the annual components overlap with, and interleave with, components before and after the activity period. The longitude of perihelion  $\Pi$  of the swarm component moves slightly backward. In addition, the annual component exhibits complex characteristics caused by the overlapping of one component with the other component from solar longitude  $\lambda_{Q} = 235^{\circ}$ . The inclination i of the swarm component has a stronger negative correlation relative to the solar longitude than does the annual component. Using the equations for the relations with solar longitude given below, I calculated the orbital elements of the swarm component from the lefthand swarm data shown in Figure 3, from which the annual component meteors had been removed:

$$a = 2.18 - 0.0013(\lambda_{\odot} - 225.06) \text{ AU (2)}$$
  
 $q = 0.369 + 0.0097(\lambda_{\odot} - 225.06) \text{ AU (3)}$   
 $\Pi = 157.8 - 0.099(\lambda_{\odot} - 225.06) \text{ deg (4)}$   
 $i = 5.37 - 0.032(\lambda_{\odot} - 225.06) \text{ deg (5)}$ 

Here,  $\lambda_{\odot}$  is the solar longitude, a is the semimajor axis, q is the perihelion distance,  $\Pi$  is the longitude of perihelion, and i is the inclination.

Asher and Izumi (1998) adopted the enhancement of fireball activity to indicate the year when the swarm component encounters the Earth. Radio observations, which mainly target small-sized meteoroids almost cannot detect the swarm-component activity (Egal et al., 2022). A hint of this difficulty is provided by the luminousmagnitude observations of the SonotaCo Network, which indicate that the swarm component is one magnitude brighter than the annual component (Shiba, 2022). The STA swarm component consists of many large particles, almost fireball-sized meteoroids. The STA swarm encounter in 2015 displayed spectacular fireballs, which led to discussions of their possible connection with asteroids (Olech et al., 2016). The possibility of STA-related meteorite falls has also been discussed affirmatively by Brown et al. (2013). In addition, Spurny et al. (2017) have pointed out that the STA meteoroids are one of the hazards for the Earth. On the other hand, the STA meteoroids have a cometary composition, which limits the chances of their hazardous impacts on the Earth, as discussed by Devillepoix et al. (2021).

Quasi-resonance Jupiter-orbit asteroids, which have a similar orbit as the STA swarm, include 2015 TX24, 2005 TF50, 2005 UR, and 2010 TU149 (Olech et al., 2017). They described these asteroids as larger fragments of the old giant parent body of the Taurid swarm. However, these asteroids themselves are not the parent bodies of the Taurid swarm because their perihelia differ from that of 2P/Encke. Clark et al. (2019) were looking forward to finding similar new asteroids. For example, asteroid 2015 TX24 has been interpreted as debris from its parent body (Devillepoix et

al., 2021), and Egal et al. (2021) consider 2015 TX24 to be the primary candidate for the source of the STA 7:2 resonance meteoroids with Jupiter. In addition, asteroids 2005 TF50 and 2005 UR exist in quasi-resonant orbits with Jupiter. The orbits of 2019 UN12 and 2014 WD7 are also near resonance with Jupiter; however, their orbits are similar to those of the Northern Taurids (NTA, #17) but not to those of the STA meteoroids.

The SonotaCo Network captured three meteors of the daytime  $\zeta$  Perseid (ZPE, #172) in 2010 and 2017. The ZPE meteor shower has been interpreted as a member of the Taurids complex (Egal et al., 2022). However, if the ZPE meteoroid stream contains resonance meteoroids, the observed meteors arrived a year earlier than predicted (see *Section 4*), so the observed meteors do not appear to be part of the STA swarm.

#### 3.2 κ Cygnids (KCG, #12)

The second resonance meteor shower considered in this study is the κ Cygnid shower (KCG, #12), (Shiba, 2017) which has complex characteristics (Koseki, 2014). The periodic activity of the KCG has been documented in reports (Koseki, 2014; Moorhead et al., 2015). Previous photographic observation data revealed a seven-year active cycle of the KCG (Lindblad, 1995). However, negative reports of periodic activity were obtained from visual observations (Rendtel and Arlt, 2016). These results indicated that only bright meteors exhibit periodic activity; therefore, while photographic or TV observations can successfully detect periodic activity, visual and radio observations cannot. Using precise orbital data based on fireball observations, Borovicka et al. (2025) pointed out the possibility of a 5:3 KCG resonance with Jupiter, which has since been confirmed by their observed periodic activity. In the SonotaCo Network observations, the active KCG years are 2007, 2014, and 2021. The integrated radiant-distribution map for these three years is shown in Figure 4A. Figure 4B shows the integrated radiant distribution during the 11 years in which no KCG swarm was observed; it also excludes 2013, when only a few KCG meteors were observed. The left side of Figure 4, marked with "A", is the KCG swarm radiant distribution stacked for the observing years 2007, 2014, and 2021. The right side, marked with "B", is the KCG radiant distribution stacked for the eleven years 2008, 2009, 2010, 2011, 2012, 2015, 2016, 2017, 2018, 2019, 2020, 2022, 2023, and 2024 all when strong KCG activity remained absent. The compact radiant concentration visible in both Figure 4A and Figure 4B at R.A. =  $280^{\circ}$  and Decl. =  $+51^{\circ}$  is the long-period meteor shower July γ Draconids (GDR, #184).

The arc-shaped radiant concentration in *Figure 4B* corresponds to the August Draconids (AUD, #197) but not the KCG. The radiant positions of both meteor showers are particularly close, early in each activity period, i.e., in the middle – last part of July, when it is difficult to identify to which shower the individual meteors belong. The  $\kappa$  Lyrids (KLY, #464) and  $\mu$  Lyrids (MUL, #413) are presumed to be the early parts of the KCG meteor shower. Shiba (2017)

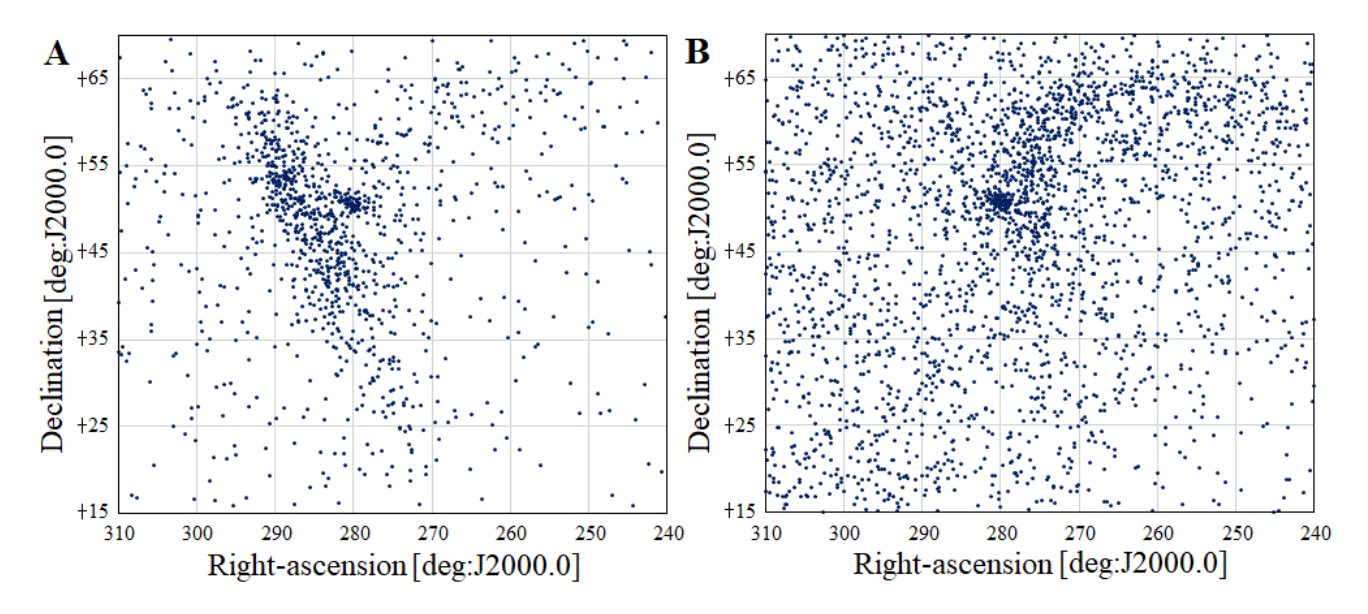


Figure 4 – KCG radiant distribution.

judged the AUDs to be the same as that part of the  $\kappa$  Cygnids labeled as E, F, and G in *Figure 5* of Koseki (2014). The differences in meteor shower identifications by individual researchers should be carefully analyzed when referencing previous reports.

The AUD orbital period is presumed to have a 7:3, 9:4, or 11:5 resonance with Jupiter (Borovicka et al., 2025). However, the SonotaCo Network results indicate no such periodic activity (*Figure 5*).

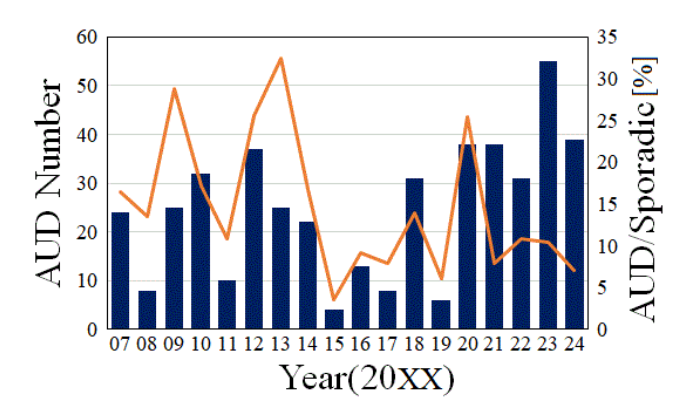


Figure 5 – The bar graph is the number of meteors classified as AUD meteors and the line graph is the AUD rate against the number of sporadic meteors.

The KCG meteors have high luminous altitudes, with often spectacular explosive fireballs. The KCG-meteoroid material either is easily evaporated or else is mechanically weak. This feature may be related to their large orbital perihelion, about one astronomical unit, which is in the habitable zone.

Jones et al. (2006) pointed out that the asteroids 2001 MG1 and 2004 LA12 have a common origin with the KCG meteoroids. Sergienko et al. (2019) identified 2001 MG1 and 2002 LV as possible parent bodies, but these asteroids do not exist in resonance with Jupiter. Consequently, although they will be widely acceptable as the possible

parent body of the AUDs, they cannot be the parent body of the KCG. The orbit of 2014 HZ198 has a 5:3 resonance with Jupiter, which is the same as the KCG; however, the difference between the two orbital directions is not negligible.

#### 3.3 η Virginids (EVI, #11)

This meteor shower has been active for two years and in turn absent for the next two years (Shiba, 2018; Koseki, 2020). The EVI meteor shower includes many fireballs, some with conspicuously low luminous-trajectory ending altitudes. These meteoroids are thought to consist of mechanically hard materials (Broek et al., 2021). This characteristic may result from the perihelion position being located inside Mercury's orbit, close to the Sun.

The estimated parent body of this meteor shower is the asteroid 2003 FB5, which has an orbit similar to that of EVI meteors. However, the orbital period is slightly longer than the resonance period, so its aphelion position will be located close to Jupiter in late March 2085. Still, it will be interesting to see whether the asteroid's future orbit evolution will bring it into the resonance position. Babadzhanov et al. (2015) discussed the relationship of asteroid 2007 CA19 with the EVI meteoroids, but 2003 FB5 is the more probable parent body of the EVI because of the similarity and near-resonance of its orbit.

Three asteroids, 2016 GX221, 2023 PC1, and 2023 HO, have a 3:1 resonance with Jupiter's orbit, and they may form a dynamical asteroid group, however, their orbital directions are different from both those of EVI and OAV. These asteroids have similar orbital directions as those of the o Piscids (OMP, #1207) and the daytime April Cetids (DAC, #419), but their orbit parameters are not established.

#### 3.4 h-Virginids (HVI, #343)

In the SonotaCo Network observations, a significant radiant concentration of the HVI was observed in 2008 and 2020, a weak activity was recorded in 2009, 2015, and 2019. The

EDMOND 2014 observations yielded a few meteors with characteristic radiant concentrations. These results suggest a 5.5-year cycle, which is also given in Koseki (2020). The estimated period ratio with Jupiter is 2:1. However, the calculated mean orbital period (*Table 1*) is not a 2:1 resonance but shorter than 5.38 years. Observations from the "Camera for All-Sky Meteor Surveillance" or CAMS (Jenniskens et al., 2016b) yield a semimajor axis of 2.28 AU, which corresponds to a 3.44-year period. Roggemans et al. (2020) suggested a 2.97 AU semi-major axis and 5.12-year orbital period based on BeNeLux 2020 data. Thus, the orbital-period data obtained in the previous several research results and present work do not relatively agree enough.

Sergienko et al. (2021) pointed out that 2001 SZ269 may be a related asteroid, but it is not in a resonance orbit with Jupiter. Conversely, 2017 GM has a near 2:1 resonance orbit with Jupiter, although its orbital direction does not agree with the HVI orbit. If HVI is not in a 2:1 resonance but instead in a 7:3 resonance, 2022 HC3 may be a possible parent-body candidate.

#### 3.5 68 Virginids (OAV, #651)

The northern  $\lambda$  Virginids identified in Lindblad (1971) may be the same as the OAV. Significant OAV activity was recorded only in 2011 and 2023, although the EDMOND observational results (Kornos et al., 2013) indicated weak activity in 2018 and 2019. Additional weak activity was found in the 2007 EDMOND results. Also, the Belarusian video network and the CAMS data indicated enhanced activity in 2023 (Harachka et al., 2023).

Figure 1 shows the EVI and OAV orbits. Both meteor showers have the same four-year activity cycle as the 3:1 resonance with Jupiter, but the difference in directions of the major axes of the meteoroid orbits corresponds to Jupiter's orbital 0.9-year differences of revolution. As a result, the active years of these two meteor showers differ by one year (Figure 2). Both meteor showers may be part of an "η Virginids complex" and may have a common origin or evolution.

Asteroid 2017 FY64 is in a similar orbit as the OAV and is just about on the resonance-orbit period. The orbital inclination of 2017 FY64 is somewhat different from that of the OAV, but 2017 FY64 exists near the swarm position. Therefore, an examination of 2017 FY is expected to reveal whether it, and the parent body of the OAV, may have a common origin.

#### 3.6 x Cygnids (CCY, #757)

The active period of the CCY is five years, which suggests a 7:3 resonance with Jupiter equal to a 5.08 yr period (Koseki, 2022). The details of the 2020 CCY activity are described in Jenniskens (2020) and Miskotte (2021). This meteor shower has some characteristics that are similar to those of the KCG. First, the encounter position with the Earth is near the perihelion of the meteor-shower orbit. Second, which may be related, the radiant drift is not to the east but to the north. Third, the meteors' luminous altitude is especially high. Fourth, the orbital inclination is directly

proportional to the solar longitude (*Figure 6*). In contrast, many faint meteors are included in the CCY but not in the KCG.

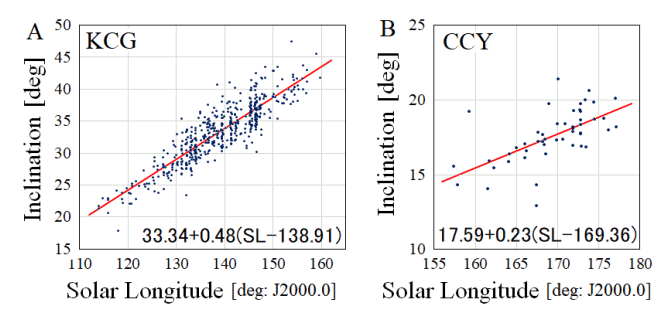


Figure 6 – Solar longitude and inclination of the KCG and CCY.

Jenniskens (2020) described 2020 RF as having a similar orbit to the CCY meteor shower and a 5:3 resonance with Jupiter, and possible interloper to Earth. However, the 2020 RF resonance ratio does not agree with CCY so it is not the parent or rerate object. The parameters of 2021 QP2 are listed for this meteor stream in *Table 1*. The period is near the resonance period, but the inclination is quite different from that of the CCY meteor shower.

# 4 A simple geometric model: Theory vs. observations

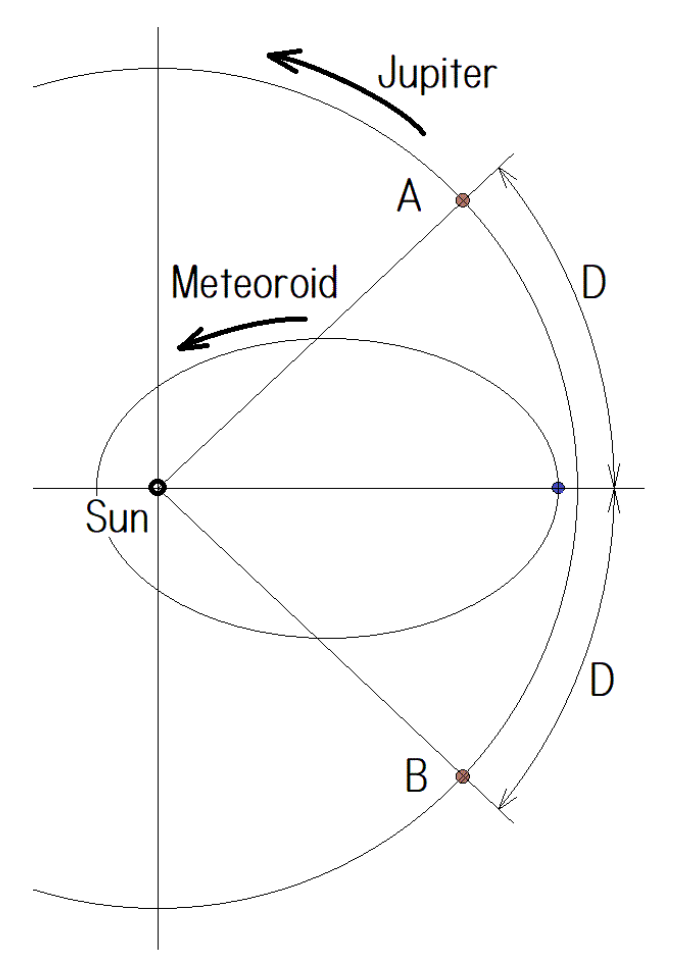


Figure 7 – A simple geometric model.

Figure 7 shows a diagram of Jupiter's orbit, with the meteoroid revolving counterclockwise around its orbit in the plane of the solar system. If a meteoroid particle is at the

aphelion point simultaneously as when Jupiter is located in position "A", then Jupiter's gravity will accelerate the meteoroid. This effect makes the semimajor axis of the meteoroid orbit slightly larger. According to Kepler's third law, the expanded orbit makes the orbital period longer; thus, the meteoroid returns to its next aphelion position later than the previous time when Jupiter was in the "A" position. As a result, the meteoroid becomes increasingly distant from Jupiter. Conversely, if Jupiter is located at position "B" when the meteoroid is at aphelion, then Jupiter's gravity makes the meteoroid's orbital period shorter, which likewise moves its orbit away from Jupiter. That is, the meteoroids always want to escape from Jupiter (Asher and Clube, 1993). The stable mean anomaly of the meteoroid particle occurs when it reaches aphelion when Jupiter is positioned at the same angle D either before or behind the meteoroid's aphelion direction; i.e., at either position "A" or position "B." Positions "A" and "B" invariably occur alternately in both orbital revolutions. The angle D is determined by the ratio of the orbital periods between Jupiter and the meteoroid. If this ratio is m:n, the angle D is given by:

$$2D = \frac{360}{m}$$
 (°) (6)

The angle D is listed in *Table 2* for each resonance meteor shower. Searching for the position of the stable mean anomaly of the center of the meteoroid swarm is thus the same as searching for the moment when Jupiter is located

at angle D in position "A" or "B." At that moment, the swarm center must exist at the meteoroids' orbital aphelion position. For meteor showers with orbital period ratios 7:2, 7:3, and 5:3, there are two or more potential positions for the meteoroid "swarm." However, the observations show that only a single swarm exists for individual meteor showers. That is, only one potential point is an exact solution, and the other points are false solutions.

*Table 2* – Differential angle *D*.

Shower	Ratio	D (°)
STA	7:2	25.7
EVI	3:1	60
KCG	5:3	36
HVI	2:1	90
OAV	3:1	60
CCY	7:3	25.7

The calculated times at which each swarm is predicted to encounter Earth's orbit are shown in *Table 3*, together with the observational results. The false solutions have been compared with observation results and were excluded.

The calculated results prove to be good predictions for the STA, EVI, OAV, and CCY encounter years. However, there are more than half-year differences between the calculations and observations for KCG and HVI.

*Table 3* – Resonance meteor shower's swarm encounter years.

	S	ГΑ	E	VI	K	CG	Н	VI
Estimated period in years <sup>1</sup>	3.39		3.	3.95		7.12		93
Phase angle $D$ (°) <sup>2</sup>	25.73		6	0	36		90	
Swarm at aphelion (years) <sup>3</sup>	2010.9		2015.9		2017.4		2017.1	
Maximum day (years) <sup>4</sup>	0.85		0.21		0.62		0.33	
Swarm encounter (years) <sup>5</sup>	2012.4		2017.8		2020.9		2020.0	
	Obs	Cal	Obs	Cal	Obs	Cal	Obs	Cal
		2005.7				1999.5		2002.2
Swarm return	2008.8	2009.1	2009.4	2009.9	2007.6	2006.7	2008.9	2008.1
Encounter years <sup>6</sup>	2012.8	2012.4	2013.6	2013.8	2014.4	2013.8	2014.9	2014.0
	2015.8	2015.8	2017.5	2017.8	2021.6	2020.9	2020.1	2020.0
	2019.3	2019.2	2021.4	2021.7		2028.0		2025.9
	2022.8	2022.6		2025.7				
		2026.0						
$O - C (years)^7$	0.	11	-0	.31	0.	77	0.59	

<sup>&</sup>lt;sup>1</sup> Estimated orbital period by resonance period ratio with Jupiter.

 $<sup>^{2}</sup>$  Jupiter's phase difference angle D from the meteoroid orbital aphelion's direction at the estimated swarm existence at the aphelion.

<sup>&</sup>lt;sup>3</sup> An adopted year of matching the above *D* condition in the SonotaCo Network observation period.

<sup>&</sup>lt;sup>4</sup> The meteor shower maximum month and day expressed in a year unit.

<sup>&</sup>lt;sup>5</sup> The time of the estimated swarm center described above encountering the Earth's orbit.

<sup>&</sup>lt;sup>6</sup> The estimated sequence of swarm center return years to the Earth (Cal) based on the above original encounter year, compared to the observations (Obs) expressed in years for the observed number of shower meteors during two years of observed swarm activity.

<sup>&</sup>lt;sup>7</sup> The average of the difference between the observed and the calculated encounter of the swarm activity.

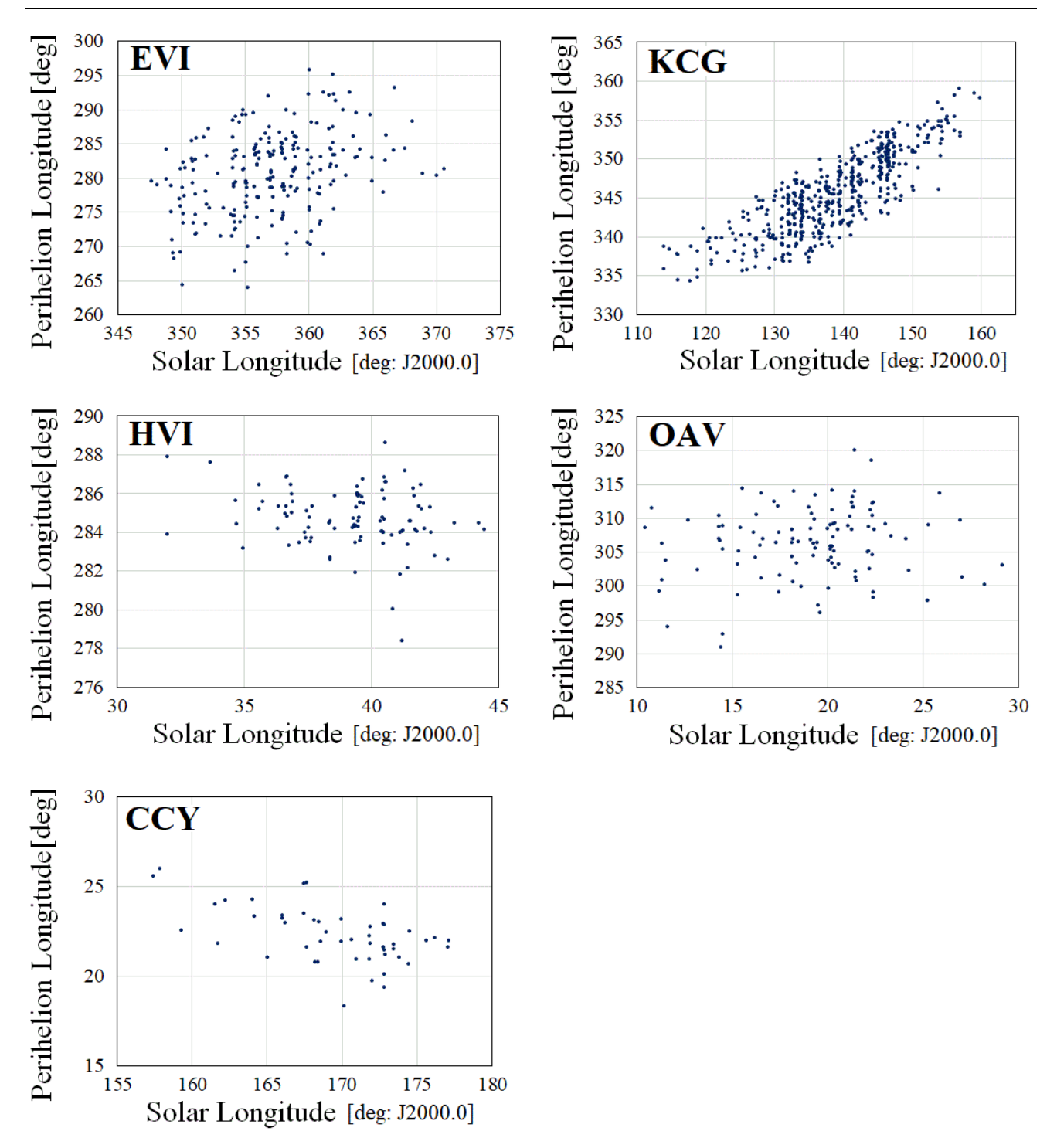


Figure 8 – Solar longitude and longitude of perihelion.

#### 5 Longitude of perihelion feature

Figure 8 shows the relationship between perihelion and solar longitudes for individual meteor showers, except for the STA meteors (which was already shown in Figure 3). There are no consistent characteristics found for each meteor shower in Figure 8. Each meteor that was thought to belong to the swarm, was stacked. The characteristics of individual meteor showers depend on the differences in the distribution of meteoroids along their orbit.

Figure 9 shows the differences between the years of actual observed swarms and calculated swarm-center encounter year on the horizontal axis and the mean longitude of perihelion at that year on the vertical axis for the individual

meteor showers. The data labels are observed years. The HVI was removed because the estimated resonance ratio is doubtful. The line is a first-order approximation. All meteor showers exhibit positive correlations, with slopes in the range of 1.0 to 4.9 degrees per year.

#### 6 Discussion

The resonance ratios of the STA, KCG, and CCY meteoroids are 7:2, 5:3, and 7:3, respectively. Each of them has two or more possible resonance positions, but the swarm exists in only one position for an individual meteor shower. These swarms did not evolve from an accumulation of evenly distributed meteoroid particles but rather from a

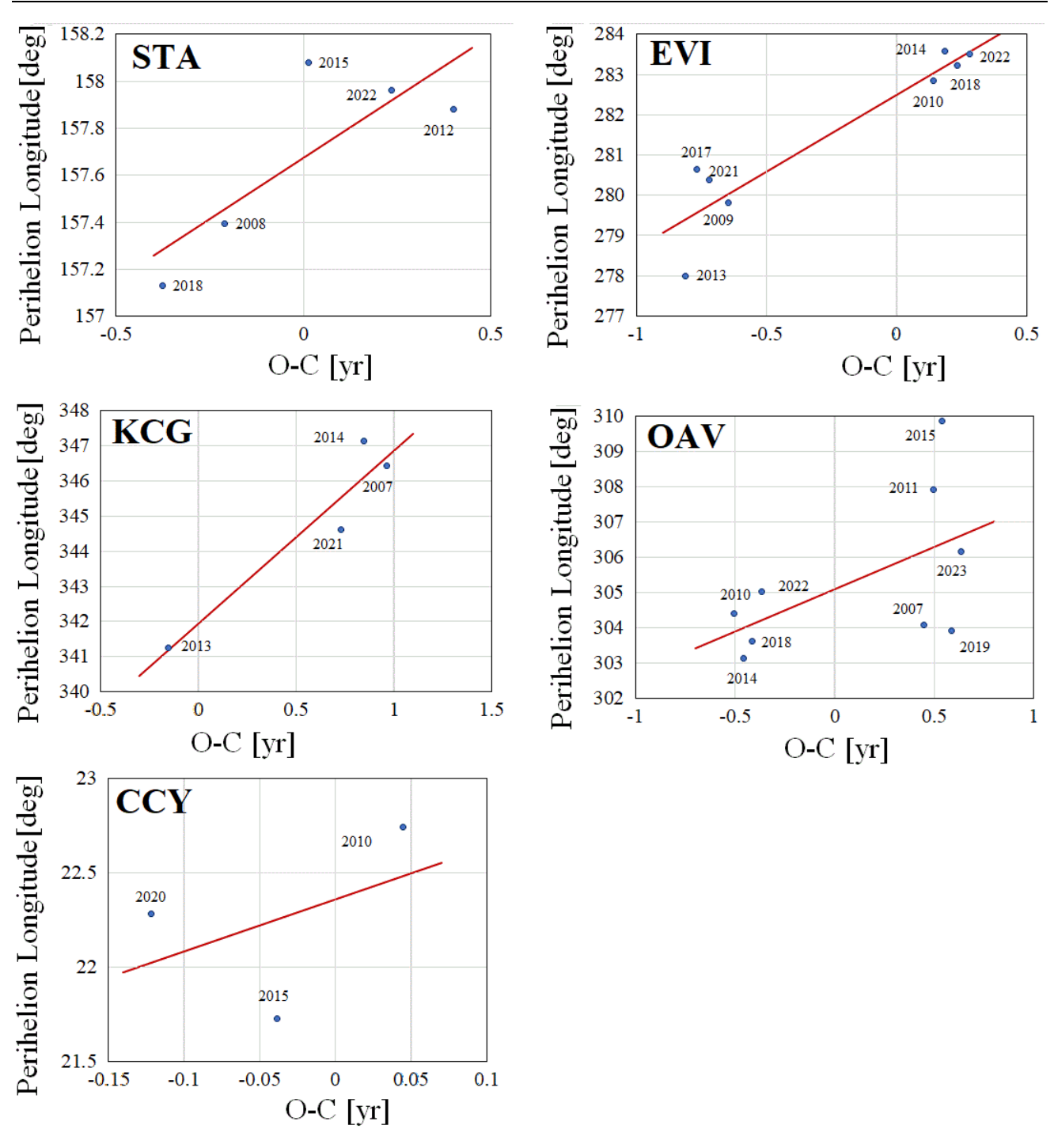


Figure 9 – Longitude or perihelion for different years with the predicted swarm center.

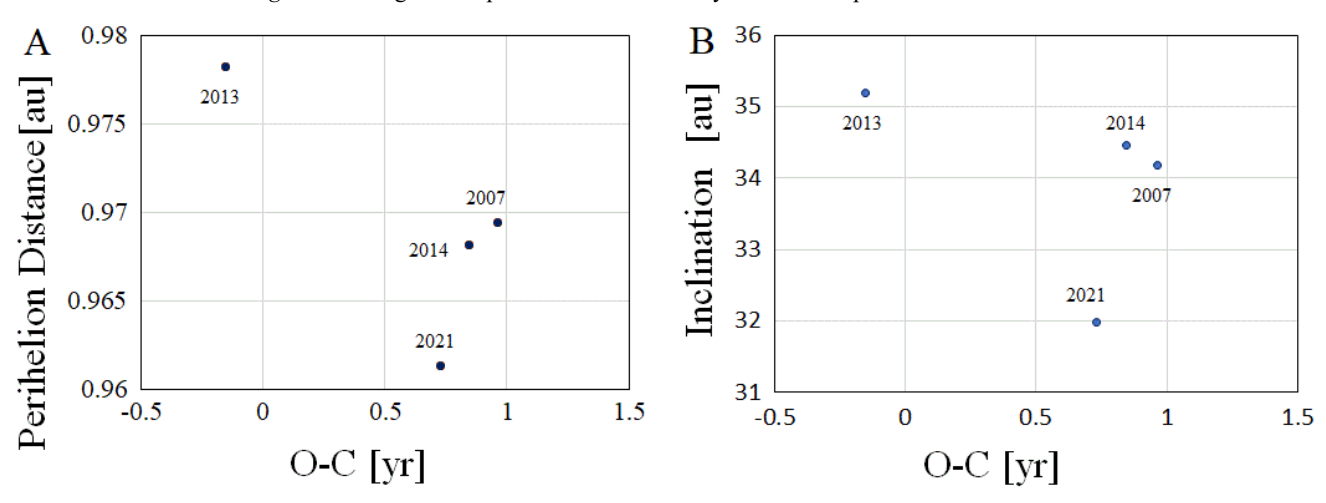


Figure 10 – Perihelion distance and inclination of the KCG.

parent body at the resonance position that broke apart or released the meteoroid particles. If the parent body survived unbroken, or if extra-large particles were produced, we can expect to find it/them in the swarm. To search for a parent or associated object, the technique is primarily crucial to find if the object is in the same resonance as the meteor shower, rather than using the D-criteria. Meteoroids in the resonance position are estimated to remain in a stable position for some thousands of years (Egal et al., 2021).

In the present study, the existence of the meteoroid swarm and its position on the orbital mean anomaly of Jovianresonance meteor showers has been predicted by a simple geometric model. The results are good for the STA, EVI, OAV, and CCY swarms, which exist near the predicted positions for each case. However, this prediction is not successful for the KCG and HVI meteor showers. The KCG shower has been observed only in 2013 near the predicted swarm-center year, when a few meteors were observed. However, the 2013 KCG data may suggest the reason why the observational results do not agree with the prediction. Figure 10 shows the orbital-element data for the perihelion distance and the inclination during the years in which the KCG meteors were observed in function of the differences between the predicted swarm-encounter years and the observed years of activity. The 2013 KCG perihelion distance and inclination were larger than those in 2007, 2014, and 2021. These results can be interpreted as indicating that the path of the center of the KCG meteoroid swarm lay outside of Earth's orbit in 2013, making it difficult to encounter enough meteors. We might be unable to observe the entire KCG meteoroid stream from the Earth.

The uncertainties are too large on the orbital elements of the HVI swarm and its activity data to enable a detailed examination of the resonance phenomena; we therefore hope to acquire more observational data in the future.

A delay of one active year for the OAV from the EVI was consistent with the prediction.

The phase difference D is the smallest (=  $25.7^{\circ}$ ) for the meteor showers STA and CCY; consequently, the effect of Jupiter's gravity will be the largest for them. As a result, the meteoroids in the stream will be swept up powerfully into a narrow region concentrated around the swarm center. Observations for both meteor showers indicate that the swarm encountered the Earth only in a single year. An exception were the STA meteor showers in 2018 and 2019, which were continuous encounters with the swarm when the swarm center existed in both intermediate years. The meteor shower KCG had a next smallest angle  $D (= 36^{\circ})$ . It exhibited two years of continuous activity, in 2013 and 2014, but 2021 was only a single-year swarm encounter. Results from the IMO Video Meteor Network, indicated enhancement of the KCG meteors on 21-25 August in 1999, followed by two years of continuous activity to 2000 (Borovicka et al., 2025). The meteor showers EVI and OAV, which each have a large angle  $D (= 60^{\circ})$  exhibit two years with continuously active swarms, which were observed at every encounter with the Earth. The mean anomalies of the swarm distributions in the orbits of the EVI and OAV meteoroids were observed to exceed  $90^{\circ}$ . The observed extent in the mean anomaly of the swarm distribution on the orbit was inversely proportional to the phase difference D, and reasonably.

The relation in *Figure 9* indicates that the front of a swarm has a smaller longitude of perihelion, while the rear of the swarm tends to have a larger longitude of perihelion. This trend has a rational relation with the position of Jupiter revolving around its orbit. However, it has a smaller variation proportion than Jupiter's rotation angular velocity (= 30.3 deg/yr).

The alpha Capricornids (CAP, #1) may have a 3:1 resonance with the Jupiter meteor shower. However, no indications of periodic activity were detected in the SonotaCo Network observations, although some meteoroids may nevertheless have resonance orbits.

# Acknowledgments

This study was based on daily contributions from the SonotaCo Network observers. This precious observational data was accumulated by video filming, data analysis, and uploads. I thank the amateur observers of the SonotaCo Network for their contributions, some of whom have sadly already passed away, and the network proprietor, Mr. SonotaCo, who has operated this network over the long term. The orbital elements of the asteroids depend on the NASA JPL site, which updates these precious data constantly. I pay tribute to the JPL site administrators.

#### References

- Asher D.J., Clube S. (1993). "An Extraterrestrial Influence during the Current Glacial-Interglacial". *The Quarterly Journal of the Royal Astronomical Society*, **34**, 481.
- Asher D.J. and Izumi K. (1998). "Meteor observations in Japan: new implications for a Taurid meteoroid swarm". *Monthly Notices of the Royal Astronomical Society*, **297**, 23–27.
- Babadzhanov P.B., Kokhirova G.I, Obrubov Yu. V. (2015). "The potentially hazardous asteroid 2007CA19 as the parent of the η Virginids meteoroid stream". *Astronomy and Astrophysics*, **579**, A119.
- Beech M., Hargrove M., Brown P. (2004). "The running of the bulls: a review of Taurid fireball activity since 1962". *The Observatory*, **124**, 277–284.
- Borovicka J., Spurný P., Kotková L., Molau S., Tomko D., Weiland T. (2025). "The structure of κ Cygnid and August Draconid meteoroid streams". *Astronomy and Astrophysics*, **695**, id. A83. eprint arXiv: **2502**.02178.
- Breek A., Borovicka J., Spurny P. (2021). "Orbital and physical properties of η-Virginids from the data of

the European Fireball Network". WGN, Journal of the International Meteor Organization, 49, 98–101.

- Brown P., Marchenko V., Moser D.E., Weryk R., Cooke W. (2013). "Meteorites from meteor showers: A case study of the Taurids". *Meteoritics & Planetary Science*, **48**, 270–288.
- Clark D.L., Wiegert P., Brown P.G. (2019). "The 2019 Taurid resonant swarm: prospects for ground detection of small NEOs". *Monthly Notices of the Royal Astronomical Society*, **487**, L35–L39.
- Devillepoix H.A.R., Jenniskens P., Bland P. A., Sansom E. K., Towner M. C., Shober P., Cupák M., Howie R. M., Hartig B. A. D., Anderson S., Jansen-Sturgeon T., Albers J. (2021). "Taurid stream #628: A reservoir of large cometary impacters". *Planetary Science Journal*, **2**, id.223, 1–13.
- Drummond J.D. (1981). "A test of comet and meteor shower associations". *Icarus*, **45**, 545–553.
- Dubietis A., Arlt R. (2007). "Taurid resonant-swarm encounters from two decades of visual observations". *Monthly Notices of the Royal Astronomical Society*, **376**, 890–894.
- Egal A., Wiegart P., Brown P.G., Spurny P., Borovicka J., Valsecchi G.B. (2021). "A dynamical analysis of the Taurid Complex: evidence for past orbital convergences". *Monthly Notices of the Royal Astronomical Society*, **507**, 2568–2591.
- Egal A., Brown P.G., Wiegert P., Kipreos Y. (2022). "An observational synthesis of the Taurid meteor complex". *Monthly Notices of the Royal Astronomical Society*, **512**, 2318–2336.
- Harachka Y., Sergei I., Zavadich R. (2023). "Increased activity 68 Virginid (OAV#00651) in 2023". eMetN Meteor Journal, 8, 183–184.
- Jones D.C., Williams I.P., Porubcan V. (2006). "The Kappa Cygnids meteoroids complex". *Monthly Notices of the Royal Astronomical Society*, **371**, 684–694.
- Jenniskens P., Nénon Q., Albers J., Gural P.S., Haberman B., Holman D., Morales R., Grigsby B.J., Samuels D., Johannink C. (2016a). "The established meteor showers as observed by CAMS". *Icarus*, 266, 331–354.
- Jenniskens P., Nénon Q., Gural P.S., Albers J., Haberman B., Johnson B., Holman D., Morales R., Grigsby B.J., Samuels D., Johannink C. (2016b). "CAMS confirmation of previously reported meteor showers". *Icarus*, 266, 355–370.
- Jenniskens P. (2020). "The 2020 chi-Cygnids". WGN, Journal of the International Meteor Organization, 48, 146–149.

Johannink C., Miskotte K. (2006). "Taurid activity 1988-2005". WGN, Journal of the International Meteor Organization, 34, 7–10.

- Koseki M. (2014). "Various meteor scenes II: Cygnid-Draconid Complex (κ-Cygnids)". WGN, Journal of the International Meteor Organization, 42, 181–197.
- Koseki M. (2020). "Three Virginid showers". *eMetN Meteor Journal*, **5**, 245–251.
- Koseki M. (2022). "SonotaCo net vs CAMS vs EDMOND vs GMN in the case of the chi Cygnids (CCY#0757)". eMetN Meteor Journal, 7, 381–389.
- Kornos L., Koukal J., Piffl R., Toth J. (2013). "Database of meteoroid orbits from several European video networks". In, Gyssens M. and Roggemans P., editors, *Proceedings of the I.M.C.*, La Palma, 20-23 Sep. 2012. IMO, ISBN 978-2-87355-024-4, 21-25.
- Lindblad B.A. (1971). "A computerized stream search among 2401 photographic meteor orbits". Smithsonian Contributions to Astrophysics, 12, 14–24.
- Lindblad B.A. (1995). "The orbit of the Kappa Cygnids and related meteor streams". *Earth, Moon & Planets*, **68**, 397–404.
- Miskotte K. (2021). "The chi Cygnids (CCY#757) in 2020, a visual analysis". *eMetN Meteor Journal*, **6**, 540–542
- Moorhead A.V., Brown P.G., Spurny P., Cooke W.J., Shrbeny L. (2015). "The 2014 KCG Meteor Outburst:Clues to a Parent Body". *The Astronomical Journal*, **150**, Article ID: 122, 1–13.
- Olech A., Żołądek P., Wiśniewski M., Rudawska R., Bęben M., Krzyżanowski T., Myszkiewicz M., Stolarz M., Gawroński M., Gozdalski M., Suchodolski T., Węgrzyk W., Tymiński Z. (2016). "2015 Southern Taurid fireballs and asteroids 2005 UR and 2005 TF50". Monthly Notices of the Royal Astronomical Society, 461, 674–683.
- Olech A., Żołądek P., Wiśniewski M., Tymiński Z., Stolarz M., Bęben M., Dorosz D., Fajfer T., Fietkiewicz K., Gawroński M., Gozdalski M., Kałużny M., Krasnowski M., Krygiel H., Krzyżanowski T., Kwinta M., Łojek T., Maciejewski M., Miernicki S., Myszkiewicz M., Nowak P., Polak K., Polakowski K., Laskowski J., Szlagor M., Tissler G., Suchodolski T., Węgrzyk W., Woźniak P., Zaręba P. (2017). "Enhanced activity of the Southern Taurids in 2005 and 2015". *Monthly Notices of the Royal Astronomical Society*, **469**, 2077–2088.

Rendtel J., Arlt R. (2016). "Kappa Cyginid rate variations over 41 years". WGN, Journal of the International Meteor Organization, 44, 62–66.

- Roggemans P., Johannink C., Sekiguchi T. (2020). "h Virginids (HVI #343) activity enhancement in 2020". *eMetN Meteor Journal*, **5**, 233–244.
- Scholl H., Froeschle C. (1988). "Gravitational breaking of meteor streams in resonance with Jupiter". *Astronomy and Astrophysics*, **195**, 345–349.
- Sergienko M.V., Sokolova M.G., Andreev A.O., Nefedyev Y.A. (2019). "The kappa Cygnid meteoroid shower and its connection with near-Earth asteroids". 82nd Annual Meeting of The Meteoritical Society 2019 (LPI Contrib. No. 2157, 2019, id.6057).
- Sergienko M.V., Sokolova M.G., Andreev A.O., Nefedyev Y.A. (2021). "Search for possible connections of the h-Virginids meteor shower with near-Earth asteroids". *Journal of Physics: Conference*, PhysicA. SPb /2021, 1–7.

- Shiba Y. (2016). "Taurid swarm exists only in southern branch (STA)". WGN, Journal of the International Meteor Organization, 44, 78–91.
- Shiba Y. (2017). "Kappa Cygnids (KCG) by TV observation results". WGN, Journal of the International Meteor Organization, 45, 127–143.
- Shiba Y. (2018). "Eta Virginids (EVI) four year cycle". WGN, Journal of the International Meteor Organization, 46, 184–190.
- Shiba Y. (2022). "Jupiter Family Meteor Showers by SonotaCo Network Observations". WGN, Journal of the International Meteor Organization, **50**, 38–61.
- SonotaCo (2009). "A meteor shower catalog based on video observations in 2007-2008". WGN, Journal of the International Meteor Organization, 37, 55–62.
- Spurny P., Borovicka J., Mucke H., Svoren J. (2017). "Discovery of a new branch of the Taurid meteoroid stream as a real source of potentially hazardous bodies". *Astronomy and Astrophysics*, **605**, id:A68.

# **New meteor shower in Delphinus (M2025-S1)**

Damir Šegon<sup>1</sup>, Denis Vida<sup>2,3</sup> and Paul Roggemans<sup>4</sup>

<sup>1</sup> Astronomical Society Istra Pula, Park Monte Zaro 2, 52100 Pula, Croatia

<sup>2</sup> Department of Physics and Astronomy, University of Western Ontario, Richmond Street, London, N6A 3K7, Ontario, Canada

<sup>3</sup> Institute for Earth and Space Exploration, University of Western Ontario, Perth Drive, London, N6A 5B8, Ontario, Canada

denis.vida@gmail.com

#### <sup>4</sup> Pijnboomstraat 25, 2800 Mechelen, Belgium

paul.roggemans@gmail.com

A new meteor shower on a Jupiter Family Comet type orbit ( $T_J = 2.91$ ) has been detected during 2025 September 12 – 18 by the Global Meteor Network. 81 meteors belonging to the new shower were observed between  $170^{\circ} < \lambda_{\theta} < 176^{\circ}$  from a radiant at R.A. = 308.8° and Decl.= +9.7° in the constellation of Delphinus, with a geocentric velocity of 12.5 km/s. The new meteor shower has been listed in the IAU MDC Working List of Meteor Showers under the temporary name-designation: M2025-S1.

#### 1 Introduction

The GMN radiant maps for September 14–17, 2025 showed a clear concentration of related radiants in the constellation of Delphinus, south of the chi Cygnid radiant (CCY#757). 81 meteors of this meteor shower were observed by the Global Meteor Network<sup>2</sup> low-light video cameras during the period 2025 September 12–18 with most events on September 15–16 (*Figure I*). The shower was independently observed by cameras in 22 countries (Australia, Belgium, Bulgaria, Brazil, Canada, Croatia, Czechia, Denmark, Germany, France, Hungary, Italy, Luxembourg, Netherlands, New Zealand, Slovakia,

Slovenia, South Africa, South Korea, Spain, United Kingdom and United States).

The shower had a median geocentric radiant with coordinates R.A. = 308.8°, Decl. = +9.7°, within a circle with a standard deviation of  $\pm 2.6^{\circ}$  (equinox J2000.0) see *Figure 2*. The radiant drift in R.A. is +0.47° on the sky per degree of solar longitude and +0.72° in Dec., both referenced to  $\lambda_{\mathcal{O}} = 172.9^{\circ}$  (*Figures 3 and 4*). The median Sun-centered ecliptic coordinates were  $\lambda - \lambda_{\mathcal{O}} = 141.2^{\circ}$ ,  $\beta = +27.4^{\circ}$  (*Figure 5*). The geocentric velocity was  $12.5 \pm 0.1$  km/s.

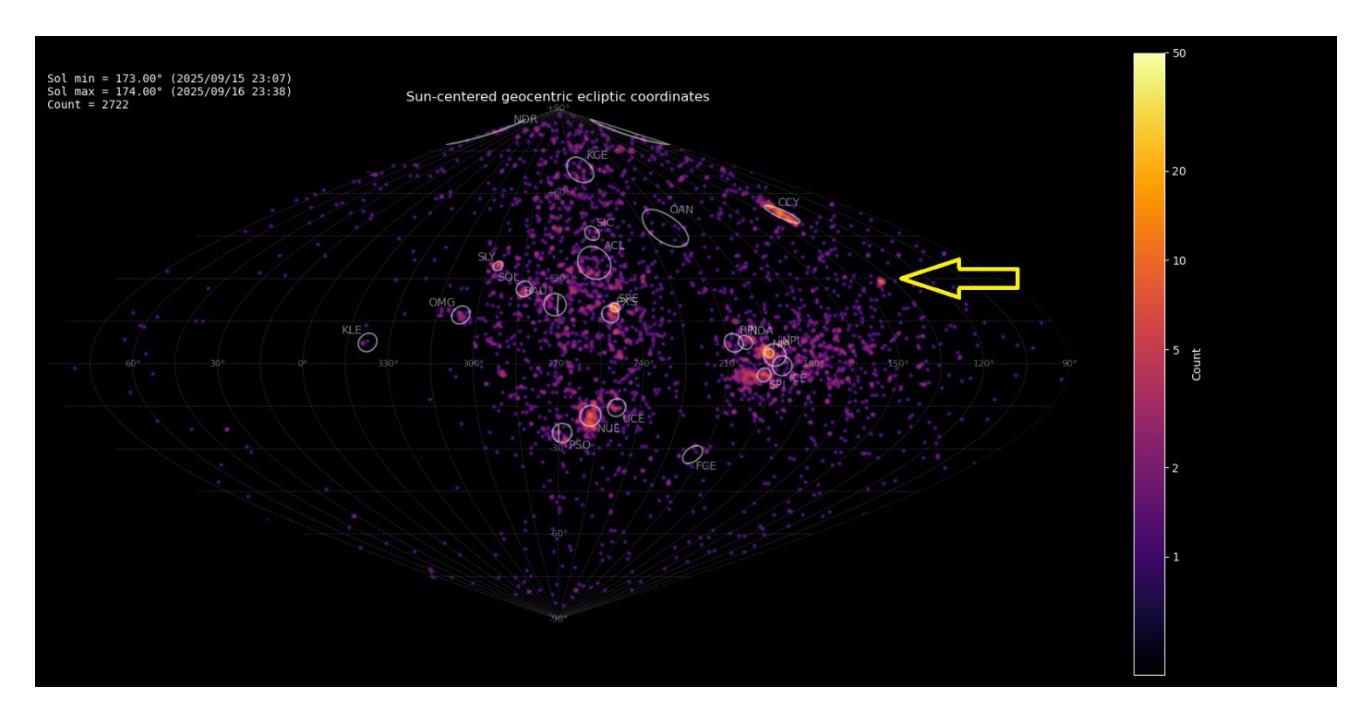


Figure 1 – Heat map with 2722 radiants obtained by the Global Meteor network on September 15 – 16, 2025. A distinct concentration is visible in Sun-centered geocentric ecliptic coordinates which was identified as a new meteor shower with the temporary identification M2025-S1. Activity from this new source was detected during several days.

<sup>&</sup>lt;sup>2</sup> https://globalmeteornetwork.org/data/

#### 2 First detection

The GMN shower association criterion assumes that meteors within 1° in solar longitude, in this case within 5.3° in radiant, and within 10% in geocentric velocity of a shower reference location are members of that shower. Further details about the shower association are explained in Moorhead et al. (2020). These are rather strict criteria since meteor showers often have a larger dispersion in radiant position, velocity and activity period. Using these meteor shower selection criteria, 81 orbits have been associated with the new shower in the GMN meteor orbit database. The mean orbit has been listed in *Table 1*. *Figures 6 and 7* clearly show that the new activity source appeared on top of the sporadic background noise.

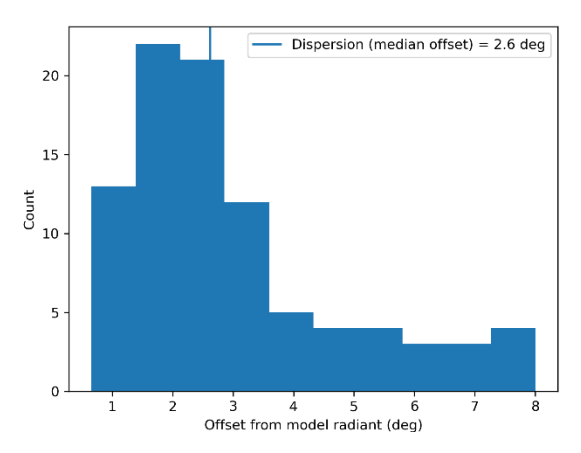


Figure 2 – Dispersion on the radiant position.

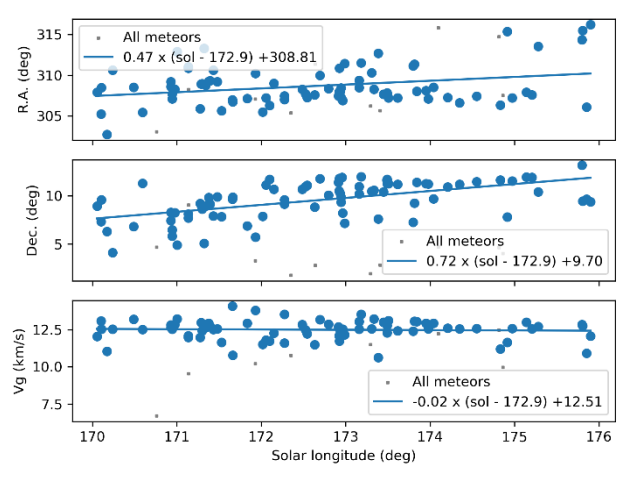


Figure 3 – The radiant drift.

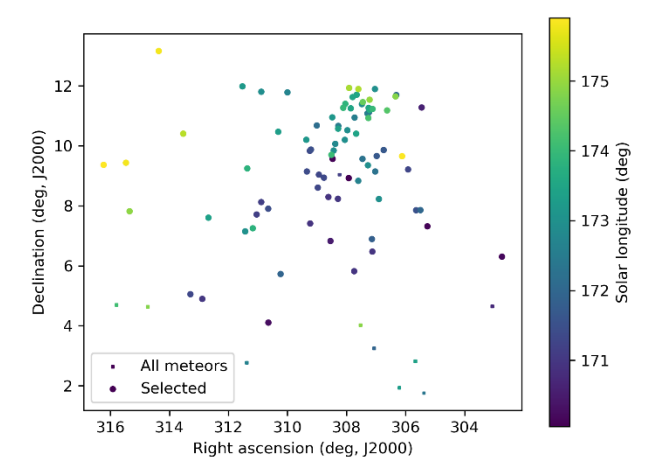


Figure 4 – The radiant distribution during the solar-longitude interval  $170^{\circ} - 176^{\circ}$  in equatorial coordinates.

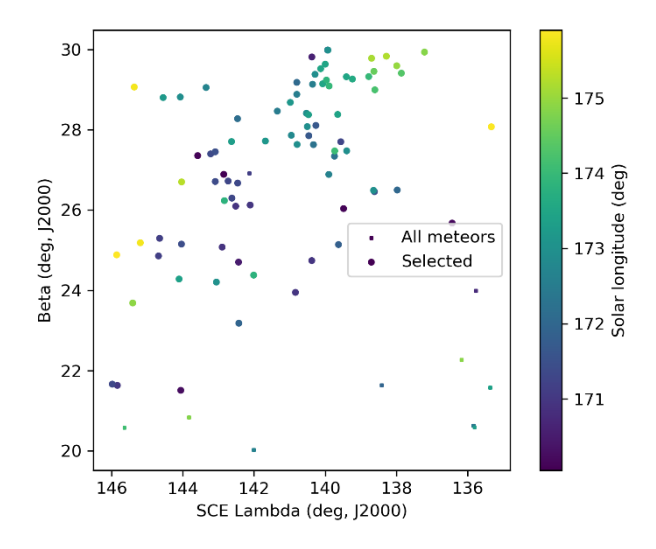


Figure 5 – The radiant distribution during the solar-longitude interval  $170^{\circ}$  –  $176^{\circ}$  in Sun centered geocentric ecliptic coordinates.

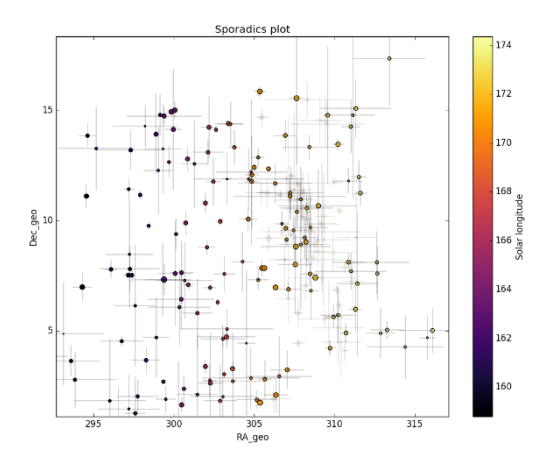


Figure 6 – All non shower meteor radiants in geocentric equatorial coordinates during the shower activity. The pale diamonds represent the new shower radiants plots, error bars represent two sigma values in both coordinates.

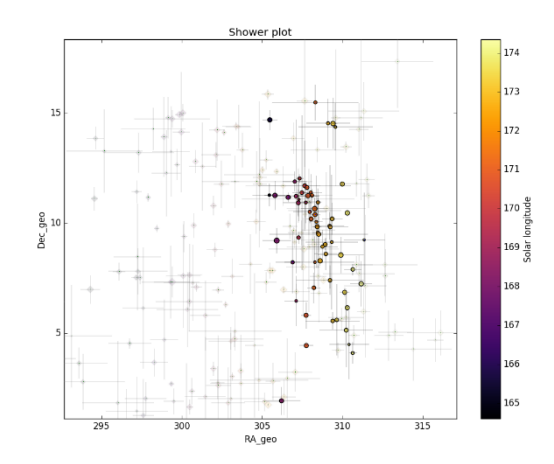


Figure 7 – The reverse of Figure 6, now the shower meteors are shown as circles and the non shower meteors as grayed out diamonds. Note that there are no other groups of meteor radiants to be seen in the vicinity of the possibly new meteor shower.

This possible new meteor shower was reported to the IAU MDC Working List of Meteor Showers and added under the temporary identification 2025-S1<sup>3</sup>.

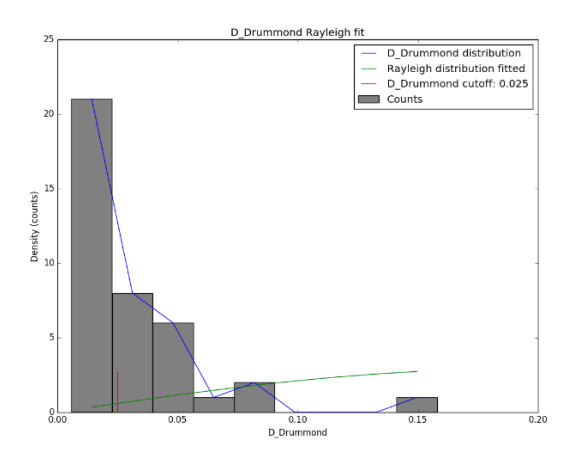


Figure 8 – Rayleigh distribution fit and Drummond  $D_D$  criterion cutoff.

#### 3 Another search method

Another method has been applied to check this new meteor shower discovery. The starting point here can be any visually spotted concentration of radiant points or any other indication for the occurrence of similar orbits. The method has been described before (Roggemans et al., 2019). The main difference with the method applied in Section 2 is that three different discrimination criteria are combined in order to have only those orbits which fit different criteria. The Dcriteria that we use are these of Southworth and Hawkins (1963), Drummond (1981) and Jopek (1993) combined. Instead of using a cutoff value for the threshold of the Dcriteria these values are considered in different classes with different thresholds of similarity. Depending on the dispersion and the type of orbits, the most appropriate threshold of similarity is selected to locate the best fitting mean orbit as the result of an iterative procedure.

The Rayleigh distribution fit indicates that a very small cutoff value is required with  $D_D > 0.025$ . The use of D-criteria requires caution for this type of low inclination short period orbits. Because of the very small cutoff of the threshold values of the D-criteria, only two classes were plotted. This method resulted in a mean orbit with 52 related orbits that fit within the similarity threshold with  $D_{SH} < 0.05$ ,  $D_D \le 0.02$  and  $D_J \le 0.05$ , recorded 2025 September 12 – 18. The plot of the radiant positions in equatorial coordinates, color coded for different D-criteria thresholds, shows a clear concentration in Right Ascension from about 305° to 310° and 7° to 13° in declination (Figure 9), see also Figure 4. A slightly more tolerant threshold of the D-criteria with  $D_{SH} < 0.075$ ,  $D_D < 0.03$  and  $D_J < 0.075$  results in 78 orbits that fit these threshold values, but with a risk of including some sporadics. Both solutions are mentioned in *Table 1*.

Looking at the Sun-centered geocentric ecliptic coordinates the radiant drift caused by of the Earth moving on its orbit around the Sun should be compensated resulting in a more compact radiant. However, *Figure 10* shows a more stretched radiant area which is due to a remarkable strong radiant drift in Sun centered ecliptic coordinates with  $\Delta(\lambda - \lambda_O) = -1.1^{\circ}$  and  $\Delta\beta = +0.7^{\circ}$ . This unusual dispersion in Sun-centered ecliptic coordinates is also found by the GMN meteor shower identification method, although less pronounced with  $\Delta(\lambda - \lambda_O) = -0.3^{\circ}$  and  $\Delta\beta = +0.6^{\circ}$ . This means that orientation of the orbits rapidly changed during the transit of the Earth through the dust stream.

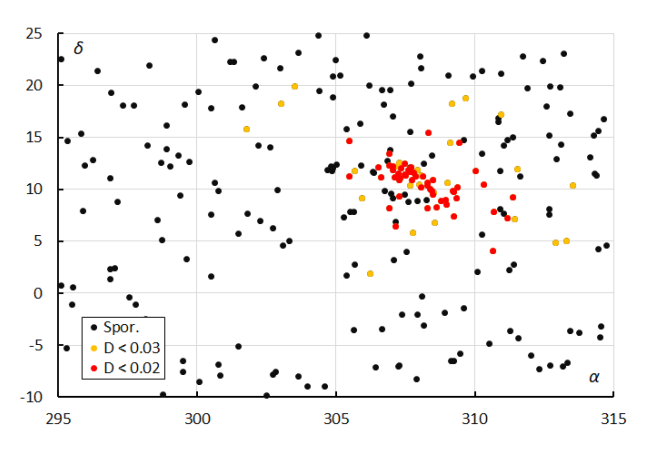


Figure 9 – The radiant distribution during the solar-longitude interval  $170^{\circ} - 176^{\circ}$  in equatorial coordinates, color coded for two threshold values of the  $D_D$  orbit similarity criterion.

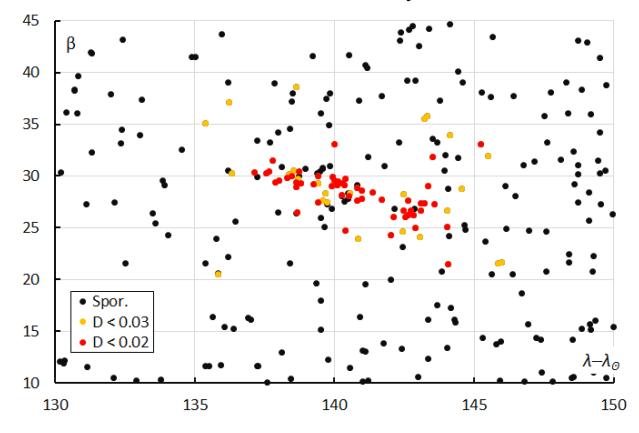


Figure 10 – The radiant distribution during the solar-longitude interval  $170^{\circ}$  –  $176^{\circ}$  in Sun-centered geocentric ecliptic coordinates, color coded for two threshold values of the  $D_D$  orbit similarity criterion.

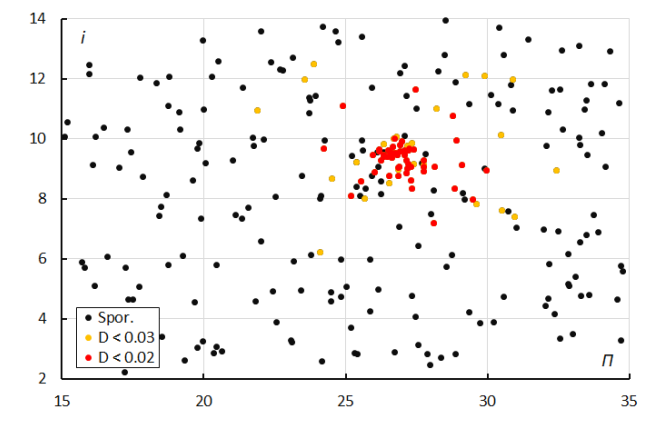


Figure 11 – The diagram of the inclination i against the longitude of perihelion  $\Pi$  color coded for two classes of D criterion threshold.

<sup>&</sup>lt;sup>3</sup> https://www.ta3.sk/IAUC22DB/MDC2022/Roje/pojedynczy\_ob\_iekt.php?lporz=02185&kodstrumienia=01238

The diagram with the inclination against the longitude of perihelion  $\Pi$  (Figure 11) shows a very clear concentration of orbits. Such a dense concentration removes any doubts about the presence of strongly related orbits.

# 4 Comparing both methods

The first method mainly looks at the radiant positions for the classification. When we apply the D criteria, only 53 of the 81 selected meteors fulfill the threshold values of  $D_{SH} < 0.075$ ,  $D_D < 0.03$  and  $D_J < 0.075$  for the mean orbit obtained by the GMN method. 25 of these 81 orbits were not identified by the second method, 56 were identified by both methods. The second method associated 22 orbits that were ignored by the first method. The reason for the discrepancies between the two methods is due to the very low geocentric velocity and unusual radiant drift in Suncentered ecliptic coordinates.

Despite the difference between the samples based on the two different methods, the final mean orbits are in very good agreement except for the radiant drift in R.A. The D-criteria method sampled more orbits on a slightly higher inclination than the GMN radiant based method as the orbits are tested with D-criteria regardless their radiant position.

Table 1 – Comparing the new meteor shower, derived by two different methods, M2025-S1 the orbital parameters as initially derived, the parameters under  $D_D < 0.03$  and  $D_D < 0.02$  were derived from the method described in Section 3.

	M2025-S1	$D_D < 0.03$	$D_D < 0.02$
λο (°)	172.9	172.8	172.95
$\lambda_{Ob}$ (°)	170.0	170.1	170.1
$\lambda_{\mathcal{O}e}$ (°)	176.0	175.5	175.5
$\alpha_g$ (°)	308.8	307.7	308.0
$\delta_{g}\left(^{\circ} ight)$	+9.7	+11.5	+10.9
$\Delta \alpha_g$ (°)	+0.47	-0.25	-0.28
$\Delta\delta_{g}$ (°)	+0.72	+0.93	+0.65
$v_g$ (km/s)	12.5	12.5	12.6
$\lambda_g$ (°)	314.08	313.5	313.6
$\lambda_g - \lambda_O$ (°)	141.18	140.7	140.4
$\beta_g$ (°)	+27.37	+29.4	+28.9
a (A.U.)	2.85	2.92	2.93
q (A.U.)	0.933	0.934	0.935
e	0.672	0.680	0.681
i (°)	8.9	9.1	9.3
ω (°)	214.7	214.3	214.0
$\mathcal{Q}\left(^{\circ}\right)$	172.7	172.65	173.0
П(°)	27.4	27.0	27.0
$T_j$	2.91	2.87	2.86
N	81	78	52

## 5 Orbit and parent body

The final mean orbits obtained by the two methods are in good agreement (Figure 11, Table 1). Figure 13 shows the

orbits in the inner solar system. The dust of M2025-S1 crosses the Earth orbit at its descending node, hitting the Earth almost from the rear, hence the very slow entrance velocity. The low inclination and aphelion close to the orbit of Jupiter means that dust trails will be much affected by this giant planet's gravitational perturbations. This could explain why this meteor shower appears to be almost absent in past observational data.

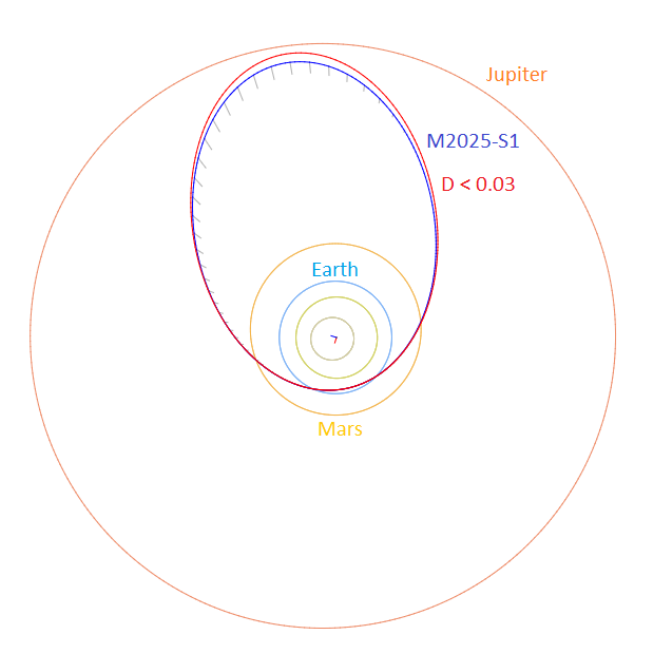


Figure 12 – Comparing the mean orbit based on the shower identification according to the two methods, blue is for M2025-S1 and red for the alternative shower search method with  $D_D < 0.03$  in Table 1. (Plotted with the Orbit visualization app provided by Pető Zsolt).

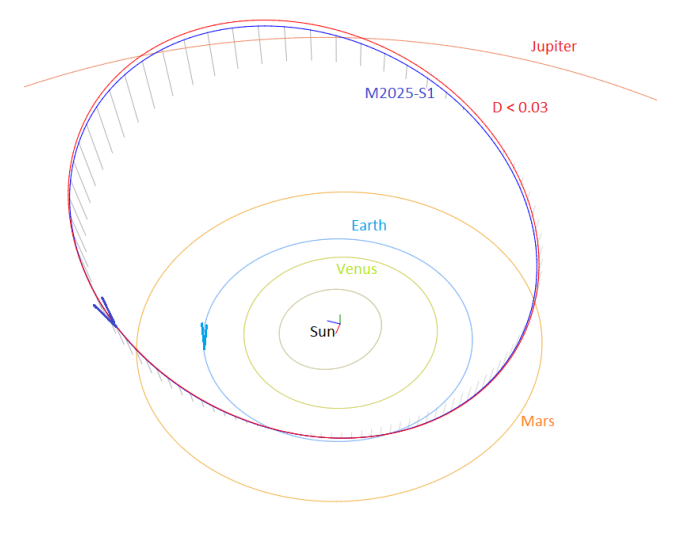


Figure 13 – Comparing the mean orbit based on the shower identification according to two methods, blue is for M2025-S1 and red for the other shower search method with  $D_D < 0.03$  in Table 1, close-up at the inner Solar System. (Plotted with the Orbit visualization app provided by Pető Zsolt).

The Tisserand's parameter  $T_j$  identifies the orbit as of a Jupiter Family Comet type orbit. A parent-body search top 10 includes candidates with a threshold for the Drummond  $D_D$  criterion value lower than 0.06 (*Table 2*). 2022 QF41

has a very similar orbit and could be the parent body. It would be up to meteoroid stream modelers to reconstruct the dynamic orbit evolution to see if there could be any connection between this object and this new meteor shower.

Table 2 – Top ten matches of a search for possible parent bodies with  $D_D < 0.06$ .

Name	$D_D$
2022 QF41	0.031
2020 MZ3	0.041
2021 RL6	0.041
1996 XX14	0.046
2010 RB12	0.051
2022 XS	0.053
2002 RC117	0.055
(419922) 2011 BJ24	0.057
2007 VG3	0.057
2005 RJ	0.059

# 6 Activity in past years

A search in older GMN orbit data resulted in seven possible orbits with  $D_D < 0.02$  in 2022, eleven in 2023 and only four orbits in 2024. SonotaCo Net has only one orbit with  $D_D < 0.02$  in 2019. EDMOND had only one orbit with  $D_D < 0.02$  in 2015. No other meteor orbit datasets were checked. The activity in the past years indicates that M2025-S1 is an annual shower but remained far below the threshold to be discovered in previous years.

#### 7 Conclusion

The discovery of a new meteor shower with a radiant in the constellation of Delphinus based on eighty-one meteors during 2025 September 12 – 18 has been confirmed by using two independent meteor shower search methods. The resulting mean orbits for both search methods are in good agreement. All meteors appeared during the solar-longitude interval  $170^{\circ} - 176^{\circ}$ , with most events around 15 - 16 September (around  $\lambda_{\theta} = 172.9^{\circ}$ ). Orbits of this meteor shower were detected in previous years, but the activity level remained well below the detection threshold. The 2025 activity appears to be an outburst compared to previous years.

#### Acknowledgment

This report is based on the data of the Global Meteor Network (Vida et al., 2020a; 2020b; 2021) which is released under the CC BY 4.0 license<sup>4</sup>. We thank all 825 participants

in the Global Meteor Network project for their contribution and perseverance. A list with the names of the volunteers who contribute to GMN has been published in the 2024 annual report (Roggemans et al., 2025).

#### References

- Drummond J. D. (1981). "A test of comet and meteor shower associations". *Icarus*, **45**, 545–553.
- Jopek T. J. (1993). "Remarks on the meteor orbital similarity D-criterion". *Icarus*, **106**, 603–607.
- Jopek T. J., Rudawska R. and Pretka-Ziomek H. (2006). "Calculation of the mean orbit of a meteoroid stream". *Monthly Notices of the Royal Astronomical Society*, **371**, 1367–1372.
- Moorhead A. V., Clements T. D., Vida D. (2020). "Realistic gravitational focusing of meteoroid streams". Monthly Notices of the Royal Astronomical Society, 494, 2982–2994.
- Roggemans P., Johannink C. and Campbell-Burns P. (2019a). "October Ursae Majorids (OCU#333)". eMetN Meteor Journal, 4, 55–64.
- Roggemans P., Campbell-Burns P., Kalina M., McIntyre M., Scott J. M., Šegon D., Vida D. (2025). "Global Meteor Network report 2024". *eMetN Meteor Journal*, **10**, 67–101.
- Southworth R. B. and Hawkins G. S. (1963). "Statistics of meteor streams". *Smithsonian Contributions to Astrophysics*, 7, 261–285.
- Vida D., Gural P., Brown P., Campbell-Brown M., Wiegert P. (2020a). "Estimating trajectories of meteors: an observational Monte Carlo approach I. Theory". Monthly Notices of the Royal Astronomical Society, 491, 2688–2705.
- Vida D., Gural P., Brown P., Campbell-Brown M., Wiegert P. (2020b). "Estimating trajectories of meteors: an observational Monte Carlo approach - II. Results". *Monthly Notices of the Royal Astronomical Society*, 491, 3996–4011.
- Vida D., Šegon D., Gural P. S., Brown P. G., McIntyre M. J. M., Dijkema T. J., Pavletić L., Kukić P., Mazur M. J., Eschman P., Roggemans P., Merlak A., Zubrović D. (2021). "The Global Meteor Network Methodology and first results". *Monthly Notices of the Royal Astronomical Society*, **506**, 5046–5074.

<sup>&</sup>lt;sup>4</sup> https://creativecommons.org/licenses/by/4.0/

# M2024-S1 activity confirmed in 2025

Paul Roggemans<sup>1</sup>, Denis Vida<sup>2,3</sup> and Damir Šegon<sup>4</sup>

<sup>1</sup> Pijnboomstraat 25, 2800 Mechelen, Belgium

paul.roggemans@gmail.com

denis.vida@gmail.com

<sup>4</sup> Astronomical Society Istra Pula, Park Monte Zaro 2, 52100 Pula, Croatia

A new meteor shower discovered in 2024 by GMN, registered by the IAU-MDC as M2024-S1 displayed distinct activity in 2025, September 21–23, from a radiant at R.A. =  $242.0^{\circ}$ , Decl. =  $+76.9^{\circ}$ . The orbit obtained in 2024 has been confirmed. Asteroid 2021 HK12 is a likely parent body and the shower may be dynamically connected with the epsilon-Ursae-Minorids (EPU#1044).

#### 1 Introduction

In 2024 Global Meteor Network discovered a new activity source on 23–24 September 2024 which was reported to the IAU-MDC and listed with the temporary identification M2024-S1 $^5$  (Vida and Šegon, 2024; Šegon et al., 2025; Harachka et al., 2024). This activity source has been detected again in 2025 (*Figure 1*) during the nights September 21–23. In total 89 meteors of this meteor shower were observed by the Global Meteor Network $^6$  low-light video cameras during the period 2025 September 19 – 30 with most events during September 21 – 24. The shower was independently observed by cameras in 20 countries

(Bosnia Herzegovina, Belgium, Bulgaria, Canada, Croatia, Czechia, Denmark, Germany, France, Hungary, Italy, Netherlands, Poland, Portugal, Romania, Slovenia, South Korea, Spain, United Kingdom and United States). The shower had a median geocentric radiant with coordinates R.A. = 242.0°, Decl. = +76.9°, within a circle with a standard deviation of  $\pm 2.2^{\circ}$  (equinox J2000.0) see *Figure 2*. The radiant drift in R.A. is  $-0.34^{\circ}$  on the sky per degree of solar longitude and  $-0.10^{\circ}$  in Dec., both referenced to  $\lambda_O = 181.4^{\circ}$  (*Figures 3 and 4*). The median Sun-centered ecliptic coordinates were  $\lambda - \lambda_O = 296.1^{\circ}$ ,  $\beta = +76.6^{\circ}$  (*Figure 5*). The geocentric velocity was  $31.8 \pm 0.1$  km/s.

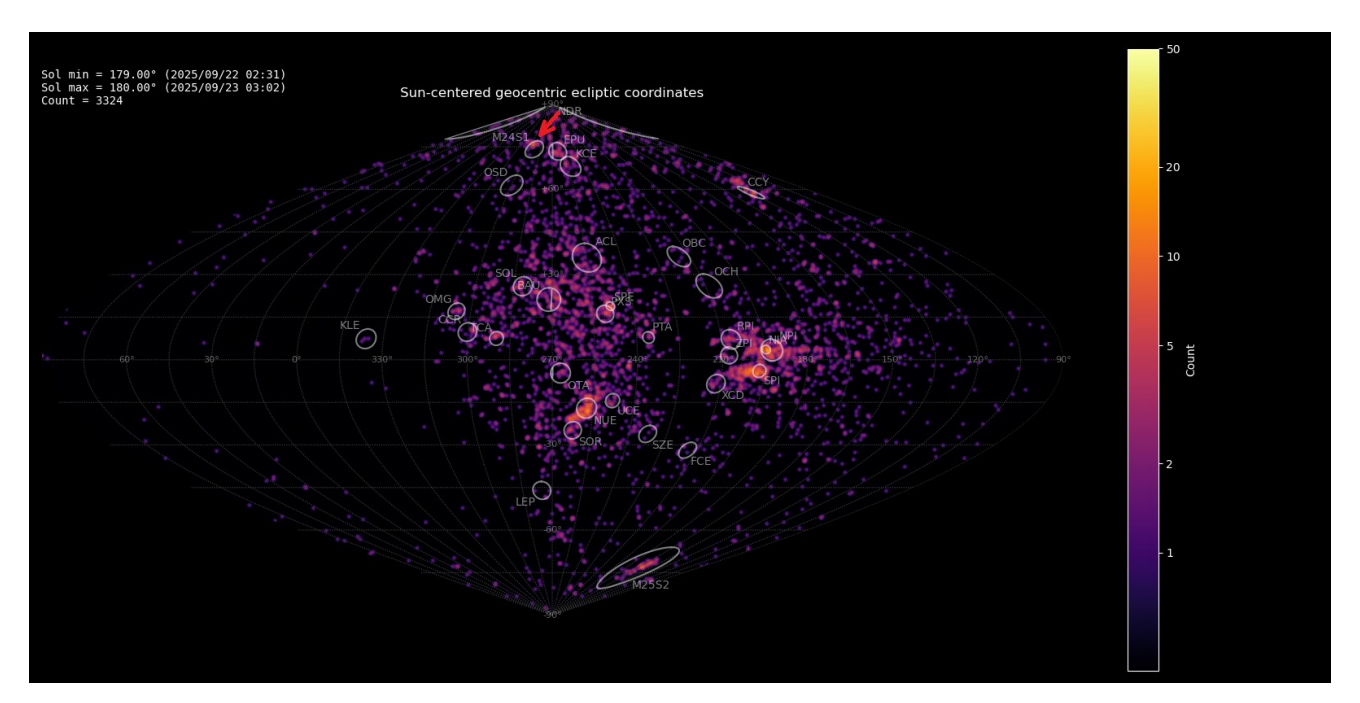


Figure 1 – Radiant plot of the Global Meteor Network data for 2025 September 22–23 in Sun-centered geocentric ecliptic coordinates. The new radiant is visible at high ecliptic altitude and marked by a red arrow.

<sup>&</sup>lt;sup>2</sup> Department of Physics and Astronomy, University of Western Ontario, Richmond Street, London, N6A 3K7, Ontario, Canada

<sup>&</sup>lt;sup>3</sup> Institute for Earth and Space Exploration, University of Western Ontario, Perth Drive, London, N6A 5B8, Ontario, Canada

<sup>&</sup>lt;sup>5</sup> https://www.ta3.sk/IAUC22DB/MDC2022/Roje/pojedynczy\_ob\_iekt.php?lporz=02172&kodstrumienia=01226

 $<sup>^{6}\,\</sup>underline{https://global meteornetwork.org/data/}$ 

#### 2 GMN shower identification results

The GMN shower association criterion assumes that meteors within 1° in solar longitude, within an association radius from radiant (4.8° in this case), and within 10% in geocentric velocity of a shower reference location are members of that shower. Further details about the shower association are explained in Moorhead et al. (2020). Using these meteor shower selection criteria, 89 orbits have been associated in 2025 with M2024-S1. The mean orbit has been listed in *Table 1*.

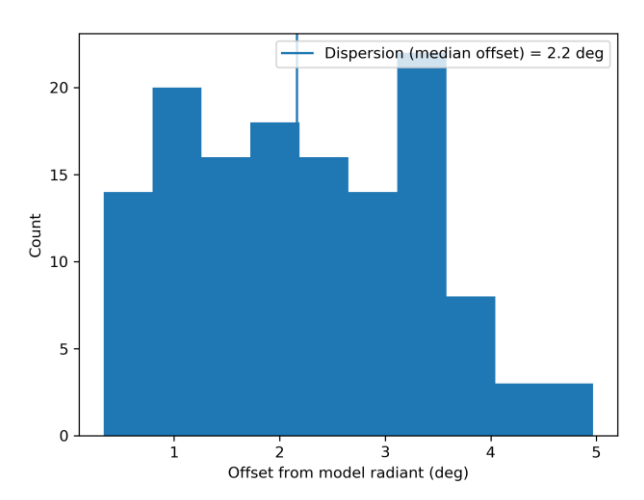


Figure 2 – Dispersion on the radiant position.

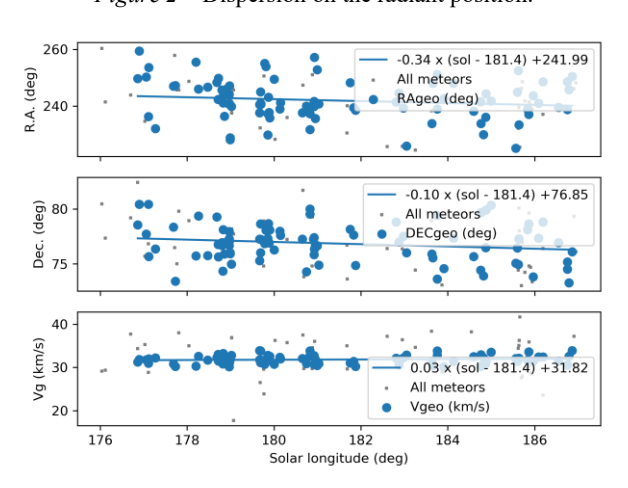


Figure 3 – The radiant drift.

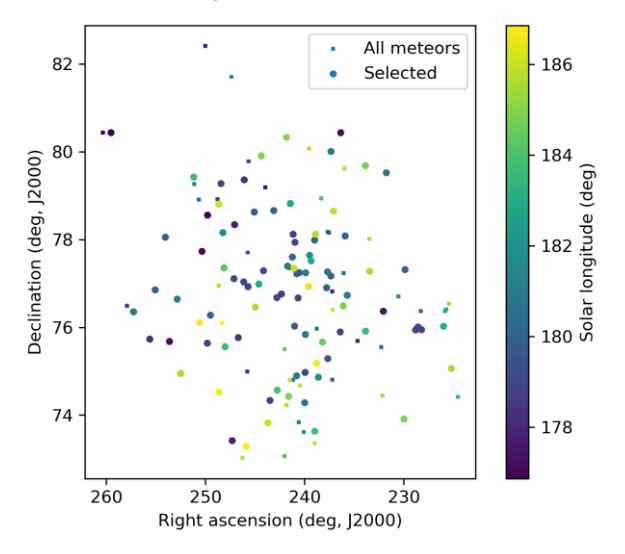


Figure 4 – The radiant distribution during the solar-longitude interval  $176^{\circ} - 187^{\circ}$  in equatorial coordinates.

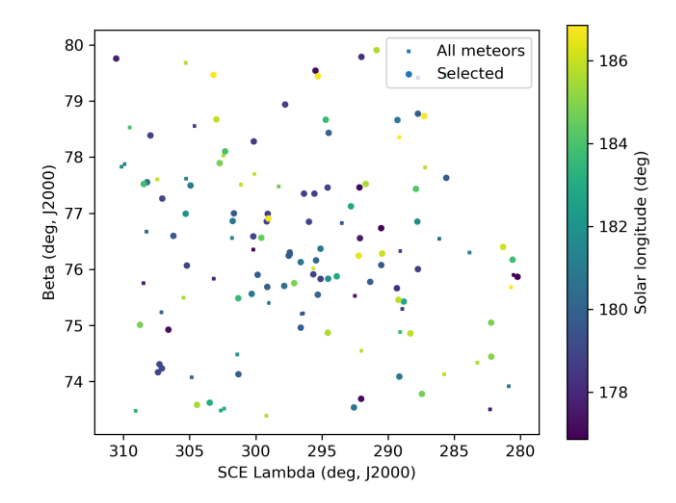


Figure 5 – The radiant distribution during the solar-longitude interval  $176^{\circ} - 187^{\circ}$  in Sun centered geocentric ecliptic coordinates.

#### 3 Another search method

Meteor shower identification strongly depends on the methodology used to select candidate shower members. The sporadic background is everywhere present at the sky which risks to contaminate selections of shower candidates. Using a radiant location is a straightforward method to classify shower meteors. In order to double check GMN meteor shower detections another method is used, based on orbit similarity criteria. This approach serves as a second opinion to make sure that no spurious radiant concentrations are mistaken as new meteor showers.

The visible concentration of radiant points was extracted for the time interval of  $178^{\circ} < \lambda_{O} < 184^{\circ}$ , arbitrarily limited in Sun-centered geocentric ecliptic coordinates with  $282^{\circ} < \lambda - \lambda_{O} < 306^{\circ}$  and  $+71^{\circ} < \beta < +78^{\circ}$ . This selection includes most of the possible meteor shower members as well as the sporadic sources within this interval. This preselection included 72 meteor orbits, used to compute a first mean orbit for this sample. We didn't use median values to derive a mean orbit since a vectoral solution like the method of Jopek et al. (2006) is more appropriate for orbital elements with angular values.

This first mean orbit serves as a reference orbit to start an iterative procedure to approach a mean orbit which is the most representative orbit for the similar orbits within the sample, removing outliers and sporadic orbits. This method has been described before (Roggemans et al., 2019). Three different discrimination criteria are combined in order to have only those orbits which fit the different criteria thresholds. The D-criteria that we use are these of Southworth and Hawkins (1963), Drummond (1981) and Jopek (1993) combined. The values are considered in five different classes with different thresholds of similarity:

- Low:  $D_{SH} < 0.2 \& D_D < 0.08 \& D_J < 0.2$ ;
- Medium Low:  $D_{SH} < 0.125 \& D_D < 0.05 \& D_J < 0.125$ ;
- Medium high:  $D_{SH} < 0.1 \& D_D < 0.04 \& D_J < 0.1$ ;
- High:  $D_{SH} < 0.075 \& D_D < 0.03 \& D_J < 0.075$ .
- Very high:  $D_{SH} < 0.05 \& D_D < 0.02 \& D_J < 0.05$ .

Working with D-criteria requires caution as the validity depends much on the type of orbits. The method works fine for high inclined long period orbits, but is less reliable for low inclination, low eccentricity short period orbits. The D-criteria values are no more than an indication for the degree of similarity between an orbit and a reference orbit.

The Rayleigh distribution fit pointed at a  $D_D$  value of 0.05 as the orbital similarity threshold value cutoff for the 2024 data of this meteor shower (Šegon et al., 2025). We compare the radiant plots of 2024 with those of 2025. In 2024 the complete activity period between 176.0° and 187.0° in solar longitude was used, in 2025 the search interval was limited to 178.0° and 184.0° in solar longitude, to focus on the main activity nights and to exclude outliers at the outskirts of the activity period. *Figure 6* compares the radiant plots in equatorial coordinates. The radiant

appears at exactly the same position as in 2024. The activity was comparable to 2024.

The radiant concentration that we see at the top left of the plot for 2025 are the epsilon-Ursae-Minorids (EPU#1044), marked with a yellow diamond, which produced an outburst in 2025 (Roggemans et al., 2025b). No concentration of radiants appeared at this position in 2024, indicating that no outburst occurred in 2024. In *Figure 6* we see the same radiant plot, but in Sun-centered geocentric ecliptic coordinates. Also, here we see the M2024-S1 radiant well apart from the position of the epsilon-Ursae-Minorids (EPU#1044). In 2025 we see a distinct concentration of radiants at the position of this meteor shower. The radiant position obtained for the epsilon-Ursae-Minorids by GMN differs about 10° from the position listed in the IAU-MDC working list<sup>7</sup>.

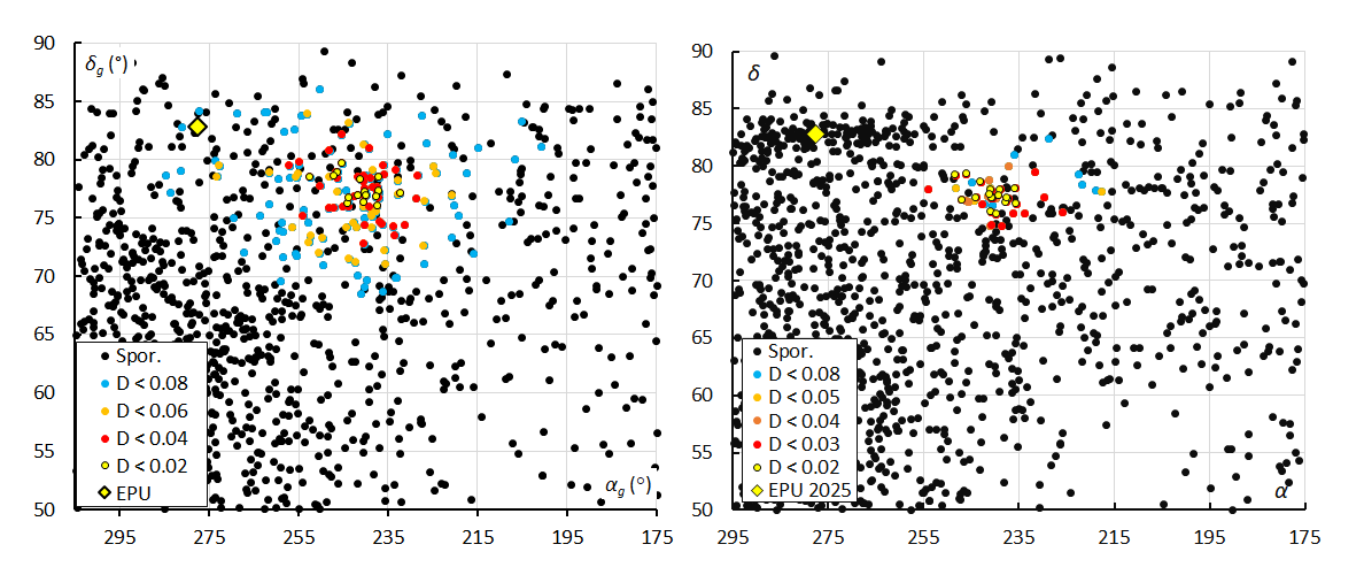


Figure 6 – The radiant distribution in equatorial coordinates, color coded for different threshold classes of the orbit similarity criteria. At left the plot for 2024 when M2024-S1 was discovered,  $\lambda_0$ [176.0–187.0], at right the plot for 2025,  $\lambda_0$ [178.0–184.0].

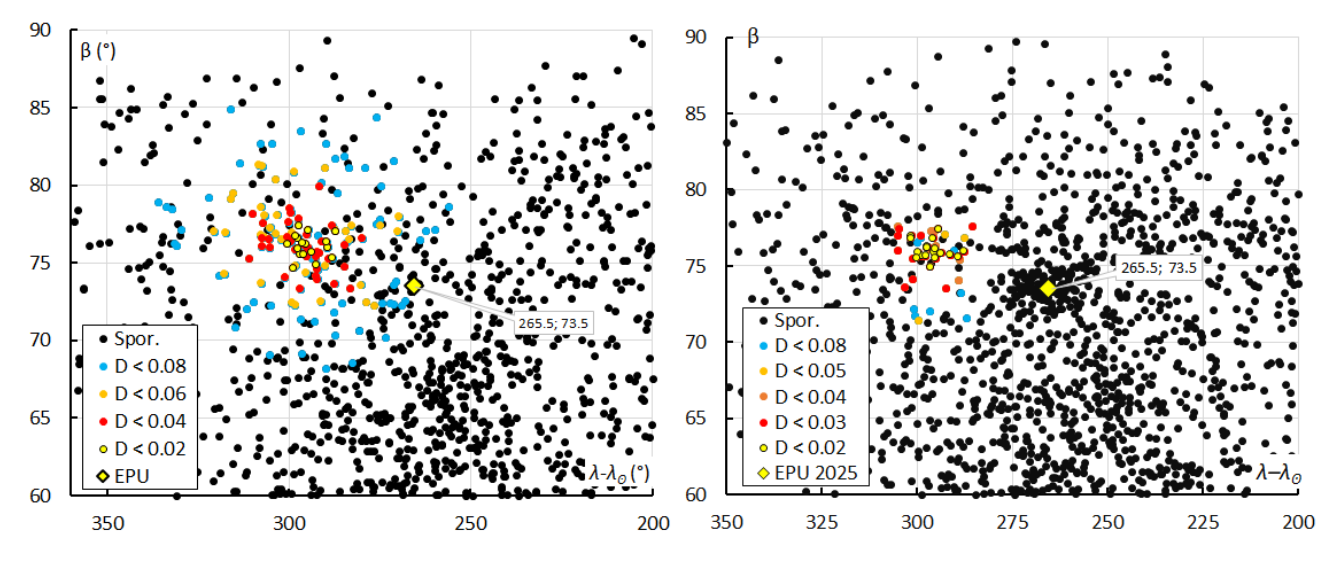


Figure 7 – The radiant distribution in Sun-centered geocentric ecliptic coordinates, color coded for different threshold classes of the orbit similarity criteria. At left the plot for 2024 when M2024-S1 was discovered,  $\lambda_0$ [176.0–187.0], at right the plot for 2025,  $\lambda_0$ [178.0–184.0].

© eMetN Meteor Journal 355

.

<sup>&</sup>lt;sup>7</sup> https://www.ta3.sk/IAUC22DB/MDC2022/Roje/pojedynczy\_ob\_iekt.php?lporz=01987&kodstrumienia=01044

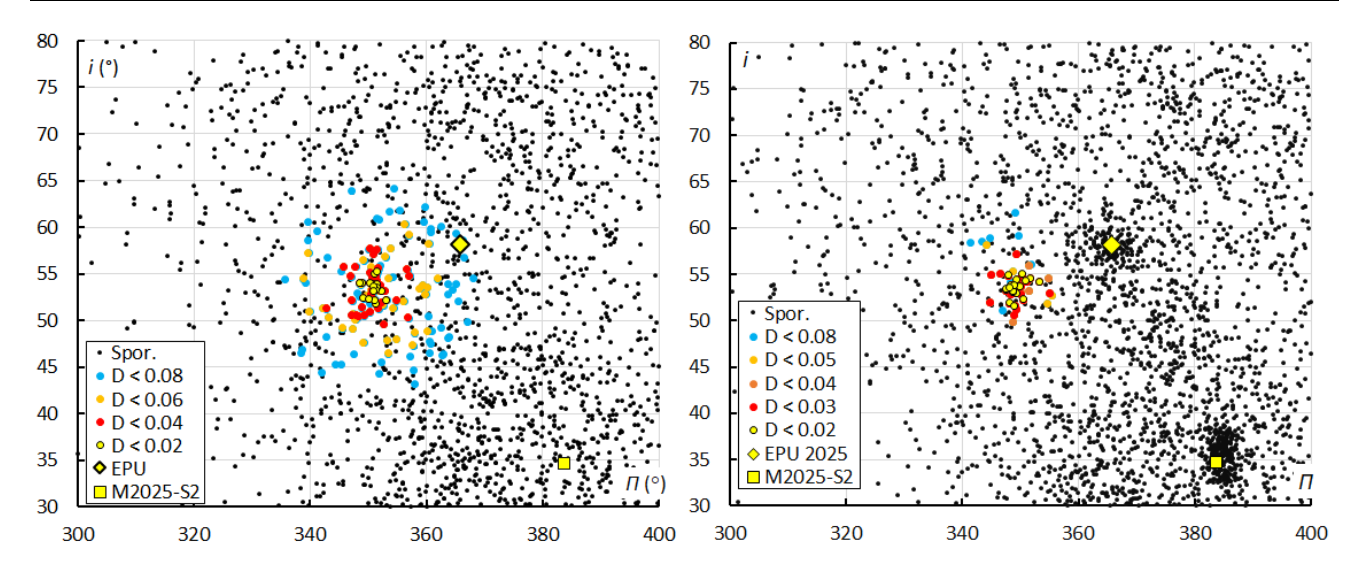


Figure 8 – Diagram of inclination *i* versus the longitude of perihelion  $\Pi$ , color coded for different threshold classes of the orbit similarity criteria. At left the plot for 2024 when M2024-S1 was discovered, sampled during the entire activity period,  $\lambda_0$ [176.0–187.0]. At right the plot for 2025, limited to the nights with highest activity  $\lambda_0$ [178.0–184.0]. The positions of two other outbursts in 2025, EPU#1044 and M2025-S2 are indicated by a yellow diamond and a yellow square.

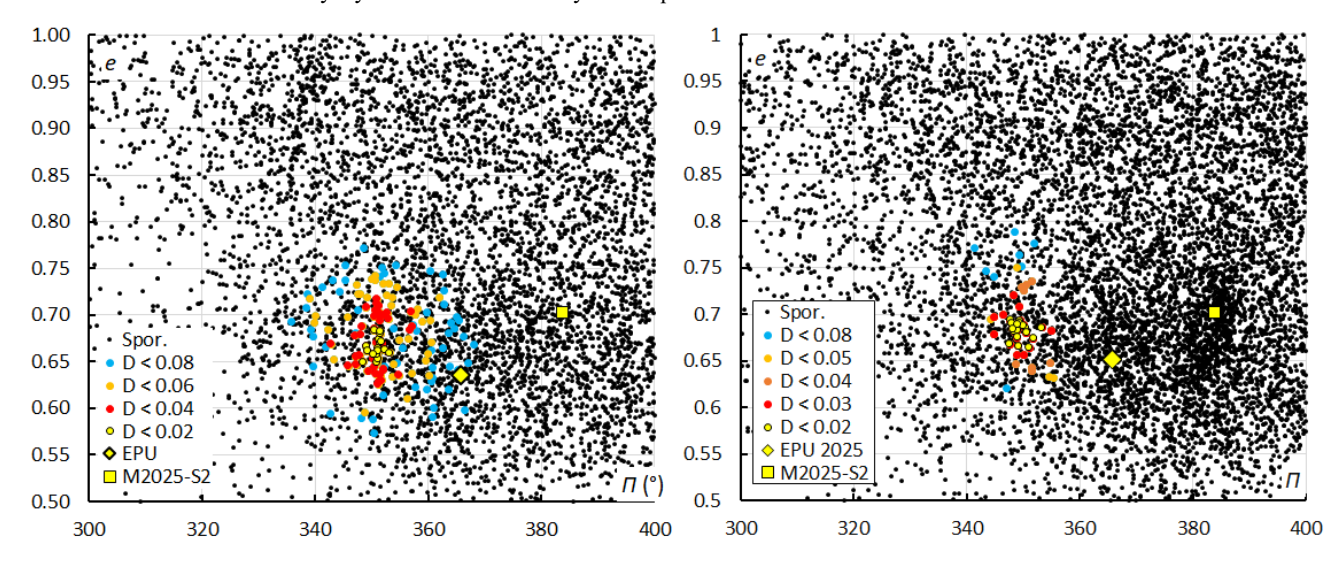


Figure 9 – Diagram of eccentricity e versus the longitude of perihelion  $\Pi$ , color coded for different threshold classes of the orbit similarity criteria. At left the plot for 2024 when M2024-S1 was discovered, sampled during the entire activity period,  $\lambda_0$ [176.0–187.0]. At right the plot for 2025, limited to the nights with highest activity  $\lambda_0$ [178.0–184.0]. The positions of two other outbursts in 2025, EPU#1044 and M2025-S2 are indicated by a yellow diamond and a yellow square.

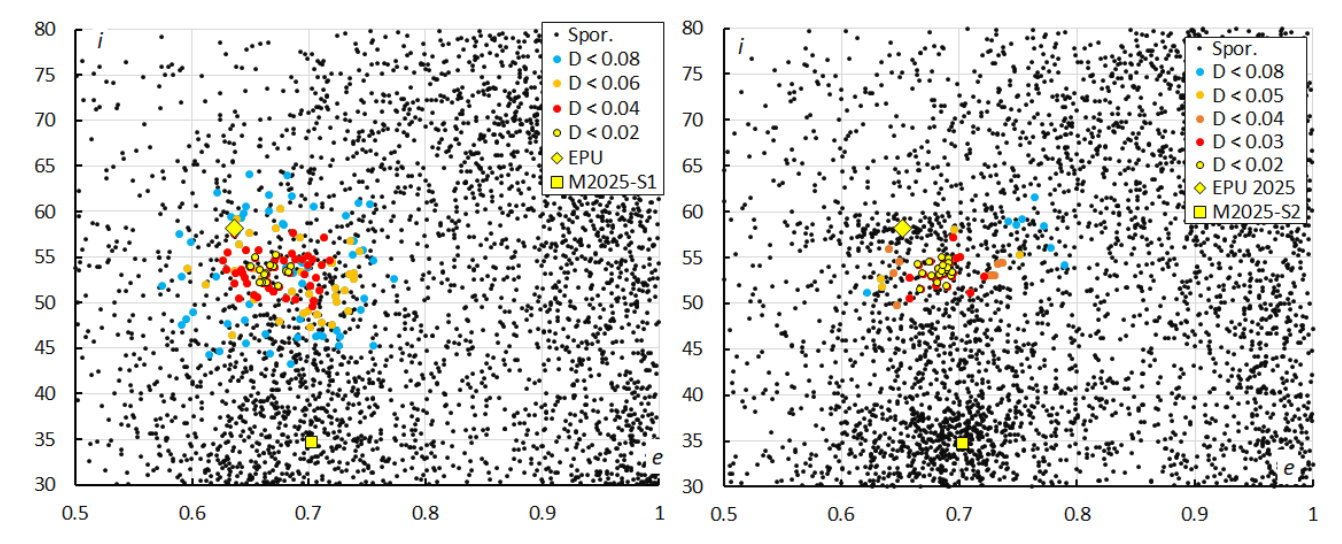


Figure 10 – Diagram of inclination i versus the eccentricity e, color coded for different threshold classes of the orbit similarity criteria. At left the plot for 2024 when M2024-S1 was discovered, sampled during the entire activity period,  $\lambda_0$ [176.0–187.0]. At right the plot for 2025, limited to the nights with highest activity  $\lambda_0$ [178.0–184.0]. The positions of two other outbursts in 2025, EPU#1044 and M2025-S2 are indicated by a yellow diamond and a yellow square.

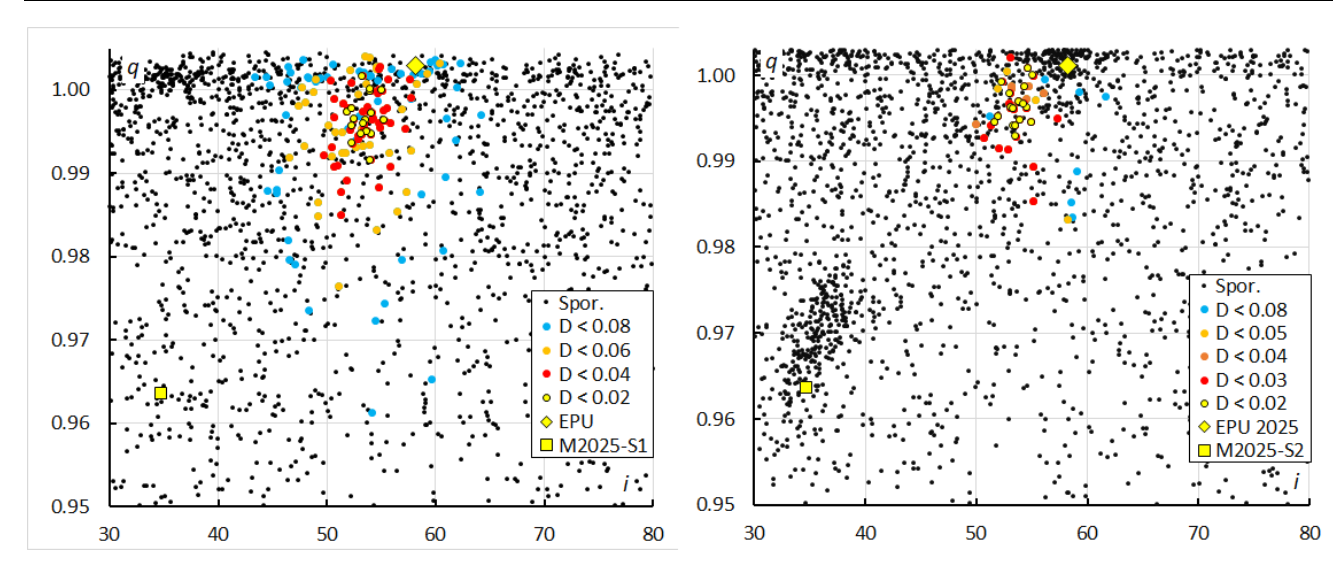


Figure 11 – Diagram of perihelion distance q versus the inclination i, color coded for different thresholds classes of the orbit similarity criteria. At left the plot for 2024 when M2024-S1 was discovered, sampled during the entire activity period,  $\lambda_0$ [176.0–187.0]. At right the plot for 2025, limited to the nights with highest activity  $\lambda_0$ [178.0–184.0]. The positions of two other outbursts in 2025, EPU#1044 and M2025-S2 are indicated by a yellow diamond and a yellow square.

Another way to visualize concentrations of meteoroid orbits is to plot the orbital elements against each other in a diagram. For orbits that belong to a meteoroid stream these parameters must appear as a concentration of points in each diagram. This way the compactness and dispersion of the stream for different orbital elements can be visualized.

Figure 8 compares inclination i against the longitude of perihelion  $\Pi$  for 2024 and 2025. M2024-S1 appears well concentrated in inclination and in longitude of perihelion. The blue dots in 2024 are outliers or chance-line-up sporadics, when the sampling bin is reduced to the same interval as used for 2025, most of these outliers disappear.

Figure 9 shows that M2024-S1 is also compact in eccentricity and longitude of perihelion. Figure 10 also shows the compactness in inclination and eccentricity. Figure 11 seems to have more dispersion in perihelion distance q but this is mainly due to the scale of the y-axis. Apart from the outliers recorded at the outskirts of the activity period, M2024-S1 appears as a distinct compact activity source.

# 4 Comparing both methods

The first method mainly looks at the radiant positions for the classification. When we apply the D criteria, only 69 of the 89 selected meteors fulfill the threshold values of  $D_{SH} < 0.125$ ,  $D_D < 0.05$  and  $D_J < 0.125$  for the mean orbit obtained by the GMN method, five meteors fail completely in the D-criteria. 30 of the 89 meteors were identified by the GMN method before solar longitude 178.0° or after 184°. Twenty-one meteors within this interval were not detected by the D-criteria method and only two orbits detected by the D-criteria method were missed by the GMN method. 37 shower members were identified by both methods in common.

Despite the difference between the samples based on the two different methods, the final mean orbits are in very good agreement except for the radiant drift in R.A which is due to the short activity interval of only four days.

Table 1 – Comparing M2024-S1 for the 2024 and 2025 solutions derived by two different methods, the parameters under  $D_D < 0.05$  were derived from the method described in *Section 3*.

	GMN 2024	GMN 2025	$D_D < 0.05$
λο (°)	181.9	181.4	180.0
λο <sub>b</sub> (°)	181.0	176.8	178.0
λ0e (°)	182.6	186.9	184.0
$a_g$ (°)	238.3	242.0	240.7
$\delta_g$ (°)	+77.3	+76.9	+77.3
$\Delta a_g$ (°)	_	-0.34	-1.8
$\Delta\delta_{g}\left(^{\circ}\right)$	_	-0.10	-0.2
$v_g$ (km/s)	32.0	31.8	31.9
$H_b$ (km)	89.7	94.3	92.1
$H_e$ (km)	79.3	82.1	81.1
$H_p$ (km)	82.7	86.0	84.3
$Mag_{Ap}$	-0.75	+0.6	-0.5
$\lambda_g$ (°)	118.09	117.47	116.7
$\lambda_g - \lambda_O$ (°)	296.19	296.07	296.5
$eta_g$ (°)	+75.80	+76.56	+76.0
a (A.U.)	3.11	3.275	3.15
q (A.U.)	0.994	0.995	0.995
e	0.680	0.696	0.684
i (°)	53.9	53.2	53.6
ω (°)	169.2	170.1	169.1
$\mathcal{Q}\left(^{\circ}\right)$	181.8	181.4	180.4
П(°)	351.0	351.5	349.6
$T_j$	2.34	2.27	2.33
N	31	89	40

# 5 Orbit and parent body

Figure 12 shows the orbits for the different solutions in the inner solar system. The dust of M2024-S1 crosses the Earth orbit at its descending node. The crossing of the ecliptic at the ascending node is close to the orbit of Jupiter what means that dust trails will be much affected by this giant planet's gravitational perturbations. This could explain a periodic activity and reason why this shower wasn't noticed sooner.

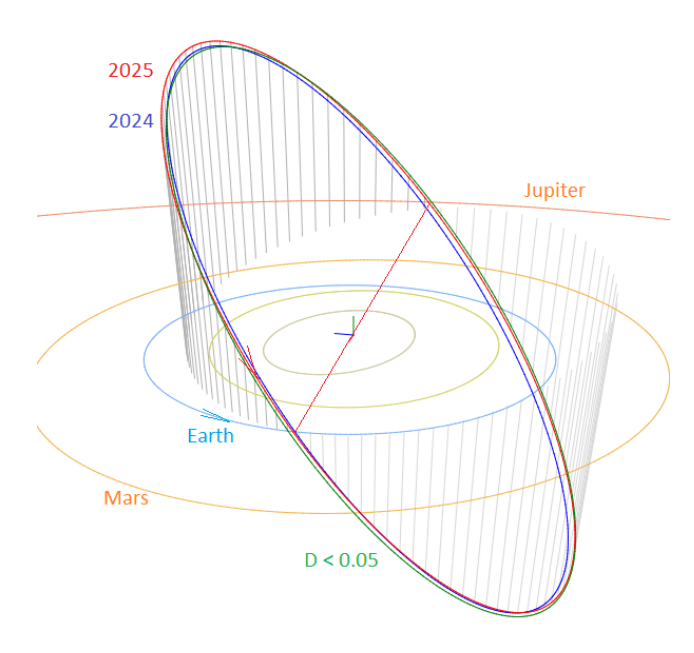


Figure 12 – Comparing the mean orbits for the solutions for M2024-S1 based on the shower identification according to two methods, blue is for 2024 data, red for 2025 data and green for the other shower search method with  $D_D < 0.05$  in Table 1, close-up at the inner Solar System. (Plotted with the Orbit visualization app provided by Pető Zsolt).

The Tisserand's parameter relative to Jupiter,  $T_j$  identifies the orbit as of a Jupiter Family Comet type orbit. A parent-body search top 10 includes candidates with a threshold for the Drummond  $D_D$  criterion value lower than 0.16 (*Table 2*). 2021 HK12 has a very similar orbit and could be the parent body. It would be up to meteoroid stream modelers to reconstruct the dynamic orbit evolution to see if there could be any connection between this object and this new meteor shower.

The list of possible parent bodies has nine candidates in common with those for the epsilon-Ursae Minorids (Roggemans et al., 2025b). Apart from common candidate parent bodies, meteoroids from both streams ablate remarkable deep in the atmosphere. This means that the particles aren't fragile dust typical for cometary material, but solid particles while the orbits nowhere get closer to the Sun than within the comfort zone of about 1 AU. The epsilon-Ursae Minorids produced an outburst in 2025, indicating a 6-year periodicity since its activity was recorded in 2019. M2024-S1 displayed distinct activity in 2024 and 2025 but remained below the threshold of

detectability in earlier years. A small number of similar orbits can be found in years before 2024, but too few to be conclusive. There were no meteor camera networks with enough capacity to detect outbursts from weak sources like M2024-S1. Both showers, EPU#1044 and M2024-S1 cross the Earth's orbit almost at the same time and also the points of their ascending nodes are relatively close to each other near Jupiter's orbit. A common origin for both meteor showers is very likely.

Table 2 – Top ten matches of a search for possible parent bodies with  $D_D < 0.16$ .

Name	$D_D$
2021 HK12	0.051
2024 RK16	0.114
2009 SG18	0.128
2010 QA5	0.132
21P/Giacobini-Zinner	0.141
2018 PF8	0.144
2020 UP3	0.145
2014 XX7	0.152
2021 VB4	0.156
(163732) 2003 KP2	0.16

#### 6 Conclusion

Activity from meteor shower M2024-S1 detected by Global Meteor Network in 2024 has been confirmed in 2025 with the same radiant position during 21–23 September, slightly earlier in time than in 2024 when it was observed on 23-24 September. The 2025 simultaneous outburst of the nearby epsilon-Ursae Minorids radiant resolved the confusion since other researchers regarded the M2024-S1 activity as a 2024 outburst of the epsilon-Ursae Minorids (Jenniskens et al., 2025). Both activity sources are different meteor showers, but dynamically related. A peculiar characteristic of this shower is the remarkable low ablation height of the meteors which indicate that the meteoroids consist of solid material. The asteroid or extinct comet 2021 HK12 is a plausible candidate as parent body. Future observations should clarify if the M2024-S1 activity is a periodic or an annual component. Orbit integrations may clarify the dynamic evolution and possible relationship with the epsilon-Ursae Minorids.

# Acknowledgment

This report is based on the data of the Global Meteor Network (Vida et al., 2020a; 2020b; 2021) which is released under the CC BY 4.0 license<sup>8</sup>. We thank all 825 participants in the Global Meteor Network project for their contribution and perseverance. A list with the names of the volunteers who contribute to GMN has been published in the 2024 annual report (Roggemans et al., 2025a).

<sup>8</sup> https://creativecommons.org/licenses/by/4.0/

#### References

- Drummond J. D. (1981). "A test of comet and meteor shower associations". *Icarus*, **45**, 545–553.
- Harachka Y., Mikulich A., Morozov K., Angelsky A. (2024). "Possible new meteor shower in Ursa Minor". *eMetN Meteor Journal*, **9**, 395–396.
- Jenniskens P., Johannink C., Moskovitz N., Howell A. (2025). "Short note on what appears to have been a 2024 outburst of epsilon-Ursae-Minorids (EPU#1044)". *eMetN Meteor Journal*, **10**, 20–21.
- Jopek T. J. (1993). "Remarks on the meteor orbital similarity D-criterion". *Icarus*, **106**, 603–607.
- Jopek T. J., Rudawska R. and Pretka-Ziomek H. (2006). "Calculation of the mean orbit of a meteoroid stream". Monthly Notices of the Royal Astronomical Society, 371, 1367–1372.
- Moorhead A. V., Clements T. D., Vida D. (2020). "Realistic gravitational focusing of meteoroid streams". Monthly Notices of the Royal Astronomical Society, **494**, 2982–2994.
- Roggemans P., Johannink C. and Campbell-Burns P. (2019). "October Ursae Majorids (OCU#333)". eMetN Meteor Journal, 4, 55–64.
- Roggemans P., Campbell-Burns P., Kalina M., McIntyre M., Scott J. M., Šegon D., Vida D. (2025a). "Global Meteor Network report 2024". *eMetN Meteor Journal*, **10**, 67–101.

- Roggemans P., Vida D., Šegon D. (2025b). "Epsilon-Ursae Minorids (EPU#1044) enhanced activity in 2025". eMetN Meteor Journal, 10, 360–367.
- Šegon D., Vida D., Roggemans P. (2025). "New meteor shower in Ursa Minor 23–24 September 2024". *eMetN Meteor Journal*, **10**, 12–19.
- Southworth R. B. and Hawkins G. S. (1963). "Statistics of meteor streams". *Smithsonian Contributions to Astrophysics*, 7, 261–285.
- Vida D., Gural P., Brown P., Campbell-Brown M., Wiegert P. (2020a). "Estimating trajectories of meteors: an observational Monte Carlo approach I. Theory". Monthly Notices of the Royal Astronomical Society, 491, 2688–2705.
- Vida D., Gural P., Brown P., Campbell-Brown M., Wiegert P. (2020b). "Estimating trajectories of meteors: an observational Monte Carlo approach - II. Results". *Monthly Notices of the Royal Astronomical Society*, 491, 3996–4011.
- Vida D., Šegon D., Gural P. S., Brown P. G., McIntyre M. J. M., Dijkema T. J., Pavletić L., Kukić P., Mazur M. J., Eschman P., Roggemans P., Merlak A., Zubrović D. (2021). "The Global Meteor Network Methodology and first results". Monthly Notices of the Royal Astronomical Society, 506, 5046–5074.
- Vida D., Šegon D. (2024). New meteor shower M2024-S1 in Ursa minor. CBET 5452. D. W. E. Green (ed.), 1 pp.

# Epsilon-Ursae Minorids (EPU#1044) enhanced activity in 2025

Paul Roggemans<sup>1</sup>, Denis Vida<sup>2,3</sup> and Damir Šegon<sup>4</sup>

<sup>1</sup> Pijnboomstraat 25, 2800 Mechelen, Belgium

paul.roggemans@gmail.com

<sup>3</sup> Institute for Earth and Space Exploration, University of Western Ontario, Perth Drive, London, N6A 5B8, Ontario, Canada

denis.vida@gmail.com

<sup>4</sup> Astronomical Society Istra Pula, Park Monte Zaro 2, 52100 Pula, Croatia

Enhanced activity has been detected during 2025 September 23 – 25 from the epsilon-Ursae Minorids (EPU#1044) by the Global Meteor Network. 102 meteors belonging to this meteor shower were observed between  $179.6^{\circ} < \lambda_{\Theta} < 182.7^{\circ}$  from a radiant at R.A. = 277.7° and Decl.= +82.8°, with a geocentric velocity of 33.8 km/s. The 2025 activity of this meteor shower confirms a 6-year periodicity since its earlier displays in 2019 and 2013.

#### 1 Introduction

While monitoring the newly detected activity source M2025-S2 far south at the southern hemisphere, another hot spot appeared on the GMN radiant density map far north at the northern hemisphere. The radiant source was automatically associated by the GMN tools as the epsilon-Ursae Minorids (EPU#1044)<sup>9</sup>, a poorly known minor meteor shower which was first reported in 2020 by Sato et al. (2020) based on thirteen detected shower meteors

captured during 2019 September 25–27 UT by the SonotaCo Network. The activity was confirmed by CAMS data as in 2019, September 24–26 UT, seven epsilon Ursae Minorids were detected by the CAMS California network and four by CAMS Florida. The discovery of this shower was based on 19 orbits, 12 from SonotaCo and 7 from CAMS. Another solution in the IAU-MDC for this meteor shower was published by Shiba (2022), based on 10 of the orbits collected by the SonotaCo network in 2019.

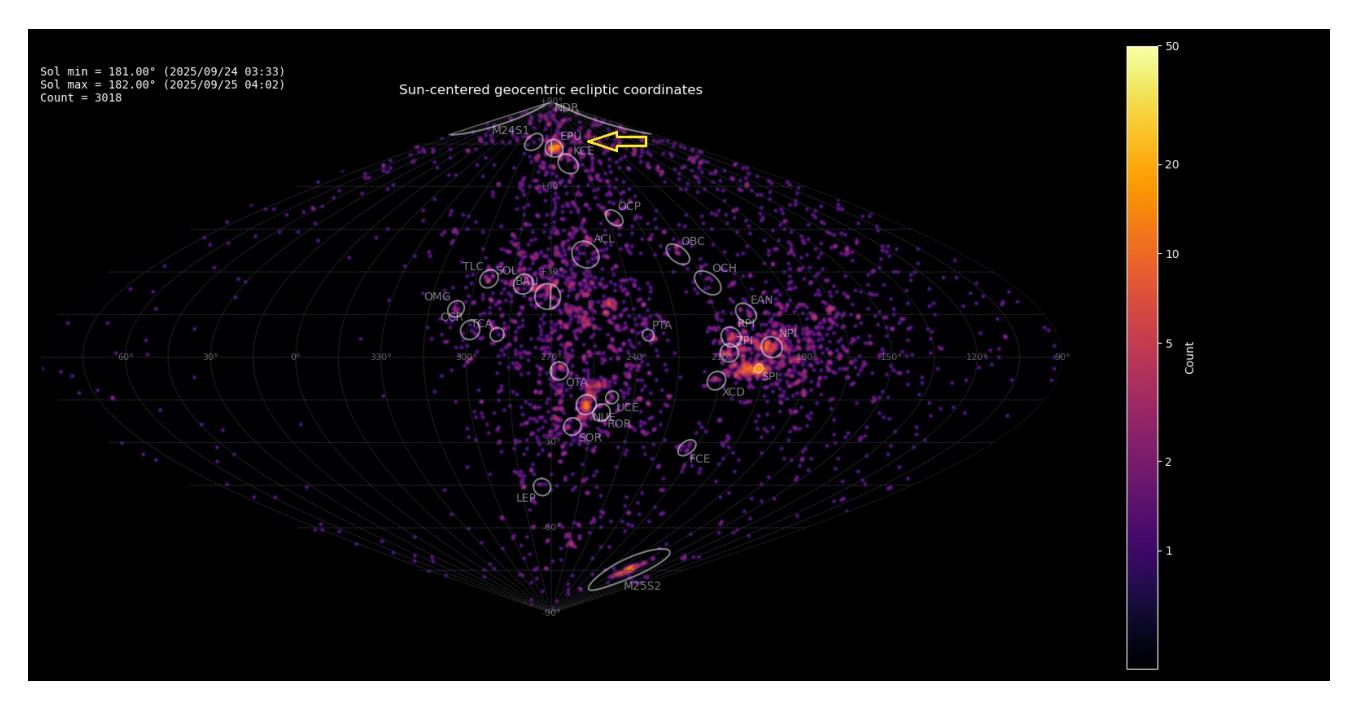


Figure 1 – Heat map with 3018 radiants obtained by the Global Meteor network on September 24 – 25, 2025. A distinct concentration is visible in Sun-centered geocentric ecliptic coordinates at the position known as the radiant of the epsilon-Ursae Minorids (EPU#1044). The activity lasted more than two days.

<sup>&</sup>lt;sup>2</sup> Department of Physics and Astronomy, University of Western Ontario, Richmond Street, London, N6A 3K7, Ontario, Canada

<sup>&</sup>lt;sup>9</sup> https://www.ta3.sk/IAUC22DB/MDC2022/Roje/pojedynczy\_obiekt.php?lporz=01987&kodstrumienia=01044

#### 2 2025 detection of EPU#1044

The GMN shower association criterion assumes that meteors within 1° in solar longitude, within an association radius, in this case of 3° in radiant, and within 10% in geocentric velocity of a shower reference location, are members of that shower. Further details about the shower association are explained in Moorhead et al. (2020). These are rather strict criteria since meteor showers often have a larger dispersion in radiant position, velocity and activity period. Using these meteor shower selection criteria, 134 orbits have been associated with the epsilon-Ursae Minorids in the GMN meteor orbit database in 2025.

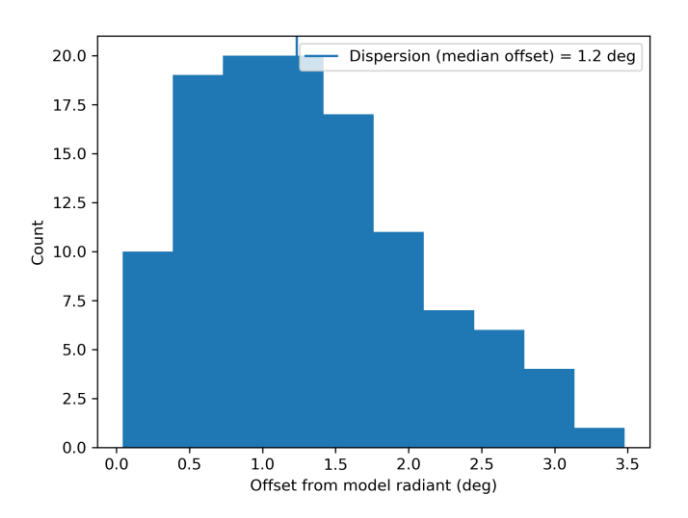


Figure 2 – Dispersion on the radiant position.

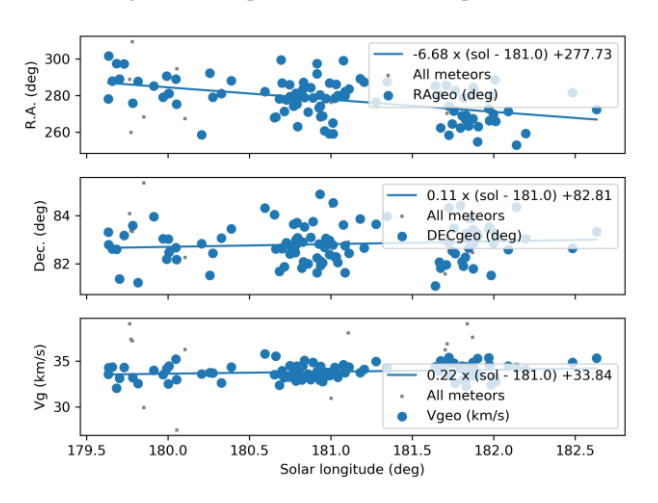


Figure 3 – The radiant drift.

The shower was independently observed by cameras in 19 countries (Belgium, Bosnia and Herzegovina, Bulgaria, Canada, Croatia, Denmark, Germany, Greece, Hungary, Ireland, Portugal, Romania, Russia, Spain, South Korea, Netherlands, Ukraine, United Kingdom and the United States).

The shower had a median geocentric radiant with coordinates R.A. = 277.7°, Decl. = +82.8°, within a circle with a standard deviation of  $\pm 1.2^{\circ}$  (equinox J2000.0) see *Figure 2*. The radiant drift in R.A. is  $-6.7^{\circ}$  on the sky per degree of solar longitude and +0.11° in Dec., both referenced to  $\lambda_{O}$  = 181.0° (*Figures 3 and 4*). The median Sun-centered ecliptic coordinates were  $\lambda - \lambda_{O}$  = 265.5°,

 $\beta$  = +73.5° (*Figure 5*). The geocentric velocity was 33.8 ± 0.1 km/s. The mean orbit has been listed in *Table 1*.

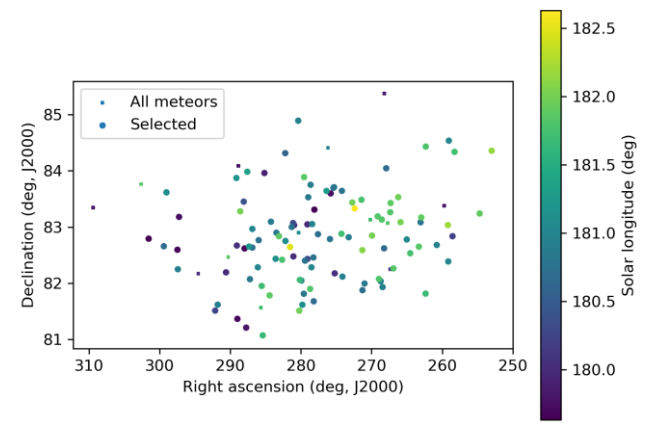


Figure 4 – The radiant distribution during the solar-longitude interval  $179.5^{\circ} - 182.5^{\circ}$  in equatorial coordinates.

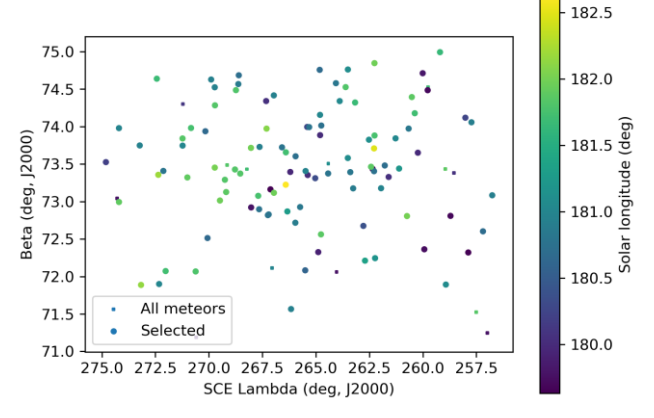


Figure 5 – The radiant distribution during the solar-longitude interval 179.5° – 182.5° in Sun centered geocentric ecliptic coordinates.

#### 3 Another search method

Another method has been applied to check this meteor shower activity in 2025. The starting point here can be any visually spotted concentration of radiant points or any other indication for the occurrence of similar orbits. The method has been described before (Roggemans et al., 2019). The main difference with the method applied in Section 2 is that three different discrimination criteria are combined in order to have only those orbits which fit different criteria. The Dcriteria that we use are these of Southworth and Hawkins (1963), Drummond (1981) and Jopek (1993) combined. Instead of using a single cutoff value for the threshold of the D-criteria these values are considered in different classes with different thresholds of similarity. Depending on the dispersion and the type of orbits, the most appropriate threshold of similarity is selected to locate the best fitting mean orbit as the result of an iterative procedure.

This method resulted in a mean orbit with 117 related orbits that fit within the similarity threshold with  $D_{SH} < 0.125$ ,  $D_D < 0.05$  and  $D_J < 0.125$ , recorded 2025 September 22 – 26. The radiant plot in geocentric Sun-centered ecliptic coordinates (*Figure 6*) shows a large dispersion due to the radiant drift with  $\Delta(\lambda - \lambda_O) = 1.8^{\circ}$ . There is also some

dispersion on the longitude of perihelion against inclination (*Figure 7*).

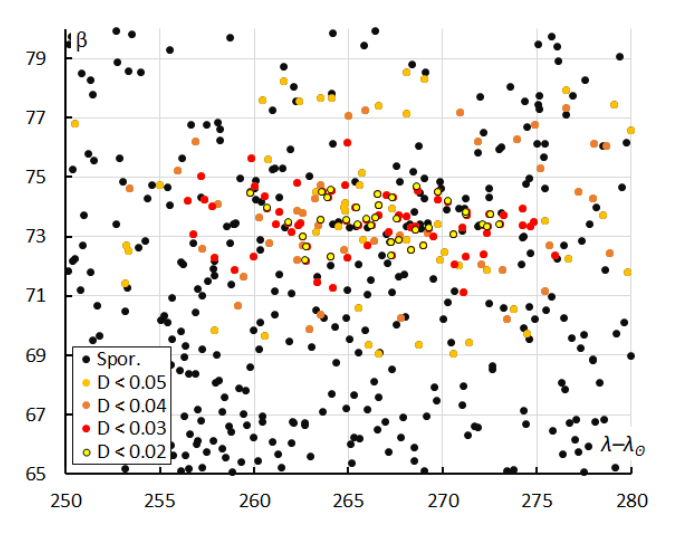


Figure 6 – The radiant distribution during the solar-longitude interval  $179^{\circ} - 183^{\circ}$  in Sun-centered geocentric ecliptic coordinates, color coded for four threshold values of the  $D_D$  orbit similarity criterion.

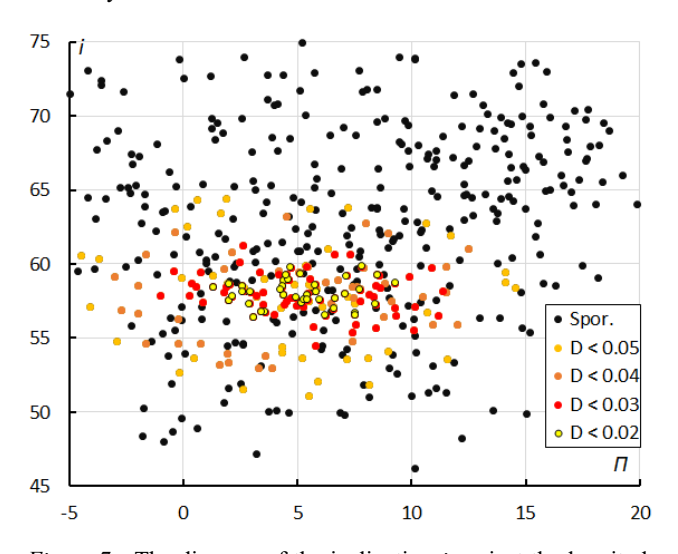


Figure 7 – The diagram of the inclination i against the longitude of perihelion  $\Pi$  color coded for four classes of D criterion threshold.

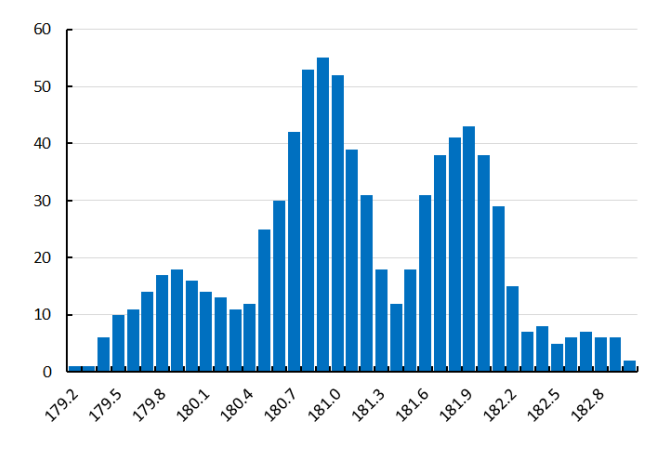


Figure 8 – Number of EPU-orbits recorded by GMN in 2025 counted in time bins of 0.2° in solar longitude.

Most EPU meteors were identified by both methods. The method based on the threshold values of the D-criteria found 18 meteors in 2025 which were not identified as EPU

meteors by the GMN method. Twenty-one of the 102 orbits used by the GMN method failed to fit the test within the similarity threshold with  $D_{SH} < 0.125$ ,  $D_D < 0.05$  and  $D_J < 0.125$ . Despite that both orbit samples include almost 20% different orbits identified as EPU meteors, the final meteor shower parameters are in very good agreement.

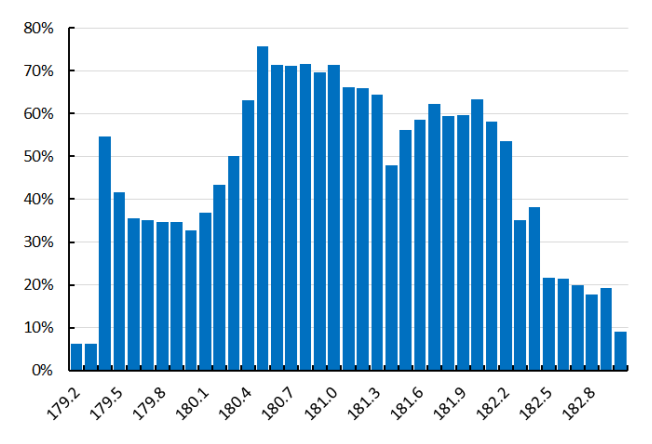


Figure 9 – Percentage of EPU-orbits relative to the total number of orbits recorded by GMN in 2025 at the Northern Hemisphere counted in time bins of 0.2° in solar longitude.

Looking at the raw counts of EPU meteors in bins of 0.2° in solar longitude (*Figure 8*), we see remarkable dips in the distribution which are due to an observational bias caused by the Pacific gap in the coverage by the network at the Northern Hemisphere. Most GMN stations at these longitudes are situated at the southern hemisphere in Australia and New Zealand where the EPU radiant remained far below the horizon. The total number of GMN cameras is much smaller in the Far East than in Europe where most of the EPU meteors were recorded. Europe had a large number of cameras with clear sky. In this case the number of EPU-meteors recorded says more about the detection capacity of the Global Meteor network than about the shower itself.

The capacity to detect weak activity from minor showers depends on the volume of atmosphere covered for which many camera-stations and clear sky are required. With about 60% of all GMN stations installed in Europe, this part of the network has a huge capacity to sample meteors from very weak sources. This explains why the EPU-activity has been mainly recorded by European cameras. If we look at the ratio EPU-meteors to non-EPU-meteors as a percentage within the sampling area at the sky in *Figure 9*, the peaks and dips from *Figure 8* disappear and it looks like the EPU meteor shower produced a plateau shaped activity profile that lasted almost 2.5 days.

The activity curve with the flux and equivalent ZHR also shows no real peak, but a rather constant level of activity during more than two days (*Figure 10*). The computed flux of the epsilon-Ursae Minorids in 2025 corresponds to a modest equivalent ZHR of 0.5. Despite such a low value, unexpected enhanced activity from weak activity minor showers is often labelled as an outburst. This can be misleading as a human visual observer will notice nothing of this activity.

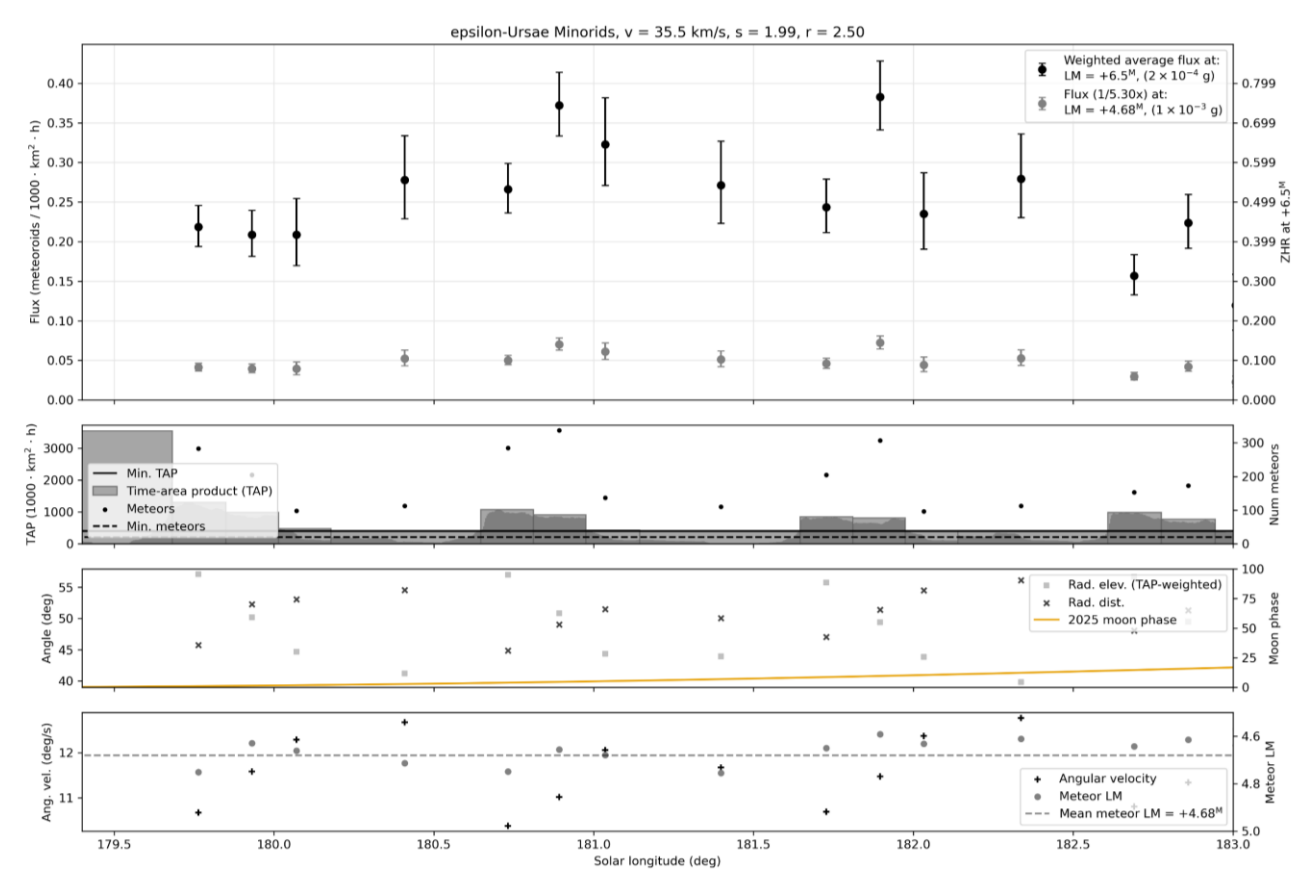


Figure 10 – Plot of the flux for the epsilon-Ursae Minorids in 2025.

# 4 Comparing past years of EPU activity

Looking up past GMN orbit data, seventeen orbits were found in 2019, thirteen of which during a short time span of 181.2° to 181.8° in solar longitude, confirming the discovery by SonotaCo network. Despite the vast expansion of the camera network of GMN, only three EPU-orbits were recorded in 2020, five in 2021, nine in 2022, sixteen in 2023 and twelve in 2024. The activity level after 2019 remained far below the threshold to attract any attention.

*Table 1* – The number of EPU orbits in the GMN orbit dataset with the time of maximum activity.

	•	
Year	EPU orbits	λοmax
2019	17	181.4
2020	3	_
2021	5	_
2022	9	180.6
2023	16	181.0
2024	12	180.7
2025	134	181.0

However, some confusion arose in 2024 when an unknown activity source was discovered by GMN, about 20° in longitude from the EPU-radiant. The GMN analysis concluded that the radiants were too far apart and therefore the detection was reported to the IAU-MDC as a new meteor shower, accepted and registered under the temporary name-designation: M2024-S1 (Vida and Šegon,

2024; Šegon et al., 2025). This new meteor shower had also been detected independently from GMN by Belarus and Ukrainian meteor cameras (Harachka et al., 2024).

Jenniskens et al. (2025) confirmed the activity reported by GMN but suggested that M2024-S1 was more likely another outburst of the epsilon-Ursae-Minorid shower which displayed better than usual activity in 2007, 2013 and 2019. Assuming a periodicity of about 5.7 years, 2024 would fit in this sequence and in that case, we could expect to see this shower again in 2025 with the dust from older ejecta accumulated in a 2:1 mean-motion resonance with Jupiter. That would predict a more regular pattern of outbursts with a 6-year period of resonance. The 2025 enhanced activity recorded by GMN confirms this outburst forecast.

GMN detected weak activity of the EPU-radiant in 2024, only 12 meteors during the shower activity period  $179.0^{\circ} < \lambda_{0} < 183.0^{\circ}$ . Figure 11 shows the radiant density plots of the northern part of the hemisphere for three nights in 2024 and three nights in 2025. The plots show a clear concentration at the position of the new M2024-S1 radiant, but barely any activity at the EPU-radiant in 2024 (top row). The bottom row in Figure 11 shows the activity in 2025 when both sources were active. In 2025 we see a very distinct activity at the EPU-radiant position which is completely missing in the 2024 plots. M2024-S1 displayed clear activity in 2025, although less pronounced than previous year. The M2024-S1 activity in 2025 has been documented in a separate follow-up report on this shower (Roggemans et al., 2025b).

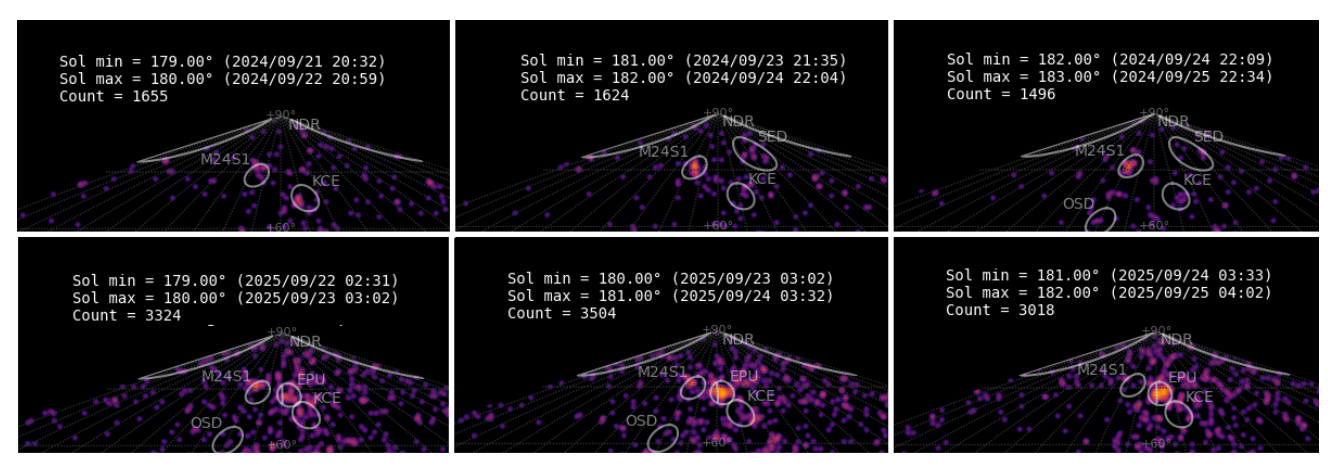


Figure 11 - Comparing the radiant density plots for M2024-S1 and EPU#1044 in 2024 (top) and 2025 (bottom).

# 5 The EPU orbit and parent body

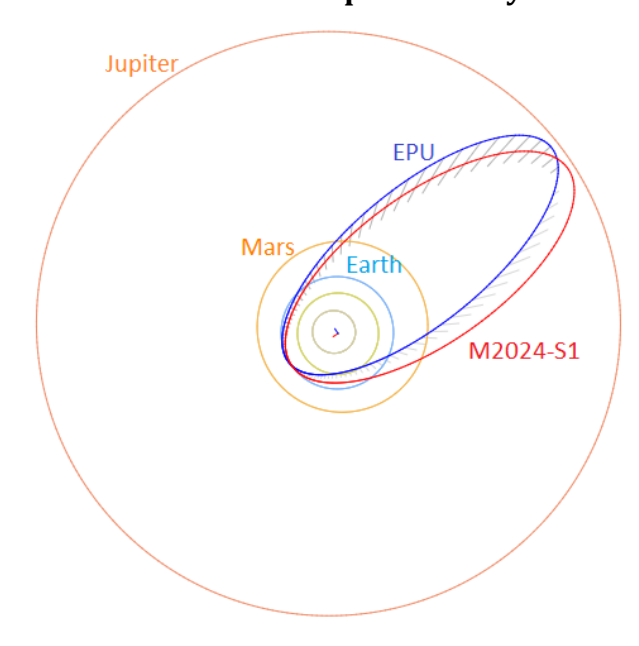


Figure 12 – Comparing the mean orbits for the epsilon-Ursae-Minorids (blue) for M2024-S1 (red), both projected in the ecliptic plane. (Plotted with the Orbit visualization app provided by Pető Zsolt).

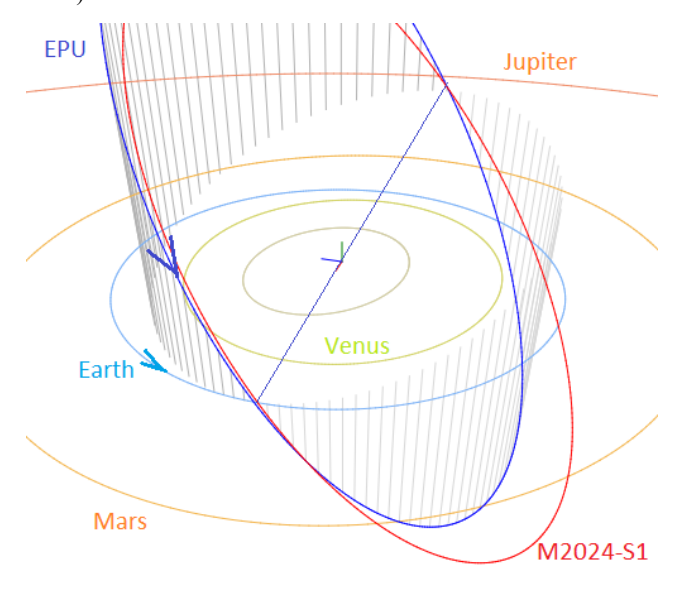


Figure 13 – Comparing the mean orbits for the epsilon-Ursae-Minorids (blue) for M2024-S1 (red), close-up at the inner Solar System. (Plotted with the Orbit visualization app provided by Pető Zsolt.

The Tisserand value relative to Jupiter indicates a Jupiter Family Comet type orbit. A top view is shown in *Figure 12*. With an inclination of 58° for the EPU orbit and 54° for the M2024-S1 orbit the aphelia remain far above the orbit of Jupiter.

Table 2 – Comparing the results for EPU#1044, derived by two different methods, the orbital parameters as derived by the GMN method for 2019 and 2025, the parameters for  $D_D < 0.05$  in 2025 and  $D_D < 0.05$  for 2019–2025, derived from the method described in Section 3.

in section 3.				
	GMN method 2019	GMN method 2025	$D_D < 0.05$ $2025$	$D_D < 0.05$ 2019– 2025
λ <sub>O</sub> (°)	181.4	181.0	181.0	181.0
$\lambda_{Ob}$ (°)	179.0	179.5	179.2	179.0
λ0e (°)	183.0	183.0	183.0	183.0
$a_g$ (°)	269.1	277.7	276.9	275.7
$\delta_g$ (°)	+82.3	+82.8	+82.7	+82.8
$\Delta \alpha_g$ (°)	-6.04	-6.68	-5.0	-4.2
$\Delta\delta_{g}\left(^{\circ}\right)$	+0.13	+0.11	-0.38	-0.2
$v_g$ (km/s)	34.0	33.8	33.7	33.8
$\lambda_g$ (°)	89.8	86.5	86.6	87.5
$\lambda_g - \lambda_{\mathcal{O}}$ (°)	268.4	265.5	265.9	266.5
$eta_g$ (°)	+74.0	+73.5	+73.7	+73.5
$H_b$ (km)	91.4	90.6	91.2	92.5
$H_e$ (km)	81.7	79.9	80.4	81.3
$H_p$ (km)	85.8	82.7	83.4	85.4
$Mag_A$	-0.19	-0.72	-0.64	-0.39
a (A.U.)	3.18	2.88	2.84	2.82
q (A.U.)	1.0018	1.0012	1.0006	1.0019
e	0.685	0.652	0.648	0.644
i (°)	58.2	58.2	57.6	58.0
ω (°)	182.4	184.6	184.3	183.9
$\mathcal{Q}\left(^{\circ}\right)$	181.6	181.1	181.1	181.2
$\Pi$ (°)	4.0	5.7	5.5	5.1
$T_j$	2.24	2.40	2.44	2.44
N	17	102	117	176

Looking in close up at the nodes we see that both showers encounter the Earth almost simultaneously at their descending nodes (*Figure 13*). The positions of the ascending nodes are relatively close to the orbit of Jupiter and the dust will be strongly affected by gravitational perturbation when the planet passes near this point. The six-year periodicity as well as the likely dynamic connection between both showers may be caused by these gravitational effects.

A remarkable characteristic of the EPU-meteors is that these penetrate deep into the atmosphere with a median beginning height at  $90.6 \pm 5.0$  km and ending height at  $79.9 \pm 4.9$  km. Most EPU meteors had negative magnitudes with a median peak absolute magnitude of -0.7. This low ablation height was noticed before by Shiba (2022) who mentioned "Luminous height is especially low". This means these meteoroids aren't fragile like expected for cometary material but rather solid particles comparable to the Geminids (GEM#4) where the perihelion distance of q = 0.14 AU close to the Sun is the explanation for the dense composition of the particles. The EPU-orbits gets nowhere much closer to the Sun than the comfort zone at about 1 AU and thus solar radiation cannot explain the solid nature of these meteoroids.

For completeness we mention the mean orbits obtained by GMN for 2019, 2023 and 2024 obtained with the D-criteria method. The number of meteors is small and thus the parameters are less certain due to small-number statistics. Note that the radiant position both in R.A. as in Suncentered ecliptic longitude for all the years of GMN data is about 10 degrees east from the radiant positions published for 2019 in the IAU-MDC working list of meteor showers<sup>10</sup>. The radiant density map in Sun-centered ecliptic coordinates for GMN on 2019, September 24–25

(Figure 14) clearly confirms the position of the radiant listed in Tables 2 and 3.

Table 3 – The results for EPU#1044, using D-criteria thresholds for  $D_{SH} < 0.125$ ,  $D_D < 0.05$  and  $D_J < 0.125$ , derived from the method described in Section 3.

$λ_O$ (°)         181.4         181.0         180.7 $λ_O$ (°)         180.3         179.2         179.0 $λ_O$ (°)         181.8         182.4         182.2 $α_g$ (°)         267.5         276.0         261.2 $δ_g$ (°)         +82.7         +80.8         +84.1 $H_b$ (km)         91.1         99.6         91.8 $H_e$ (km)         81.4         86.7         82.4 $H_P$ (km)         85.7         91.3         86.5 $Mag_A$ -0.33         +0.16         -0.40 $v_g$ (km/s)         34.0         33.1         34.4 $λ_g$ (°)         91.1         87.3         92.6 $λ_g$ - $λ_O$ (°)         269.6         265.8         271.3 $β_g$ (°)         +73.5         +75.0         +72.3 $a$ (A.U.)         2.93         2.84         2.80 $q$ (A.U.)         1.002         0.998         1.001 $e$ 0.658         0.648         0.642 $i$ (°)         58.1         56.6         60.0 $ω$ (°)         182.8         184.1         181.0				
$\lambda ob$ (°) $180.3$ $179.2$ $179.0$ $\lambda oe$ (°) $181.8$ $182.4$ $182.2$ $a_g$ (°) $267.5$ $276.0$ $261.2$ $b_g$ (°) $+82.7$ $+80.8$ $+84.1$ $H_b$ (km) $91.1$ $99.6$ $91.8$ $H_e$ (km) $81.4$ $86.7$ $82.4$ $H_p$ (km) $85.7$ $91.3$ $86.5$ $Mag_A$ $-0.33$ $+0.16$ $-0.40$ $v_g$ (km/s) $34.0$ $33.1$ $34.4$ $\lambda_g$ (°) $91.1$ $87.3$ $92.6$ $\lambda_g - \lambda_O$ (°) $269.6$ $265.8$ $271.3$ $\beta_g$ (°) $+73.5$ $+75.0$ $+72.3$ $a$ (A.U.) $2.93$ $2.84$ $2.80$ $q$ (A.U.) $1.002$ $0.998$ $1.001$ $e$ $0.658$ $0.648$ $0.642$ $i$ (°) $58.1$ $56.6$ $60.0$ $\omega$ (°) $182.8$ $184.1$ $181.0$ $\omega$ (°) $182.8$ $184.1$ $180.8$ $180.7$ <		GMN 2019	GMN 2023	GMN2024
$\lambda_{Oe}$ (°) 181.8 182.4 182.2 $\alpha_g$ (°) 267.5 276.0 261.2 $\delta_g$ (°) +82.7 +80.8 +84.1 $H_b$ (km) 91.1 99.6 91.8 $H_e$ (km) 81.4 86.7 82.4 $H_p$ (km) 85.7 91.3 86.5 $Mag_A$ -0.33 +0.16 -0.40 $\nu_g$ (km/s) 34.0 33.1 34.4 $\lambda_g$ (°) 91.1 87.3 92.6 $\lambda_g$ - $\lambda_O$ (°) 269.6 265.8 271.3 $\beta_g$ (°) +73.5 +75.0 +72.3 $\alpha$ (A.U.) 2.93 2.84 2.80 $\alpha$ (A.U.) 1.002 0.998 1.001 $\alpha$ 0.658 0.648 0.642 $\alpha$ (°) 182.8 184.1 181.0 $\alpha$ (°) 182.8 184.1 181.0 $\alpha$ (°) 181.4 180.8 180.7 $\alpha$ (°) 4.2 5.0 1.8	λο (°)	181.4	181.0	180.7
$\alpha_g$ (°) $267.5$ $276.0$ $261.2$ $\delta_g$ (°) $+82.7$ $+80.8$ $+84.1$ $H_b$ (km) $91.1$ $99.6$ $91.8$ $H_e$ (km) $81.4$ $86.7$ $82.4$ $H_p$ (km) $85.7$ $91.3$ $86.5$ $Mag_A$ $-0.33$ $+0.16$ $-0.40$ $v_g$ (km/s) $34.0$ $33.1$ $34.4$ $\lambda_g$ (°) $91.1$ $87.3$ $92.6$ $\lambda_g - \lambda_O$ (°) $269.6$ $265.8$ $271.3$ $\beta_g$ (°) $+73.5$ $+75.0$ $+72.3$ $a$ (A.U.) $2.93$ $2.84$ $2.80$ $q$ (A.U.) $1.002$ $0.998$ $1.001$ $e$ $0.658$ $0.648$ $0.642$ $i$ (°) $58.1$ $56.6$ $60.0$ $\omega$ (°) $182.8$ $184.1$ $181.0$ $\omega$ (°) $181.4$ $180.8$ $180.7$ $\Pi$ (°) $4.2$ $5.0$ $1.8$ $T_j$ $2.37$ $2.45$ $2.42$	λο <sub>b</sub> (°)	180.3	179.2	179.0
$\delta_g$ (°) +82.7 +80.8 +84.1 $H_b$ (km) 91.1 99.6 91.8 $H_e$ (km) 81.4 86.7 82.4 $H_p$ (km) 85.7 91.3 86.5 $Mag_A$ -0.33 +0.16 -0.40 $v_g$ (km/s) 34.0 33.1 34.4 $\lambda_g$ (°) 91.1 87.3 92.6 $\lambda_g$ - $\lambda_o$ (°) 269.6 265.8 271.3 $\beta_g$ (°) +73.5 +75.0 +72.3 a (A.U.) 2.93 2.84 2.80 q (A.U.) 1.002 0.998 1.001 e 0.658 0.648 0.642 i (°) 58.1 56.6 60.0 $\omega$ (°) 182.8 184.1 181.0 $\Omega$ (°) 181.4 180.8 180.7 $\Pi$ (°) 4.2 5.0 1.8 $T_j$ 2.37 2.45 2.42	$\lambda_{\mathcal{O}e}$ (°)	181.8	182.4	182.2
$H_b$ (km)       91.1       99.6       91.8 $H_e$ (km)       81.4       86.7       82.4 $H_p$ (km)       85.7       91.3       86.5 $Mag_A$ $-0.33$ $+0.16$ $-0.40$ $v_g$ (km/s)       34.0       33.1       34.4 $\lambda_g$ (°)       91.1       87.3       92.6 $\lambda_g - \lambda_O$ (°)       269.6       265.8       271.3 $\beta_g$ (°) $+73.5$ $+75.0$ $+72.3$ $a$ (A.U.)       2.93       2.84       2.80 $q$ (A.U.)       1.002       0.998       1.001 $e$ 0.658       0.648       0.642 $i$ (°)       58.1       56.6       60.0 $\omega$ (°)       182.8       184.1       181.0 $\Omega$ (°)       181.4       180.8       180.7 $\Pi$ (°)       4.2       5.0       1.8 $T_j$ 2.37       2.45       2.42	$a_g$ (°)	267.5	276.0	261.2
$H_e$ (km) 81.4 86.7 82.4 $H_p$ (km) 85.7 91.3 86.5 $Mag_A$ -0.33 +0.16 -0.40 $v_g$ (km/s) 34.0 33.1 34.4 $\lambda_g$ (°) 91.1 87.3 92.6 $\lambda_g$ - $\lambda_\theta$ (°) 269.6 265.8 271.3 $\beta_g$ (°) +73.5 +75.0 +72.3 $a$ (A.U.) 2.93 2.84 2.80 $q$ (A.U.) 1.002 0.998 1.001 $e$ 0.658 0.648 0.642 $i$ (°) 58.1 56.6 60.0 $\omega$ (°) 182.8 184.1 181.0 $\Omega$ (°) 181.4 180.8 180.7 $\Pi$ (°) 4.2 5.0 1.8 $T_j$ 2.37 2.45 2.42	$\delta_g$ (°)	+82.7	+80.8	+84.1
$H_p$ (km)       85.7       91.3       86.5 $Mag_A$ $-0.33$ $+0.16$ $-0.40$ $v_g$ (km/s)       34.0       33.1       34.4 $\lambda_g$ (°)       91.1       87.3       92.6 $\lambda_g - \lambda_O$ (°)       269.6       265.8       271.3 $\beta_g$ (°) $+73.5$ $+75.0$ $+72.3$ $a$ (A.U.)       2.93       2.84       2.80 $q$ (A.U.)       1.002       0.998       1.001 $e$ 0.658       0.648       0.642 $i$ (°)       58.1       56.6       60.0 $\omega$ (°)       182.8       184.1       181.0 $\Omega$ (°)       181.4       180.8       180.7 $\Pi$ (°)       4.2       5.0       1.8 $T_j$ 2.37       2.45       2.42	$H_b$ (km)	91.1	99.6	91.8
$Mag_A$ $-0.33$ $+0.16$ $-0.40$ $v_g$ (km/s) 34.0 33.1 34.4 $\lambda_g$ (°) 91.1 87.3 92.6 $\lambda_g - \lambda_\theta$ (°) 269.6 265.8 271.3 $\beta_g$ (°) +73.5 +75.0 +72.3 $a$ (A.U.) 2.93 2.84 2.80 $q$ (A.U.) 1.002 0.998 1.001 $e$ 0.658 0.648 0.642 $i$ (°) 58.1 56.6 60.0 $\omega$ (°) 182.8 184.1 181.0 $\Omega$ (°) 181.4 180.8 180.7 $\Pi$ (°) 4.2 5.0 1.8 $T_j$ 2.37 2.45 2.42	$H_e$ (km)	81.4	86.7	82.4
$v_g$ (km/s)       34.0       33.1       34.4 $\lambda_g$ (°)       91.1       87.3       92.6 $\lambda_g - \lambda_{\theta}$ (°)       269.6       265.8       271.3 $\beta_g$ (°)       +73.5       +75.0       +72.3 $a$ (A.U.)       2.93       2.84       2.80 $q$ (A.U.)       1.002       0.998       1.001 $e$ 0.658       0.648       0.642 $i$ (°)       58.1       56.6       60.0 $\omega$ (°)       182.8       184.1       181.0 $\Omega$ (°)       181.4       180.8       180.7 $\Pi$ (°)       4.2       5.0       1.8 $T_j$ 2.37       2.45       2.42	$H_p$ (km)	85.7	91.3	86.5
$\lambda_g$ (°) 91.1 87.3 92.6 $\lambda_g - \lambda_\Theta$ (°) 269.6 265.8 271.3 $\beta_g$ (°) +73.5 +75.0 +72.3 a (A.U.) 2.93 2.84 2.80 q (A.U.) 1.002 0.998 1.001 e 0.658 0.648 0.642 i (°) 58.1 56.6 60.0 $\omega$ (°) 182.8 184.1 181.0 $\Omega$ (°) 181.4 180.8 180.7 $\Pi$ (°) 4.2 5.0 1.8 $T_j$ 2.37 2.45 2.42	$Mag_A$	-0.33	+0.16	-0.40
$\lambda_g - \lambda_{\Theta}$ (°) 269.6 265.8 271.3 $\beta_g$ (°) +73.5 +75.0 +72.3 a (A.U.) 2.93 2.84 2.80 q (A.U.) 1.002 0.998 1.001 e 0.658 0.648 0.642 i (°) 58.1 56.6 60.0 $\omega$ (°) 182.8 184.1 181.0 $\Omega$ (°) 181.4 180.8 180.7 $\Pi$ (°) 4.2 5.0 1.8 $T_j$ 2.37 2.45 2.42	$v_g$ (km/s)	34.0	33.1	34.4
$ \beta_g(^{\circ}) $ +73.5 +75.0 +72.3 $a$ (A.U.) 2.93 2.84 2.80 $q$ (A.U.) 1.002 0.998 1.001 $e$ 0.658 0.648 0.642 $i$ ( $^{\circ}$ ) 58.1 56.6 60.0 $\omega$ ( $^{\circ}$ ) 182.8 184.1 181.0 $\Omega$ ( $^{\circ}$ ) 181.4 180.8 180.7 $\Pi$ ( $^{\circ}$ ) 4.2 5.0 1.8 $T_j$ 2.37 2.45 2.42	$\lambda_g$ (°)	91.1	87.3	92.6
$a$ (A.U.) $2.93$ $2.84$ $2.80$ $q$ (A.U.) $1.002$ $0.998$ $1.001$ $e$ $0.658$ $0.648$ $0.642$ $i$ (°) $58.1$ $56.6$ $60.0$ $\omega$ (°) $182.8$ $184.1$ $181.0$ $\Omega$ (°) $181.4$ $180.8$ $180.7$ $\Pi$ (°) $4.2$ $5.0$ $1.8$ $T_j$ $2.37$ $2.45$ $2.42$	$\lambda_g - \lambda_O$ (°)	269.6	265.8	271.3
$q$ (A.U.)       1.002       0.998       1.001 $e$ 0.658       0.648       0.642 $i$ (°)       58.1       56.6       60.0 $\omega$ (°)       182.8       184.1       181.0 $\Omega$ (°)       181.4       180.8       180.7 $\Pi$ (°)       4.2       5.0       1.8 $T_j$ 2.37       2.45       2.42	$eta_g$ (°)	+73.5	+75.0	+72.3
e       0.658       0.648       0.642 $i$ (°)       58.1       56.6       60.0 $\omega$ (°)       182.8       184.1       181.0 $\Omega$ (°)       181.4       180.8       180.7 $\Pi$ (°)       4.2       5.0       1.8 $T_j$ 2.37       2.45       2.42	a (A.U.)	2.93	2.84	2.80
$i$ (°) $58.1$ $56.6$ $60.0$ $\omega$ (°) $182.8$ $184.1$ $181.0$ $\Omega$ (°) $181.4$ $180.8$ $180.7$ $\Pi$ (°) $4.2$ $5.0$ $1.8$ $T_j$ $2.37$ $2.45$ $2.42$	q (A.U.)	1.002	0.998	1.001
$\omega$ (°) 182.8 184.1 181.0 $\Omega$ (°) 181.4 180.8 180.7 $\Pi$ (°) 4.2 5.0 1.8 $T_j$ 2.37 2.45 2.42	e	0.658	0.648	0.642
$\Omega$ (°)       181.4       180.8       180.7 $\Pi$ (°)       4.2       5.0       1.8 $T_j$ 2.37       2.45       2.42	i (°)	58.1	56.6	60.0
$\Pi$ (°) 4.2 5.0 1.8 $T_j$ 2.37 2.45 2.42	ω (°)	182.8	184.1	181.0
T <sub>j</sub> 2.37 2.45 2.42	$\mathcal{Q}\left(^{\circ}\right)$	181.4	180.8	180.7
	$\Pi$ (°)	4.2	5.0	1.8
N 14 16 12	$T_j$	2.37	2.45	2.42
	N	14	16	12

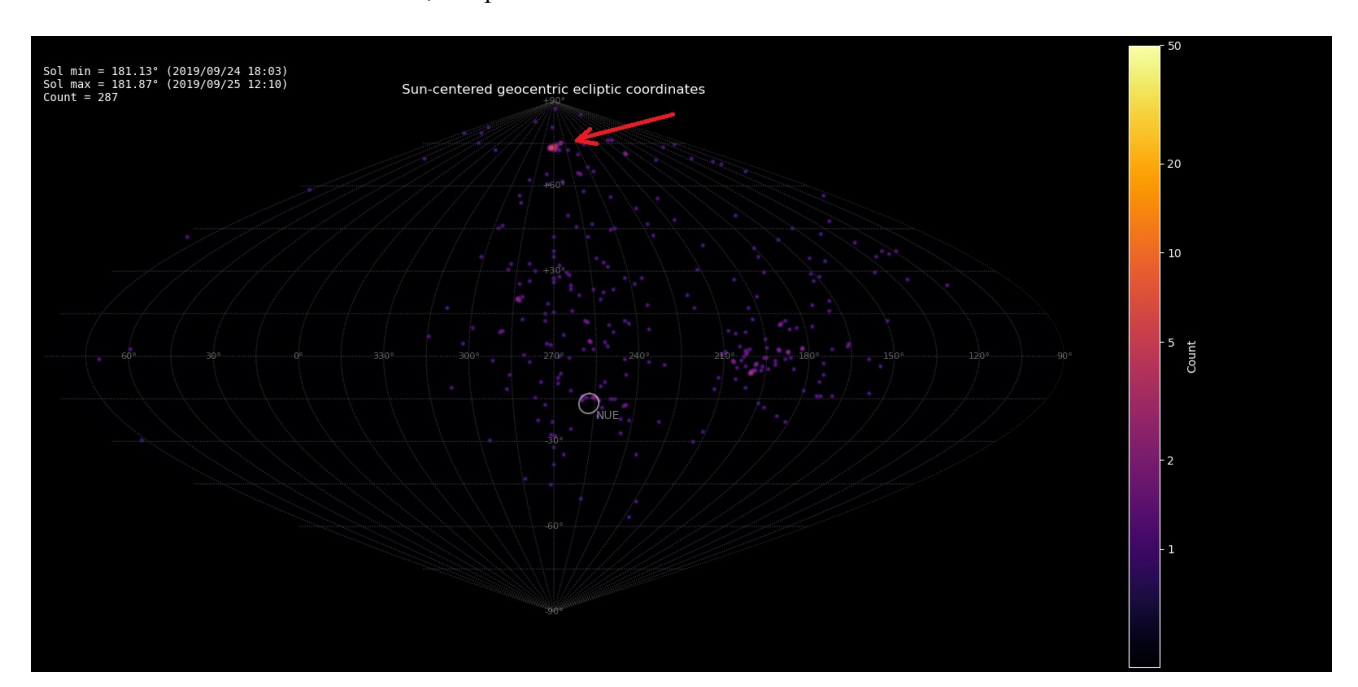


Figure 14 – Heat map with 287 radiants obtained by the Global Meteor network on September 24 – 25, 2019. A distinct concentration is visible in Sun-centered geocentric ecliptic coordinates at the position known as the radiant of the epsilon-Ursae Minorids (EPU#1044).

<sup>&</sup>lt;sup>10</sup> https://www.ta3.sk/IAUC22DB/MDC2022/Roje/pojedynczy\_obiekt.php?lporz=01987&kodstrumienia=01044

Table 4 – Top ten matches of a search for possible parent bodies with  $D_D < 0.17$ .

Name	$D_D$
2009 SG18	0.072
2021 HK12	0.088
2024 RK16	0.127
2020 UP3	0.134
(163732) 2003 KP2	0.149
2010 QA5	0.154
2021 VB4	0.156
2019 QF6	0.163
21P/Giacobini-Zinner	0.165
2014 XX7	0.167

Table 4 list ten possible parent bodies with two most likely parent bodies, 2009 SG18 and 2021 HK12. The modeling for 2009SG18 has been done in the past for a possible association with the kappa-Cepheids (KCE#751) (Šegon et al., 2017). However, the model produced no intersections with the Earth orbit for 2025 thus this is not the parent body.

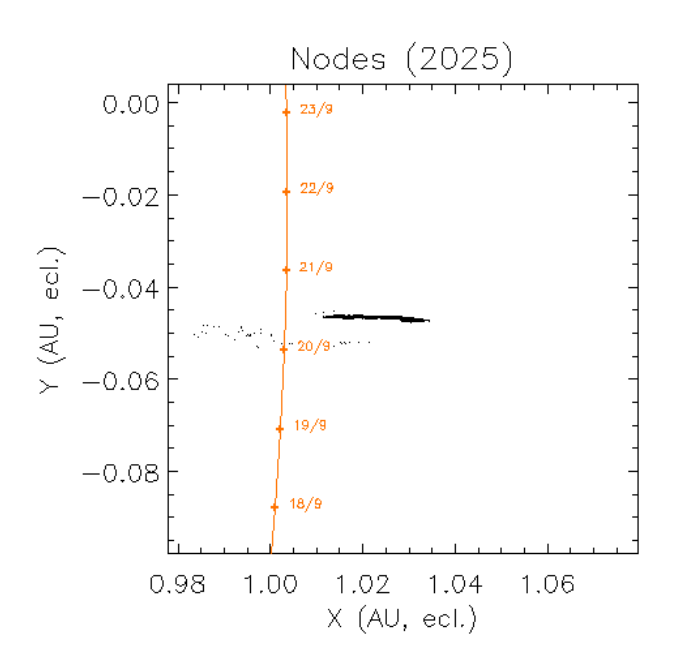


Figure 14 – Location of the nodes of the particles in 2025 released by 2009 SG18 over several centuries. (Model by J. Vaubaillon).

The next candidate, 2021 HK12, has as orbital parameters:

- q = 1.036 AU,
- e = 0.685,
- $i = 47.0^{\circ}$ ,
- $\omega = 168.8^{\circ}$ .
- $\Omega = 187.1^{\circ}$ ,
- Tj = 2.37.

This object with a Jupiter Family Comet type orbit could be related to both the epsilon-Ursae-Minorids and the new source M2024-S1.

#### 6 Conclusion

Significant enhanced activity of the epsilon-Ursae-Minorids has been observed in 2025 by the Global Meteor Network during 23-25 September. This activity confirms the prediction of a possible outburst in 2025, based on a 6-year periodicity by Jenniskens et al. (2025). A peculiar characteristic of this shower is the remarkable low ablation height of the meteors which indicate that the meteoroids consist of solid material. The simultaneous reoccurrence of the new shower discovered by GMN in 2024 and registered as M2024-S1 in the IAU-MDC Working List of Meteor Showers confirms that both activity sources should be regarded as separate meteor showers because of the differences in radiant position and orbital parameters. Both meteor showers are very likely dynamically related to each other. The asteroid 2021 HK12 remains a plausible candidate as parent body.

# Acknowledgment

This report is based on the data of the Global Meteor Network (Vida et al., 2020a; 2020b; 2021) which is released under the CC BY 4.0 license<sup>11</sup>. We thank all 825 participants in the Global Meteor Network project for their contribution and perseverance. A list with the names of the volunteers who contribute to GMN has been published in the 2024 annual report (Roggemans et al., 2025a).

#### References

Drummond J. D. (1981). "A test of comet and meteor shower associations". *Icarus*, **45**, 545–553.

Harachka Y., Mikulich A., Morozov K., Angelsky A. (2024). "Possible new meteor shower in Ursa Minor". *eMetN Meteor Journal*, **9**, 395–396.

Jenniskens P., Johannink C., Moskovitz N., Howell A. (2025). "Short note on what appears to have been a 2024 outburst of epsilon-Ursae-Minorids (IAU#1044)". *eMetN Meteor Journal*, **10**, 20–21.

Jopek T. J. (1993). "Remarks on the meteor orbital similarity D-criterion". *Icarus*, **106**, 603–607.

Jopek T. J., Rudawska R. and Pretka-Ziomek H. (2006). "Calculation of the mean orbit of a meteoroid stream". Monthly Notices of the Royal Astronomical Society, 371, 1367–1372.

Moorhead A. V., Clements T. D., Vida D. (2020). "Realistic gravitational focusing of meteoroid streams". Monthly Notices of the Royal Astronomical Society, 494, 2982–2994.

<sup>11</sup> https://creativecommons.org/licenses/by/4.0/

Roggemans P., Johannink C. and Campbell-Burns P. (2019). "October Ursae Majorids (OCU#333)". eMetN Meteor Journal, 4, 55–64.

- Roggemans P., Campbell-Burns P., Kalina M., McIntyre M., Scott J. M., Šegon D., Vida D. (2025a). "Global Meteor Network report 2024". *eMetN Meteor Journal*, **10**, 67–101.
- Roggemans P., Vida D., Šegon D. (2025b). "M2024-S1 activity confirmed in 2025". *eMetN Meteor Journal*, **10**, 353–359.
- Sato H., Jenniskens P., Howell A. (2020). "Epsilon Ursae Minorid Meteor Shower 2019". *CBET* **4860**.
- Šegon D., Vaubaillon J., Gural P.S., Vida D., Željko A., Korlevic K. and Skokic I. (2017). "Dynamical modeling validation of parent bodies associated with newly discovered CMN meteor showers". *Astronomy & Astrophysics*, **598**, A15. 13 pages.
- Šegon D., Vida D., Roggemans P. (2025). "New meteor shower in Ursa Minor 23–24 September 2024". *eMetN Meteor Journal*, **10**, 12–19.
- Shiba Y. (2022). "Jupiter Family Meteor Showers by SonotaCo Network Observations". WGN, Journal of the International Meteor Organization, 50, 38–61.

- Southworth R. B. and Hawkins G. S. (1963). "Statistics of meteor streams". *Smithsonian Contributions to Astrophysics*, 7, 261–285.
- Vida D., Gural P., Brown P., Campbell-Brown M., Wiegert P. (2020a). "Estimating trajectories of meteors: an observational Monte Carlo approach I. Theory". Monthly Notices of the Royal Astronomical Society, 491, 2688–2705.
- Vida D., Gural P., Brown P., Campbell-Brown M., Wiegert P. (2020b). "Estimating trajectories of meteors: an observational Monte Carlo approach - II. Results". *Monthly Notices of the Royal Astronomical Society*, 491, 3996–4011.
- Vida D., Šegon D., Gural P. S., Brown P. G., McIntyre M. J. M., Dijkema T. J., Pavletić L., Kukić P., Mazur M. J., Eschman P., Roggemans P., Merlak A., Zubrović D. (2021). "The Global Meteor Network Methodology and first results". *Monthly Notices of the Royal Astronomical Society*, **506**, 5046–5074.
- Vida D., Šegon D. (2024). New meteor shower M2024-S1 in Ursa minor. CBET 5452. D. W. E. Green (ed.), 1 pp.

# New meteor shower in Hydrus (M2025-S2)

Damir Šegon<sup>1</sup>, Denis Vida<sup>2,3</sup>, Paul Roggemans<sup>4</sup>, James M. Scott<sup>5</sup>, Jeff Wood<sup>6</sup>

<sup>1</sup> Astronomical Society Istra Pula, Park Monte Zaro 2, 52100 Pula, Croatia

denis.vida@gmail.com

<sup>4</sup> Pijnboomstraat 25, 2800 Mechelen, Belgium

<sup>5</sup> Department of Geoscience, Aarhus University, Høegh-Guldbergs Gade 2. DK-8000 Aarhus C, Denmark jscott@geo.au.dk

<sup>6</sup> PO Box 162, Willetton, Western Australia 6955, Australia

A new meteor shower on a Jupiter Family Comet type orbit ( $T_J = 2.53$ ) has been detected during 2025 September 9 – October 1, by the Global Meteor Network. 377 meteors belonging to the new shower were observed between  $166^{\circ} < \lambda_{O} < 188^{\circ}$  from a radiant at R.A. = 43° and Decl.= -66°, with a geocentric velocity of 22.1 km/s. Maximum activity occurred at  $\lambda_{O} = 181.3^{\circ}$  (September 24). The new meteor shower has been listed in the IAU MDC Working List of Meteor Showers under the temporary name-designation: M2025-S2.

#### 1 Introduction

The GMN radiant maps for September 20-21, 2025, showed a clear concentration of related radiants in the constellation of Hydrus. Initially 109 meteors of this meteor shower were observed by the Global Meteor Network<sup>12</sup> low-light video cameras during the period 2025 September 12-21. The shower was independently observed by cameras in five countries (Australia, Brazil, Chile, New Zealand and South Africa).

The shower had a median geocentric radiant with coordinates R.A. =  $31.6^{\circ}$ , Decl. = -66.9 (equinox J2000.0) at its discovery. The radiant drift in R.A. was +1.64° on the sky per degree of solar longitude and +0.29° in Dec., both referenced to  $\lambda_{O}=175.3^{\circ}$ . The median Sun-centered ecliptic coordinates were  $\lambda-\lambda_{O}=156.5^{\circ}$ ,  $\beta=-67.8^{\circ}$ . The geocentric velocity was  $20.6\pm0.1$  km/s. The new meteor shower was reported to the IAU-MDC and registered under the temporary identification  $2025-S2^{13}$ .

The new shower didn't fade in activity, but grew stronger and lasted for more than a week after being reported to the IAU-MDC. The radiant showed a remarkable strong drift in Sun-center ecliptic coordinates. A new analysis was required to cover the entire activity period.

#### 2 The GMN shower association method

The GMN shower association criteria assumes that meteors within 1° in solar longitude, within 4.8° in radiant in this case, and within 10% in geocentric velocity of a shower reference location are members of that shower. Further details about the shower association are explained in

Moorhead et al. (2020). These are a rather strict criteria since meteor showers often have a larger dispersion in radiant position and velocity. Using these meteor shower selection criteria, 377 orbits have been associated with the new shower in the GMN meteor orbit database in a second analysis.

The activity period lasted from September 9 to October 1 starting with the radiant in the constellation Tucana moving through Hydrus and Horologium and ending in Reticulum. When the new shower was first reported its radiant was in Hydrus, but the maximum activity occurred later at  $\lambda_O = 181.3^{\circ}$  when the radiant was located in Reticulum. The folklore of naming a meteor shower to a star near its radiant will be like a lottery in this case.

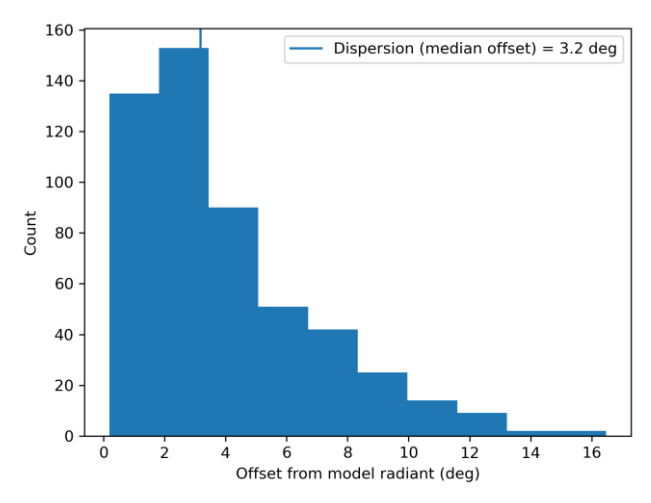


Figure 1 – Dispersion median offset on the radiant position.

<sup>&</sup>lt;sup>2</sup> Department of Physics and Astronomy, University of Western Ontario, Richmond Street, London, N6A 3K7, Ontario, Canada

<sup>&</sup>lt;sup>3</sup> Institute for Earth and Space Exploration, University of Western Ontario, Perth Drive, London, N6A 5B8, Ontario, Canada

<sup>&</sup>lt;sup>12</sup> https://globalmeteornetwork.org/data/

<sup>&</sup>lt;sup>13</sup> https://www.ta3.sk/IAUC22DB/MDC2022/Roje/pojedynczy\_obiekt.php?lporz=02188&kodstrumienia=01239

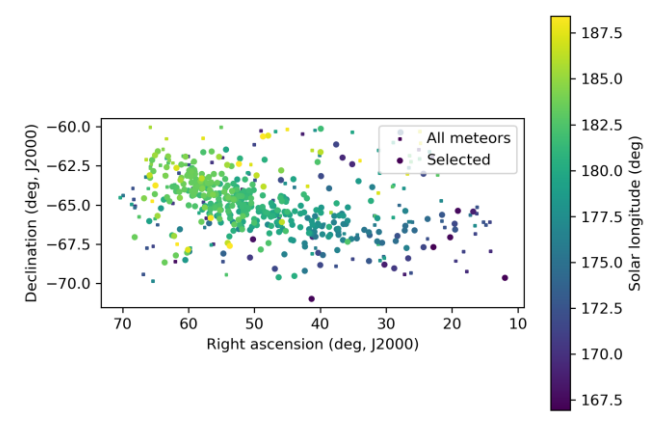


Figure 2 – The radiant distribution during the solar-longitude interval  $167^{\circ} - 188^{\circ}$  in equatorial coordinates.

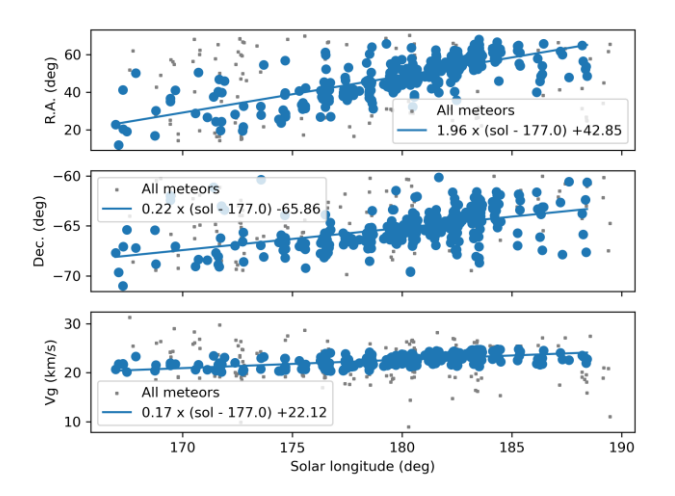


Figure 3 – The radiant drift.

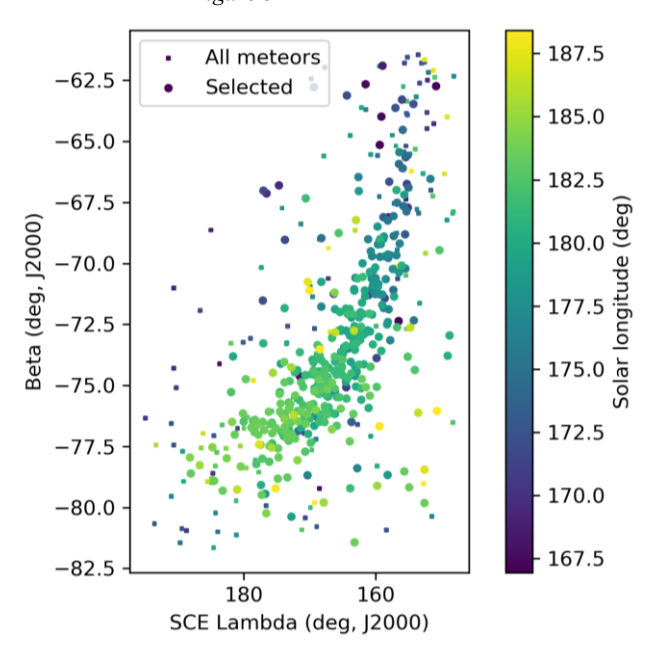


Figure 4 – The radiant distribution during the solar-longitude interval  $167^{\circ} - 188^{\circ}$  in Sun centered geocentric ecliptic coordinates.

The new GMN analysis resulted in a median geocentric radiant with coordinates R.A. = 42.9°, Decl. = -65.9 (equinox J2000.0) (*Figure 2*). The radiant drift in R.A. was +1.96° on the sky per degree of solar longitude and +0.22° in Dec., both referenced to  $\lambda_{\Theta} = 177.0^{\circ}$  (*Figure 3*). The median Sun-centered ecliptic coordinates were  $\lambda - \lambda_{\Theta} = 163.6^{\circ}$ ,  $\beta = -71.5^{\circ}$ . The geocentric velocity was

22.1  $\pm$  0.1 km/s. The Sun-centered ecliptic coordinates show a remarkably strong radiant drift with  $\Delta(\lambda - \lambda_O) = 0.84^{\circ}$ ,  $\Delta\beta = -0.65^{\circ}$  forming a long extended radiant in the shape of a sickle (*Figure 4*).

### 3 Another search method

Meteor shower identification strongly depends on the methodology used to select candidate shower members. The sporadic background is everywhere present at the sky which risks to contaminate selections of shower candidates. Using a radiant location is a straightforward method to classify shower meteors. In order to double check GMN meteor shower detections, another method, based on orbit similarity criteria is used. This approach serves to make sure that no spurious radiant concentrations are mistaken as new meteor showers.

A reference orbit is required to start an iterative procedure to approach a mean orbit, which is the most representative orbit for the meteor shower as a whole, removing outliers and sporadic orbits. This method has been described before (Roggemans et al., 2019). Three different discrimination criteria are combined in order to have only those orbits which fit the different criteria thresholds. The D-criteria that we use are these of Southworth and Hawkins (1963), Drummond (1981) and Jopek (1993) combined. The values are considered in different classes with different thresholds of similarity:

- Medium Low:  $D_{SH} < 0.125 \& D_D < 0.05 \& D_J < 0.125$ ;
- Medium high:  $D_{SH} < 0.1 \& D_D < 0.04 \& D_J < 0.1$ ;
- High:  $D_{SH} < 0.075 \& D_D < 0.03 \& D_J < 0.075$ .
- Very high:  $D_{SH} < 0.05 \& D_D < 0.02 \& D_J < 0.05$ .

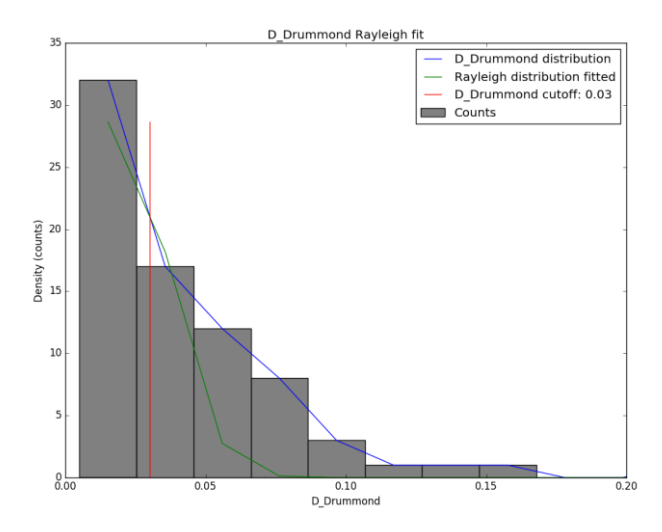


Figure 5 – Rayleigh distribution fit and Drummond  $D_D$  criterion cutoff.

The Rayleigh distribution fit pointed at a  $D_D$  value of 0.03 as the orbital similarity threshold value cutoff (*Figure 5*). The radiant drift in Sun-centered ecliptic coordinates due to changes in orbital elements during Earth's transit, makes it impossible to describe this meteoroid stream with a single reference orbit. The D-criteria values are no more than an indication for the degree of similarity between an orbit and

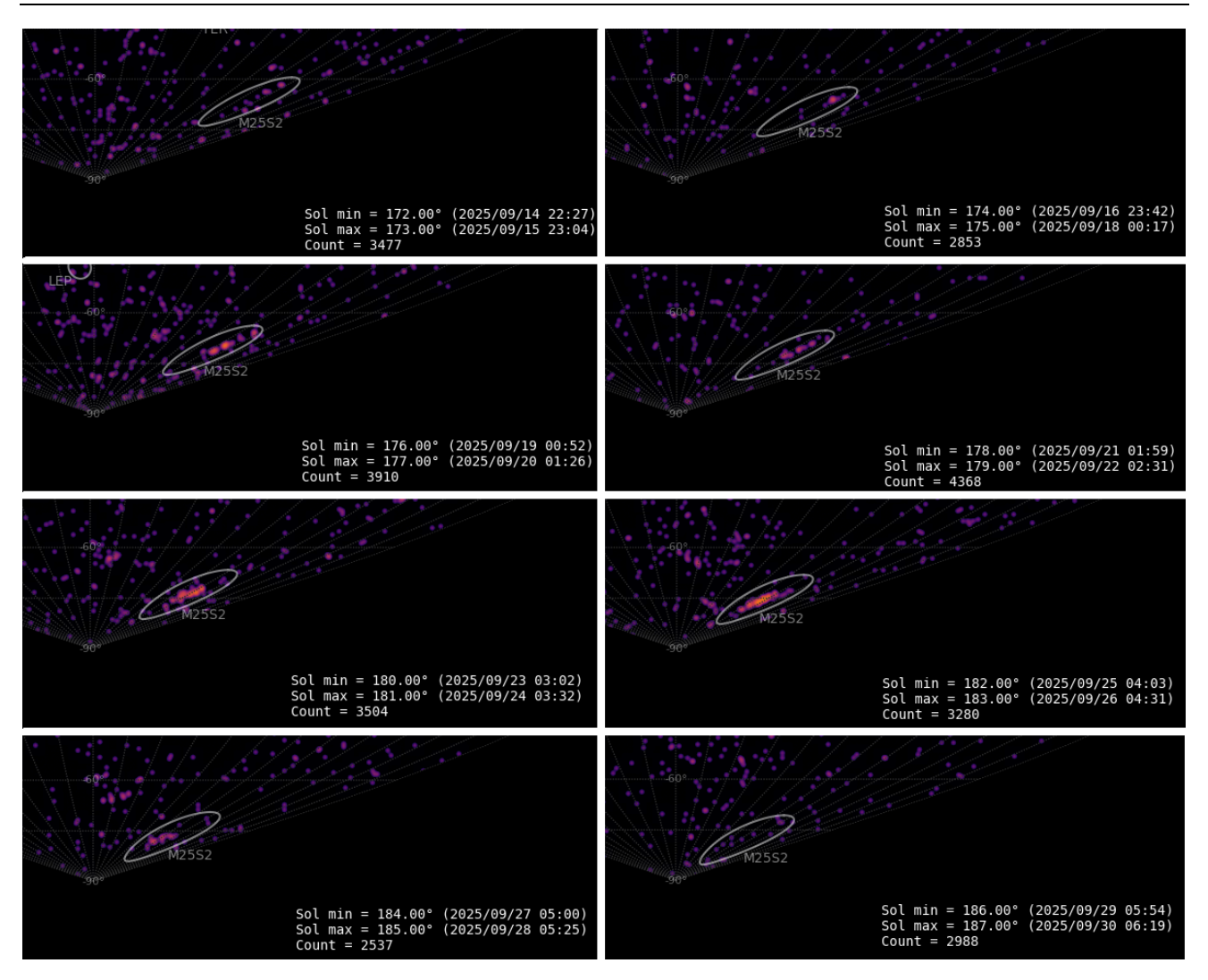


Figure 6 – The evolution of the radiant of M2025-S2 on the GMN radiant density maps during the activity period, plotted in Sun-centered geocentric ecliptic coordinates.

a reference orbit. Working with D-criteria requires caution like in this case when the orbital elements change significantly during Earth's transit. *Figure 6* shows the changes in the radiant position and appearance during the activity period and requires an adapted approach.

All GMN orbit data was extracted for the time interval of  $165^{\circ} < \lambda_{\mathcal{O}} < 187^{\circ}$ , limited in Sun-centered geocentric ecliptic coordinates with  $139^{\circ} < \lambda - \lambda_{\mathcal{O}} < 206^{\circ}$  and  $-57^{\circ} < \beta < -84^{\circ}$ . The method was applied on four intervals of  $7^{\circ}$  in solar longitude, with an overlap of  $2^{\circ}$ :

- $165^{\circ} < \lambda_{\mathcal{O}} < 172^{\circ}$
- 170° < λ<sub>⊙</sub> < 177°</li>
- 175° < λ<sub>O</sub> < 182°
- 180° < λ<sub>O</sub> < 187°</li>

For each time bin a mean orbit was computed as a reference orbit to start the iteration to approach the best fitting mean orbit for each interval. We didn't use median values to derive a mean orbit since a vectoral solution like the method of Jopek et al. (2006) is more appropriate for orbital elements with angular values. This method resulted in 277 orbits that fit with the mean orbit for each interval within

the similarity threshold with  $D_{SH} < 0.075$ ,  $D_D < 0.03$  and  $D_J < 0.075$ .

A single solution for the entire activity period is impossible to define with D-criteria since the orbits changed too much during the three weeks of activity. The solutions obtained for each of the four intervals solved the problem. Counting the number of M2025-S2 meteors per solar longitude relative to the total number of meteors recorded at the Southern Hemisphere allows reconstruction of the activity profile. The profiles obtained for the two methods of shower association are superimposed in *Figure 7*. When the shower was first noticed (at  $\lambda_O = 175.0^{\circ}$ ), the best of the activity had still to come. The skew activity profile indicates maximum activity at  $\lambda_O = 181.5^{\circ}$  with an abrupt end of the activity after  $\lambda_O = 188^{\circ}$ . The GMN method associated more meteors as M2025-S2 than the D-criteria method.

Figures 8 to 11 show close-ups and appearance and drift of the radiants for the solution within each interval in solar longitude. The drift of the radiant in Sun-centered longitude and latitude from week to week is clearly visible. The increasing number of radiant dots is in line with the activity profile in Figure 7. Combining all data in a single plot results in a long extended radiant with the shape of a sickle

(Figure 12). Note that most radiants correspond to orbits with a very small similarity threshold of  $D_{SH} < 0.05$ ,  $D_D < 0.02$  and  $D_J < 0.05$ .

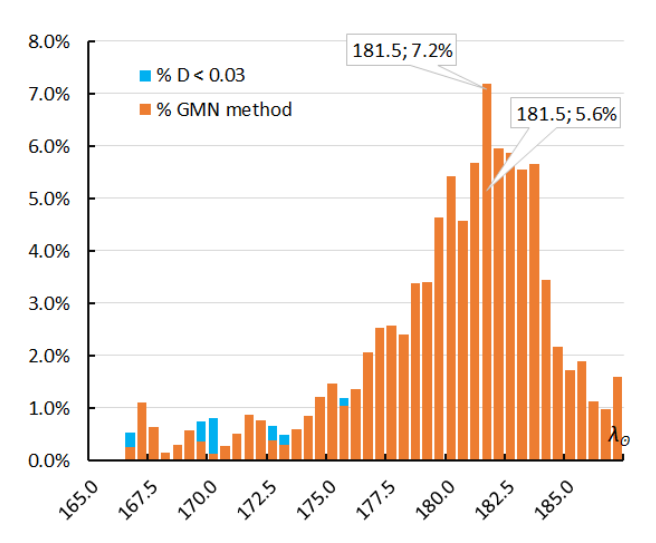


Figure 7 – The percentage of M2025-S2 meteors relative to the total number of meteors recorded by cameras at the Southern Hemisphere. Orange is the result for the GMN shower classification, blue for the D-criteria threshold method.

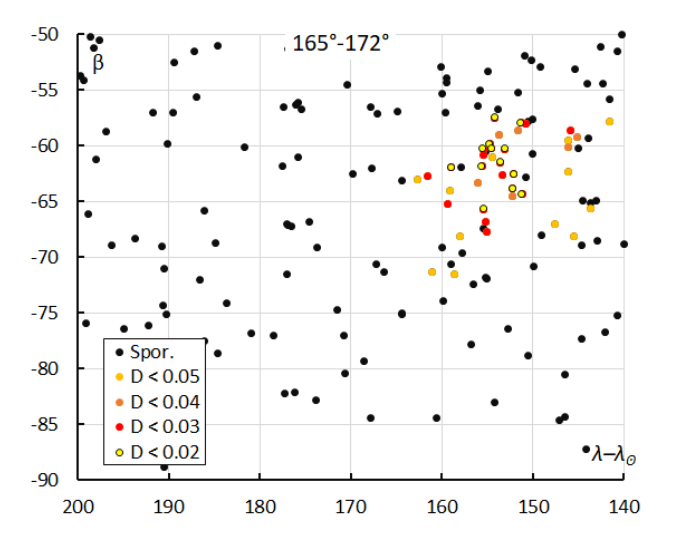


Figure 8 – The radiant distribution during the solar-longitude interval  $165^{\circ} - 172^{\circ}$  in Sun centered ecliptic coordinates.

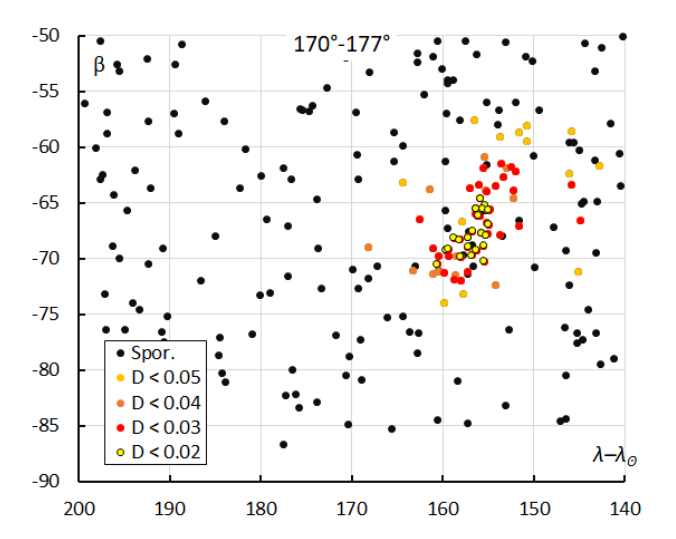


Figure 9 – The radiant distribution during the solar-longitude interval  $170^{\circ} - 177^{\circ}$  in Sun centered ecliptic coordinates.

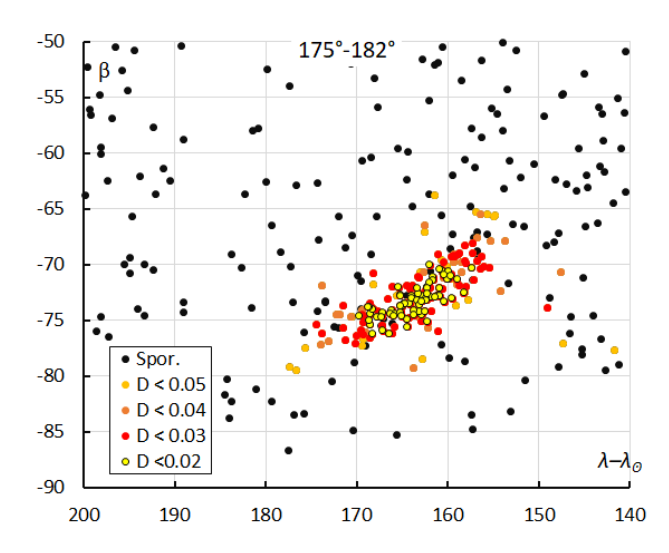


Figure 10 – The radiant distribution during the solar-longitude interval  $175^{\circ}$  –  $182^{\circ}$  in Sun centered ecliptic coordinates.

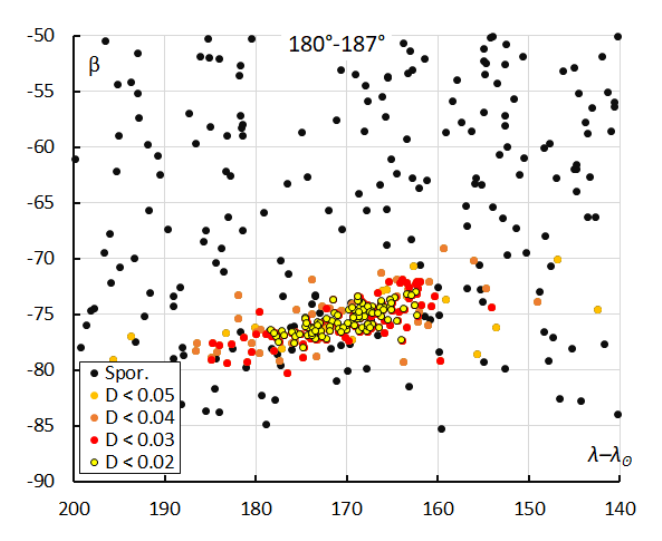


Figure 11 – The radiant distribution during the solar-longitude interval  $180^{\circ} - 187^{\circ}$  in Sun centered ecliptic coordinates.

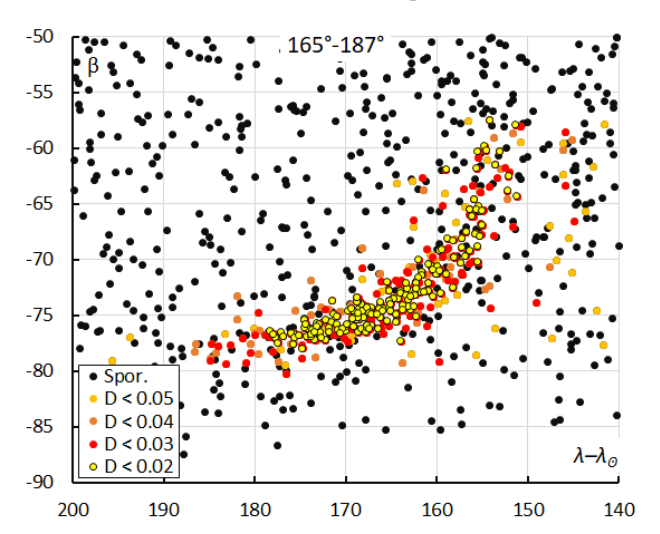


Figure 12 – The radiant distribution during the solar-longitude interval  $165^{\circ} - 187^{\circ}$  in Sun centered ecliptic coordinates.

Table I – GMN 1<sup>st</sup> is the solution reported when M2025-S2 was first discovered, GMN 2<sup>nd</sup> the solution when the activity had ended. The solutions for four intervals in solar longitude were derived from the method described in Section 3, valid for  $D_D < 0.03$ .

	GMN 1st	$GMN \ 2^{nd}$	165°–172°	170°–177°	175°–182°	180°–187°
λο (°)	175.3	181.3	170.2	175.4	180.1	182.3
λ <i>ω</i> <sub>b</sub> (°)	166.9	166.9	166.7	170.5	175.4	180.0
λ <sub>Θe</sub> (°)	178.1	188.4	171.7	176.8	182.0	186.5
$\alpha_g$ (°)	31.6	42.9	15.2	28.5	47.3	55.2
$\delta_{g}\left(^{\circ} ight)$	-66.9	-65.9	-66.1	-66.7	-65.6	-64.4
$\Delta \alpha_g$ (°)	1.64	1.96	0.75	2.64	2.78	2.99
$\Delta\delta_{g}\left(^{\circ}\right)$	+0.29	+0.22	-0.17	+0.12	+0.36	+0.46
$v_g$ (km/s)	20.6	22.1	19.3	20.7	22.3	23.4
$H_b$ (km)	93.9	95.8	93.8	94.3	95.8	96.4
$H_e$ (km)	83.1	84.1	83.1	81.8	83.5	84.1
$H_p$ (km)	87.0	88.3	87.4	86.4	88.3	88.5
$Mag_{Ap}$	+0.9	+0.4	+0.7	+0.5	+0.2	+0.1
$\lambda_g$ (°)	331.83	344.89	325.1	330.9	343.6	349.9
$\lambda_g - \lambda_{\mathcal{O}}$ (°)	156.53	163.59	154.7	155.9	163.3	168.9
$eta_g$ (°)	-67.82	-71.48	-61.9	-66.9	-65.6	-75.5
a (A.U.)	3.203	3.237	3.33	3.34	3.27	3.28
q (A.U.)	0.956	0.965	0.944	0.955	0.966	0.970
e	0.701	0.702	0.717	0.714	0.705	0.704
i (°)	29.7	34.8	27.1	29.9	34.0	36.3
ω (°)	27.6	23.7	31.1	27.9	24.2	22.5
$\Omega$ (°)	354.1	0.4	350.1	354.7	359.8	2.4
П(°)	21.7	24.1	21.2	22.6	24.0	24.8
$T_j$	2.60	2.53	2.56	2.53	2.52	250
N	109	377	22	51	131	158

## 4 Orbit and parent body

The final mean orbits based on the meteors identified as M2025-S2 according to the GMN method and the D-criteria method for the different intervals in solar longitude are in general in good agreement but show that meteor shower orbit parameters strongly depend on the sample that is used.

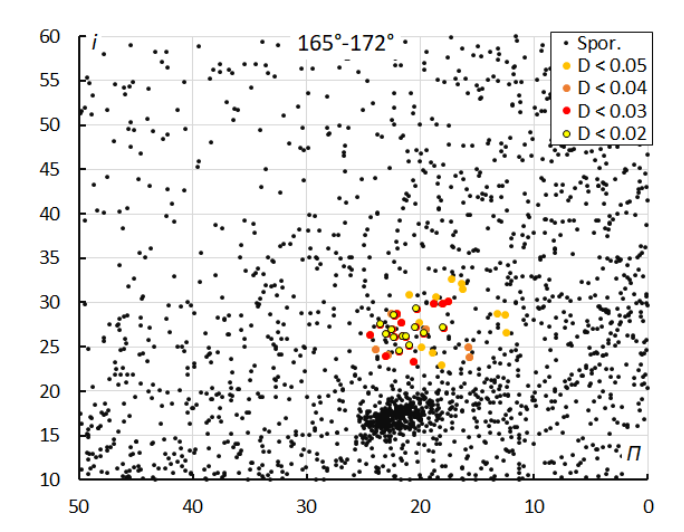


Figure 13 – The diagram of the inclination i against the longitude of perihelion  $\Pi$  color coded for different classes of D criterion threshold, for  $\lambda_{\mathcal{O}}$  between 165° and 172°.

Looking at the diagram of inclination versus longitude of perihelion for each interval, we can see the inclination and the longitude of perihelion slightly increasing. The dense concentration just below the M2025-S2 meteors are the chi Cygnids (CCY#757), a shower active at the same time with very similar characteristics but visible at the Northern Hemisphere.

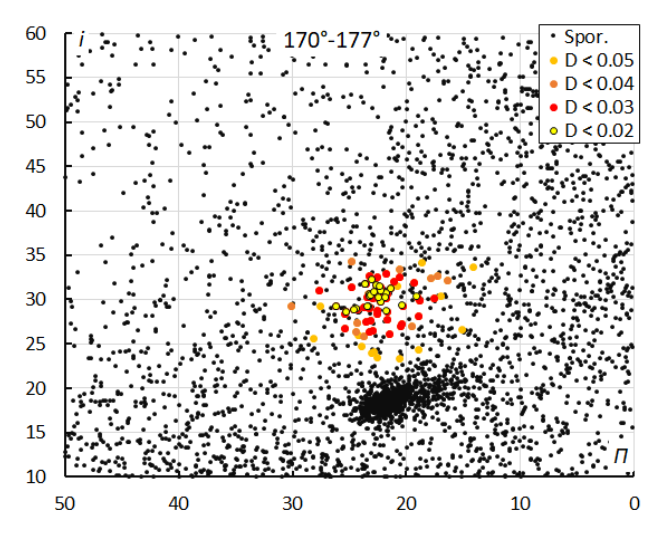


Figure 14 – The diagram of the inclination i against the longitude of perihelion  $\Pi$  color coded for different classes of D criterion threshold, for  $\lambda_{\theta}$  between 170° and 177°.

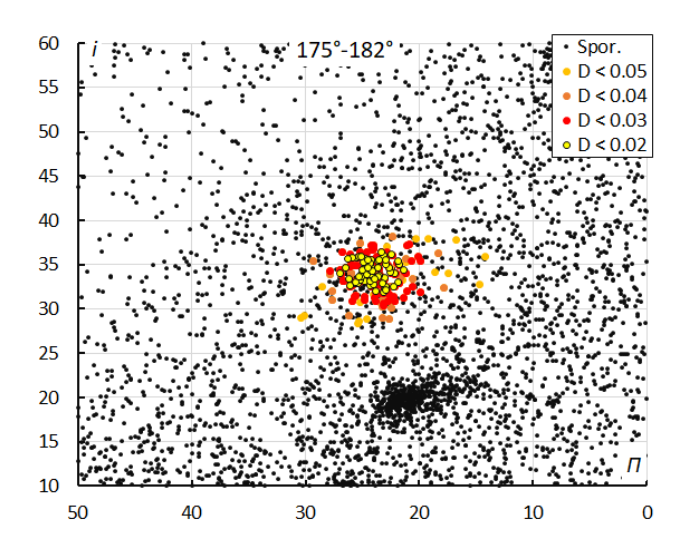


Figure 15 – The diagram of the inclination i against the longitude of perihelion  $\Pi$  color coded for different classes of D criterion threshold, for  $\lambda_{\theta}$  between 175° and 182°.

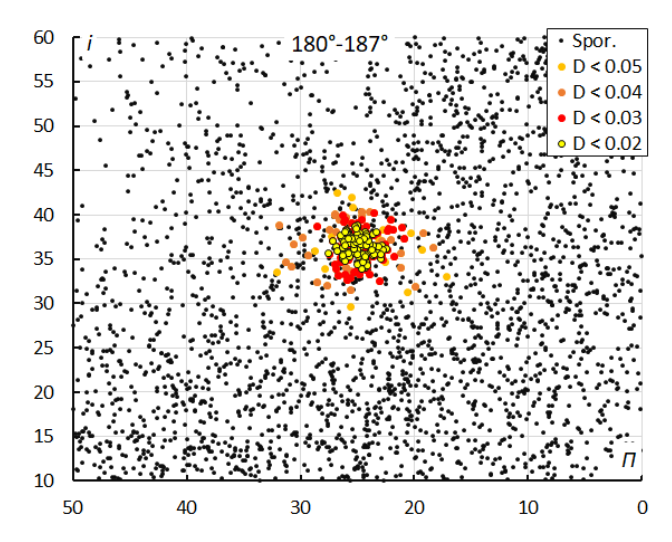


Figure 16 – The diagram of the inclination i against the longitude of perihelion  $\Pi$  color coded for different classes of D criterion threshold, for  $\lambda_{\theta}$  between 180° and 187°.

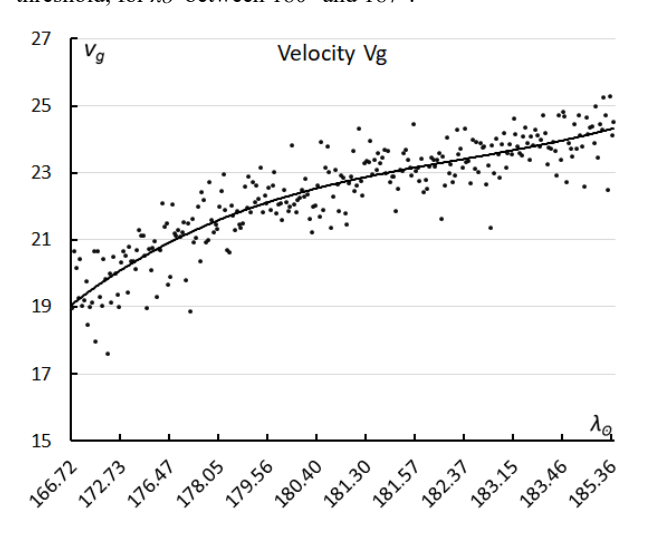


Figure 17 - The geocentric velocity in function of the solar longitude.

During the activity of the M2025-S2 meteor shower, the geocentric velocity increased, from about 19 km/s to more than 24 km/s (*Figure 17*). The change in velocity is also visible in the plot of the radiants in Sun-centered ecliptic

coordinates, which compensate the radiant drift caused by the rotation of the Earth around the Sun. The remarkable strong drift in Sun-centered ecliptic coordinates increased during the activity period from  $\Delta(\lambda-\lambda_O)=+0.52^\circ$ ,  $\Delta\beta=-0.86^\circ$  in the second week to  $\Delta(\lambda-\lambda_O)=2.85^\circ$ ,  $\Delta\beta=-0.97^\circ$  in the last week. The first week had too few data to determine radiant drift. This change in drift explains the sickle shaped radiant plot in *Figure 18*.

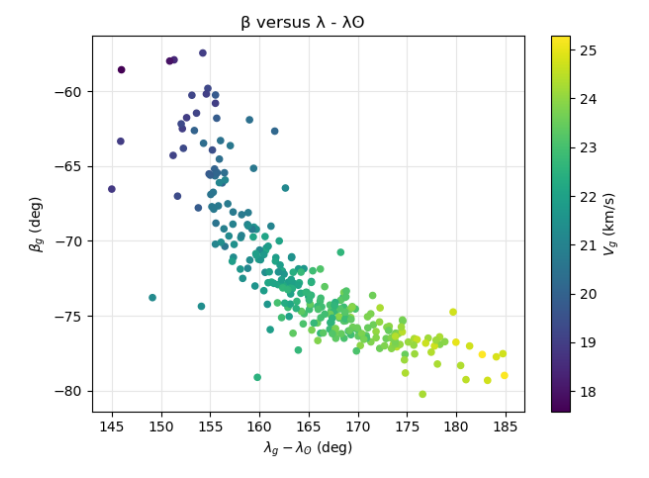


Figure 18 – The radiant distribution during the solar-longitude interval 165° – 187° in Sun centered ecliptic coordinates, color-coded in function of the geocentric velocity.

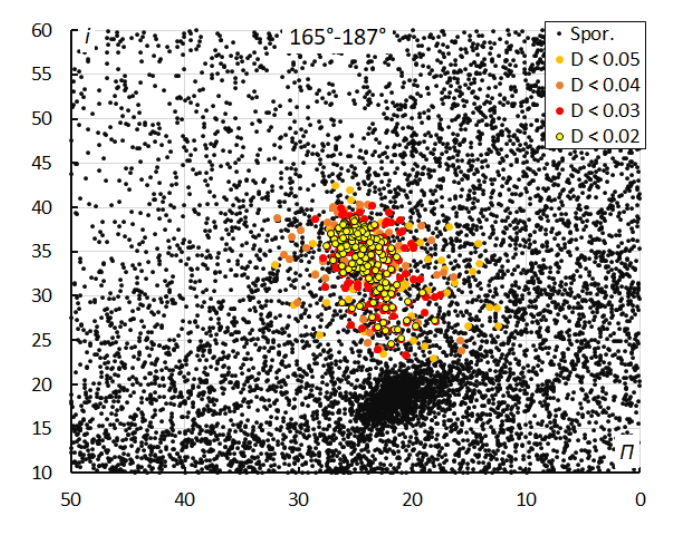


Figure 19 – The diagram of the inclination i against the longitude of perihelion  $\Pi$  color-coded for different classes of D criterion threshold, for  $\lambda_{\theta}$  between 165° and 187°.

Figure 19 seem to shows how the orbits changed in inclination and longitude of perihelion during the entire activity period. In reality, the orbits are rather concentrated if considered in short time intervals. The dispersion is due to the rapid change in inclination and longitude of perihelion. This drift in inclination is shown in Figure 20 and in longitude of perihelion in Figure 21. Both line graphs show the evolution in time.

Figure 22 shows the same diagram as Figure 19 but color-coded for velocity. At the start of the activity slower M2025-S2 meteors have a lower inclination and smaller longitude of perihelion. Towards the end of the shower

activity these meteors are much faster with a higher inclination and larger longitude of perihelion.

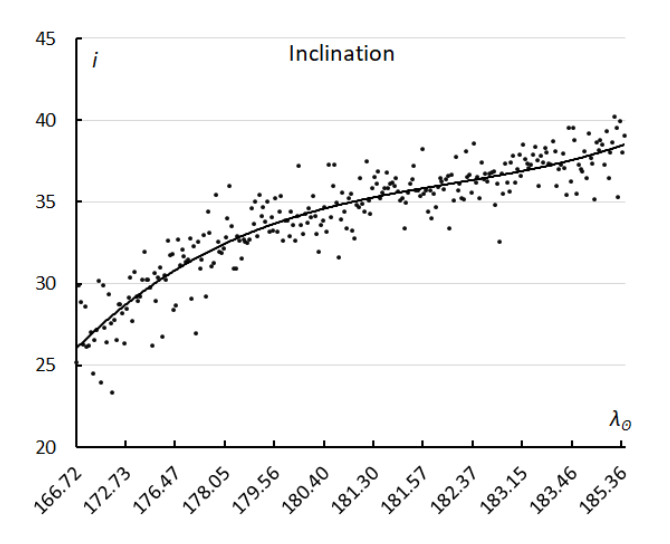


Figure 20 – The inclination i in function of the solar longitude.

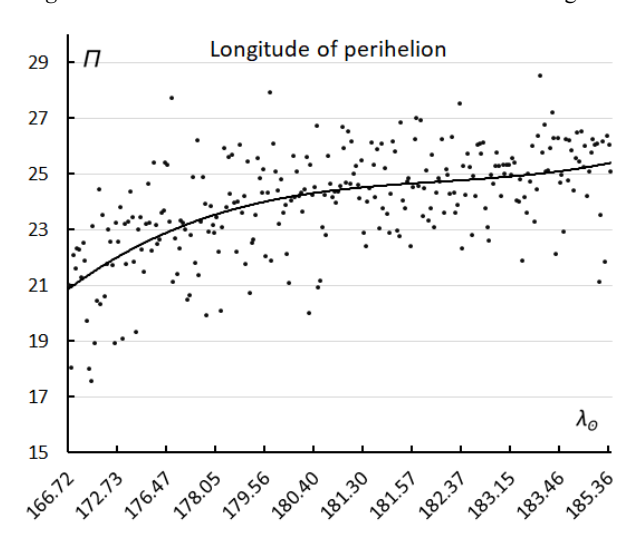


Figure 21 – The longitude of perihelion  $\Pi$  in function of the solar longitude.

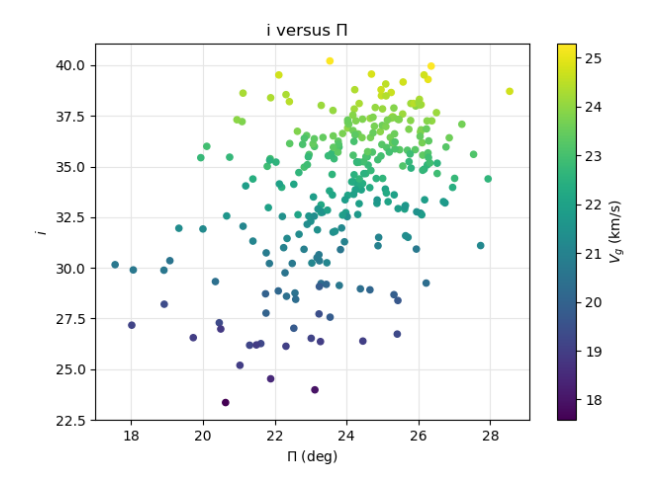


Figure 22 – The diagram of the inclination i against the longitude of perihelion  $\Pi$ , color-coded in function of the geocentric velocity.

Figure 23 shows less dispersion in eccentricity than in inclination (Figure 19). The eccentricity seems to decrease slightly during the activity period (Figure 24). There is some correlation between the velocity and the longitude of perihelion, but in eccentricity the velocity looks randomly

distributed. The dense concentration immediately right-below of the M2025-S2 concentration are again the chi Cygnids (CCY#757).

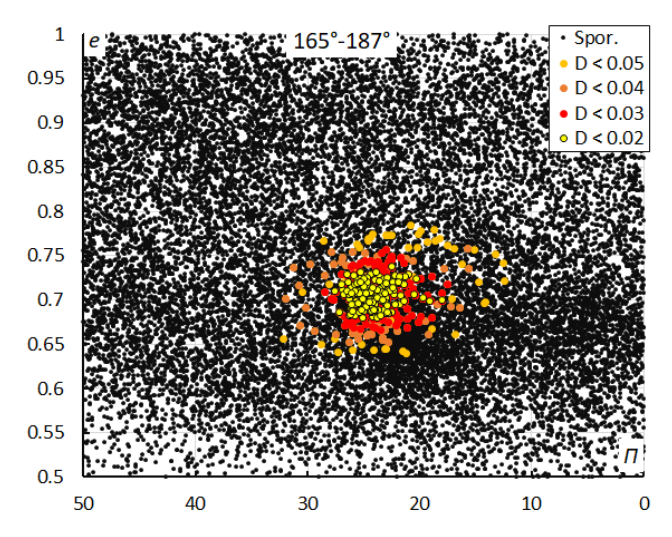


Figure 23 – The diagram of the eccentricity e against the longitude of perihelion  $\Pi$  color-coded for different classes of D criterion threshold, for  $\lambda_{\theta}$  between 165° and 187°.

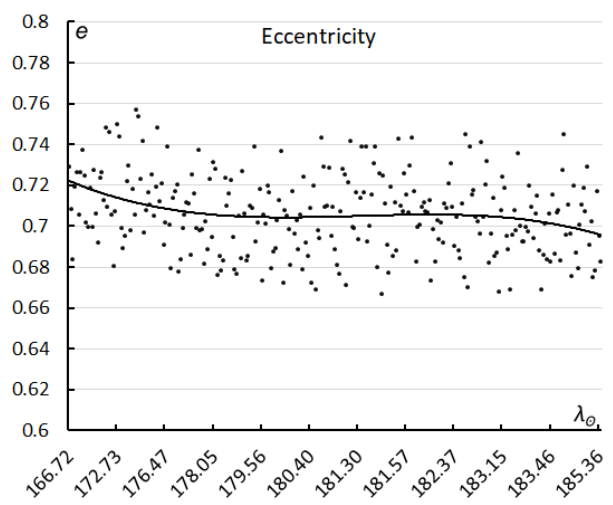


Figure 24 – The eccentricity e in function of the solar longitude.

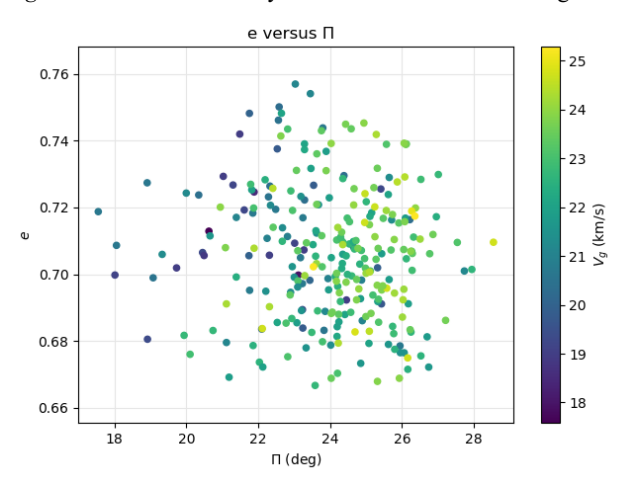


Figure 25 – The diagram of the eccentricity e against the longitude of perihelion  $\Pi$ , color-coded in function of the geocentric velocity.

Looking at the diagram of the eccentricity versus the inclination the orbits appear mainly dispersed in inclination (*Figure 26*). The dense concentration of orbits just left from

the M2025-S2 orbits, are the chi Cygnids (CCY#757) which have a slightly lower inclination and eccentricity. The drift in velocity is mainly visible in the inclination in *Figure 27*. The faster the meteors the higher the inclination.

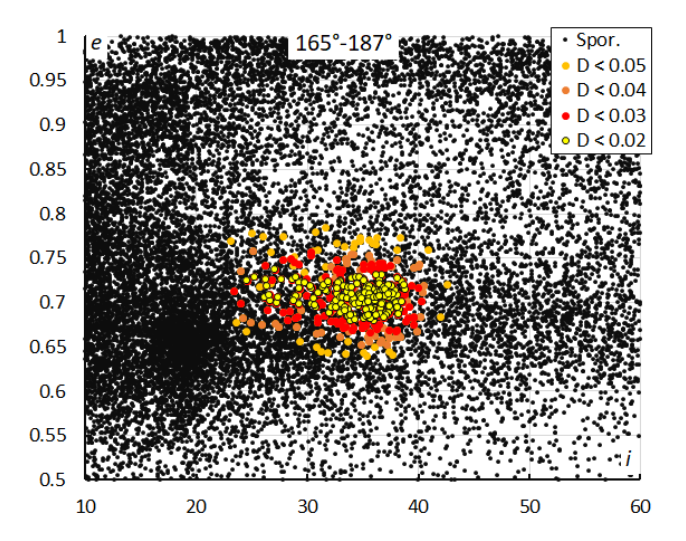


Figure 26 – The diagram of the eccentricity e against the inclination i color-coded for different classes of D criterion threshold, for  $\lambda_0$  between 165° and 187°.

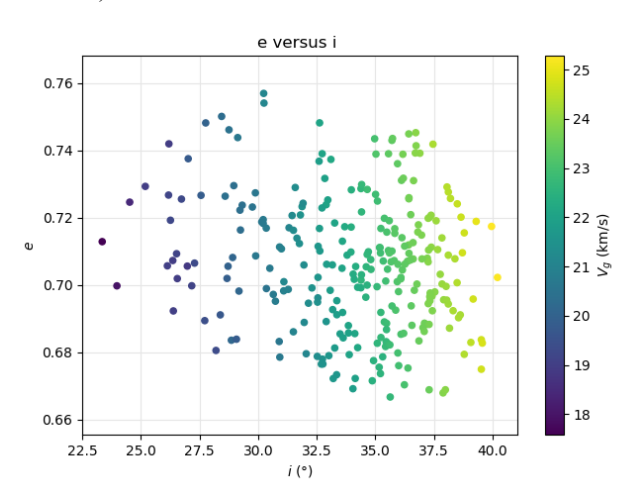


Figure 27 – The diagram of the eccentricity *e* against the inclination *i*, color-coded in function of the geocentric velocity.

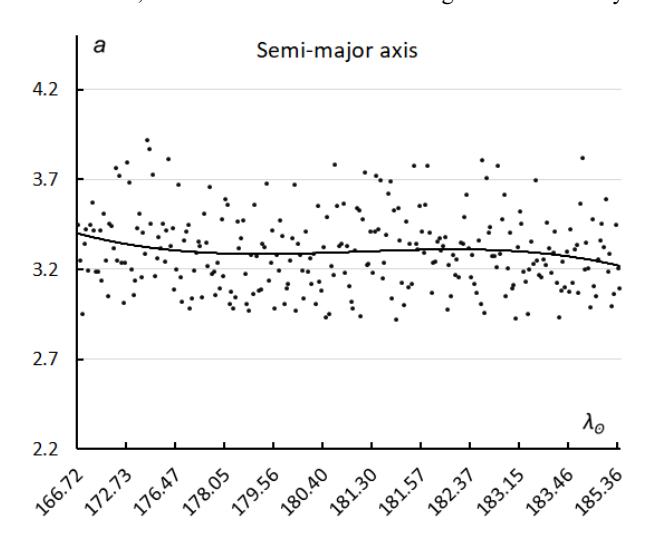


Figure 28 – The semi-major axis a in function of the solar longitude.

During the shower activity we see no significant change in

semi-major axis a (Figure 28). There is a clear increase in perihelion distance q. The diagram of the perihelion distance versus the inclination shows a long-stretched trail in both inclination and perihelion distance. The dark concentration left from M2025-S2 are again the chi Cygnids (Figure 29).

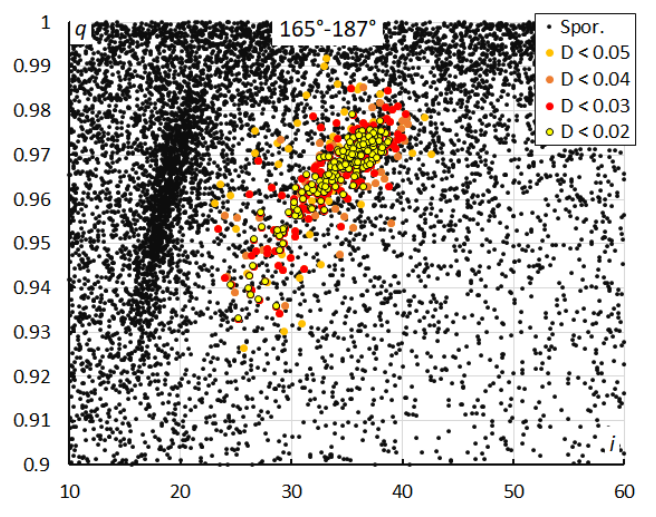


Figure 29 – The diagram of the perihelion distance q against the inclination i color-coded for different classes of D criterion threshold, for  $\lambda_0$  between 165° and 187°.

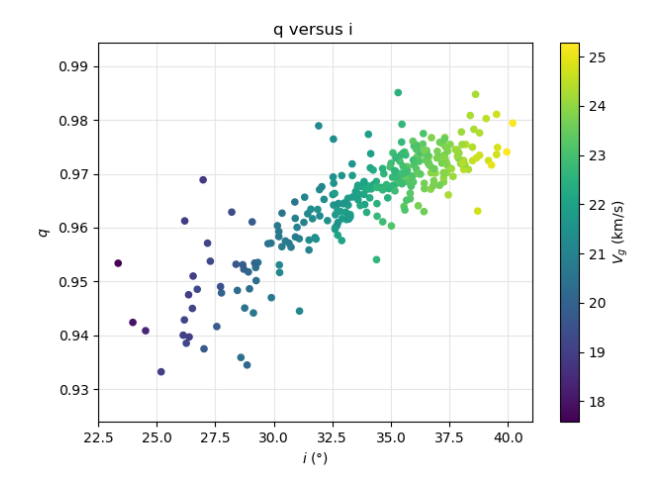


Figure 30 – The diagram of the perihelion distance q against the inclination i, color-coded in function of the geocentric velocity.

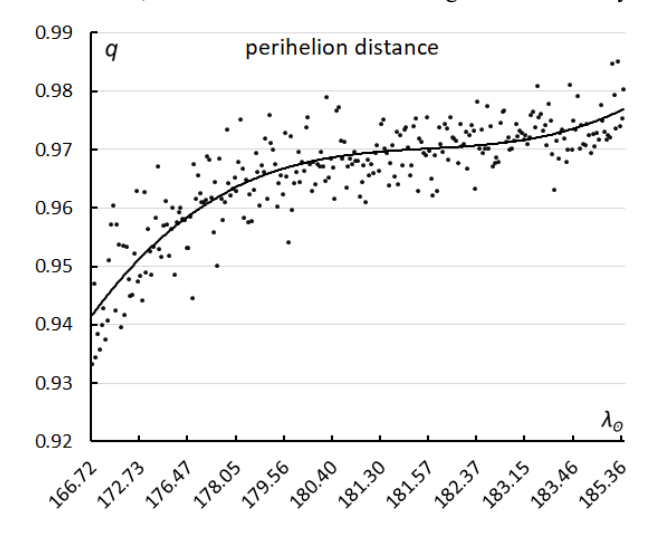


Figure 31 – The perihelion distance q in function of the solar longitude.

Figures 30 and 31 combined show how the perihelion distance and inclination increase with the velocity during the activity period of M2025-S2.

Figures 8 to 31 were all derived from the selection based on the method with D-criteria, which has 277 M2025-S2 meteors against the GMN method which has 377. Only 6 meteors selected by D-criteria were ignored by the GMN method. 106 meteors identified by the GMN method were not detected by the D-criteria method, of which ten orbits do not even fit the low threshold class similarity for the mean orbit obtained by the GMN method. The rapidly changing orbit parameters during the activity makes it impossible to apply D criteria on a single solution reference orbit. Therefore, the activity period has been split into four intervals in solar longitude. The solutions for the two methods correspond best for the interval 175°-182°.

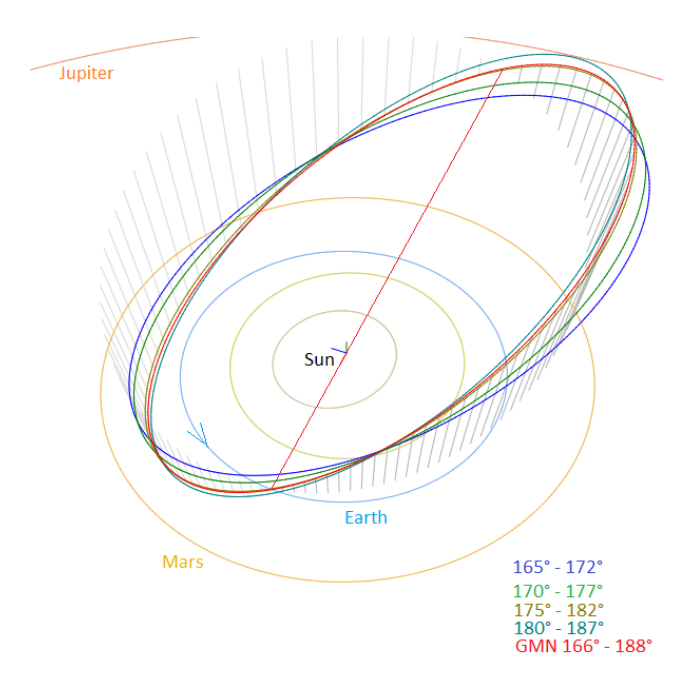


Figure 32 – Comparing the mean orbits for the solutions for M2025-S2 based on the shower identification according to two methods, red for the 2025GMN solution, the other colors for the intervals used for the D-criteria shower search method with  $D_D < 0.03$  in Table 1, close-up at the inner Solar System. (Plotted with the Orbit visualization app provided by Pető Zsolt).

The Tisserand's parameter relative to Jupiter,  $T_j$  (= 2.53) identifies the orbit as of a Jupiter Family Comet type orbit. *Figure 32* shows the orbits for the different solutions in the inner solar system. The dust of M2025-S2 crosses the Earth orbit at its ascending node from south of the ecliptic radiating from a circumpolar radiant at the Southern Hemisphere. Comparing the orbits for the different time bins in solar longitude, we see that the orbital plane gradually changes in orientation. This layered structure is what we see in the changing orbital parameters and the strong drift in Sun-centered ecliptic coordinates during the activity period. The mean orbit obtained by the GMN method is very close to the solution for the time interval  $175^{\circ}$ – $182^{\circ}$  obtained with the D-criteria method.

The orbit crosses the ecliptic at its descending node close to the orbit of Jupiter, which means that dust trails will be much affected by this giant planet's gravitational perturbations. Although the Jupiter Family Comet type orbit suggests a cometary origin, meteoroids of M2025-S2 have a deep ablation height in the atmosphere uncommon for fragile cometary material.

Three other sources observed around the same time, the epsilon Ursae-Minorids (EPU#1044) (Roggemans et al., 2025b), M2024-S1 discovered in 2024 (Vida and Šegon, 2024; Šegon et al., 2025) and observed again in 2025 (Roggemans et al., 2025c) and the chi Cygnids (CCY#757) were all three in outburst in 2025. All three cross the Earth orbit at their descending node at about the same time as M2025-S2 crossed its ascending node. All these meteoroid streams cross the ecliptic near the Earth orbit at one node and have the position of the other node as well as the aphelion relatively close to the orbit of Jupiter. All have the same characteristic with meteors penetrating deep into the atmosphere. The epsilon Ursae-Minorids and chi Cygnids are known as episodic showers. It would be worthwhile to run orbit integrations to understand the mechanism that gave these showers their periodic nature and peculiar characteristics.

A list of possible parent bodies is listed in *Table 2*. Stream modelers may reconstruct the dynamics of this meteoroid stream. It is uncertain if the parent body still exists or if it has already been discovered. There is no convincing evidence among the known candidates in *Table 2*.

Table 2 – Top ten matches of a search for possible parent bodies with  $D_D < 0.13$ .

Name	$D_D$
2022 SJ48	0.099
1994 RB	0.105
2017 TO4	0.113
2020 WB3	0.116
2010 UY6	0.117
2009 RD4	0.121
2014 SO260	0.122
2011 TA4	0.123
2019 WF1	0.125
2014 SM142	0.127

### 5 Past observations

The Global Meteor Network got good coverage at the Southern Hemisphere since 2022, but only a few orbits could be associated with M2025-S2 in past years (three in 2024 and two in 2023). No other video camera network data is available for the Southern Hemisphere for earlier years. There are visual observations from the  $20^{th}$  century mentioning activity from this part of the sky. The first possible sightings may have been from Cuno Hoffmeister in Namibia in 1938 with a radiant at RA 48° and decl.–68° at  $\lambda_{\rm O}$  167.9° (eq.1925). No later possible sightings could be

found from South Africa or New Zealand. Michael Buhagiar in the 1970's made mention that there may be a weak shower in later September near the South Celestial Pole but didn't provide any details just an opinion/feeling. Others, like WAMS/NAPOMS observers in Australia either didn't report activity from this part of the sky, or the radiant positions don't fit with our data. We can conclude that there are no records that reveal any striking activity from M2025-S2 in the past. Its sudden appearance in 2025 may indicate this is a dust trail with a periodic nature or a one-year event.

## 6 Conclusion

Activity from a new meteor shower M2025-S2 discovered by Global Meteor Network has been analyzed by two different meteor shower association methods. The shower displayed an exceptional strong radiant drift in Suncentered ecliptic coordinates. During the three weeks activity period the shower gradually increased in activity to reach its maximum activity at  $\lambda_0 = 181.3^{\circ}$  (2025, September 24). The orientation of the orbital plane of the meteoroid stream changes during Earth's transit and resulted in rapidly changing inclination, longitude of perihelion and distance of perihelion. This layered structure is very similar to the chi Cygnids active at the Northern Hemisphere around the same time.

## Acknowledgment

This report is based on the data of the Global Meteor Network (Vida et al., 2020a; 2020b; 2021) which is released under the CC BY 4.0 license<sup>14</sup>. We thank all 825 participants in the Global Meteor Network project for their contribution and perseverance. A list with the names of the volunteers who contribute to GMN has been published in the 2024 annual report (Roggemans et al., 2025a).

## References

- Drummond J. D. (1981). "A test of comet and meteor shower associations". *Icarus*, **45**, 545–553.
- Jopek T. J. (1993). "Remarks on the meteor orbital similarity D-criterion". *Icarus*, **106**, 603–607.
- Jopek T. J., Rudawska R. and Pretka-Ziomek H. (2006). "Calculation of the mean orbit of a meteoroid stream". Monthly Notices of the Royal Astronomical Society, 371, 1367–1372.
- Moorhead A. V., Clements T. D., Vida D. (2020). "Realistic gravitational focusing of meteoroid streams". Monthly Notices of the Royal Astronomical Society, 494, 2982–2994.

- Roggemans P., Johannink C. and Campbell-Burns P. (2019). "October Ursae Majorids (OCU#333)". eMetN Meteor Journal, 4, 55–64.
- Roggemans P., Campbell-Burns P., Kalina M., McIntyre M., Scott J. M., Šegon D., Vida D. (2025a). "Global Meteor Network report 2024". *eMetN Meteor Journal*, **10**, 67–101.
- Roggemans P., Vida D., Šegon D. (2025b). "Epsilon-Ursae Minorids (EPU#1044) enhanced activity in 2025". eMetN Meteor Journal, 10, 360–367.
- Roggemans P., Vida D., Šegon D. (2025c). "M2024-S1 activity confirmed in 2025". *eMetN Meteor Journal*, **10**, 353–359.
- Šegon D., Vida D., Roggemans P. (2025). "New meteor shower in Ursa Minor 23–24 September 2024". *eMetN Meteor Journal*, **10**, 12–19.
- Southworth R. B. and Hawkins G. S. (1963). "Statistics of meteor streams". *Smithsonian Contributions to Astrophysics*, 7, 261–285.
- Vida D., Gural P., Brown P., Campbell-Brown M., Wiegert P. (2020a). "Estimating trajectories of meteors: an observational Monte Carlo approach I. Theory". Monthly Notices of the Royal Astronomical Society, 491, 2688–2705.
- Vida D., Gural P., Brown P., Campbell-Brown M., Wiegert P. (2020b). "Estimating trajectories of meteors: an observational Monte Carlo approach - II. Results". *Monthly Notices of the Royal Astronomical Society*, 491, 3996–4011.
- Vida D., Šegon D., Gural P. S., Brown P. G., McIntyre M. J. M., Dijkema T. J., Pavletić L., Kukić P., Mazur M. J., Eschman P., Roggemans P., Merlak A., Zubrović D. (2021). "The Global Meteor Network Methodology and first results". Monthly Notices of the Royal Astronomical Society, 506, 5046–5074.
- Vida D., Šegon D. (2024). New meteor shower M2024-S1 in Ursa minor. CBET 5452. D. W. E. Green (ed.), 1 pp.

<sup>14</sup> https://creativecommons.org/licenses/by/4.0/

# Delta-Horologiids (DHO#1146) in 2025

Paul Roggemans<sup>1</sup>, Damir Šegon<sup>2</sup>, Denis Vida<sup>3,4</sup>, James M. Scott<sup>5</sup>, Jeff Wood<sup>6</sup>

<sup>1</sup> Pijnboomstraat 25, 2800 Mechelen, Belgium

paul.roggemans@gmail.com

<sup>2</sup> Astronomical Society Istra Pula, Park Monte Zaro 2, 52100 Pula, Croatia

<sup>3</sup> Department of Physics and Astronomy, University of Western Ontario, Richmond Street, London, N6A 3K7, Ontario, Canada

<sup>4</sup> Institute for Earth and Space Exploration, University of Western Ontario, Perth Drive, London, N6A 5B8, Ontario, Canada

denis.vida@gmail.com

<sup>5</sup> Department of Geoscience, Aarhus University, Høegh-Guldbergs Gade 2. DK-8000 Aarhus C , Denmark jscott@geo.au.dk

<sup>6</sup> PO Box 162, Willetton, Western Australia 6955, Australia

A case study on the delta-Horologiids (DHO#1146) based on Global Meteor Network orbit data identified 34 possible DHO-orbits in 2025. The radiant position was derived as R.A. =  $61.4^{\circ}$  and decl.=  $-40.6^{\circ}$  with a geocentric velocity of 42.9 km/s. GMN data confirms the existence of this minor meteor shower.

#### 1 Introduction

While looking for unknown sources of meteor activity sometimes radiants are spotted that are unknown to the GMN meteor shower list. The IAU MDC Meteor Shower List<sup>15</sup> includes many more meteor showers than the GMN list, often poorly documented entries that have been detected in recent years. Before the official procedure to announce the discovery of an unknown meteor shower is made, unidentified radiant concentrations are verified with the IAU MDC list. This procedure was followed for a

suspect activity in the constellation of Horologium during the night of 9–10 September, 2025. This meteor shower had been reported in 2023 and registered as the delta-Horologiids (#1146)<sup>16</sup>, based on 66 meteors recorded by CAMS and 856 meteors recorded by SAAMER radar (Jenniskens, 2023). Apart from the radiant position, the orbital parameters between the two datasets differ a lot. The IAU-MDC working list of meteor showers contains only the orbit parameters based on CAMS-data. An analysis has been made, based on GMN-data and the solution has been reported to the IAU-MDC.

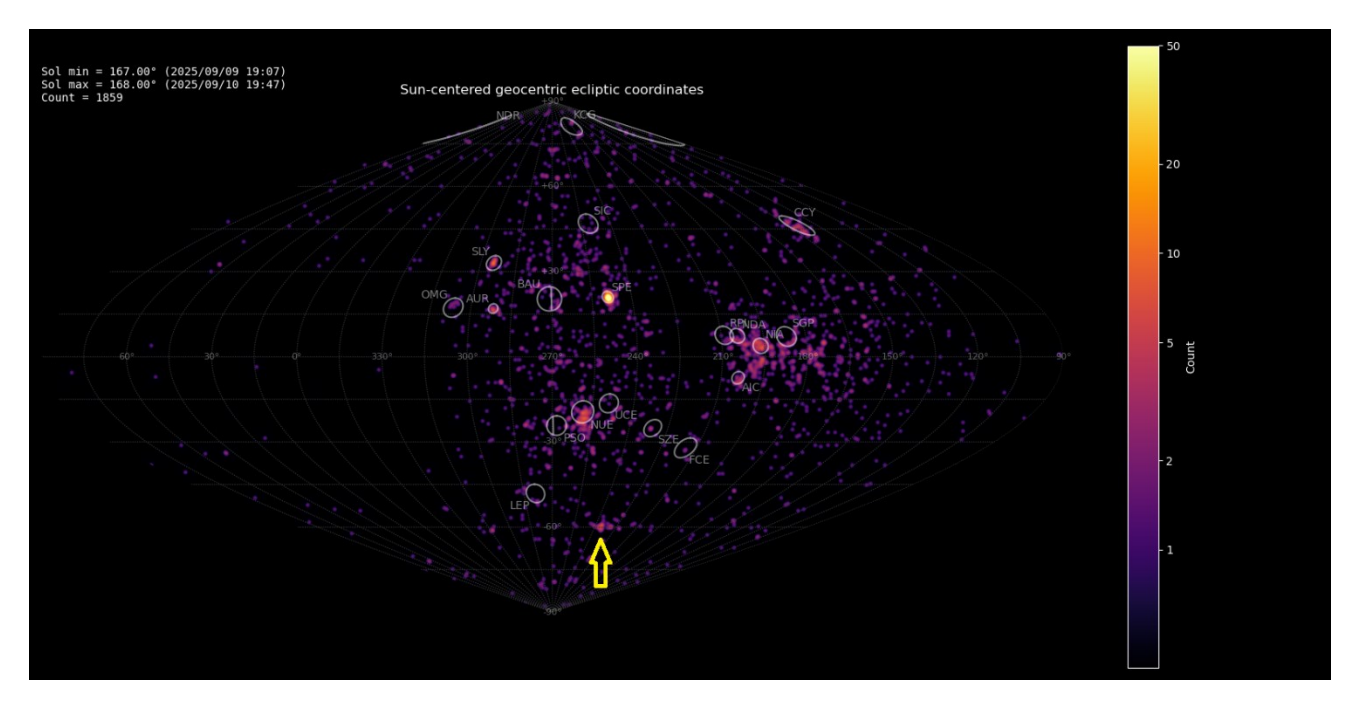


Figure 1 – Heat map with 1859 radiants obtained by the Global Meteor network in 9–10 September, 2025. The position of the delta-Horologiids in Sun-centered geocentric ecliptic coordinates is marked with a yellow arrow.

https://www.ta3.sk/IAUC22DB/MDC2022/Roje/roje lista.php?corobic\_roje=0&sort\_roje=0

<sup>&</sup>lt;sup>16</sup> https://www.ta3.sk/IAUC22DB/MDC2022/Roje/pojedynczy obiekt.php?lporz=02094&kodstrumienia=01146

## 2 GMN shower identification results

The GMN shower association criterion assumes that meteors within 1° in solar longitude, within an association radius from radiant (2.9° in this case), and within 10% in geocentric velocity of a shower reference location are members of that shower. Further details about the shower association are explained in Moorhead et al. (2020). Using these meteor shower selection criteria, 34 orbits have been associated in 2025 with the delta-Horologiids. The mean orbit has been listed in *Table 1*.

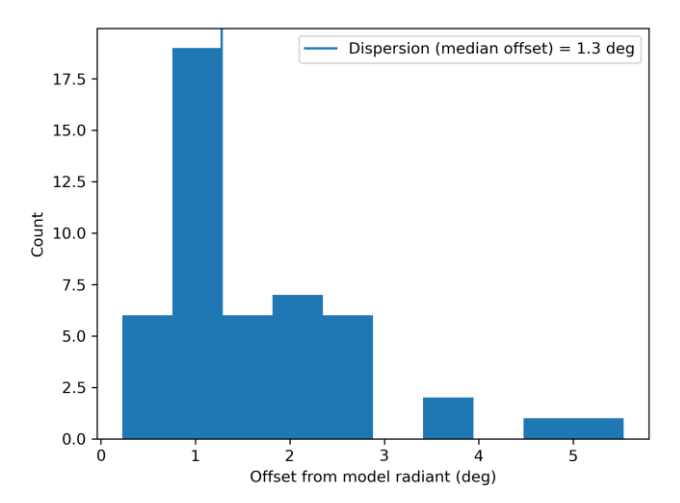


Figure 2 – Dispersion on the radiant position.

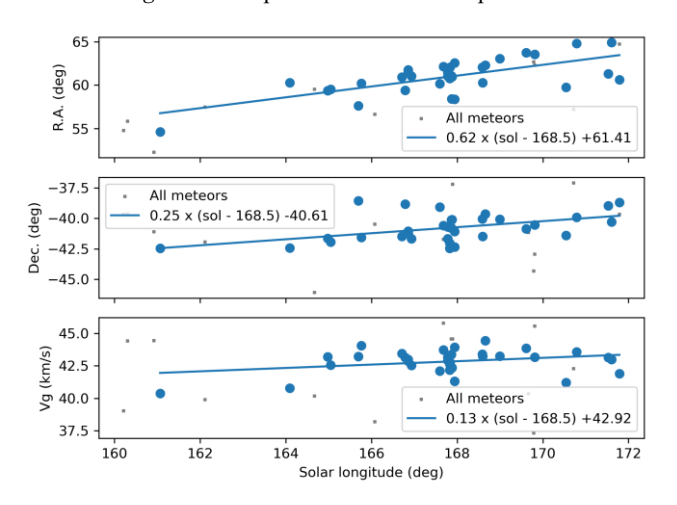


Figure 3 – The radiant drift.

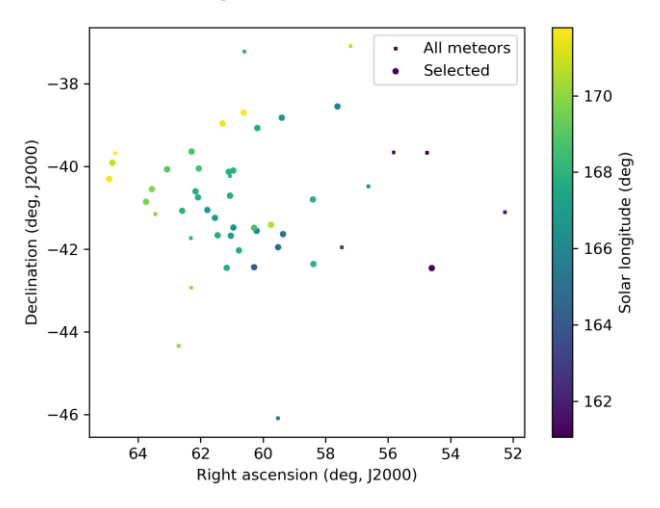


Figure 4 – The radiant distribution during the solar-longitude interval  $161.0^{\circ} - 172.0^{\circ}$  in equatorial coordinates.

Figures 5 and 6 clearly show that the shower activity source appeared on top of the sporadic background noise.

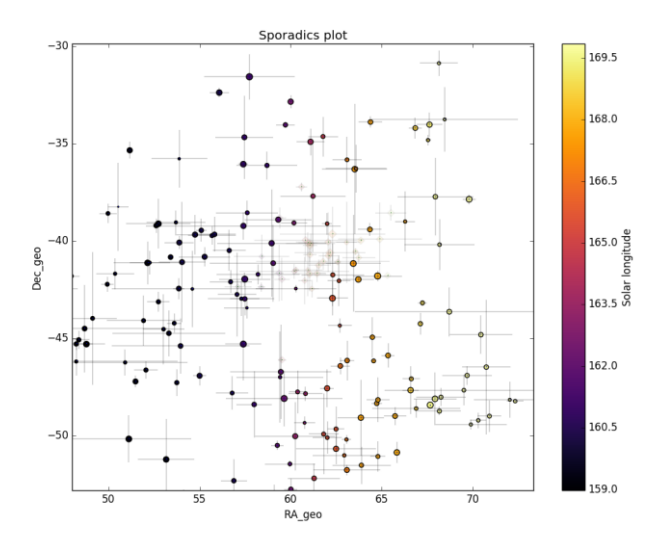


Figure 5 – All non shower meteor radiants in geocentric equatorial coordinates during the shower activity. The pale diamonds represent the new shower radiants plots, error bars represent two sigma values in both coordinates.

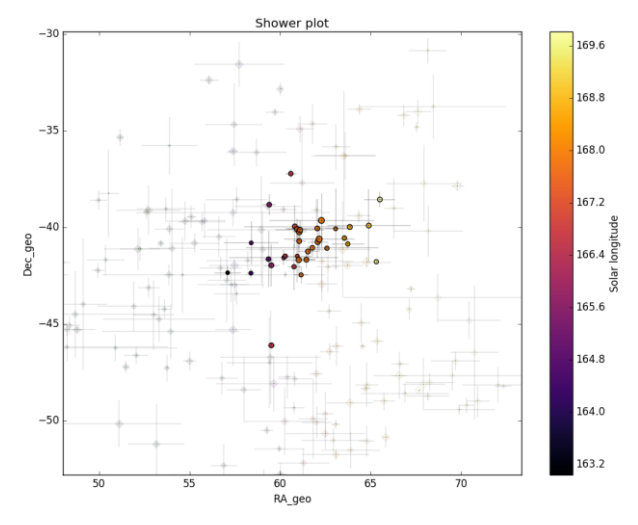


Figure 6 – The reverse of Figure 5, now the shower meteors are shown as circles and the non shower meteors as grayed out diamonds. Note that there are no other groups of meteor radiants to be seen in the vicinity of the possibly new meteor shower.

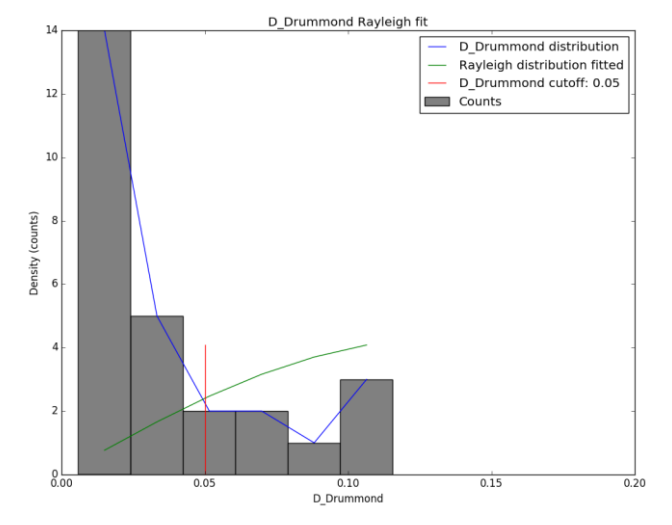


Figure 7 – Rayleigh distribution fit and Drummond  $D_D$  criterion cutoff.

### 3 Another search method

Meteor shower identification strongly depends on the methodology used to select candidate shower members. The sporadic background is everywhere present at the sky which risks to contaminate selections of shower candidates. Using a radiant location is a straightforward method to classify shower meteors. In order to double check GMN meteor shower detections another method is used, based on orbit similarity criteria. This approach serves as a second opinion to make sure that no spurious radiant concentrations are mistaken as new meteor showers.

The visible concentration of radiant points was extracted for the time interval of  $161^{\circ} < \lambda_{\mathcal{O}} < 172^{\circ}$ , arbitrarily limited in Sun-centered geocentric ecliptic coordinates with  $220^{\circ} < \lambda - \lambda_{\mathcal{O}} < 250^{\circ}$  and  $-48^{\circ} < \beta < -69^{\circ}$ . This selection includes most of the possible meteor shower members as well as the sporadic sources within this interval. This preselection included 162 meteor orbits, used to compute a first mean orbit for this sample. We didn't use median values to derive a mean orbit since a vectoral solution like the method of Jopek et al. (2006) is more appropriate for orbital elements with angular values.

This first mean orbit serves as a reference orbit to start an iterative procedure to approach a mean orbit which is the most representative orbit for the similar orbits within the sample, removing outliers and sporadic orbits. This method has been described before (Roggemans et al., 2019). Three different discrimination criteria are combined in order to have only those orbits which fit the different criteria thresholds. The D-criteria that we use are these of Southworth and Hawkins (1963), Drummond (1981) and Jopek (1993) combined. The values are considered in five different classes with different thresholds of similarity:

- Low:  $D_{SH} < 0.2 \& D_D < 0.08 \& D_J < 0.2$ ;
- Medium Low:  $D_{SH} < 0.125 \& D_D < 0.05 \& D_J < 0.125$ ;
- Medium high:  $D_{SH} < 0.1 \& D_D < 0.04 \& D_J < 0.1$ ;
- High:  $D_{SH} < 0.075 \& D_D < 0.03 \& D_J < 0.075$ .
- Very high:  $D_{SH} < 0.05 \& D_D < 0.02 \& D_J < 0.05$ .

Working with D-criteria requires caution as the validity depends much on the type of orbits. The method works fine for high inclined long period orbits, but is less reliable for low inclination, low eccentricity short period orbits. The Dcriteria values are no more than an indication for the degree of similarity between an orbit and a reference orbit.

The Rayleigh distribution fit pointed at a  $D_D$  value of 0.05 as the orbital similarity threshold value cutoff (*Figure 7*). This method resulted in a mean orbit with 31 related orbits that fit within the similarity threshold with  $D_{SH} < 0.125$ ,  $D_D < 0.05$  and  $D_J < 0.125$ , recorded 2025 September 5 – 14. The plot of the radiant positions in equatorial coordinates, color coded for different D-criteria thresholds, shows a clear concentration in Right Ascension from about 57° to 66° and  $-38^\circ$  to  $-43^\circ$  in declination (*Figure 9*), see also *Figure 4*.

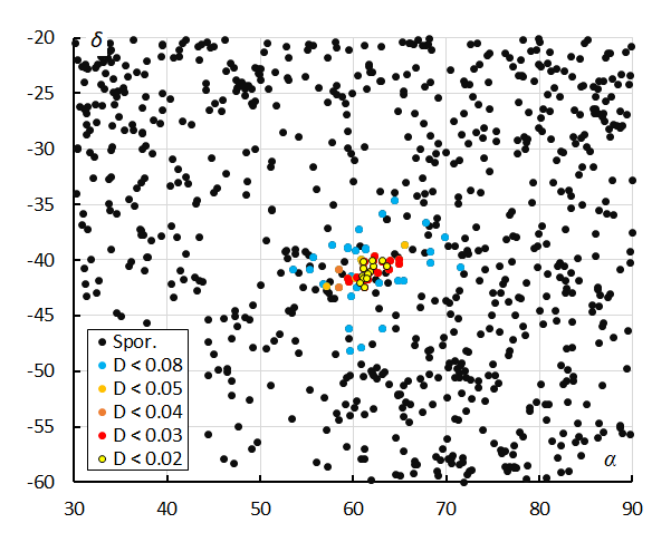


Figure 8 – The radiant distribution during the solar-longitude interval  $161^{\circ} - 172^{\circ}$  in equatorial coordinates, color coded for five threshold values of the  $D_D$  orbit similarity criterion.

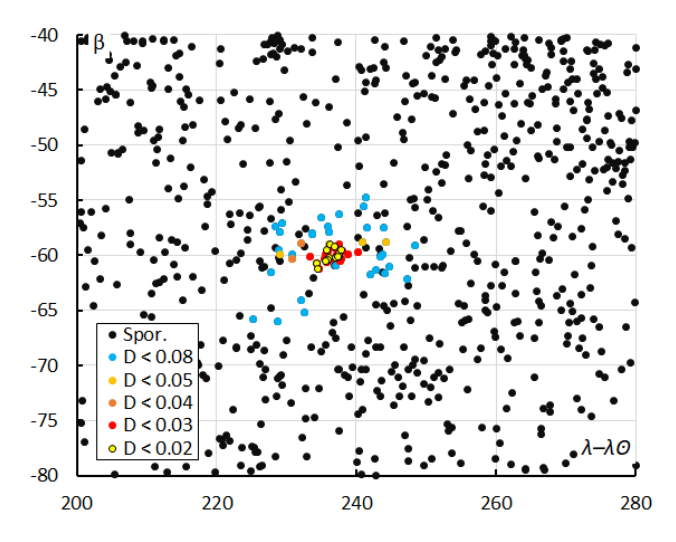


Figure 9 – The radiant distribution during the solar-longitude interval  $161^{\circ} - 172^{\circ}$  in Sun-centered geocentric ecliptic coordinates, color coded for five threshold values of the  $D_D$  orbit similarity criterion.

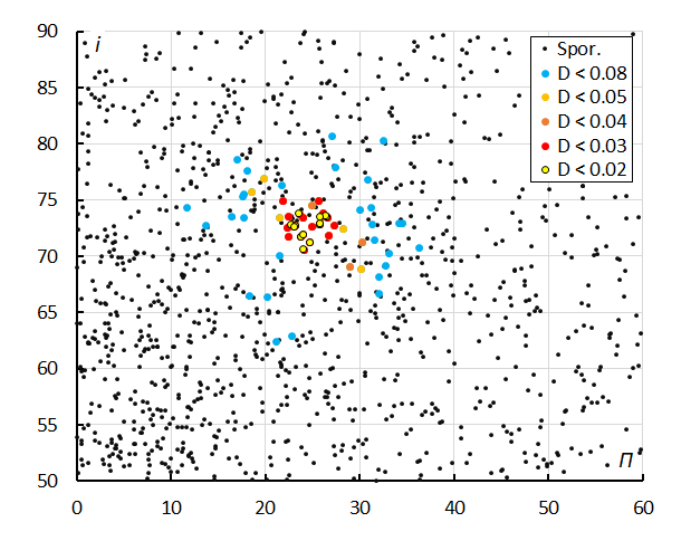


Figure 10 – The diagram of the inclination i versus the longitude of perihelion  $\Pi$  color coded for five classes of D criterion threshold.

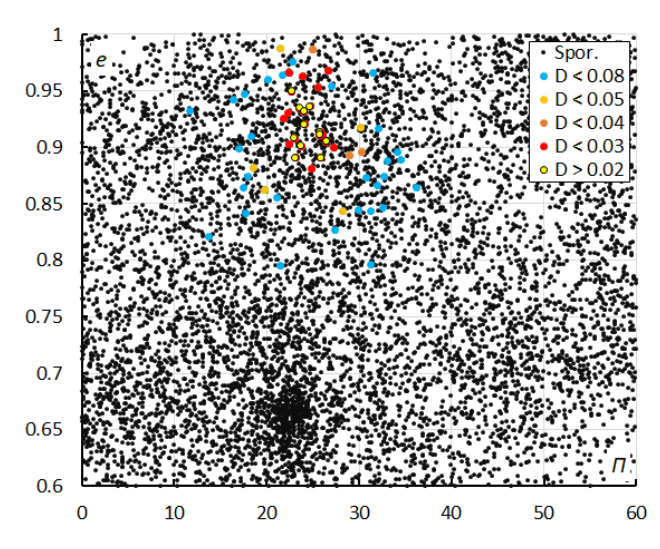


Figure 11 – Diagram of eccentricity e versus the longitude of perihelion  $\Pi$ , color coded for different threshold classes of the orbit similarity criteria.

Figure 10 shows inclination i against the longitude of perihelion II. The delta-Horologiids appear well concentrated in inclination and in longitude of perihelion. Figure 11 shows that there is more dispersion in eccentricity against longitude of perihelion. The blue dots are associations that fit the threshold class with  $D_{SH} < 0.2$  &  $D_D < 0.08$  &  $D_J < 0.2$  and appear to be outliers, indicating that the cutoff value  $D_D < 0.05$  obtained from the Rayleigh distribution fit is valid. The concentration below DHO#1146 are the chi-Cygnids (CCY#757) and the newly discovered M2025-S1 meteors. Figure 12 shows the distribution of eccentricity versus inclination.

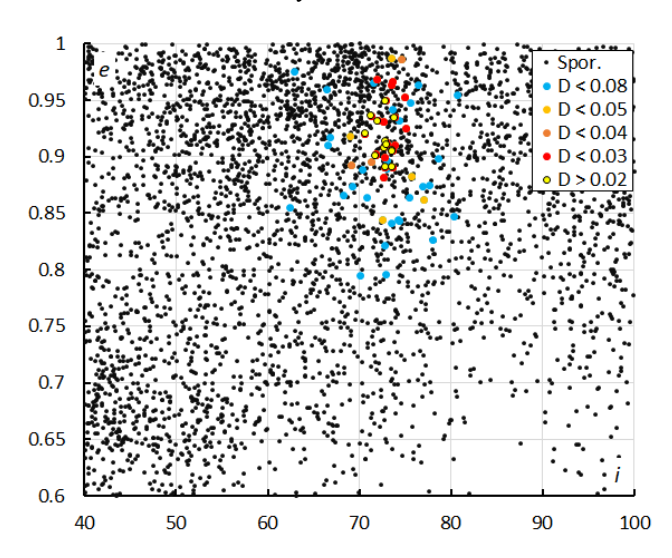


Figure 12 – Diagram of eccentricity e versus inclination i, color coded for different threshold classes of the orbit similarity criteria.

### 4 Comparing both methods

The first method mainly looks at the radiant positions for the classification. When we apply the D-criteria, 28 of the 34 selected meteors fulfill the threshold values of  $D_{SH} < 0.125$ ,  $D_D < 0.05$  and  $D_J < 0.125$  for the mean orbit obtained by the GMN method, an outlier at  $\lambda_O = 161.07^\circ$  fails completely in the D-criteria. The activity period probably starts after  $\lambda_O = 163^\circ$ .

26 meteors were identified as DHO#1146 by both methods, eight were found by the GMN method but ignored by the D-criteria method. Five were found by the D-criteria method but ignored by the GMN method. Despite the difference between the samples based on the two different methods, the final mean orbits are in very good agreement although the method based on D-criteria thresholds tends to select slightly faster meteors.

## 5 Orbit and parent body

Figure 13 shows the orbits for the different solutions in the inner solar system. The dust of DHO#1146 crosses the Earth orbit at its ascending node. Meteoroids hit the Earth from deep south of the ecliptic. With an inclination of about 72° the orbital plane of this meteoroid stream is very steep on the ecliptic. The descending node crosses the ecliptic plane relatively close to the orbit of Jupiter.

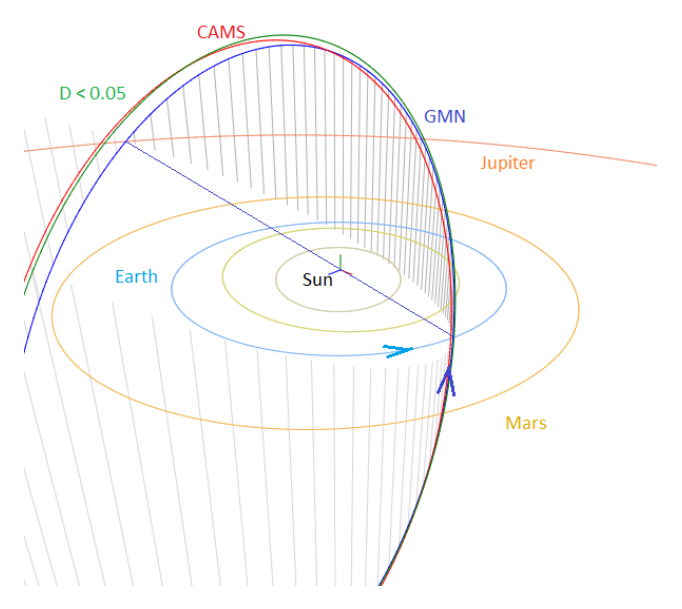


Figure 13 – Comparing the mean orbits for different solutions, blue is based on the GMN method, green for the D-criteria method with  $D_D < 0.05$  and red for CAMS data in *Table 1*, close-up at the inner Solar System. (Plotted with the Orbit visualization app provided by Pető Zsolt).

The Tisserand's parameter relative to Jupiter,  $T_j$  identifies the orbit as of a Mellish-type toroidal shower, because of its high inclination, named after comet C/1917 F1 (Mellish) which was the first numbered of this type. A parent-body search top 10 includes candidates with a threshold for the Drummond  $D_D$  criterion value lower than 0.26 (*Table 2*). It would be up to meteoroid stream modelers to reconstruct the dynamic orbit evolution to see if any of these objects might be dynamically related to this shower. The ablation height in the atmosphere is relatively high and indicate fragile cometary material.

The orbital parameters obtained by GMN in 2025 agree fairly well with the solution published for CAMS by Peter Jenniskens (2023). The orbital parameters derived from SAAMER radar data do not correspond, either these refer to another dust population or reflect some instrumental bias.

Table 1 – Comparing CAMS to GMN 2025 solutions derived by two different methods, the parameters under  $D_D < 0.05$  were derived from the method described in Section 3.

	GMN 2025	$D_D < 0.05$	CAMS
λο (°)	168.5	167.9	168.5
λο <sub>b</sub> (°)	160.0	163.0	163
$\lambda_{\mathcal{O}e}$ (°)	175.0	171.6	173
$\alpha_g$ (°)	61.4	61.2	60.8
$\delta_g$ (°)	-40.6	-40.8	-40.0
$\Delta \alpha_g$ (°)	+0.62	+0.59	+0.10
$\Delta\delta_{g}\left(^{\circ} ight)$	+0.25	+0.13	+0.77
$v_g$ (km/s)	42.9	43.2	43.6
$H_b$ (km)	106.3	106.6	108.0
$H_e$ (km)	93.1	93.0	92.0
$H_p$ (km)	100.1	100.8	100.3
$Mag_{Ap}$	-0.1	-0.4	-
$\lambda_g$ (°)	44.15	43.9	43.76
$\lambda_g - \lambda_O$ (°)	235.65	236.2	235.26
$eta_g$ (°)	-59.56	-59.9	-58.8
a (A.U.)	8.782	11.3	13.6
q (A.U.)	0.902	0.910	0.907
e	0.897	0.919	0.935
i (°)	72.4	72.7	74.1
ω (°)	38.3	36.8	37.4
$arOmega\left(^{\circ} ight)$	347.8	348.0	348.5
П(°)	26.2	24.8	25.2
$T_j$	0.94	0.81	0.71
N	34	31	66

Table 2 – Top ten matches of a search for possible parent bodies with  $D_D < 0.26$ .

····	
Name	$D_D$
C/1932 P1 (Peltier-Whipple)	0.083
35P/Herschel-Rigollet	0.136
2010 QE2	0.147
2022 KL8	0.226
C/1900 O1 (Borrelly-Brooks)	0.227
C/1984 V1 (Levy-Rudenko)	0.228
161P/Hartley-IRAS	0.236
2018 ND1	0.244
C/390 Q1	0.253
C/1982 M1 (Austin)	0.258

## 6 Past years activity

In 2024 Global Meteor Network detected 40 DHO#1146 meteors with  $D_{SH} < 0.125$ ,  $D_D < 0.05$  and  $D_J < 0.125$ , eleven were detected in 2023, four in 2022 and nothing in the years before. These numbers say more about the Global

A search through older visual observations shows it has been detected in the past by visual observers. Cuno Hoffmeister was the first who had at least four radiants possibly related to this activity when he was in Namibia in 1937–1938. Dedicated meteor observers such as R. MacIntosh (1926–1935) and J. Morgan (1972–1981) in New Zealand didn't notice any activity, most likely because both did very little observing from mid-August to late September.

In Australia, Shinkfield from Adelaide observed this activity on one occasion on the night of 8 September 1948 ( $\lambda_{\rm O}=166^{\circ}$ ) with a radiant at RA 61° and Dec  $-40^{\circ}$ , mentioning in a letter that there was a burst of activity reaching 5 per hour that night. Maurice Clark's group recorded them in 1979 when one of his observers, Andrew Pearce, recorded a radiant from RA 60° and Dec.  $-45^{\circ}$  in the predawn hours of 9 September ( $\lambda_{\rm O}=166^{\circ}$ ) and again on 12 September ( $\lambda_{\rm O}=169^{\circ}$ ) with a radiant at RA 64° and Dec.  $-43^{\circ}$ .

WAMS/NAPOMS observers detected them as delta-Horologiids on several occasions from 1979 to 1998. In summary meteors were recorded from around 2 September through to 17 September with what appears to be a maximum ZHR being between 2 and 4 per hour. The mean radiant position at maximum was RA 62° and Dec. –44°.

## 7 Conclusion

Global Meteor network observations confirm the existence of the minor meteor shower known as the delta-Horologiids and first reported by Peter Jenniskens based on CAMS lowlight video cameras. Visual observers noticed weak activity from this source in the past.

The solution derived from GMN data for 2025 is in good agreement with the result published for CAMS-data, but differs a lot from orbit parameters based on SAAMER radar data as published in Jenniskens (2023)..

## Acknowledgment

This report is based on the data of the Global Meteor Network (Vida et al., 2020a; 2020b; 2021) which is released under the CC BY 4.0 license<sup>17</sup>. We thank all 825 participants in the Global Meteor Network project for their contribution and perseverance. A list with the names of the volunteers who contribute to GMN has been published in the 2024 annual report (Roggemans et al., 2025).

382

Meteor Network expansion at the Southern Hemisphere than about the shower activity since the number of cameras increased a lot since 2021. No other camera network data is publicly available to check this Southern Hemisphere activity.

<sup>&</sup>lt;sup>17</sup> https://creativecommons.org/licenses/by/4.0/

### References

- Drummond J. D. (1981). "A test of comet and meteor shower associations". *Icarus*, **45**, 545–553.
- Jenniskens P. (2023). Atlas of Earth's meteor showers. Elsevier, Cambridge, United states. ISBN 978-0-443-23577-1. Page 199.
- Jopek T. J. (1993). "Remarks on the meteor orbital similarity D-criterion". *Icarus*, **106**, 603–607.
- Jopek T. J., Rudawska R. and Pretka-Ziomek H. (2006). "Calculation of the mean orbit of a meteoroid stream". Monthly Notices of the Royal Astronomical Society, 371, 1367–1372.
- Moorhead A. V., Clements T. D., Vida D. (2020). "Realistic gravitational focusing of meteoroid streams". Monthly Notices of the Royal Astronomical Society, 494, 2982–2994.
- Roggemans P., Johannink C. and Campbell-Burns P. (2019). "October Ursae Majorids (OCU#333)". eMetN Meteor Journal, 4, 55–64.
- Roggemans P., Campbell-Burns P., Kalina M., McIntyre M., Scott J. M., Šegon D., Vida D. (2025). "Global Meteor Network report 2024". *eMetN Meteor Journal*, **10**, 67–101.

- Southworth R. B. and Hawkins G. S. (1963). "Statistics of meteor streams". *Smithsonian Contributions to Astrophysics*, 7, 261–285.
- Vida D., Gural P., Brown P., Campbell-Brown M., Wiegert P. (2020a). "Estimating trajectories of meteors: an observational Monte Carlo approach I. Theory". Monthly Notices of the Royal Astronomical Society, 491, 2688–2705.
- Vida D., Gural P., Brown P., Campbell-Brown M., Wiegert P. (2020b). "Estimating trajectories of meteors: an observational Monte Carlo approach II. Results". Monthly Notices of the Royal Astronomical Society, 491, 3996–4011.
- Vida D., Šegon D., Gural P. S., Brown P. G., McIntyre M.
  J. M., Dijkema T. J., Pavletić L., Kukić P., Mazur M.
  J., Eschman P., Roggemans P., Merlak A., Zubrović D. (2021). "The Global Meteor Network Methodology and first results". Monthly Notices of the Royal Astronomical Society, 506, 5046–5074.

# **August 2025 CARMELO report**

Mariasole Maglione<sup>1</sup>, Lorenzo Barbieri<sup>2</sup>

<sup>1</sup>GAV, Gruppo Astrofili Vicentini, Italy mariasole@astrofilivicentini.it

<sup>2</sup> CARMELO network and AAB: Associazione Astrofili Bolognesi, Italy

carmelometeor@gmail.com

The CARMELO network (Cheap Amateur Radio Meteor Echoes LOgger) is a collaboration of SDR radio receivers aimed at detecting meteor echoes. This report presents the data for August 2025.

### 1 Introduction

August is the month of the Perseids. This year, although the shower is as scattered as ever, a peak in meteor activity was recorded on the night of August 13.

### 2 Methods

The CARMELO network consists of SDR radio receivers. In them, a microprocessor (Raspberry) performs three functions simultaneously:

- By driving a dongle, it tunes the frequency on which the transmitter transmits and tunes like a radio, samples the radio signal and through the FFT (Fast Fourier Transform) measures frequency and received power.
- By analyzing the received data for each packet, it detects meteor echoes and discards false positives and interference.
- It compiles a file containing the event log and sends it to a server.

The data are all generated by the same standard, and are therefore homogeneous and comparable. A single receiver can be assembled with a few devices whose total current cost is about 210 euros.

To participate in the network read the instructions on this page<sup>18</sup>.

## 3 August data

In the plots that follow, all available at this page<sup>19</sup>, the abscissae represent time, which is expressed in UT (Universal Time) or in solar longitude (Solar Long), and the ordinates represent the hourly rate, calculated as the total number of events recorded by the network in an hour divided by the number of operating receivers.

In *Figure 1*, the trend of signals detected by the receivers for the month of August.

### 4 Perseids

The Perseids (PER) are one of the most famous and spectacular meteor showers of the year, active from late July until almost the end of August. Peak activity occurs around mid-August, but the shower is notable for its rather long duration: the meteors can be observed for several weeks, making it a widespread phenomenon that is not limited to a single night.

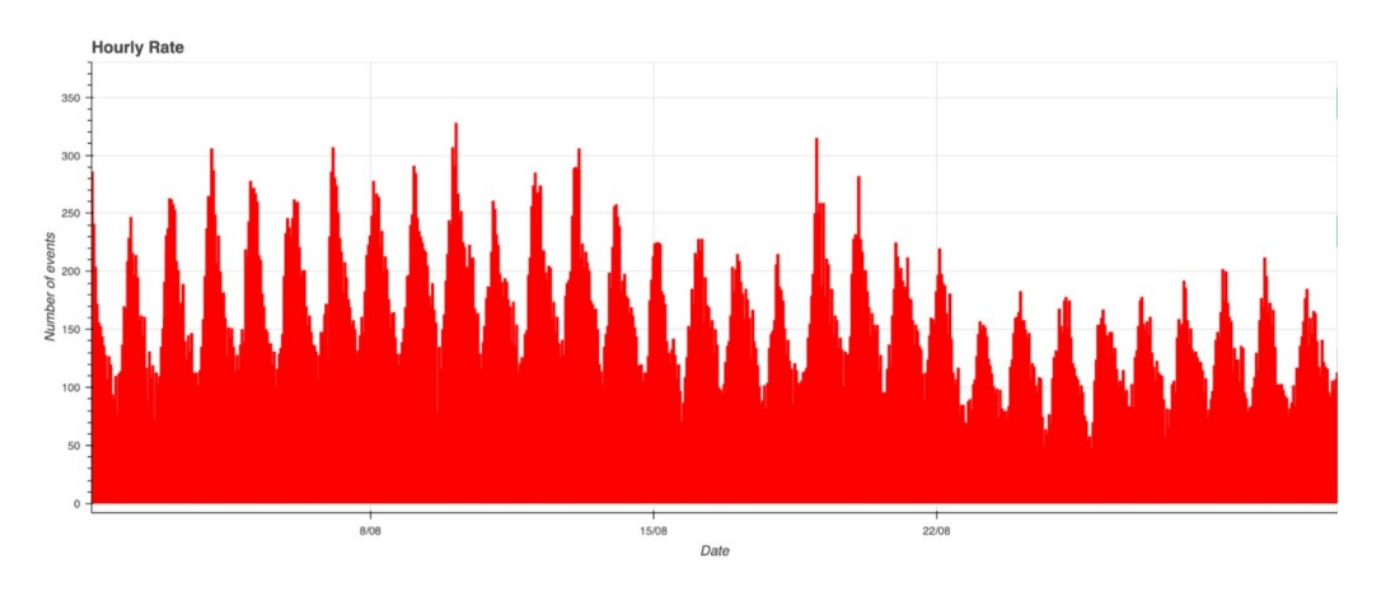


Figure 1 – August 2025 data trend.

<sup>18</sup> http://www.astrofiliabologna.it/about carmelo

<sup>&</sup>lt;sup>19</sup> http://www.astrofiliabologna.it/graficocarmelohr

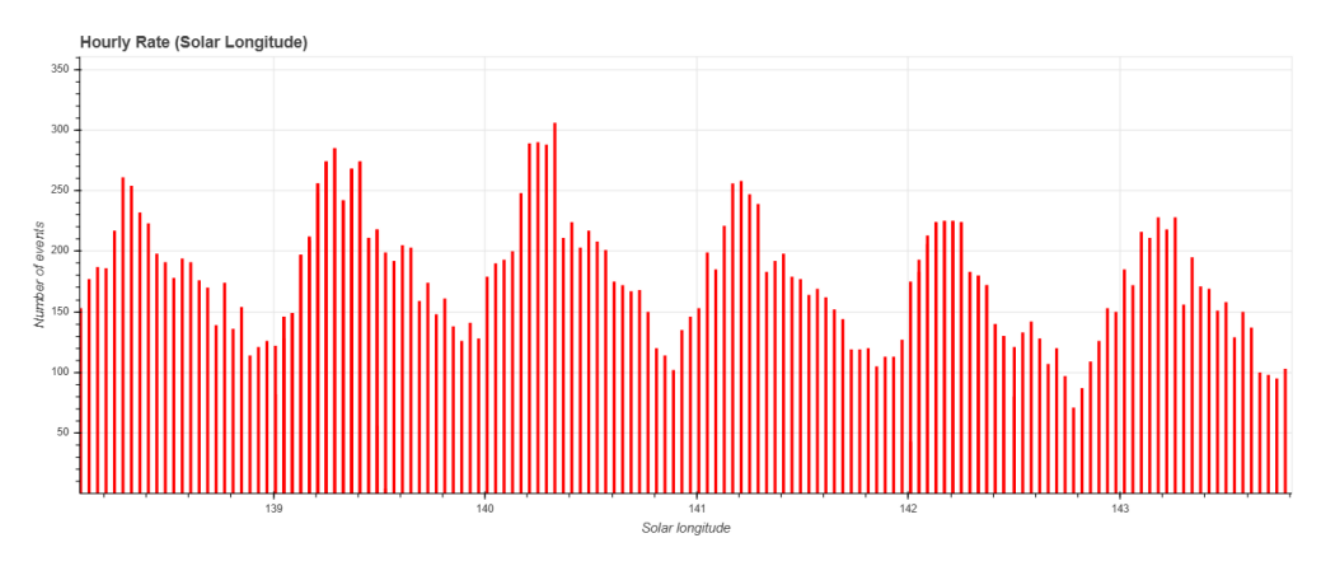


Figure 2 – Maximum meteor activity recorded between solar longitudes 140.1° and 140.4°.

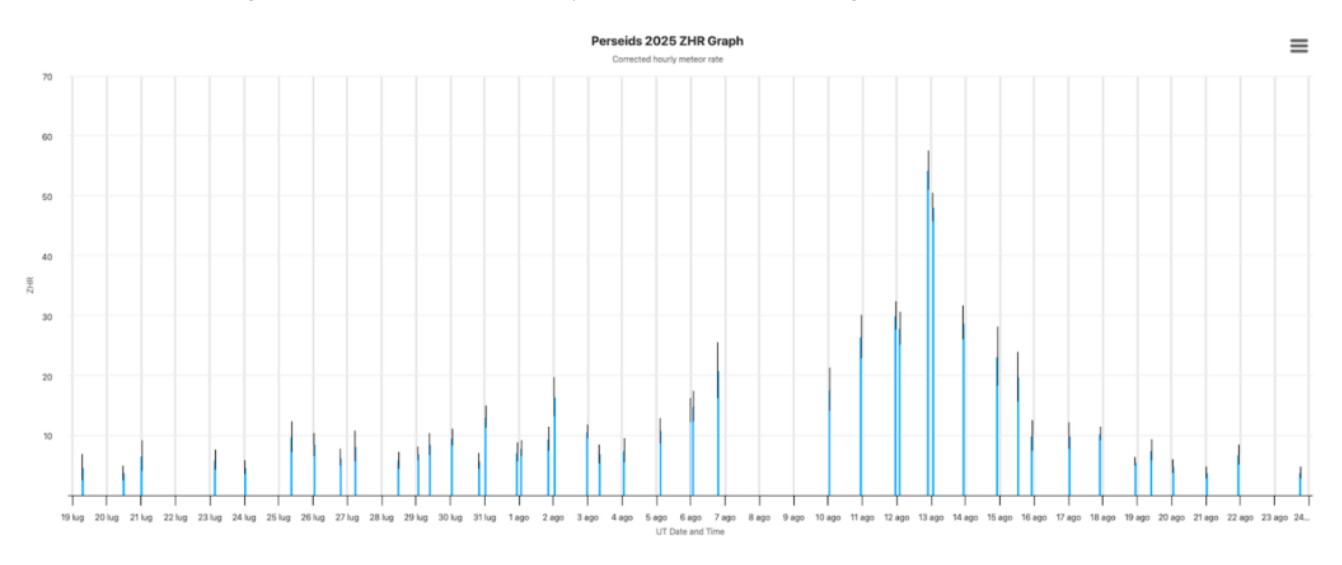


Figure 3 – Plot of the ZHR (Zenithal Hourly Rate) recorded by IMO.

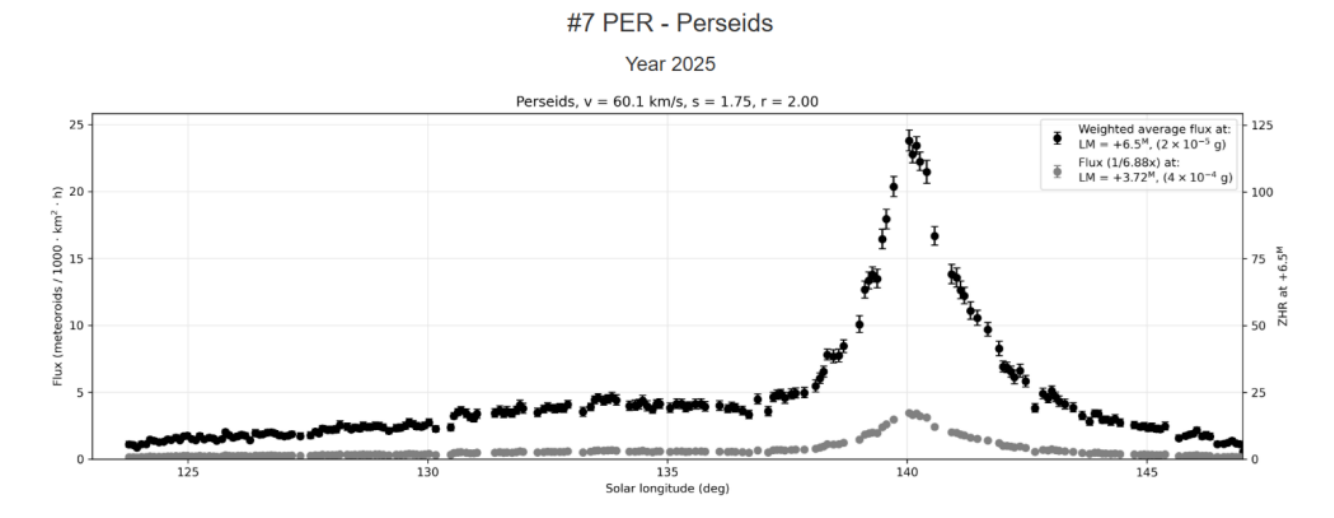


Figure 4 – Plot of the meteoroid flux in the atmosphere recorded by GMN cameras.

The Perseids originate from debris left behind by the comet Swift-Tuttle, which the Earth encounters every year at this time. The radiant is located in the Perseus constellation, from which the shower takes its name. The meteors are particularly fast, with an entry speed into the atmosphere of about 61 km/s, and produce bright and persistent trails,

often accompanied by traces of ionization that are easily detectable even through radio observations.

This year, the CARMELO network recorded the highest activity of the swarm on the night of August 13, lasting about 5–6 hours, between solar longitudes  $140.1^{\circ}$  and  $140.4^{\circ}$ , as shown in *Figure 2*.

Visual observations from the International Meteor Organization (IMO)<sup>20</sup>, shown in *Figure 3*, and camera data from the Global Meteor Network  $(GMN)^{21}$ , shown in *Figure 4*, also indicate a peak in the shower's activity around August 13.

Returning to our radio data, we observe an increase around  $08^{h}00^{m}$ – $09^{h}00^{m}$  UT on August 12, both in the received power plot (*Figure 5*) and in the meteor echo duration plot (*Figure 6*).

We know that the duration of a radio echo depends on the time required for the meteor trail to dissipate (saturation of the cylinder): the greater the number of ionized atoms, the longer the deionization process lasts. The number of ionized atoms is also proportional to the kinetic energy of the bodies colliding with the upper layers of the ionosphere: the more

energetic the impact, the more atoms are disintegrated, and consequently the denser the radio meteor appears.

Since kinetic energy is given by:

$$E_c = \frac{1}{2}mv^2$$

and since all meteors belonging to the same shower move at the same velocity v, it follows that the only varying parameter is m, namely the mass.

Therefore, we can hypothesize that around  $08^h00^m-09^h00^m$  UT on August 12, at solar longitude 139.57°, an increase in kinetic energy was measured. This suggests that meteoroids of greater mass than the average Perseids entered the atmosphere, about thirty hours in advance of the peak hourly rate.

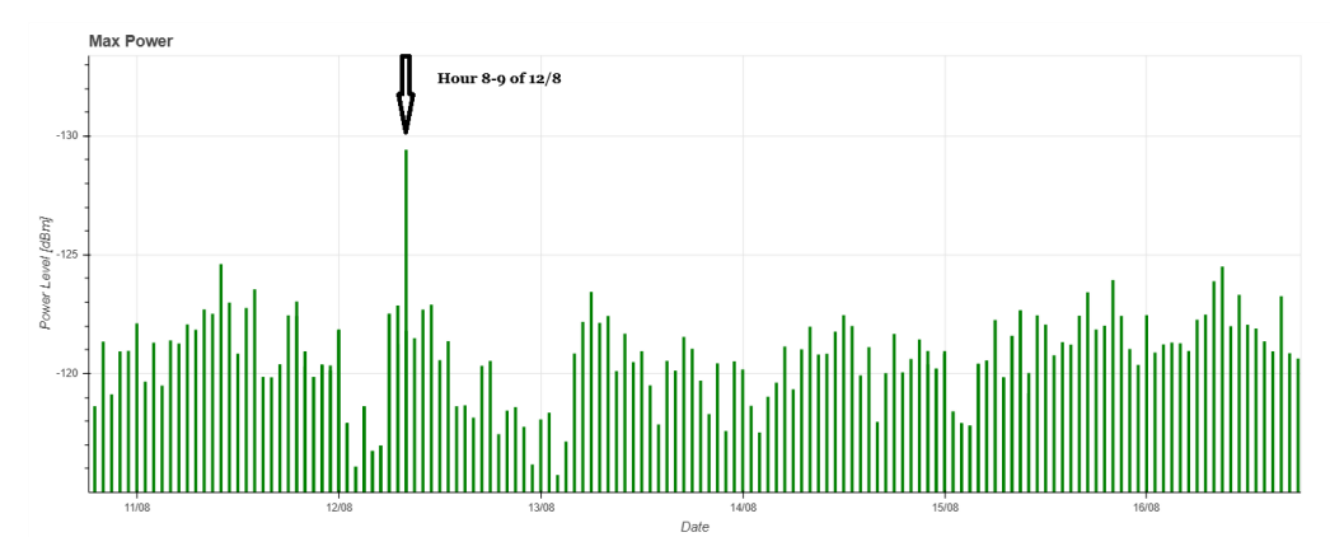


Figure 5 – Plot of the meteor echo power showing a peak at solar longitude 139.57°.

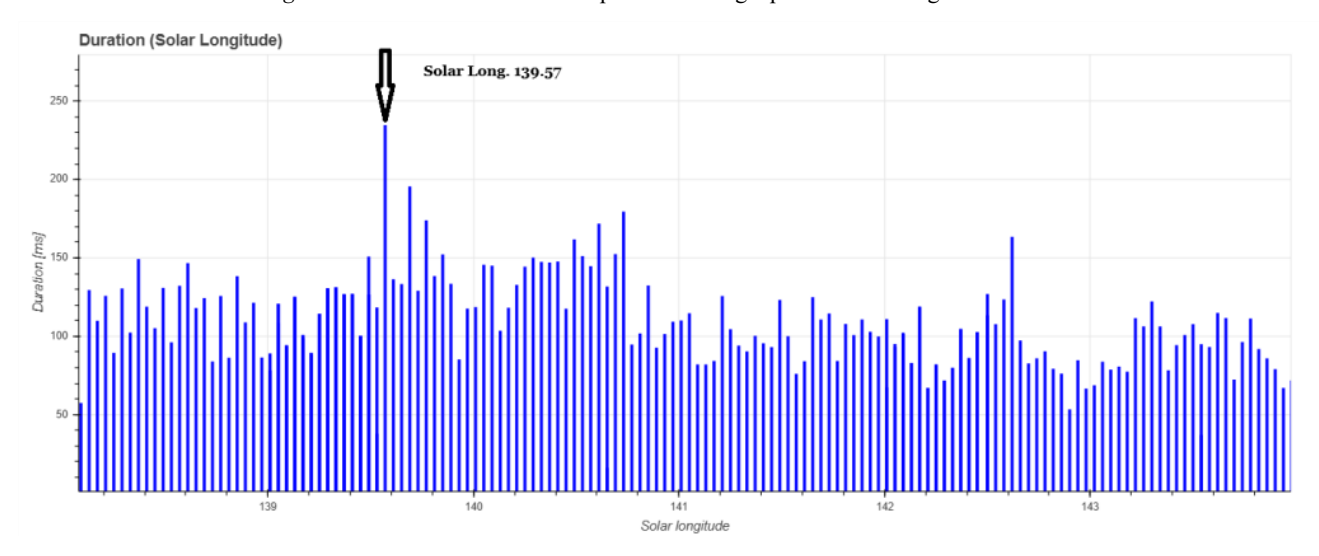


Figure 6 – Plot of the meteor echo duration showing a peak at solar longitude 139.57°.

### 5 The CARMELO network

The network currently consists of 14 receivers, 13 of which are operational, located in Italy, the UK, Croatia and the USA. The European receivers are tuned to the Graves radar

station frequency in France, which is 143.050 MHz. Participating in the network are:

- Lorenzo Barbieri, Budrio (BO) ITA;
- Associazione Astrofili Bolognesi, Bologna ITA;

<sup>&</sup>lt;sup>20</sup> International Meteor Organization

<sup>&</sup>lt;sup>21</sup> Global Meteor Network

- Associazione Astrofili Bolognesi, Medelana (BO) ITA:
- Paolo Fontana, Castenaso (BO) ITA;
- Paolo Fontana, Belluno (BL) ITA;
- Associazione Astrofili Pisani, Orciatico (PI) ITA;
- Gruppo Astrofili Persicetani, San Giovanni in Persiceto (BO) ITA;
- Roberto Nesci, Foligno (PG) ITA;
- MarSEC, Marana di Crespadoro (VI) ITA;
- Gruppo Astrofili Vicentini, Arcugnano (VI) ITA;

- Associazione Ravennate Astrofili Theyta, Ravenna (RA) ITA;
- Akademsko Astronomsko Društvo, Rijeka CRO;
- Mike German a Hayfield, Derbyshire UK;
- Mike Otte, Pearl City, Illinois USA.

The authors' hope is that the network can expand both quantitatively and geographically, thus allowing the production of better-quality data.

# **September 2025 CARMELO report**

Mariasole Maglione<sup>1</sup>, Lorenzo Barbieri<sup>2</sup>

<sup>1</sup>GAV, Gruppo Astrofili Vicentini, Italy mariasole@astrofilivicentini.it

<sup>2</sup> CARMELO network and AAB: Associazione Astrofili Bolognesi, Italy

carmelometeor@gmail.com

The CARMELO network (Cheap Amateur Radio Meteor Echoes LOgger) is a collaboration of SDR radio receivers aimed at detecting meteor echoes. This report presents the data for September 2025.

### 1 Introduction

In September, the meteor activity detected by the CARMELO network was moderate and did not allow us to highlight peaks in the activity of specific showers. We therefore decided to take this opportunity to think about the possibility of evaluating, at least qualitatively, the behavior of meteor showers based on the network data.

#### 2 Methods

The CARMELO network consists of SDR radio receivers. In them, a microprocessor (Raspberry) performs three functions simultaneously:

- By driving a dongle, it tunes the frequency on which the transmitter transmits and tunes like a radio, samples the radio signal and through the FFT (Fast Fourier Transform) measures frequency and received power.
- By analyzing the received data for each packet, it detects meteor echoes and discards false positives and interference.
- It compiles a file containing the event log and sends it to a server.

The data are all generated by the same standard, and are therefore homogeneous and comparable. A single receiver can be assembled with a few devices whose total current cost is about 210 euros.

To participate in the network read the instructions on this page<sup>22</sup>.

## 3 September data

In the plots that follow, all available at this page<sup>23</sup>, the abscissae represent time, which is expressed in UT (Universal Time) or in solar longitude (Solar Long), and the ordinates represent the hourly rate, calculated as the total number of events recorded by the network in an hour divided by the number of operating receivers.

In *Figure 1*, the trend of signals detected by the receivers for the month of September.

In September, meteor activity recorded by the CARMELO network was more or less constant. There were no peaks in activity associated with any particular meteor shower.

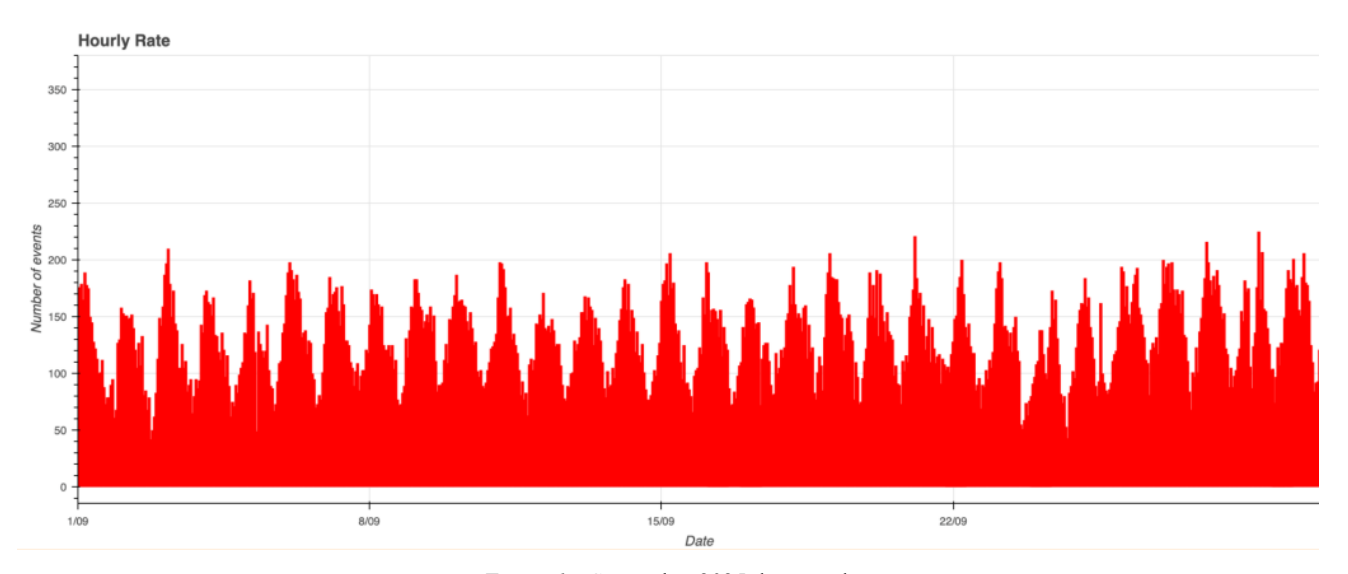


Figure 1 – September 2025 data trend.

<sup>&</sup>lt;sup>22</sup> http://www.astrofiliabologna.it/about carmelo

<sup>&</sup>lt;sup>23</sup> http://www.astrofiliabologna.it/graficocarmelohr

### 4 The behavior of meteor showers

As we have already seen, amateur observation of meteors using radio meteor scatter suffers from the serious limitation of not being able to define orbits. As a result, it is impossible to classify individual meteors.

On the other hand, as is well known, this type of observation is independent of weather conditions and the presence or absence of the Sun or Moon. It can therefore be useful in assessing, at least qualitatively, the behavior of meteor showers. Let us therefore try to hypothesize a use of CARMELO data for this purpose.

Let us assume that a meteor shower, at the moment of its formation, has a homogeneous structure, i.e., that the particles that compose it are uniformly distributed within the cylinder created by the release of dust from the parent body.

As is well known, over time this homogeneity is lost due to certain perturbing forces. The best known of these is the Poynting-Robertson effect. This effect can be explained by the fact that particles heated by the Sun tend to cool down by re-emitting the same energy in the infrared, in all directions.

By examining the average behavior of all particles, thus attributing spherical symmetry to them, if the particle were stationary, the radiation emitted would be the same in all directions, with equal quantity and equal frequency.

However, all particles move in the Solar System at a speed of about 30 km/s, so in the direction of movement, the frequency of the radiation emitted is higher than that emitted in the opposite direction, due to the Doppler effect (Jenniskens, 2006).

According to Planck's law, the famous law underlying quantum mechanics:

$$\varepsilon = h \nu$$

Where e is energy, h is Planck's constant, and  $\nu$  is frequency.

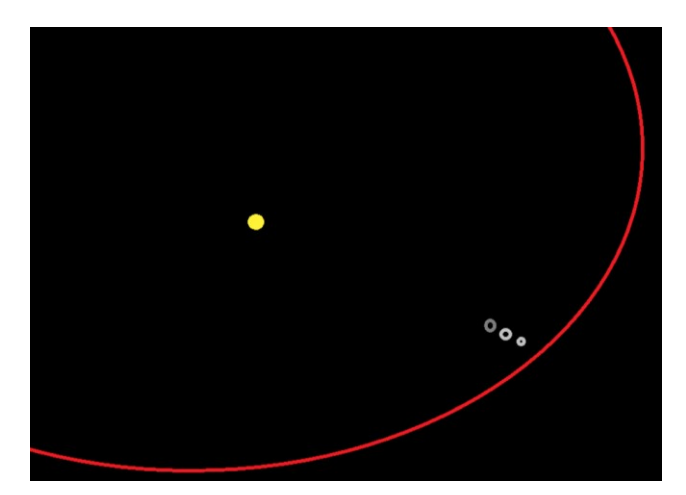


Figure 2 – Differentiation of orbits according to mass.

The energy released in the direction of movement is greater than that released in the opposite direction: it follows, therefore, that the particle undergoes a braking action. This braking action will not be the same for all particles, but will be proportional to their ability to receive and re-emit heat and therefore, among other quantities, to their mass.

The more a body is slowed down, the more its orbit 'tightens', i.e. the axes of the orbit become smaller. It follows that different particles are induced by the Poynting-Robertson effect to differentiate their orbits according to their mass (see *Figure 2*).

Over the years, the shower gradually loses its symmetry. There are two parameters, derived from visual observations, that analytically describe this phenomenon:

- The meteoric flux density.
- The mass index.

The meteor flux density is indicated by  $Q(m_{\theta})$  and is defined as the quantity of meteoroids of mass  $m_{\theta}$  per unit of time, in a unit of area perpendicular to the direction of motion.

For example, for  $m_0 = 10$  mg, we can have  $Q(m_0) = 0.001$  billionths per square meter per second.

The mass index is the exponent (s) in a power distribution of meteoroid masses, a method for modeling the number of meteoroids of different sizes that exist. The formula is:

$$\frac{dN}{dM} = N_0 (\frac{M}{M^*})^{-s}$$

where dN is the number of meteoroids in a mass interval dM,  $N_0$  is a constant,  $M^*$  is a characteristic mass, and s is the mass index (Belkovich et al., 2005).

The following plot shows the comparison between  $Q(m_0)$  and s for a generic shower: the x-axis represents the solar longitude, i.e., time.

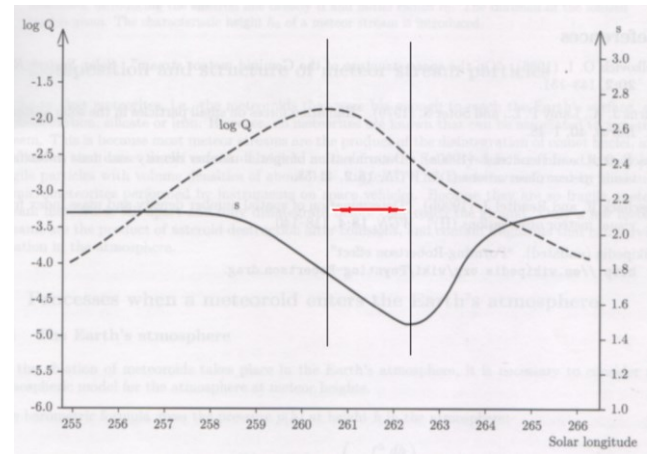


Figure 3 – Comparison between  $Q(m_{\theta})$  and s in a generic meteor shower. (Belkovich et al., 2005).

The difference between the maximum of  $Q(m_{\theta})$  and the maximum of s represents the time interval between the maximum particle density and the maximum of the more

massive particles, and is proportional to the age of the shower: the younger the shower, the more the length of the red arrow in *Figure 3* tends towards zero.

To complicate matters, we must consider the inclination of the orbits, which changes the way the Earth encounters the shower (see *Figure 4*).

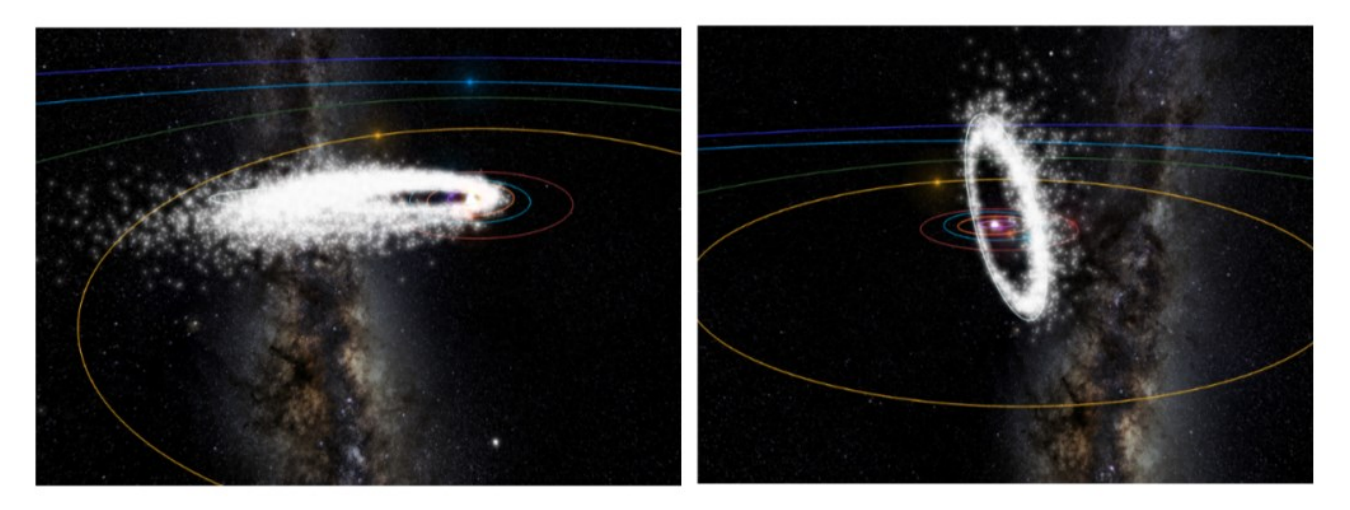


Figure 4 – Low inclination orbit on the ecliptic (left) and high inclination orbit (right, with progenitor body originating from the Kuiper belt).

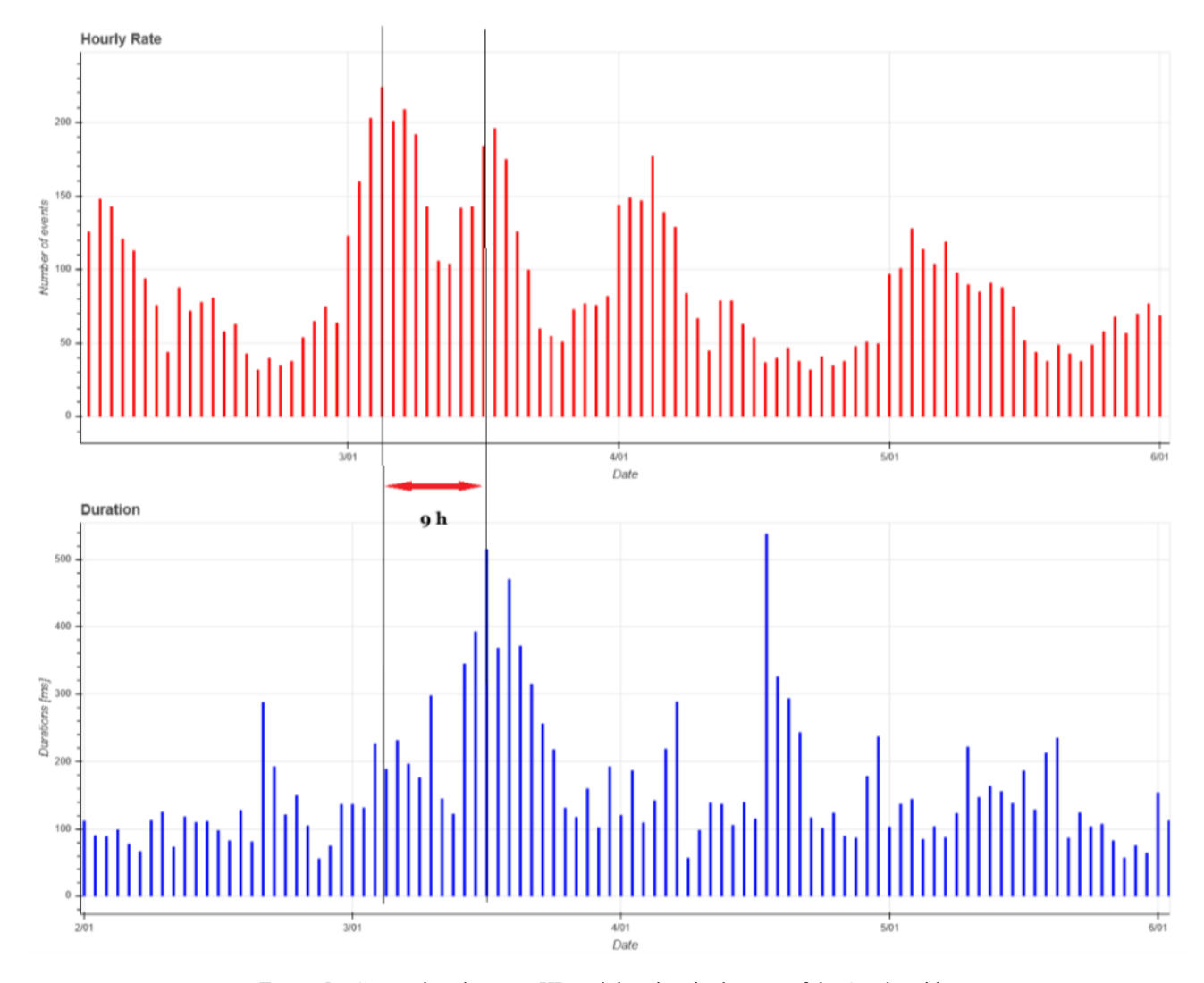


Figure 5 - Comparison between HR and duration, in the case of the Quadrantids.

CARMELO, analyzing the number of recorded events, produces the Hourly Rate (HR, in red here) plot. This plot does not distinguish between different showers or between showers and sporadic meteors, but assuming that on days

when a particular shower is active, the majority of radio meteors recorded belong to that shower, it can be considered, with a high degree of approximation, that this

data is comparable to the  $Q(m_0)$  calculated from visual observations.

The same page also shows the duration plot (in blue), which records the duration of the radio signals received by the CARMELO receivers. These durations depend on the degree of saturation of the cylinder of free electrons formed by the impact of the meteor with the molecules of the ionosphere.

There are many variables that determine the degree of saturation of a radiometeor, including: velocity (squared), mass, cross section (i.e., size), altitude of the point of specular reflection, frequency, transmitter power, receiver impedance, gains of the two antennas, and atmospheric pressure (Belkovich and Verbeeck, 2005).

In order to simplify the search for the predominant quantities, we can roughly state that the share of point P of specular reflection, the frequency, the transmitter power, the receiver impedance, and the gains of the two antennas are always the same, and ignore atmospheric pressure. In the case of a shower, speed can also be ignored, considering that the particles belonging to it impact the atmosphere at the same speed and therefore, even with gross simplifications, we can try to consider the duration of the echoes as comparable to the mass index s.

In *Figure 5*, we propose a comparison between the Hourly Rate and duration in the case of the Quadrantids.

This is a notoriously "young" shower, but even at its age, a noticeable discrepancy between the two maxima can be observed.

Assuming that these considerations have a scientific basis despite the simplifications made, we could also go so far as to estimate the order of magnitude of the distances involved.

Considering that:

$$s = v * t$$

and that the speed v of the Earth in the Solar System is approximately 30 km/s, in 9 hours the distance traveled will be:

$$s = 30*9*60*60 = 972000 \text{ Km}$$

In other words, the shift toward an inner orbit by the most massive particles resulted in a distance between orbits of the order of magnitude of one million kilometers.

The reliability of the comparison we propose here will need to be verified in the future with other showers.

### 5 The CARMELO network

The network currently consists of 14 receivers, 13 of which are operational, located in Italy, the UK, Croatia and the USA. The European receivers are tuned to the Graves radar station frequency in France, which is 143.050 MHz. Participating in the network are:

- Lorenzo Barbieri, Budrio (BO) ITA;
- Associazione Astrofili Bolognesi, Bologna ITA;
- Associazione Astrofili Bolognesi, Medelana (BO) ITA;
- Paolo Fontana, Castenaso (BO) ITA;
- Paolo Fontana, Belluno (BL) ITA;
- Associazione Astrofili Pisani, Orciatico (PI) ITA;
- Gruppo Astrofili Persicetani, San Giovanni in Persiceto (BO) ITA;
- Roberto Nesci, Foligno (PG) ITA;
- MarSEC, Marana di Crespadoro (VI) ITA;
- Gruppo Astrofili Vicentini, Arcugnano (VI) ITA;
- Associazione Ravennate Astrofili Theyta, Ravenna (RA) ITA;
- Akademsko Astronomsko Društvo, Rijeka CRO;
- Mike German a Hayfield, Derbyshire UK;
- Mike Otte, Pearl City, Illinois USA.

The authors' hope is that the network can expand both quantitatively and geographically, thus allowing the production of better-quality data.

## References

Jenniskens P. (2006). Meteor showers and their parent comets. Cambridge University Press.

Belkovich O., Pajovic D., Wislez J M. (2005). "Basic elements of meteor stream theory". *Proceedings of the radio meteor school 2005*, from p. 17.

Belkovich O., Verbeeck C. (2005). "The physics of meteoroid ablation and the formation of ionized meteor trails". *Proceedings of the radio meteor school 2005*, from p. 21.

# Radio meteors August 2025

## Felix Verbelen

### Vereniging voor Sterrenkunde & Volkssterrenwacht MIRA, Grimbergen, Belgium

felix.verbelen@gmail.com

An overview of the radio observations during August is given.

### 1 Introduction

The graphs show both the daily totals (*Figure 1 and 2*) and the hourly numbers (*Figure 3 and 4*) of "all" reflections counted automatically, and of manually counted "overdense" reflections, overdense reflections longer than 10 seconds and longer than 1 minute, as observed here at Kampenhout (BE) on the frequency of our VVS-beacon (49.99 MHz) during the month of August 2025.

The hourly numbers, for echoes shorter than 1 minute, are weighted averages derived from:

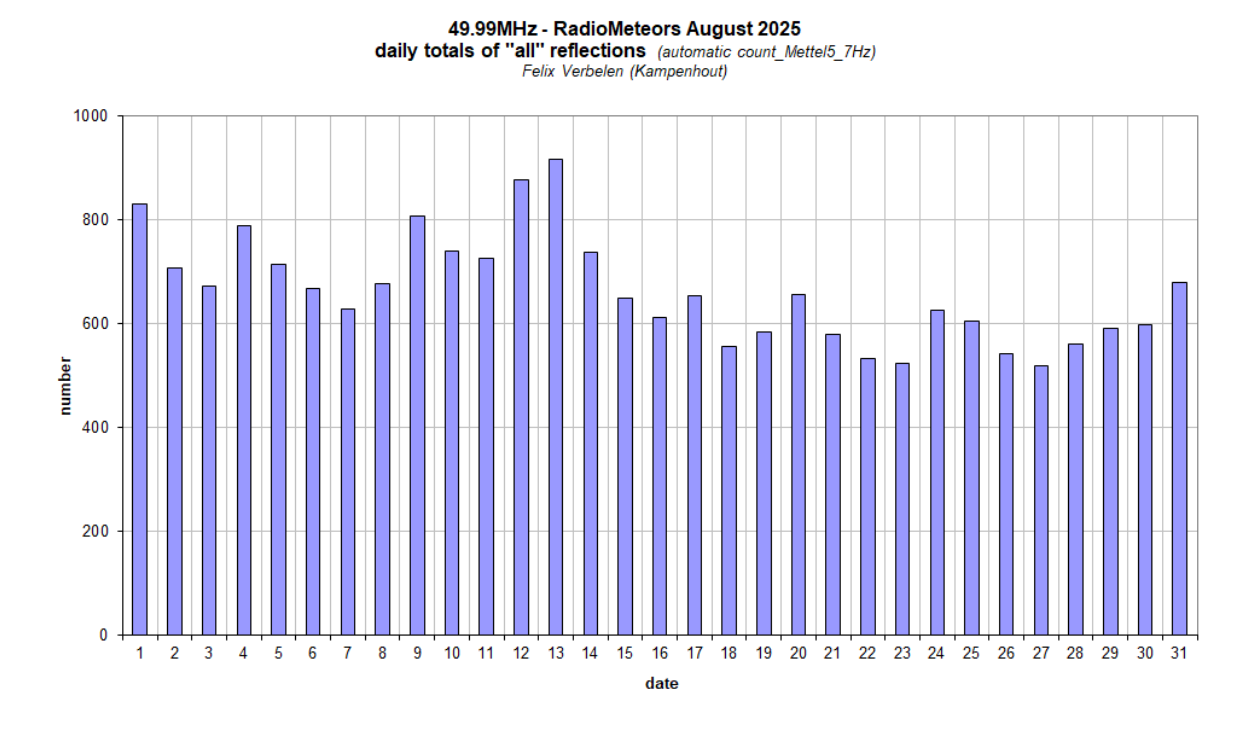
$$N(h) = \frac{n(h-1)}{4} + \frac{n(h)}{2} + \frac{n(h+1)}{4}$$

Local interference and unidentified noise remained quite limited, and some lightning activity was only recorded on 5 days. There were however frequent solar eruptions, mostly of Type III. The highlights of the month were, of course, the Perseids, which, as every year, produced numerous long-lasting reflections. After a start-up period with increased activity in the first part of the month, the shower reached its forecasted maximum on August 12–13, after which activity quickly declined.

Over the entire month, 51 reflections longer than 1 minute were recorded here. *Figures 5 to 46* show a selection, along with some other interesting images. Many more are available upon request.

In addition to the usual graphs, you will also find the raw counts in cvs-format<sup>24</sup> from which the graphs are derived. The table contains the following columns: day of the month, hour of the day, day + decimals, solar longitude (epoch J2000), counts of "all" reflections, overdense reflections, reflections longer than 10 seconds and reflections longer than 1 minute, the numbers being the observed reflections of the past hour.

<sup>&</sup>lt;sup>24</sup> https://www.emeteornews.net/wp-content/uploads/2025/09/202508 49990 FV rawcounts.csv



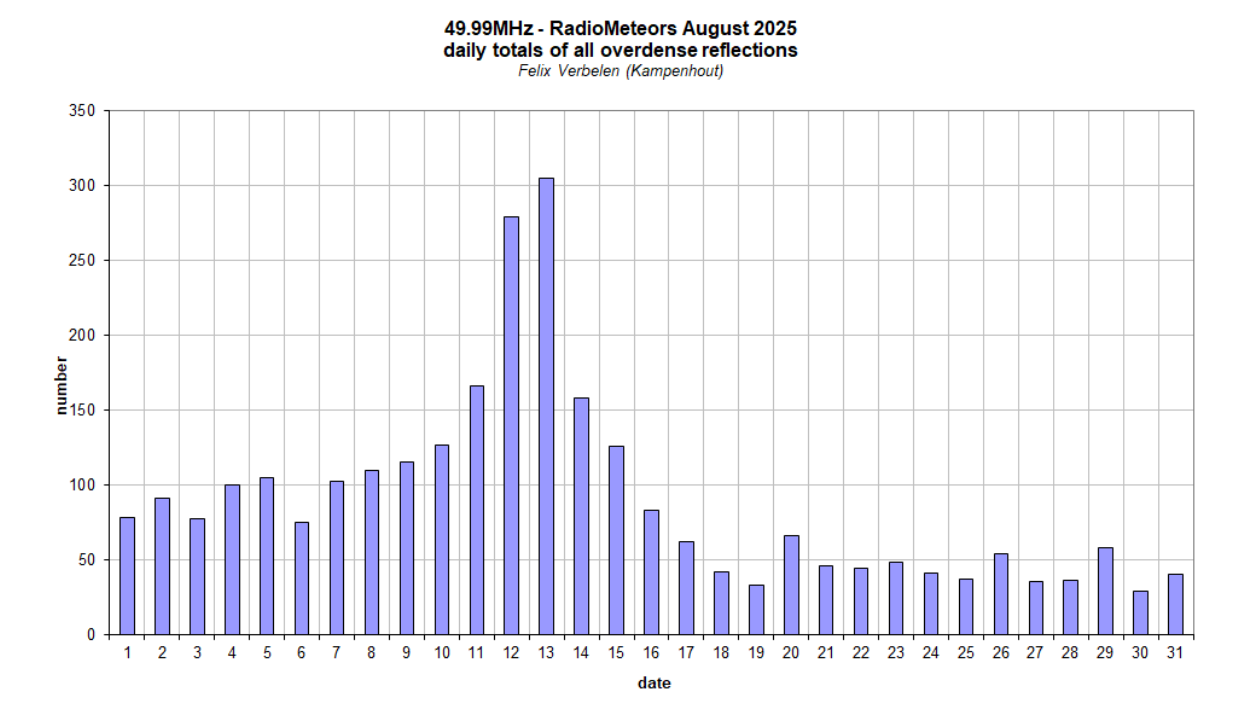
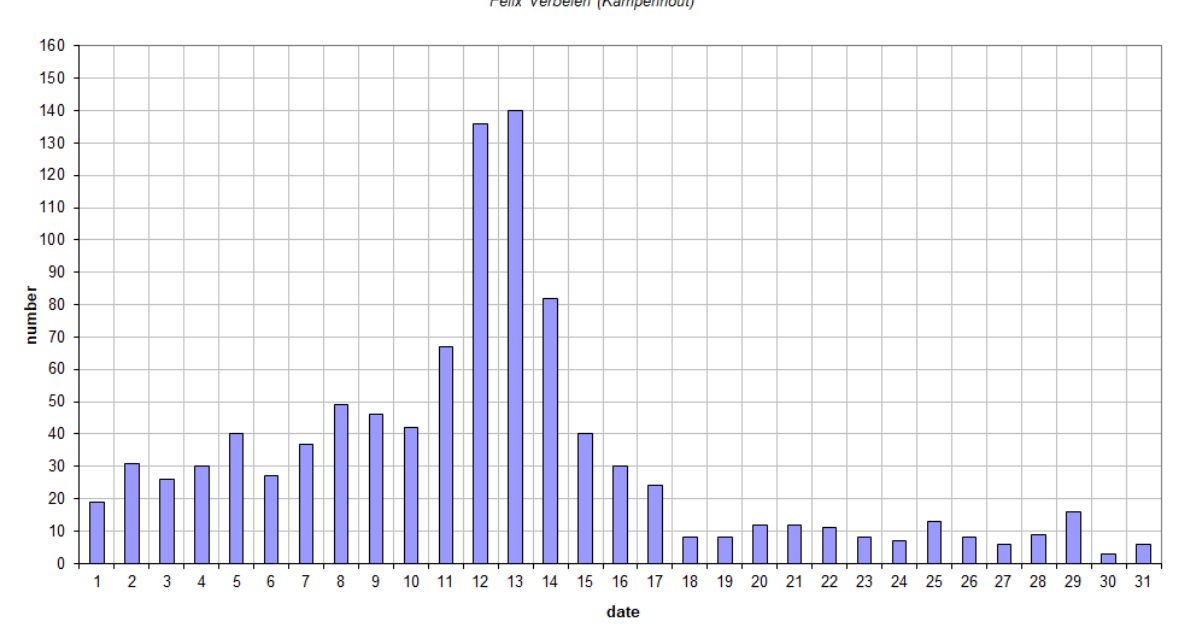


Figure 1 – The daily totals of "all" reflections counted automatically, and of manually counted "overdense" reflections, as observed here at Kampenhout (BE) on the frequency of our VVS-beacon (49.99 MHz) during August 2025.

#### 49.99MHz - RadioMeteors August 2025 daily totals of reflections longer than 10 seconds Felix Verbelen (Kampenhout)



# 49.99MHz - RadioMeteors August 2025 daily totals of reflections longer than 1 minute

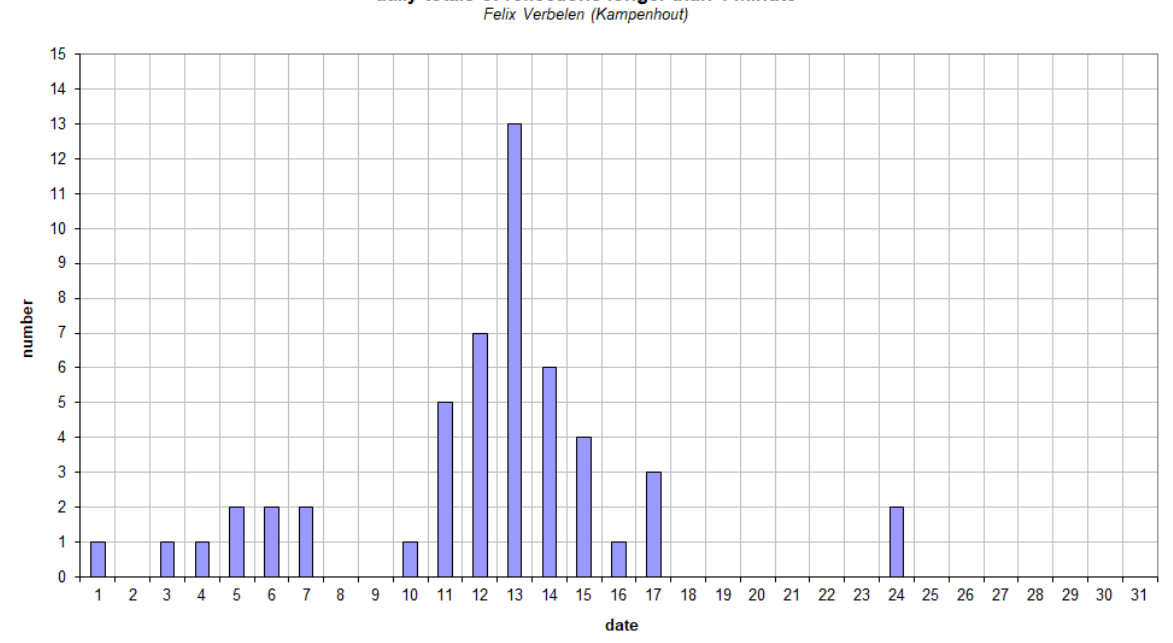
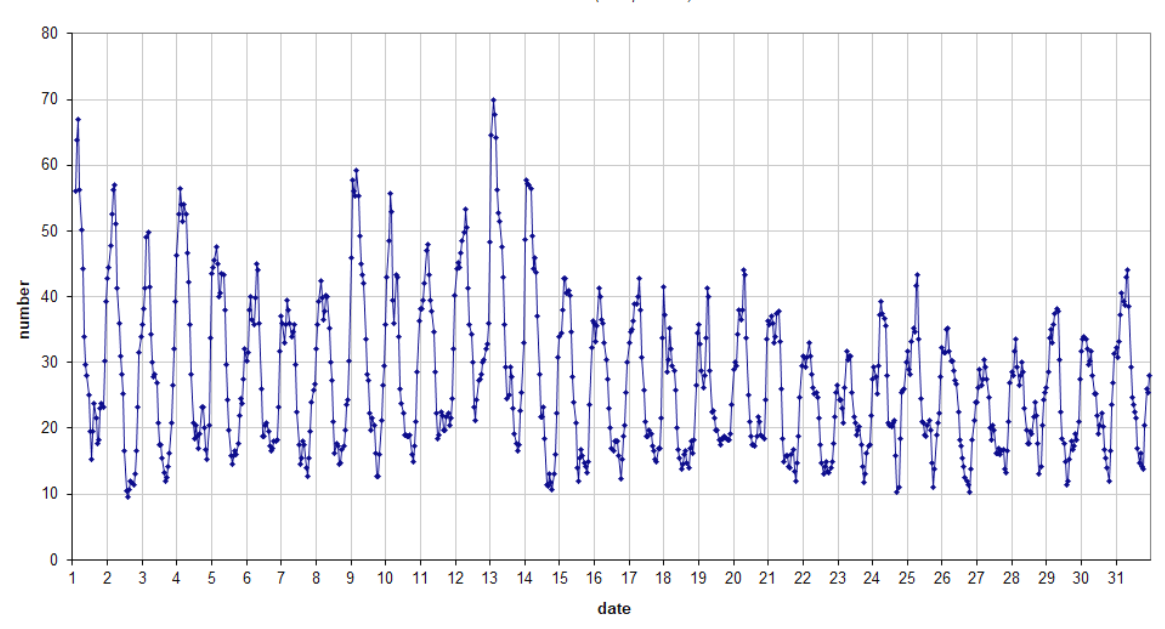


Figure 2 – The daily totals of overdense reflections longer than 10 seconds and longer than 1 minute, as observed here at Kampenhout (BE) on the frequency of our VVS-beacon (49.99 MHz) during August 2025.





#### 49.99MHz - RadioMeteors August 2025 number of overdense reflections per hour (weighted average) Felix Verbelen (Kampenhout)

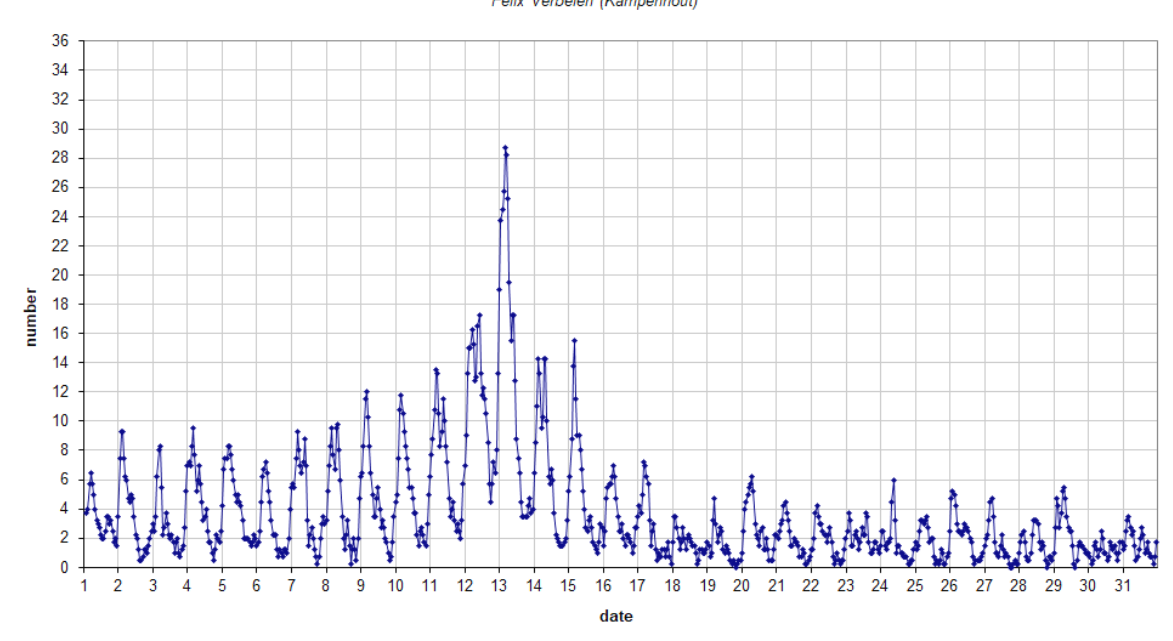
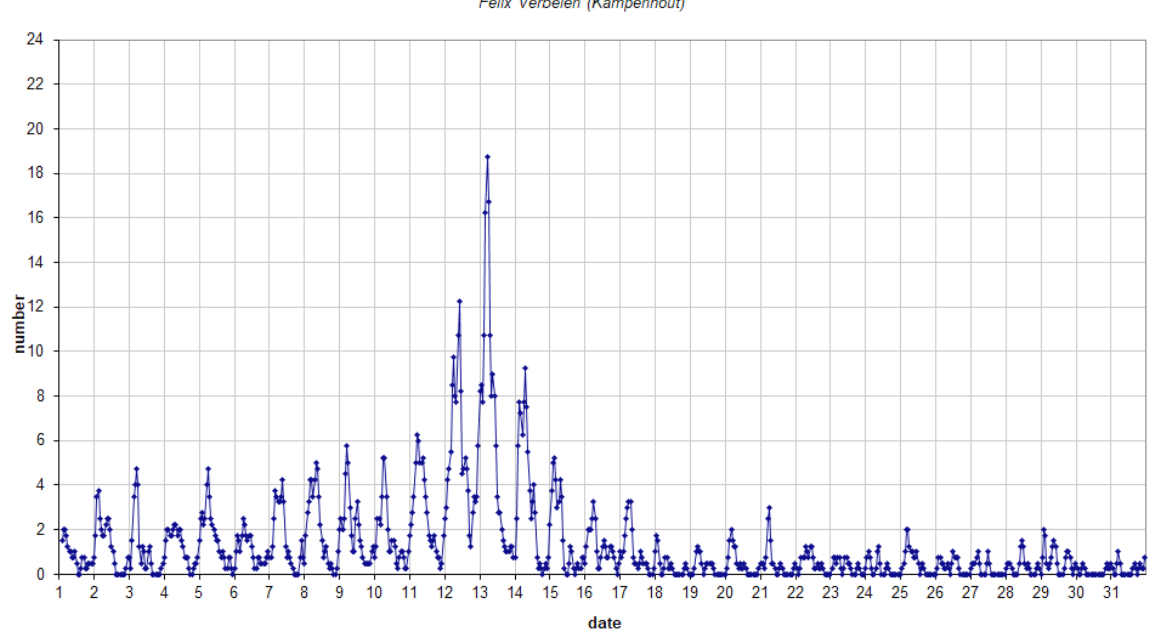


Figure 3 – The hourly numbers of "all" reflections counted automatically, and of manually counted "overdense" reflections, as observed here at Kampenhout (BE) on the frequency of our VVS-beacon (49.99 MHz) during August 2025.

#### 49.99MHz - RadioMeteors August 2025 number of reflections >10 seconds per hour (weighted average) Felix Verbelen (Kampenhout)



#### 49.99MHz - RadioMeteors August 2025 hourly totals of overdense reflections longer than 1 minute Felix Verbelen (Kampenhout/BE)

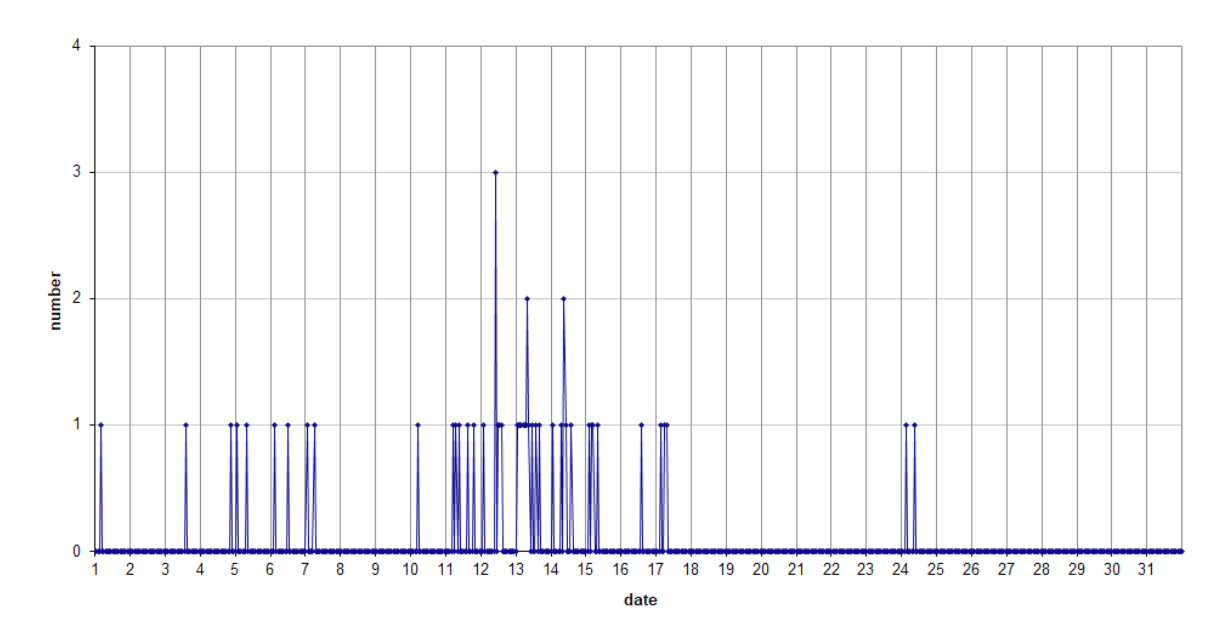


Figure 4 – The hourly numbers of overdense reflections longer than 10 seconds and longer than 1 minute, as observed here at Kampenhout (BE) on the frequency of our VVS-beacon (49.99 MHz) during August 2025.

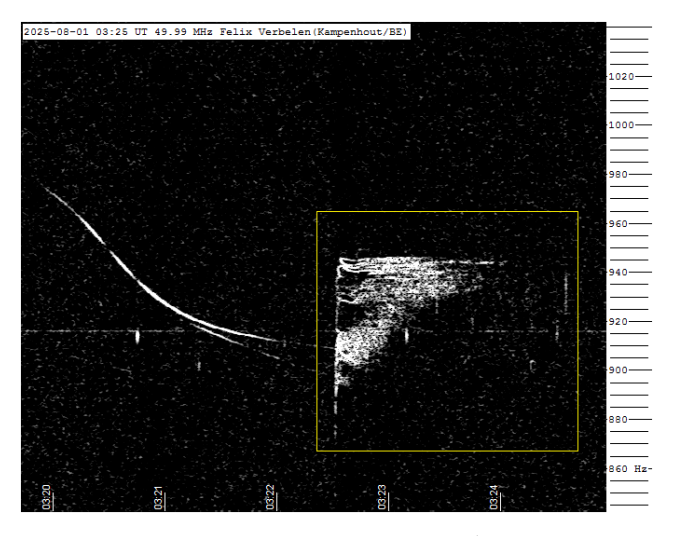


Figure 5 – Meteor echoes August 1, 3<sup>h</sup>25<sup>m</sup> UT.

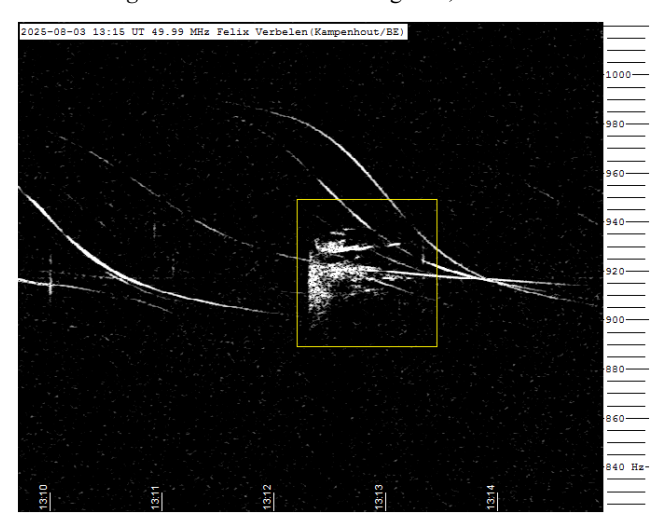


Figure 6 – Meteor echoes August 3, 13<sup>h</sup>15<sup>m</sup> UT.

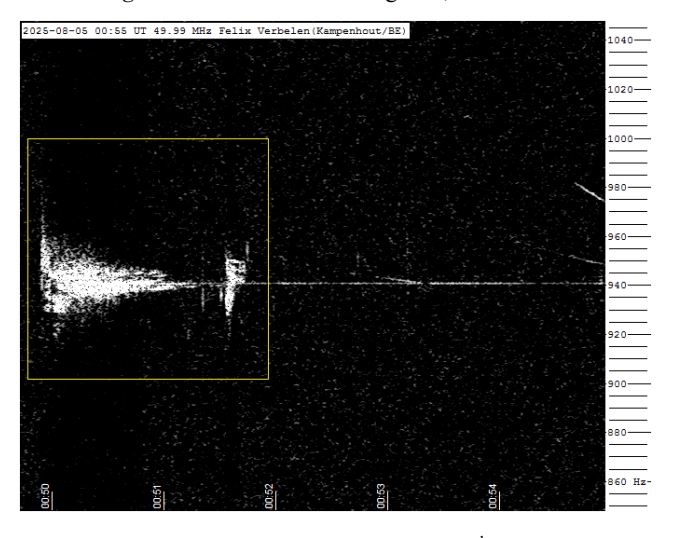


Figure 7 – Meteor echoes August 5, 00<sup>h</sup>55<sup>m</sup> UT.

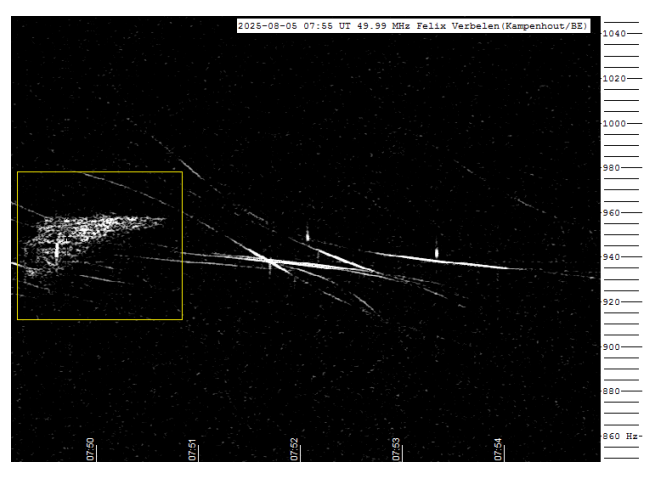


Figure 8 – Meteor echoes August 5, 07h55m UT.

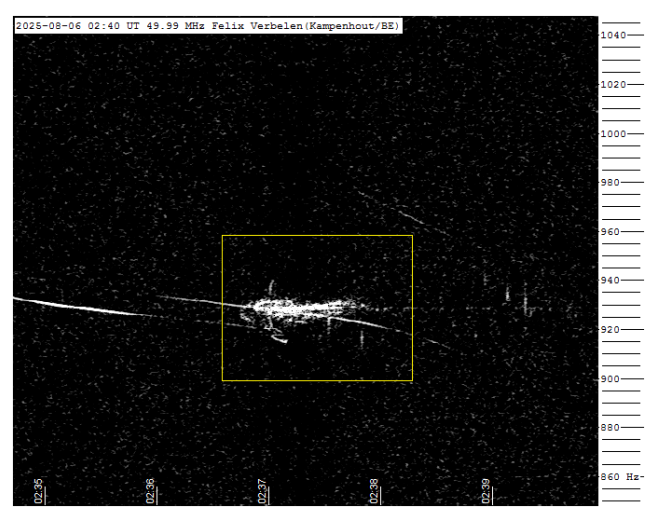


Figure 9 – Meteor echoes August 6, 02<sup>h</sup>40<sup>m</sup> UT.

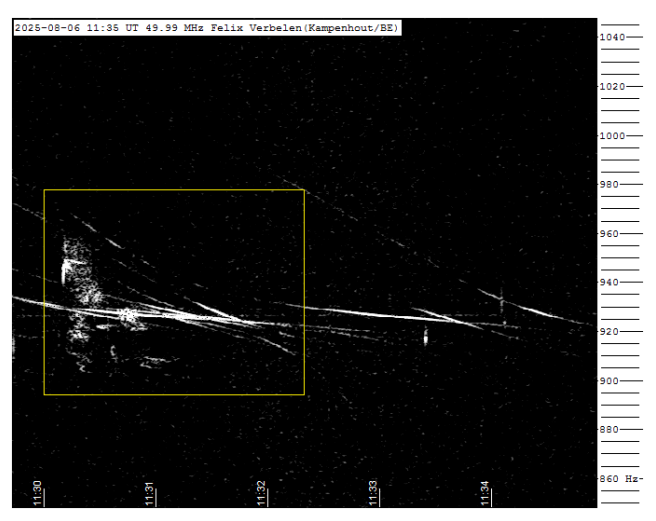


Figure 10 – Meteor echoes August 6, 11h35m UT.

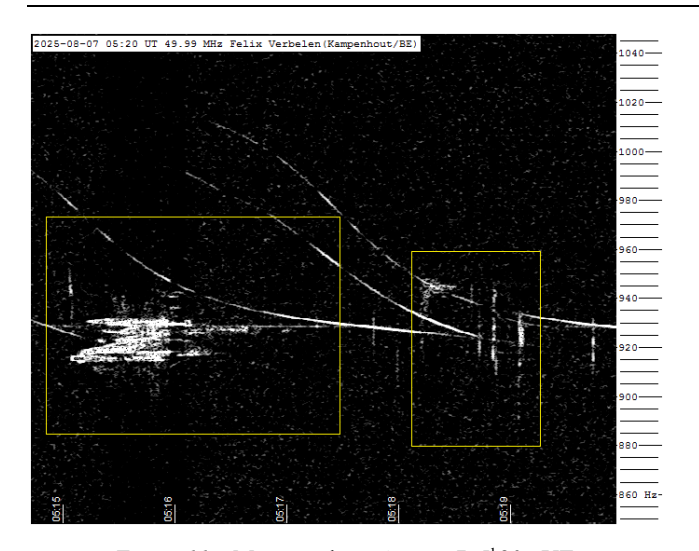


Figure 11 – Meteor echoes August 7, 5<sup>h</sup>20<sup>m</sup> UT.

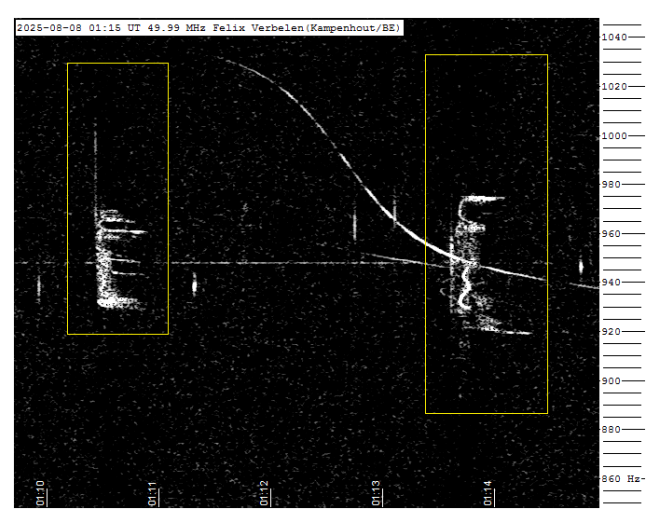


Figure 12 – Meteor echoes August 8, 1h15m UT.

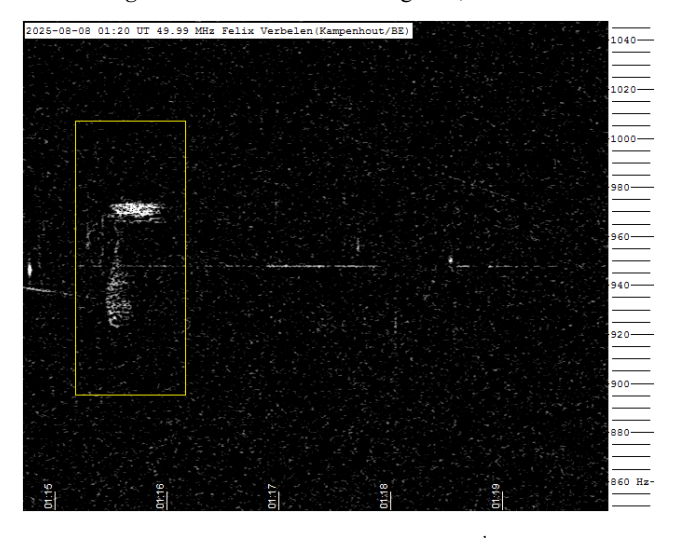


Figure 13 – Meteor echoes August 8, 1<sup>h</sup>20<sup>m</sup> UT.

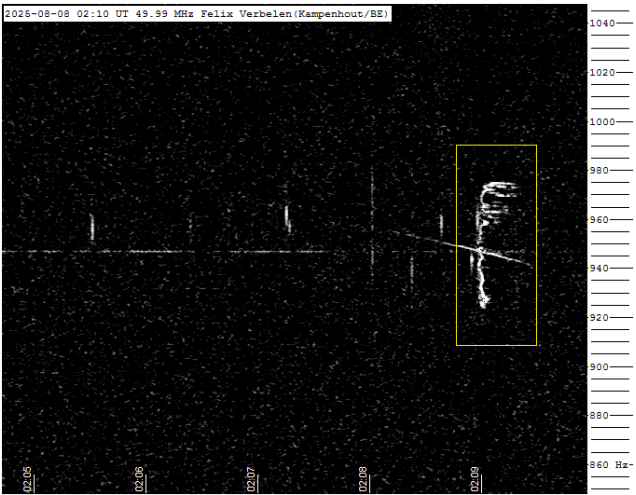


Figure 14 – Meteor echoes August 8,  $2^h10^m$  UT.

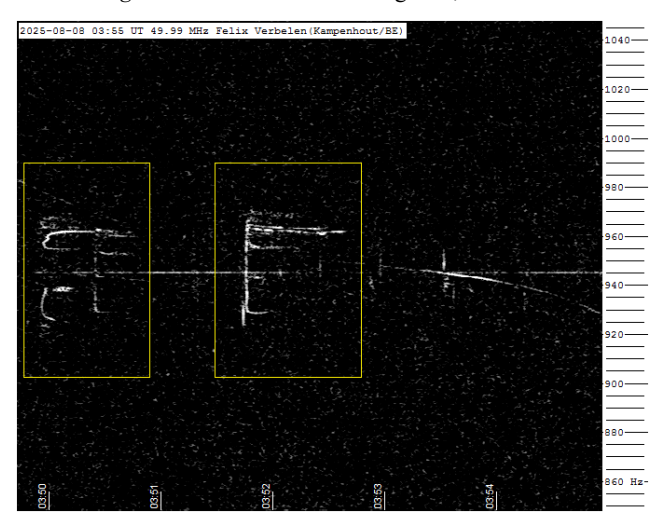


Figure 15 – Meteor echoes August 8, 3h55m UT.



Figure 16 – Meteor echoes August 8, 4h10m UT.

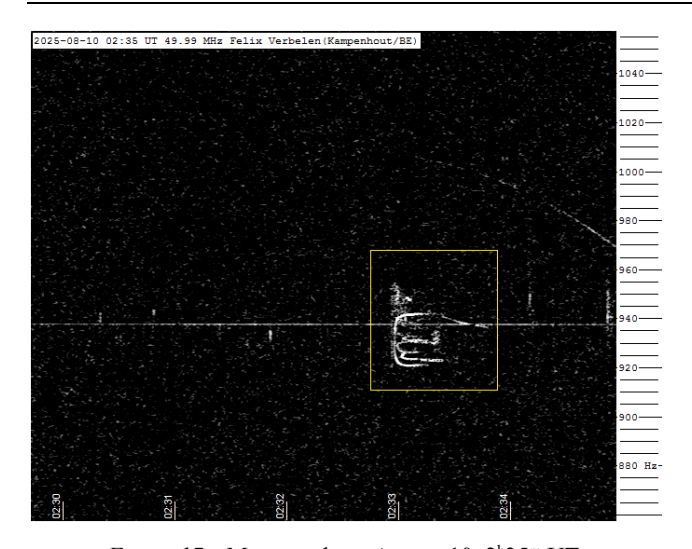


Figure 17 – Meteor echoes August 10, 2h35m UT.

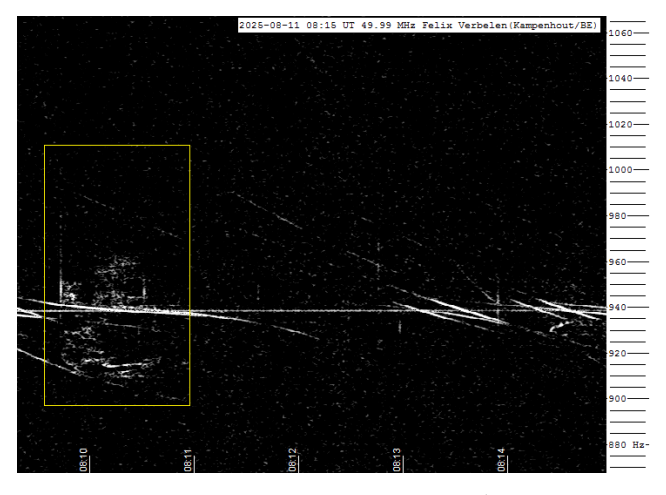


Figure 18 – Meteor echoes August 11, 8h15m UT.

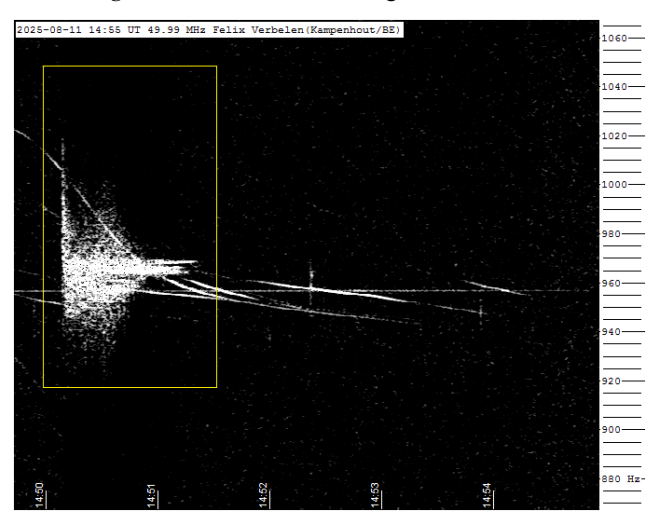


Figure 19 – Meteor echoes August 11, 14h55m UT.

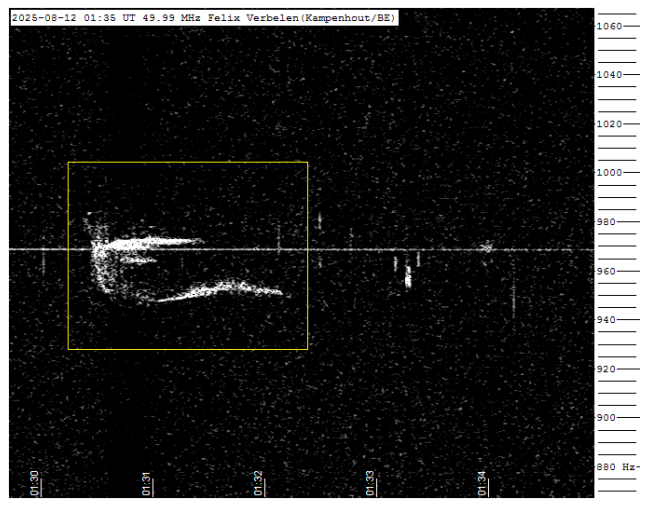


Figure 20 – Meteor echoes August 12, 1h35m UT.

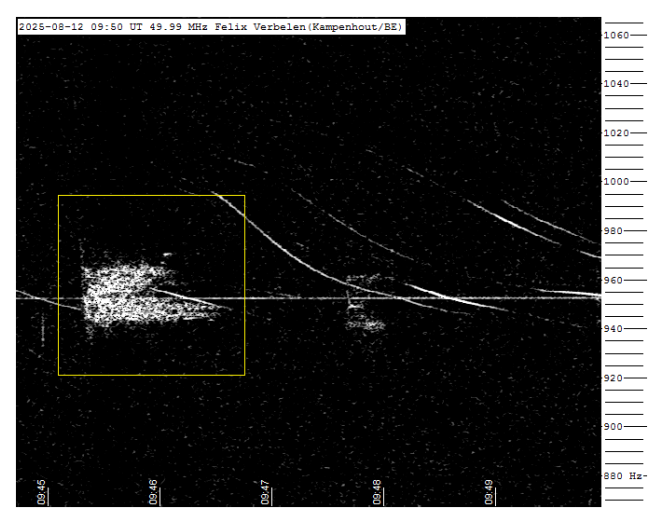


Figure 21 – Meteor echoes August 12, 9h50m UT.

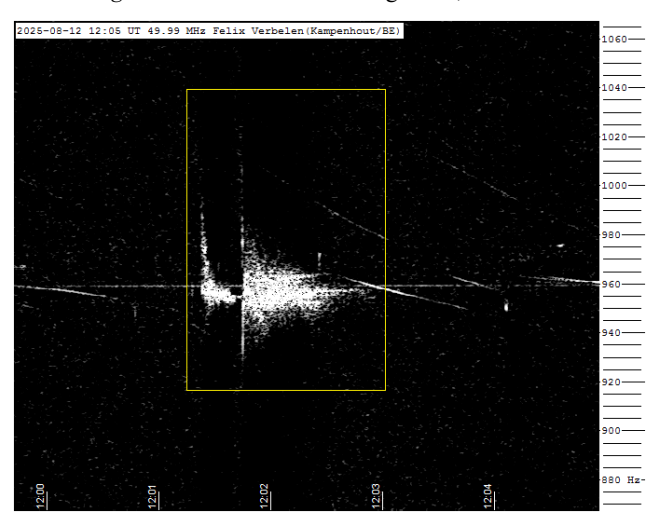


Figure 22 – Meteor echoes August 12, 12h05m UT.

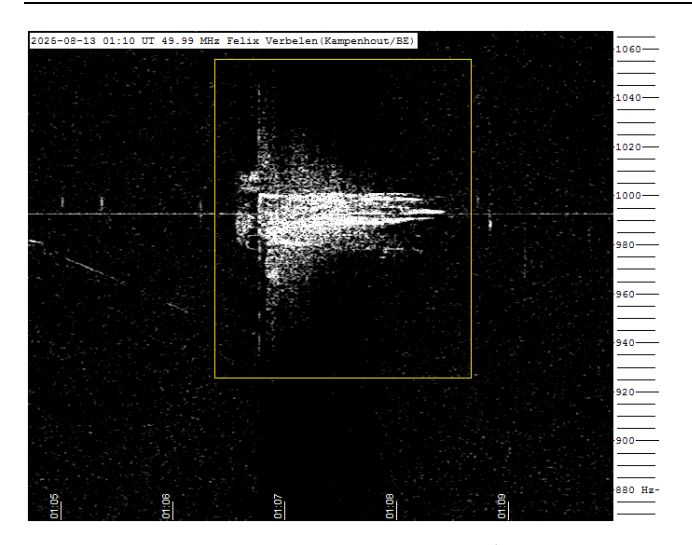


Figure 23 – Meteor echoes August 13, 1<sup>h</sup>10<sup>m</sup> UT.

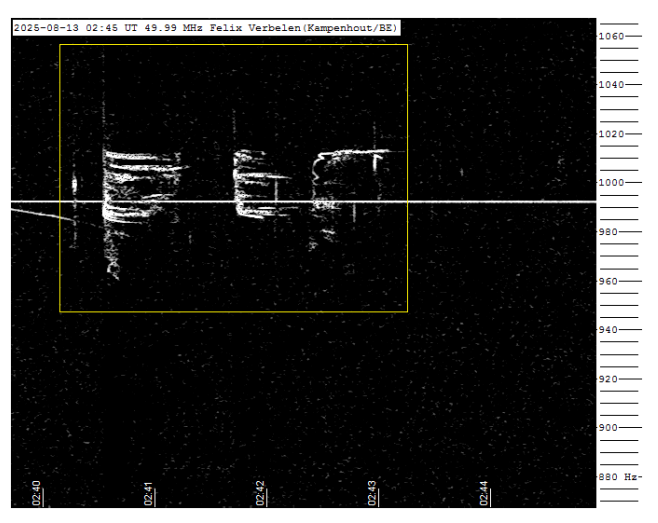


Figure 24 – Meteor echoes August 13, 2h45m UT.

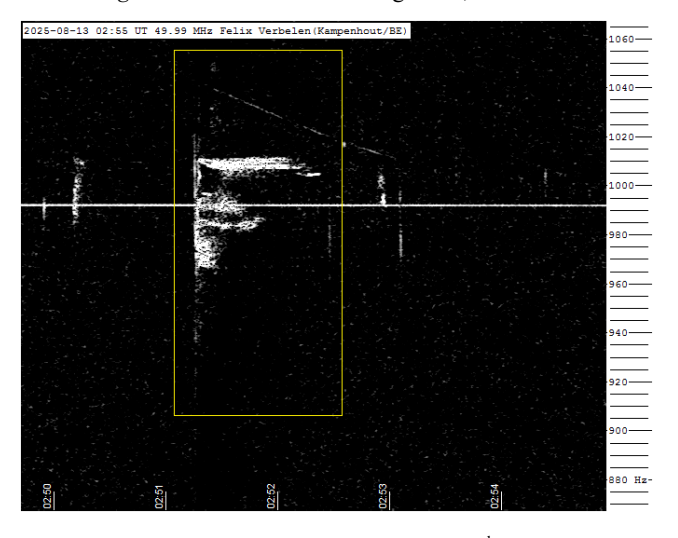


Figure 25 – Meteor echoes August 13, 2h55m UT.

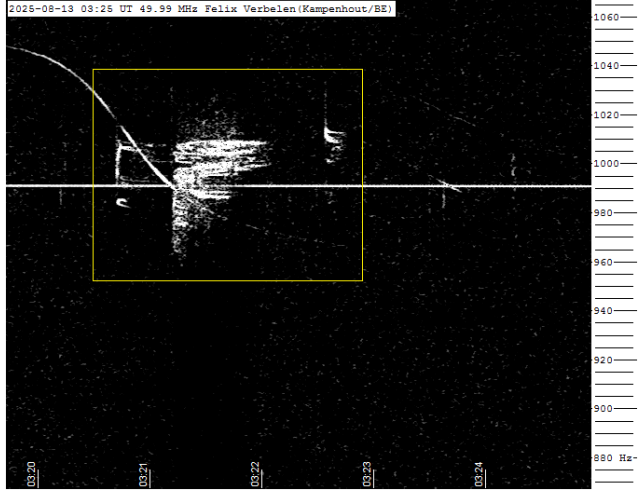


Figure 26 – Meteor echoes August 13, 3<sup>h</sup>25<sup>m</sup> UT.

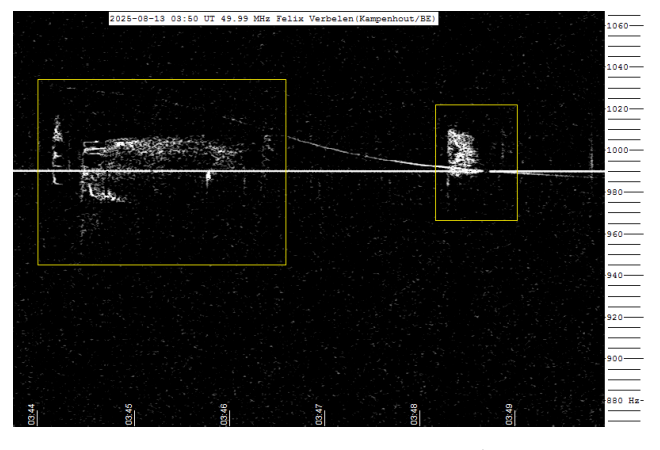


Figure 27 – Meteor echoes August 13, 3<sup>h</sup>50<sup>m</sup> UT.

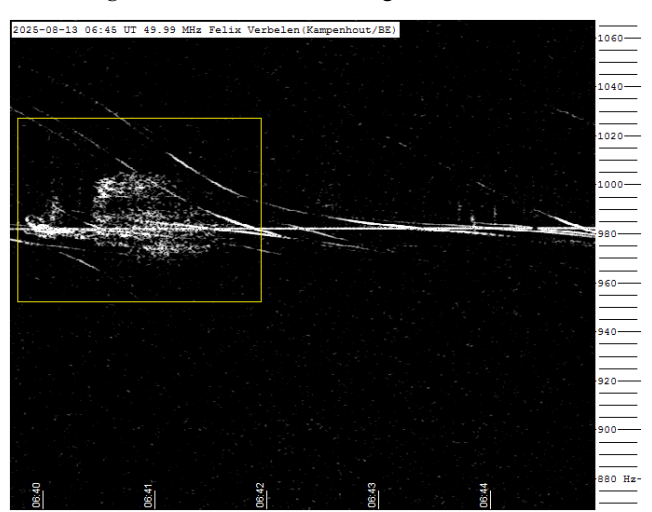


Figure 28 – Meteor echoes August 13, 6h45m UT.

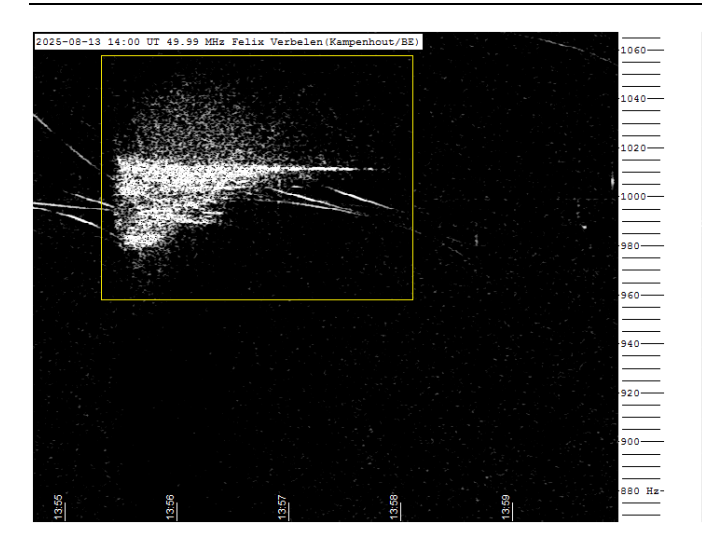


Figure 29 – Meteor echoes August 13, 14h00m UT.

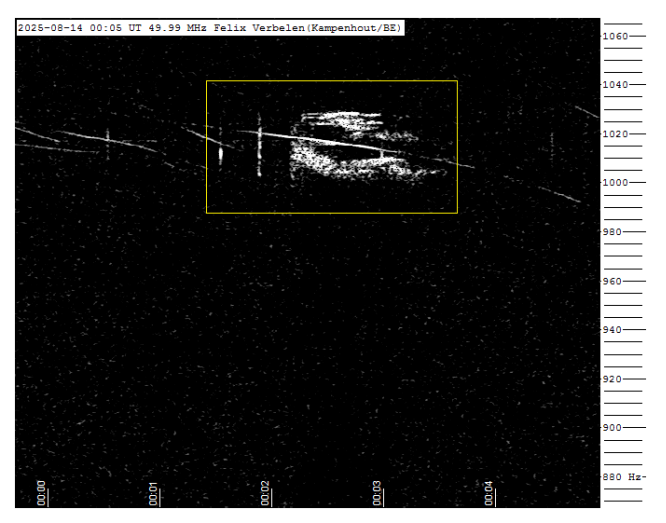


Figure 30 – Meteor echoes August 14,  $00^{\rm h}05^{\rm m}$  UT.

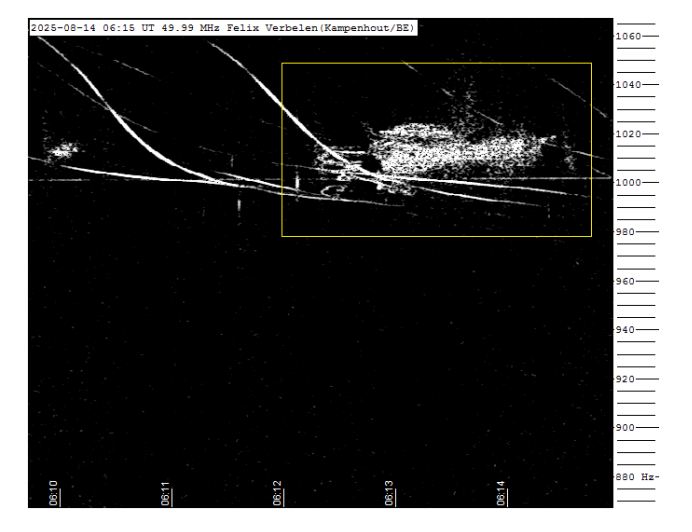


Figure 31 – Meteor echoes August 14, 06h15m UT.

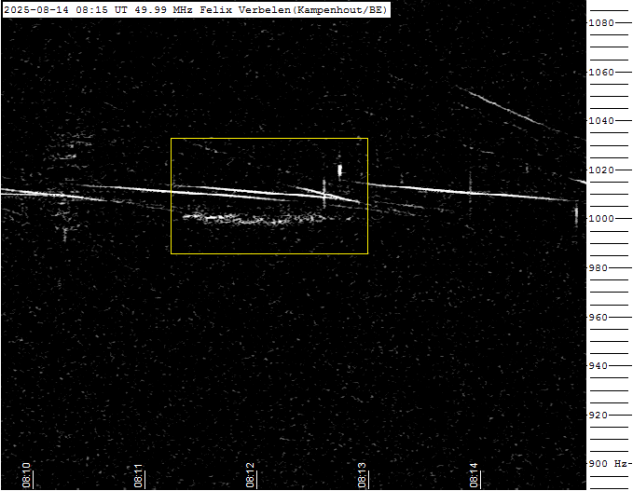


Figure 32 – Meteor echoes August 14, 08h15m UT.

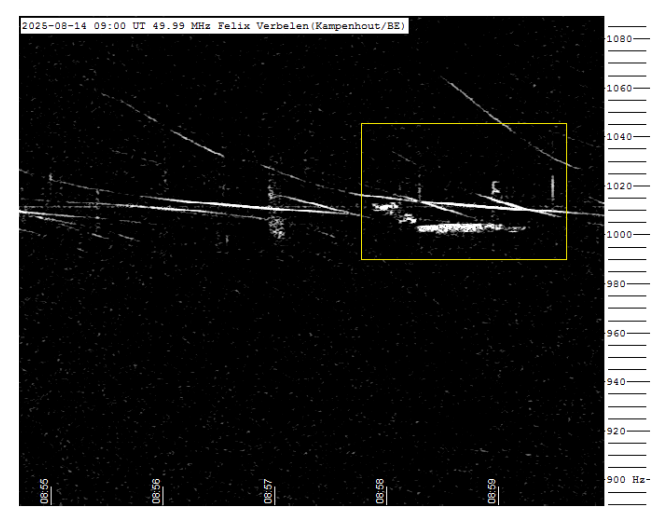


Figure 33 – Meteor echoes August 14, 09h00m UT.

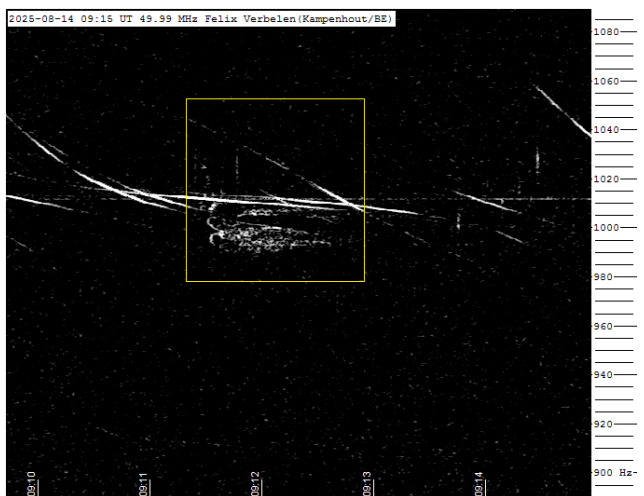


Figure 34 – Meteor echoes August 14, 09h15m UT.

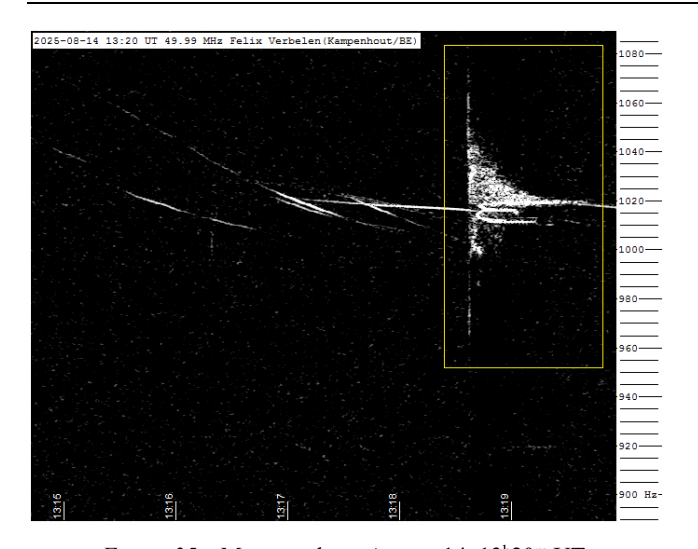


Figure 35 – Meteor echoes August 14, 13<sup>h</sup>20<sup>m</sup> UT.

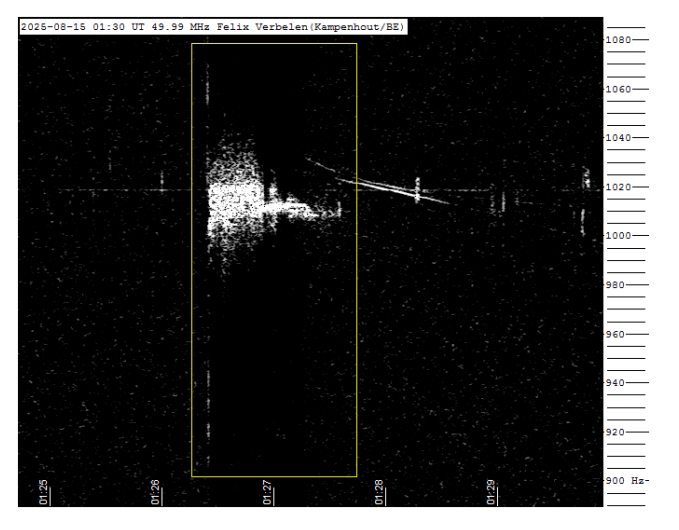


Figure 36 – Meteor echoes August 15, 1h30m UT.

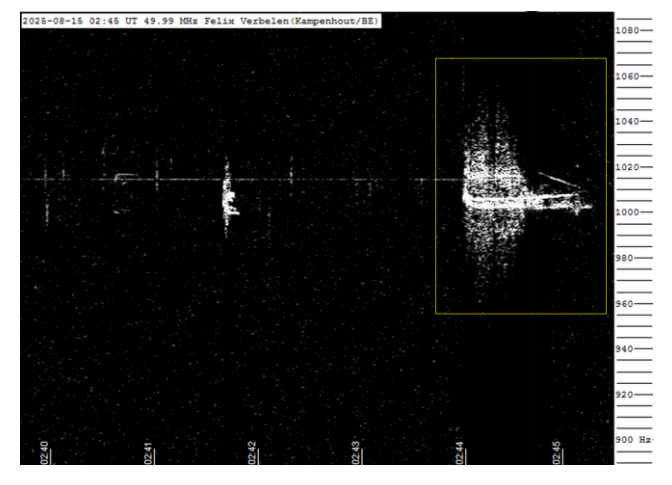


Figure 37 – Meteor echoes August 15, 2h45m UT.

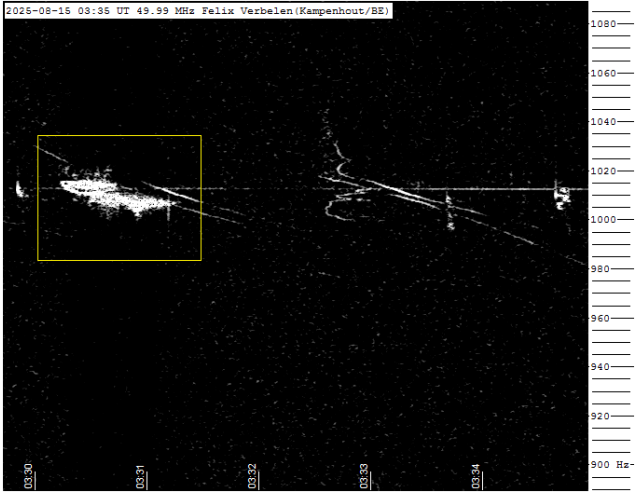


Figure 38 – Meteor echoes August 15, 3h35m UT.

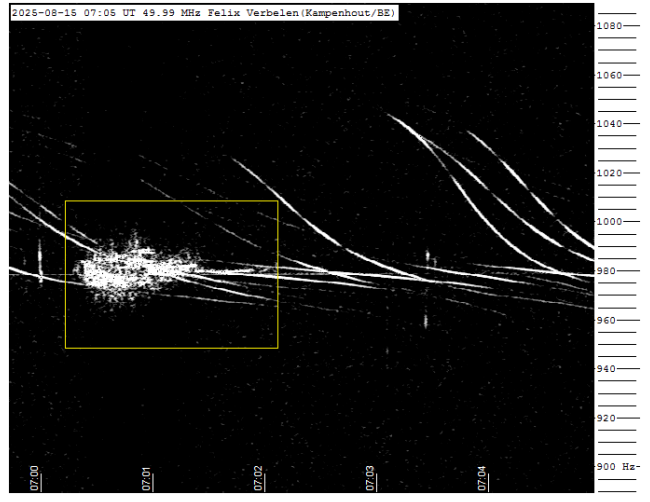


Figure 39 – Meteor echoes August 15,  $7^h05^m$  UT.

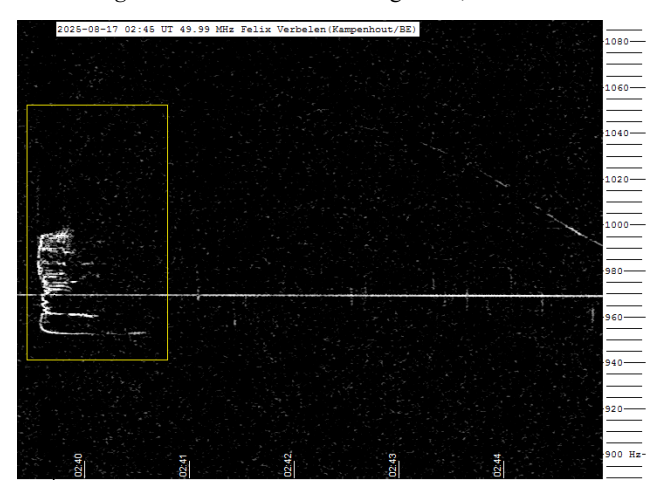


Figure 40 – Meteor echoes August 17, 2h45m UT.

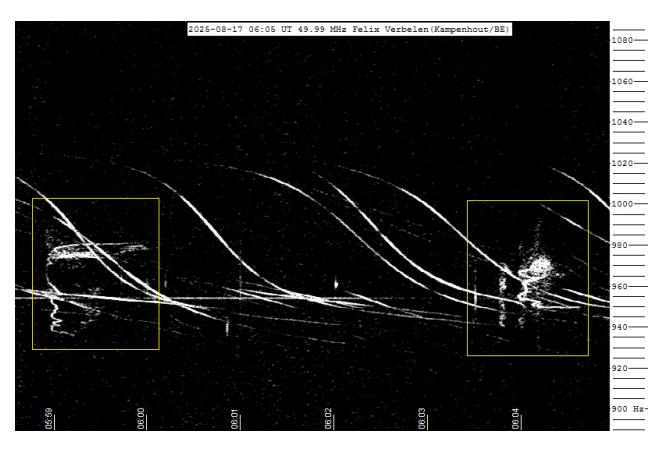


Figure 41 – Meteor echoes August 17,  $6^h05^m$  UT.

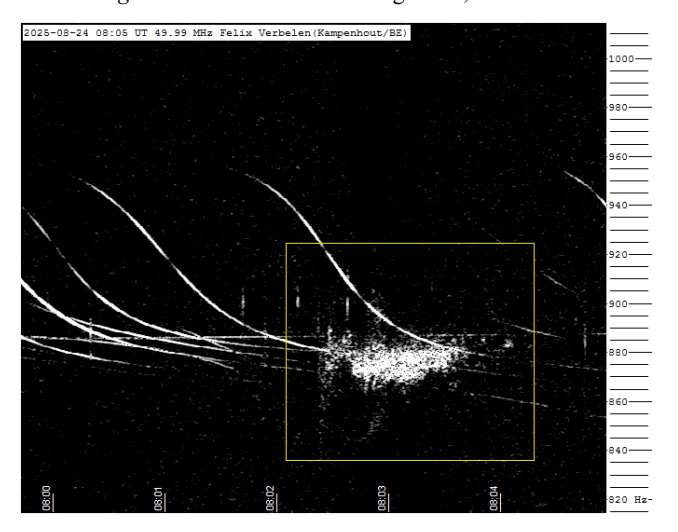


Figure 42 – Meteor echoes August 24,  $8^h05^m$  UT.

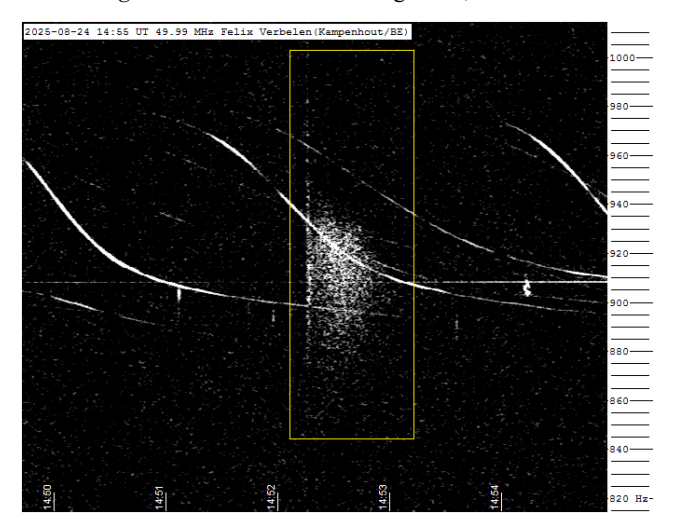


Figure 43 – Meteor echoes August 24,  $14^{\rm h}55^{\rm m}$  UT.

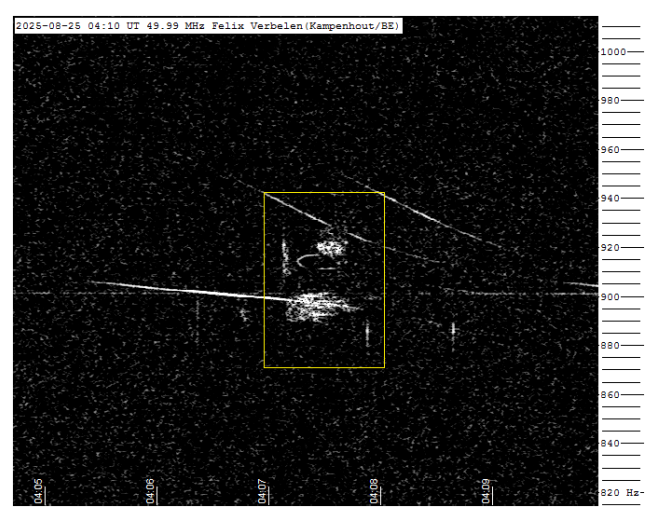


Figure 44 – Meteor echoes August 25, 4h10m UT.

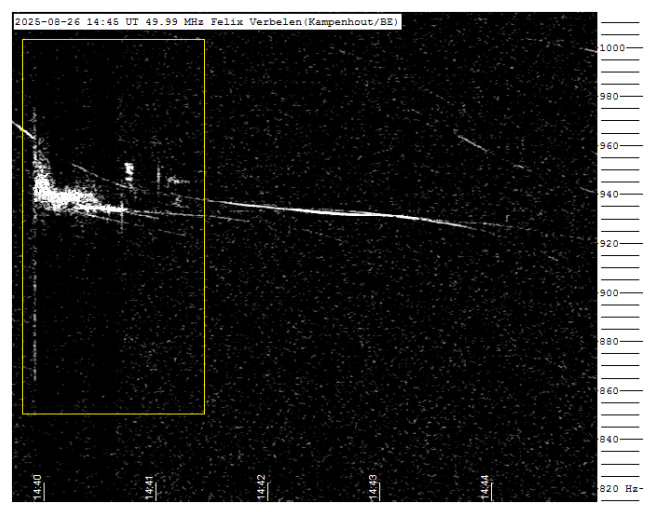


Figure 45 – Meteor echoes August 26,  $14^h45^m$  UT.

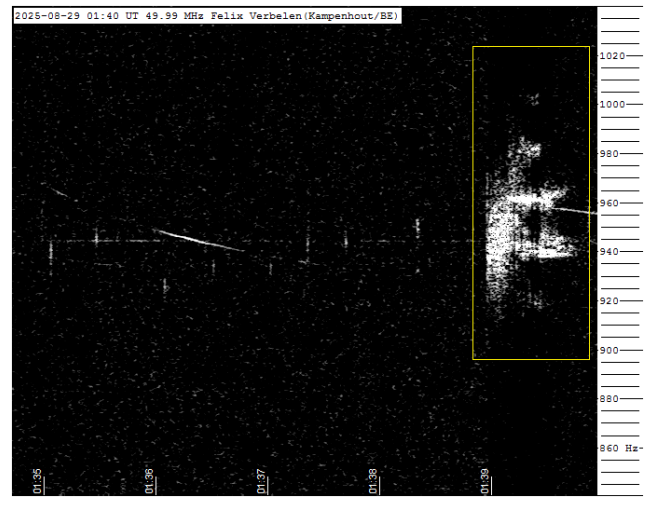


Figure 46 – Meteor echoes August 29, 1<sup>h</sup>40<sup>m</sup> UT.

# Radio meteors September 2025

### Felix Verbelen

Vereniging voor Sterrenkunde & Volkssterrenwacht MIRA, Grimbergen, Belgium

felix.verbelen@gmail.com

An overview of the radio observations during September is given.

## 1 Introduction

The graphs show both the daily totals (*Figure 1 and 2*) and the hourly numbers (*Figure 3 and 4*) of "all" reflections counted automatically, and of manually counted "overdense" reflections, overdense reflections longer than 10 seconds and longer than 1 minute, as observed here at Kampenhout (BE) on the frequency of our VVS-beacon (49.99 MHz) during the month of September 2025.

The hourly numbers, for echoes shorter than 1 minute, are weighted averages derived from:

$$N(h) = \frac{n(h-1)}{4} + \frac{n(h)}{2} + \frac{n(h+1)}{4}$$

Local interference and unidentified noise generally remained low. Weak lightning activity was recorded on 3 days, while very strong activity was noted on September 13<sup>th</sup> when a thunderstorm occurred in the immediate vicinity of the beacon.

Solar activity remained quite strong.

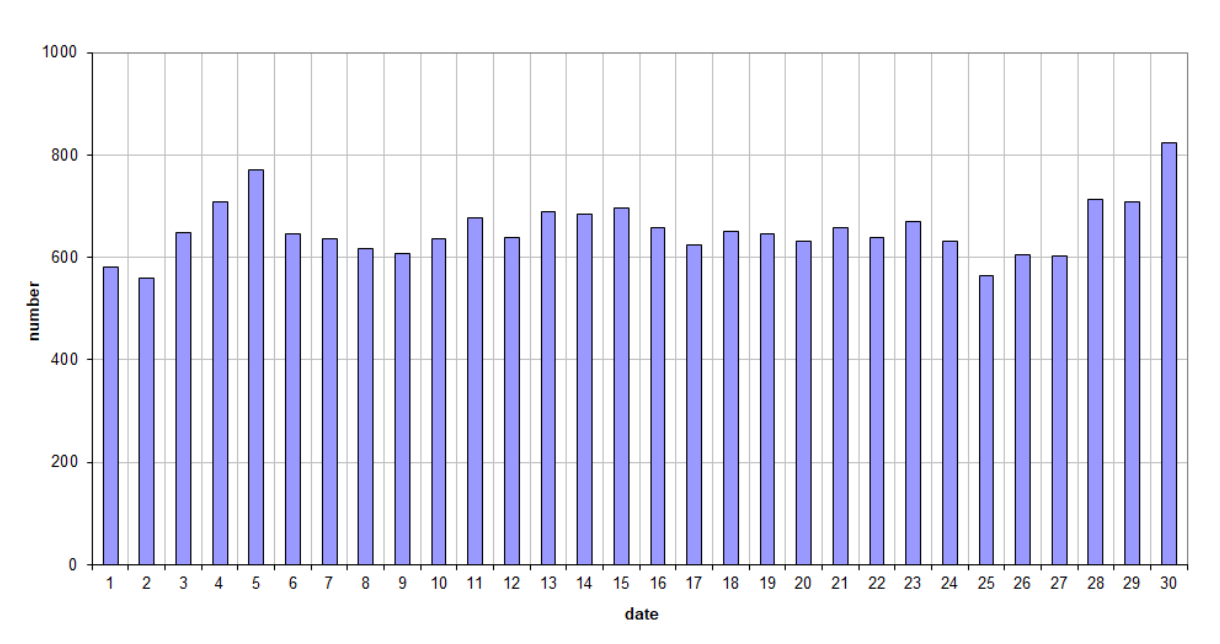
During this month, there were no truly prominent meteor showers active, but the activity nevertheless remained interesting, with both a number of smaller showers and a fair number of long reflections.

Across the entire month, 14 reflections longer than 1 minute were recorded. A selection, along with some other interesting reflections is presented in *Figures 5 to 19*.

In addition to the usual graphs, you will also find the raw counts in cvs-format<sup>25</sup> from which the graphs are derived. The table contains the following columns: day of the month, hour of the day, day + decimals, solar longitude (epoch J2000), counts of "all" reflections, overdense reflections, reflections longer than 10 seconds and reflections longer than 1 minute, the numbers being the observed reflections of the past hour.

<sup>&</sup>lt;sup>25</sup> https://www.emeteornews.net/wp-content/uploads/2025/10/202509 49990 FV rawcounts.csv





## 49.99MHz - RadioMeteors September 2025 daily totals of all overdense reflections

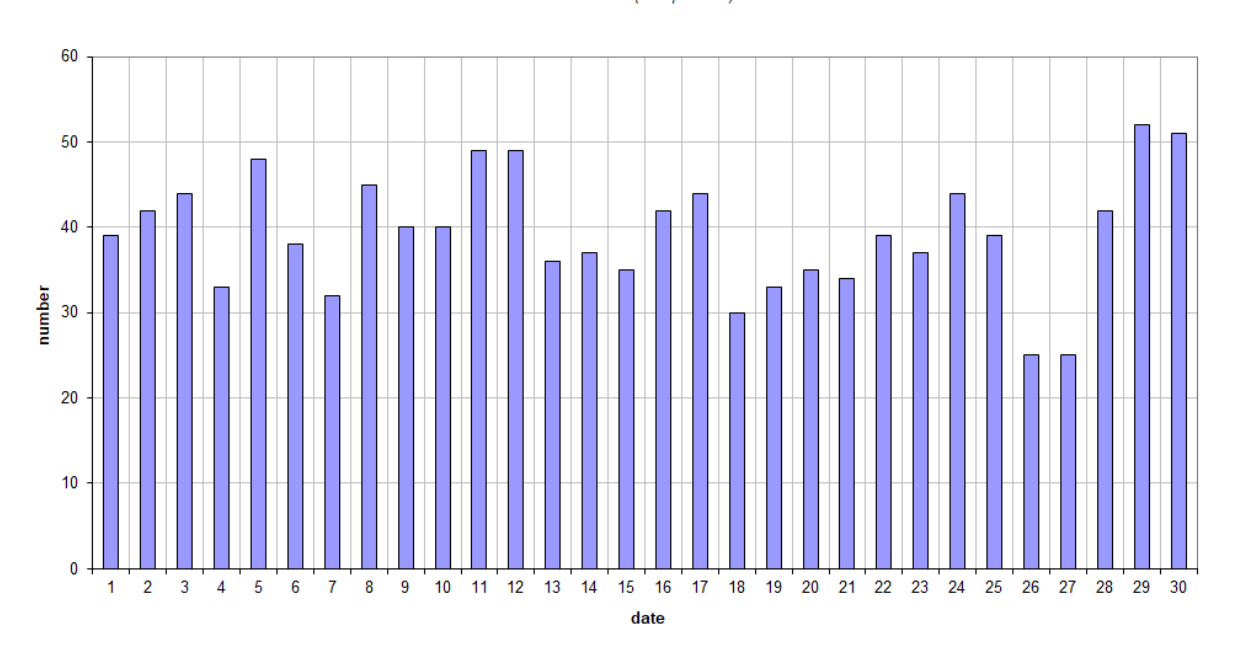
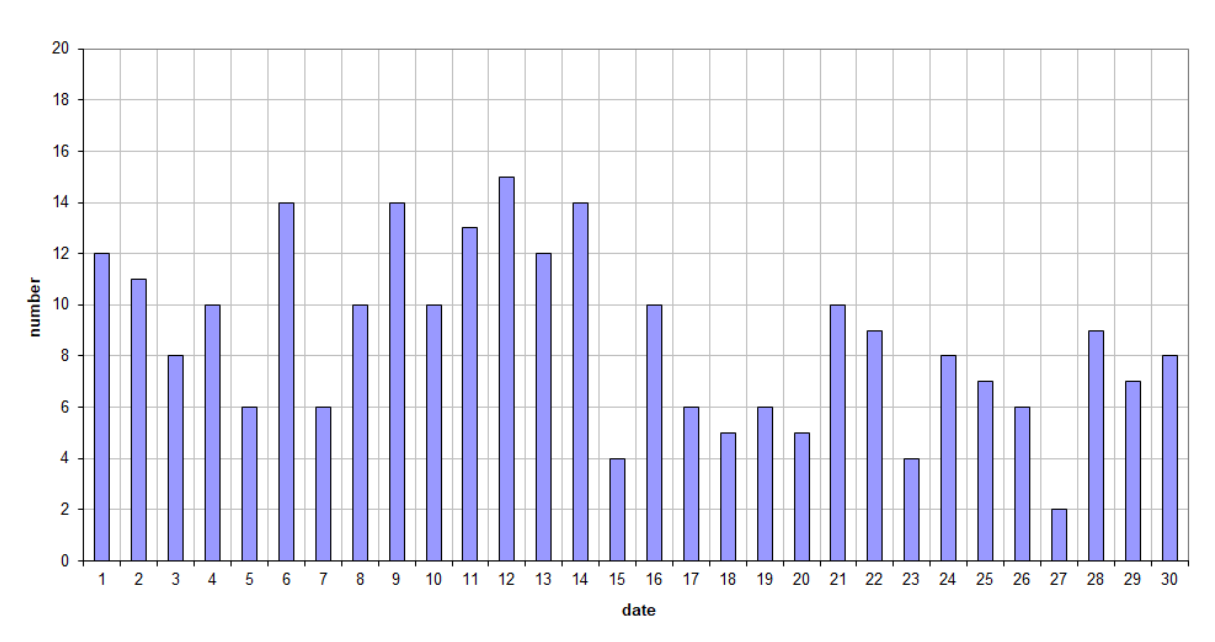


Figure 1 – The daily totals of "all" reflections counted automatically, and of manually counted "overdense" reflections, as observed here at Kampenhout (BE) on the frequency of our VVS-beacon (49.99 MHz) during September 2025.

## 49.99MHz - RadioMeteors September 2025 daily totals of reflections longer than 10 seconds

Felix Verbelen (Kampenhout)



#### 49.99MHz - RadioMeteors September 2025 daily totals of reflections longer than 1 minute Felix Verbelen (Kampenhout)

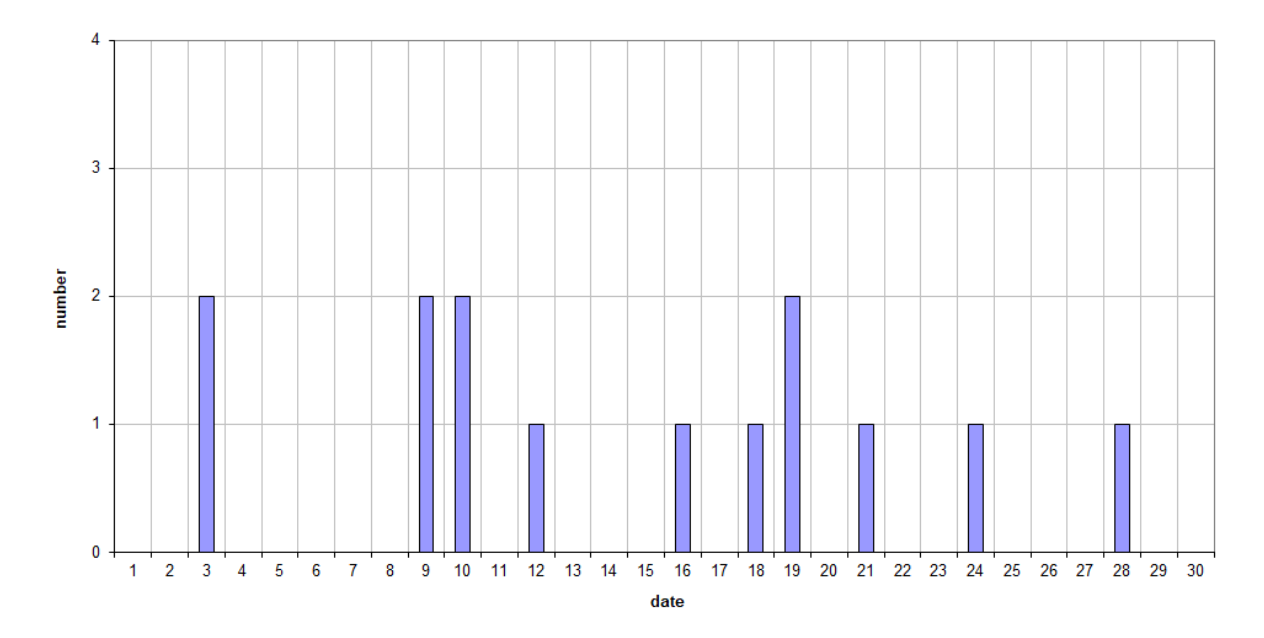
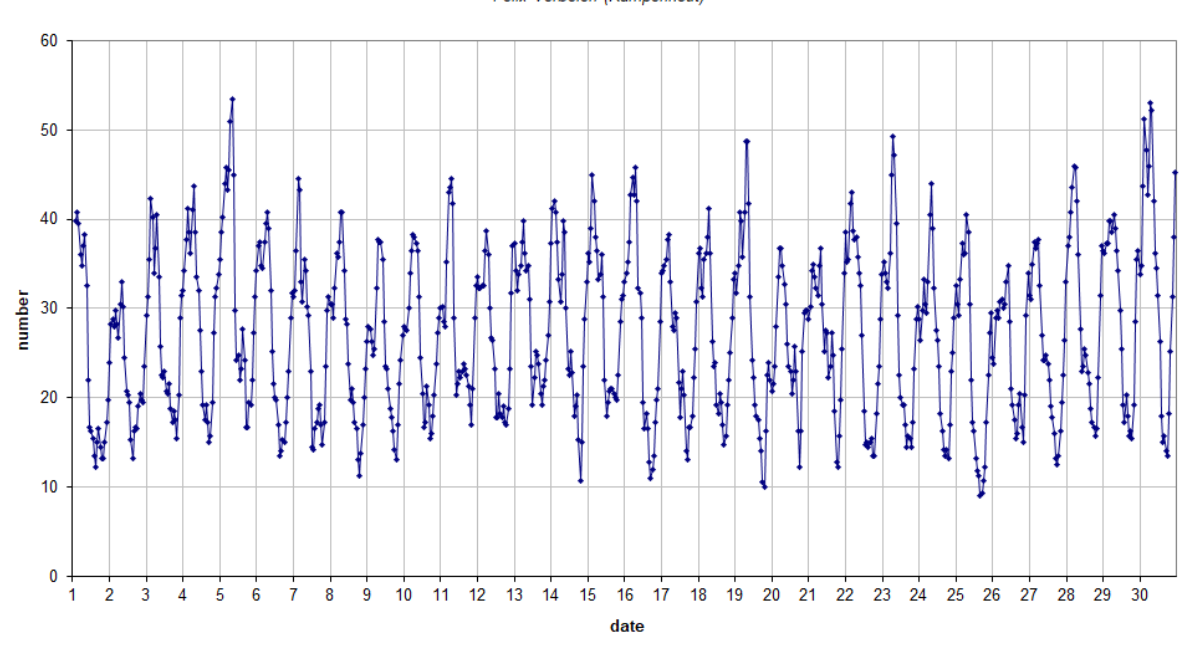


Figure 2 – The daily totals of overdense reflections longer than 10 seconds and longer than 1 minute, as observed here at Kampenhout (BE) on the frequency of our VVS-beacon (49.99 MHz) during September 2025.

#### 49.99 MHz - RadioMeteors September 2025 number of "all" refections per hour (weighted average) (automatic count\_Mettel5\_7Hz) Felix Verbelen (Kampenhout)



#### 49.99MHz - RadioMeteors September 2025 number of overdense reflections per hour (weighted average) Felix Verbelen (Kampenhout)

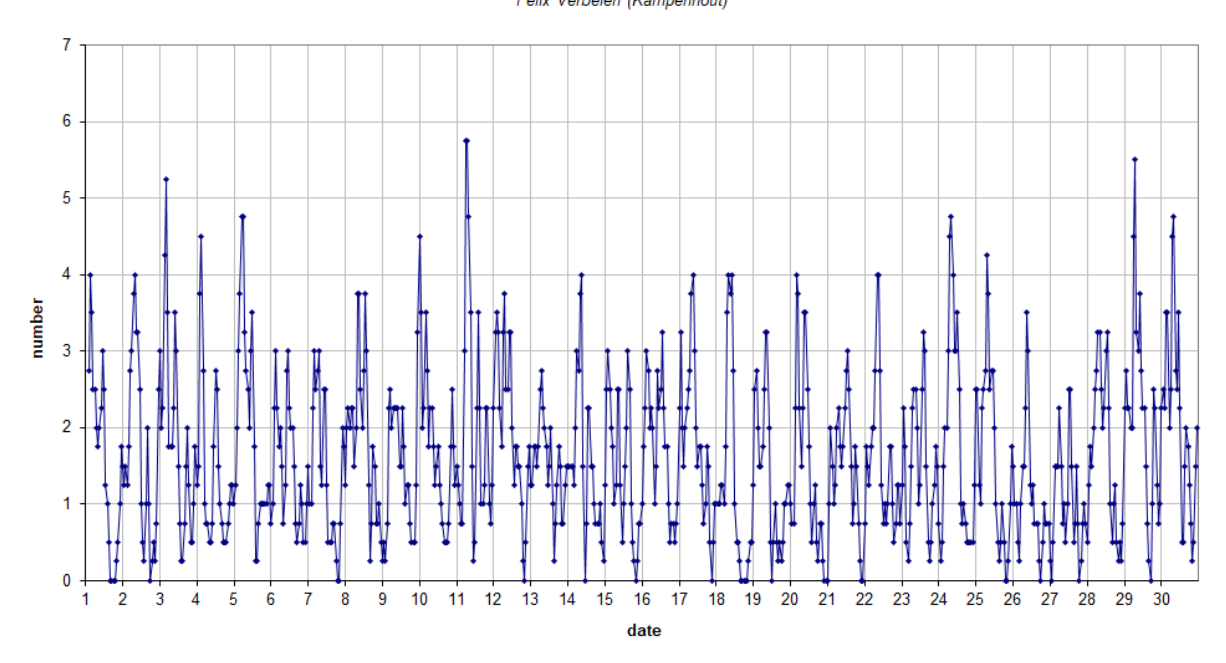
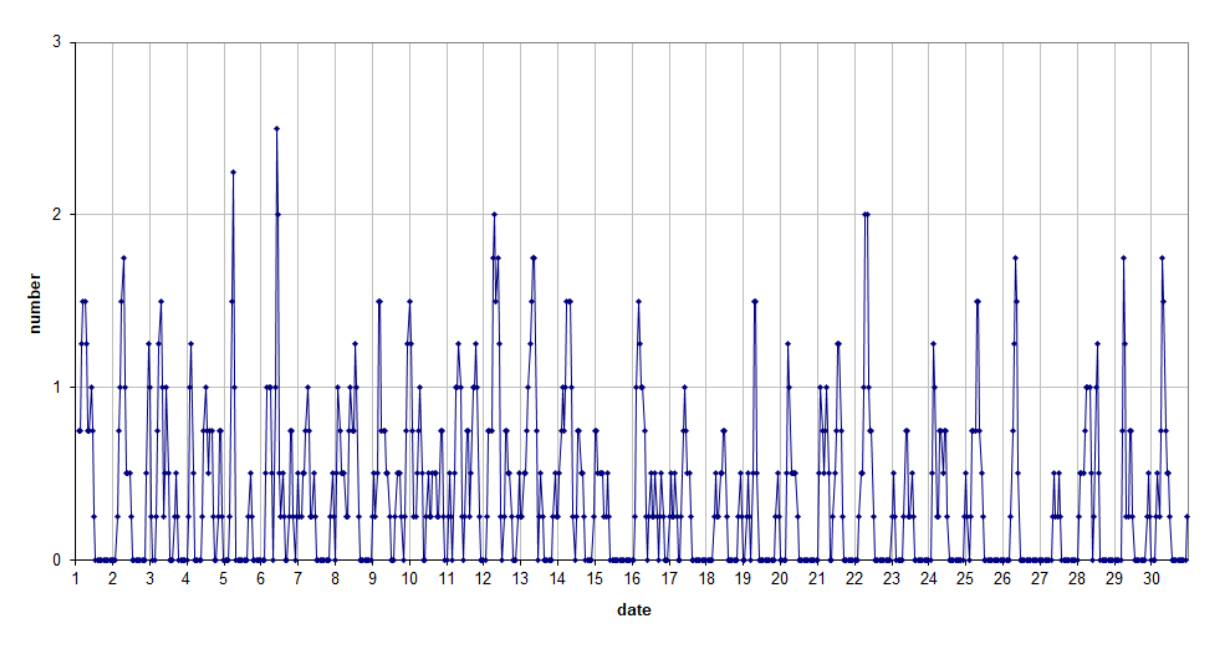


Figure 3 – The hourly numbers of "all" reflections counted automatically, and of manually counted "overdense" reflections, as observed here at Kampenhout (BE) on the frequency of our VVS-beacon (49.99 MHz) during September 2025.

### 49.99MHz - RadioMeteors September 2025 number of reflections >10 seconds per hour (weighted average)

Felix Verbelen (Kampenhout)



#### 49.99MHz - RadioMeteors September 2025 hourly totals of overdense reflections longer than 1 minute Felix Verbelen (Kampenhout/BE)

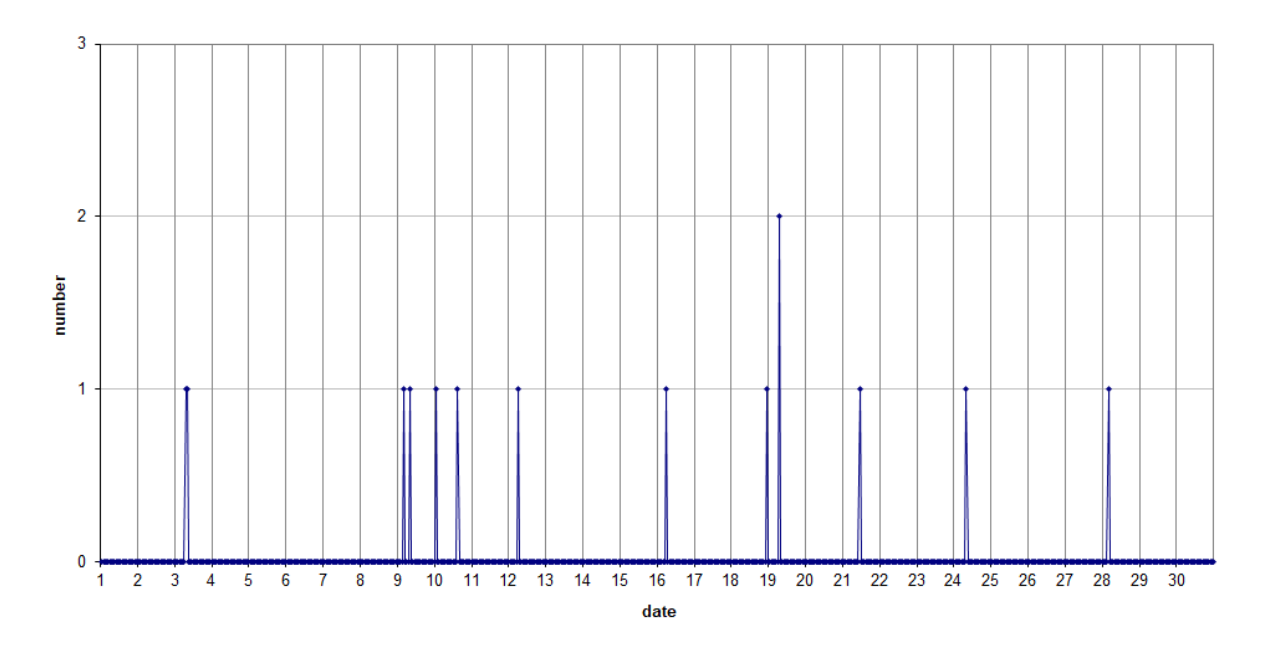


Figure 4 – The hourly numbers of overdense reflections longer than 10 seconds and longer than 1 minute, as observed here at Kampenhout (BE) on the frequency of our VVS-beacon (49.99 MHz) during September 2025.

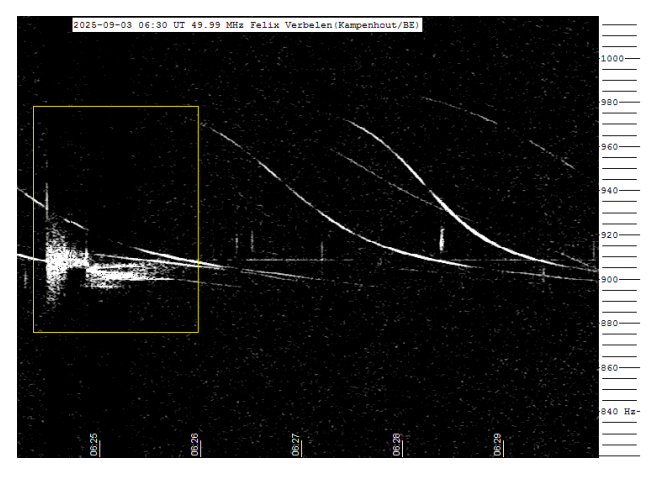


Figure 5 – Meteor echoes September 3,  $6^h30^m$  UT.

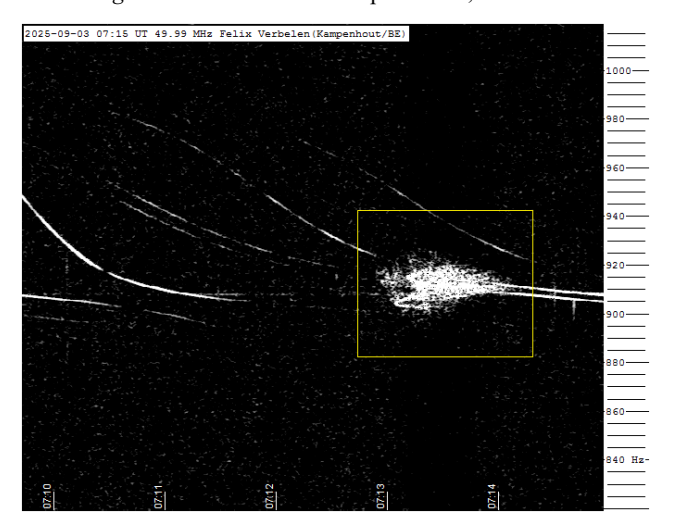


Figure 6 – Meteor echoes September 3, 7h15m UT.

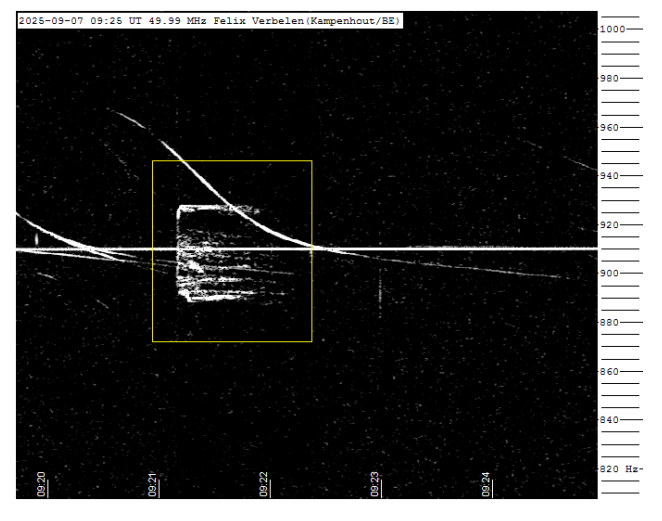


Figure 7 – Meteor echoes September 7, 9h25m UT.

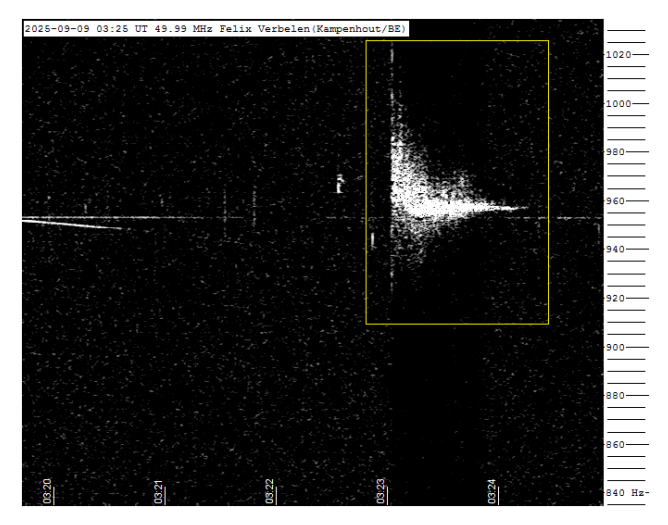


Figure 8 – Meteor echoes September 9,  $3^{\rm h}25^{\rm m}$  UT.

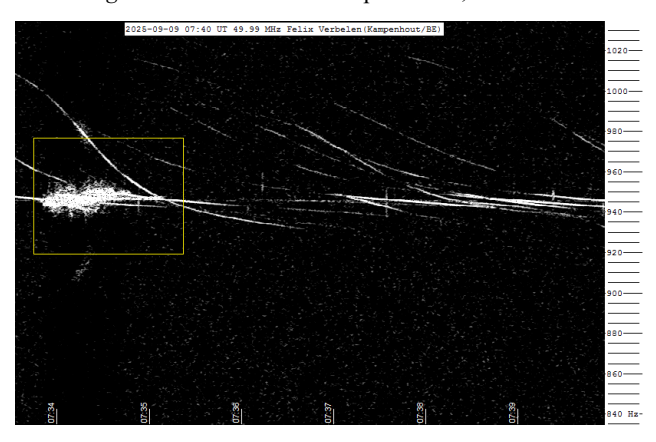


Figure 9 – Meteor echoes September 9, 7<sup>h</sup>40<sup>m</sup> UT.

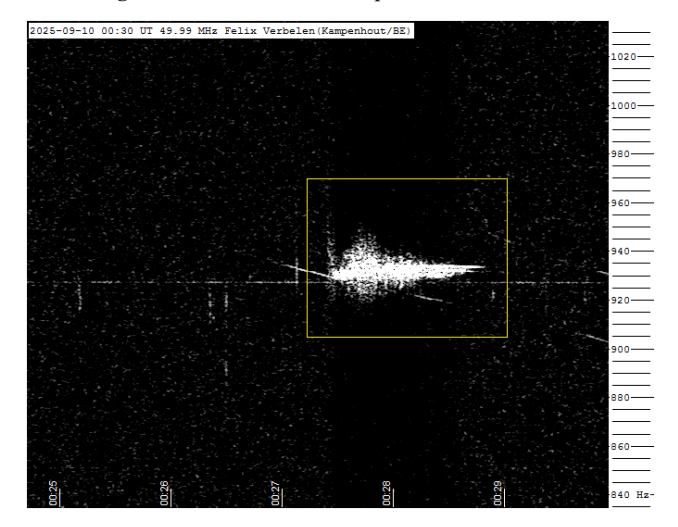


Figure 10 – Meteor echoes September 9,  $0^{\rm h}30^{\rm m}$  UT.

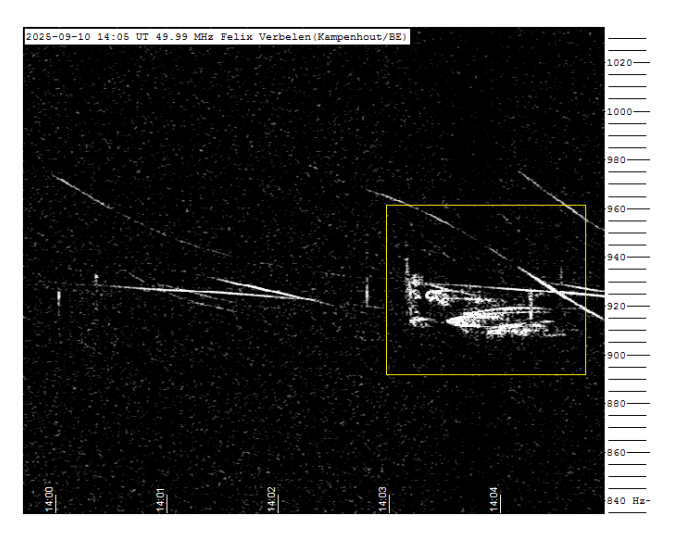


Figure 11 – Meteor echoes September 10,  $14^h05^m$  UT.

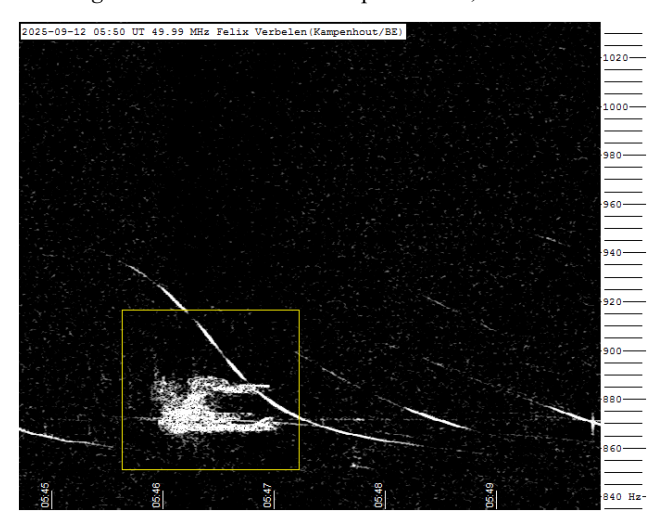


Figure 12 – Meteor echoes September 12,  $5^{\rm h}50^{\rm m}$  UT.

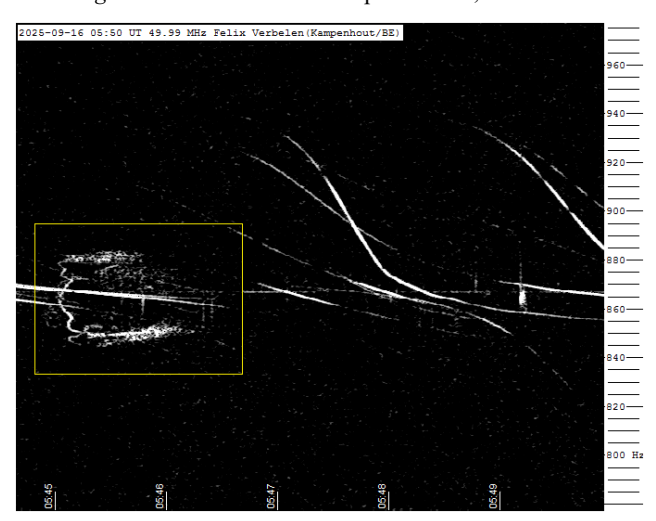


Figure 13 – Meteor echoes September 16, 5h50m UT.

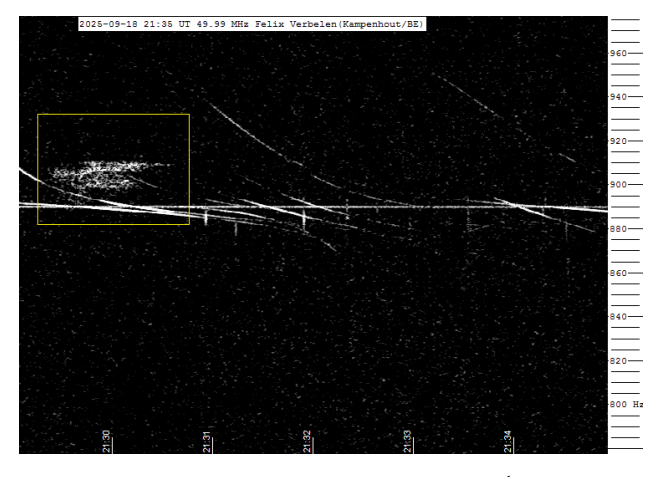


Figure 14 – Meteor echoes September  $18, 21^{\rm h}35^{\rm m}$  UT.

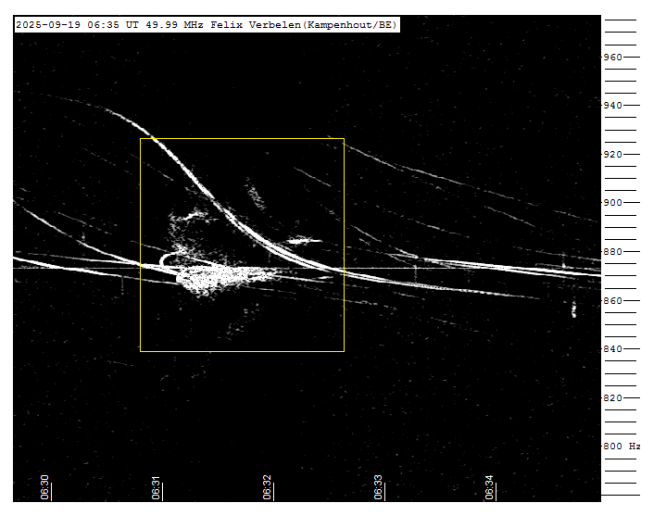


Figure 15 – Meteor echoes September 19, 6h35m UT.

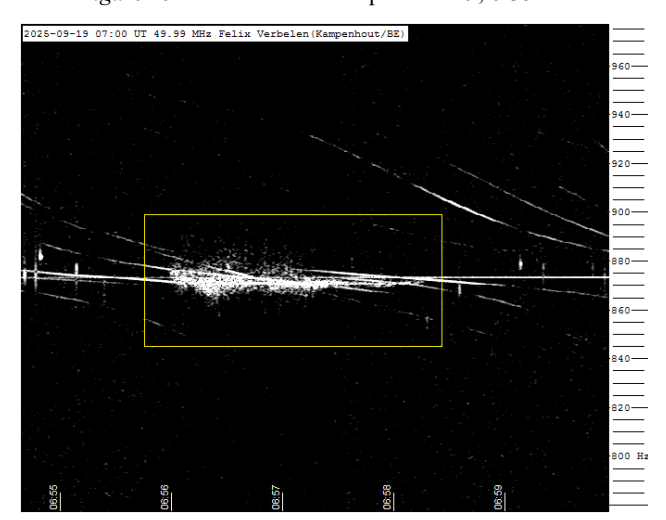


Figure 16 – Meteor echoes September 19,  $7^h00^m$  UT.

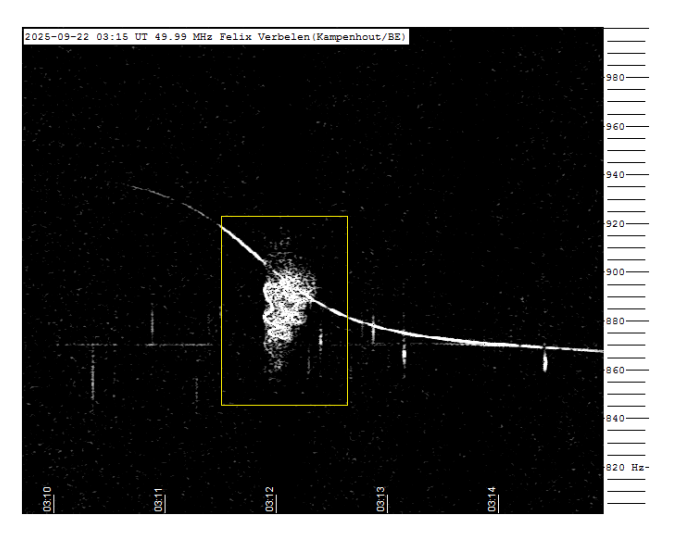


Figure 17 – Meteor echoes September 22,  $3^h15^m$  UT.

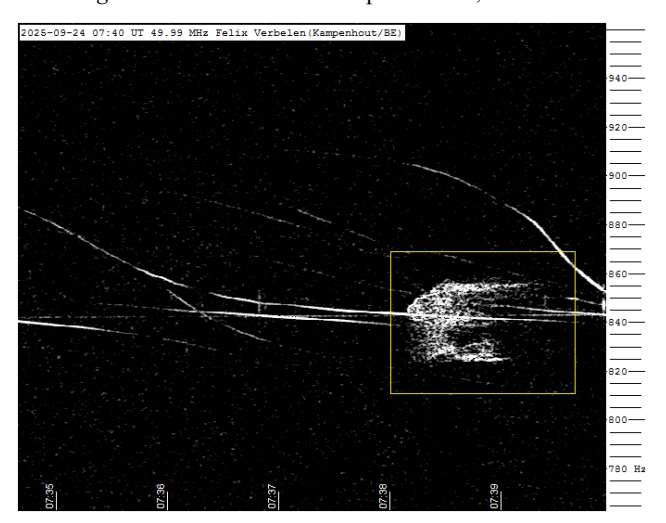


Figure 18 – Meteor echoes September 24,  $7^{h}40^{m}$  UT.

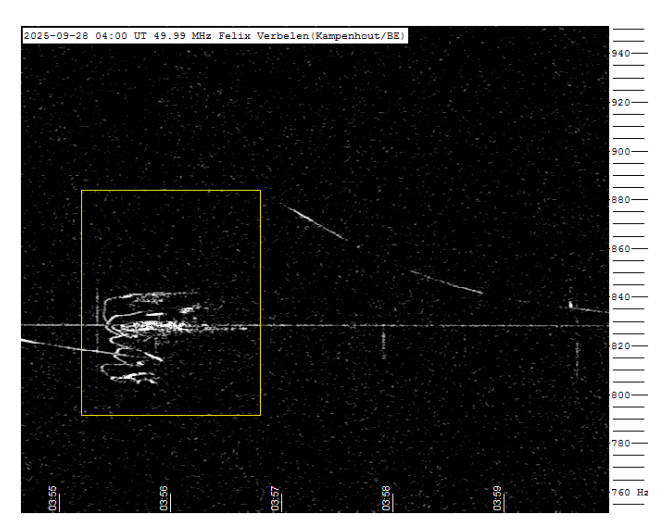


Figure 19 – Meteor echoes September 28,  $4^{h}00^{m}$  UT.

# Remarkable fireballs spotted in the framework of the Southwestern Europe Meteor Network from February to April 2025

J.M. Madiedo<sup>1</sup>, J.L. Ortiz<sup>1</sup>, F. Aceituno<sup>1</sup>, J. Aceituno<sup>2</sup>, E. de Guindos<sup>2</sup>, D. Ávila<sup>3</sup>, A. Gómez-Hernández<sup>4</sup>, J. Gómez-Martínez<sup>4</sup>, A. García<sup>5</sup>, and A.I. Aimee<sup>6</sup>

<sup>1</sup> Departamento de Sistema Solar, Instituto de Astrofísica de Andalucía (IAA-CSIC), 18080 Granada, Spain madiedo@cica.es, ortiz@iaa.es, fja@iaa.es

<sup>2</sup> Observatorio Astronómico de Calar Alto (CAHA), E-04004, Almería, Spain aceitun@caha.es, guindos@caha.es

<sup>3</sup> Estación de Meteoros de Ayora, Ayora, Valencia, Spain David ayora007@hotmail.com

<sup>4</sup> Estación de Registro La Lloma, Olocau, Valencia, Spain curso88@gmail.com

<sup>5</sup> Estación de Meteoros de Cullera (Faro de Cullera), Valencia, Spain antonio.garcia88@joseantoniogarcia.com

<sup>6</sup> Southwestern Europe Meteor Network, 41012 Sevilla, Spain

swemn.server@gmail.com

Some of the brightest fireballs registered in the framework of the Southwestern Europe Meteor Network from February to April 2025 are described in this report. They have been spotted from the Iberian Peninsula. Their absolute magnitude ranges from -6 to -12. One of these fireballs was a potential meteorite-producing fireball. Meteors included here were associated with different sources: the sporadic background, major meteoroid streams, and poorly-known streams.

#### 1 Introduction

The Southwestern Europe Meteor Network (SWEMN) is conducting the SMART project (Spectroscopy of Meteoroids by means of Robotic Technologies) since 2006 in order to analyze the physical and chemical properties of meteoroids ablating in the Earth's atmosphere. For this purpose we employ an array of automated cameras and spectrographs deployed at different meteor-observing stations in Spain (Madiedo, 2014; Madiedo, 2017). This allows to derive the luminous path of meteors and the orbit of their progenitor meteoroids, and also to study the evolution of meteor plasmas from the emission spectrum produced by these events (Madiedo, 2015a; 2015b). SMART also provides important information for our MIDAS project (Moon Impacts Detection and Analysis System). MIDAS is being conducted by the Institute of Astrophysics of Andalusia (IAA-CSIC) to study lunar impact flashes produced when large meteoroids hit the Moon (Madiedo et al., 2015; Madiedo et al., 2018; Madiedo et al. 2019; Ortiz et al., 2015).

This paper describes the preliminary analysis of eight bolides observed by our meteor stations. This work has been fully written by AIMEE (acronym for Artificial Intelligence with Meteoroid Environment Expertise) by employing the records listed in the SWEMN fireball database (Madiedo et al., 2021; Madiedo et al., 2022).

#### 2 Equipment and methods

The events presented here have been recorded by using Watec 902H2 and Watec 902 Ultimate cameras. Their field of view ranges from  $62 \times 50$  degrees to  $14 \times 11$  degrees. To record meteor spectra we have attached holographic diffraction gratings (1000 lines/mm) to the lens of some of these cameras. We have also employed digital CMOS color cameras (models Sony A7S and A7SII) operating in HD video mode (1920 × 1080 pixels). These cover a field of view of around 70 × 40 degrees. A detailed description of this hardware and the way it operates was given in previous works (Madiedo, 2017). Besides digital CMOS cameras manufactured by ZWO (model ASI185MC) were used. The atmospheric path of the events were triangulated by means of the SAMIA software, developed by J.M. Madiedo. This program employs the planes-intersection (Ceplecha, 1987).

# 3 Description of the 2025 February 3 fireball

We spotted this bright event from the meteor-observing stations located at Huelva, La Hita (Toledo), Calar Alto, Sierra Nevada, La Sagra (Granada), and Sevilla (*Figure 1*). The bolide was captured on 2025 February 3, at  $4^h04^m51.0 \pm 0.1^s$  UT. The maximum brightness exhibited by the fireball was equivalent to an absolute magnitude of

 $-7.0 \pm 1.0$ . The code assigned to the bolide in the SWEMN meteor database is SWEMN20250203\_040451.

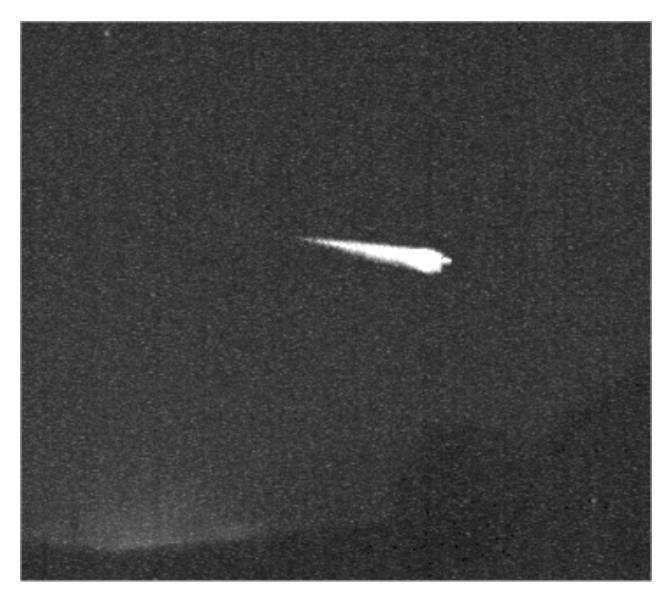


Figure 1 – Stacked image of the SWEMN20250203\_040451 "Serrato" fireball.



Figure 2 – Atmospheric path of the SWEMN20250203\_040451 bolide, and its projection on the ground.

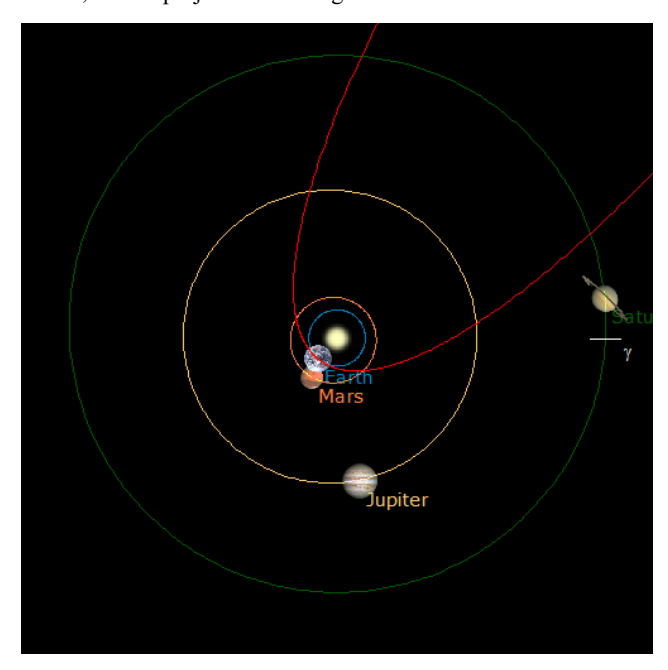


Figure 3 – Projection on the ecliptic plane of the orbit of the parent meteoroid of the SWEMN20250203 040451 event.

#### Atmospheric trajectory, radiant and orbit

This bolide overflew the Mediterranean Sea and the province of Málaga (southern Spain). Its initial altitude was  $H_b = 119.2 \pm 0.5\,$  km. The bright meteor penetrated the atmosphere till a final height  $H_e = 85.3 \pm 0.5\,$  km. The equatorial coordinates of the apparent radiant yield  $\alpha = 216.37^{\circ}$ ,  $\delta = -23.99^{\circ}$ . Besides, we inferred that the meteoroid entered the atmosphere with a velocity  $v_{\infty} = 72.4 \pm 0.4\,$  km/s. The calculated atmospheric path of the bolide is shown in *Figure 2*. The heliocentric orbit of the meteoroid is drawn in *Figure 3*.

*Table 1* – Orbital data (J2000) of the progenitor meteoroid before its encounter with our planet.

a (AU)	22.3 ± 18.	ω (°)	$8.9 \pm 00.2$
e	$0.95 \pm 0.03$	$\Omega$ (°)	$134.237705 \pm 10^{\text{-}5}$
q (AU)	$0.9797 \pm 0.0001$	i (°)	$163.52 \pm 0.07$

We named this bolide "Serrato", since the bright meteor was located near the zenith of this locality during its final phase. The parameters of the orbit in the Solar System of the progenitor meteoroid before its encounter with our planet have been included in *Table 1*. The value calculated for the geocentric velocity was  $v_g = 71.4 \pm 0.4$  km/s. The Tisserand parameter referred to Jupiter ( $T_J = -0.93$ ) indicates that before hitting our atmosphere the meteoroid was moving on a cometary (HTC) orbit. By taking into account these data and the derived radiant position, the event was associated with the  $\pi$ -Hydrids (IAU meteor shower code PIH#0101) (Molau and Rendtel, 2009).

#### 4 The 2025 February 5 bolide

This fireball was recorded by our devices at  $4^{\rm h}24^{\rm m}54.0 \pm 0.1^{\rm s}$  UT on 2025 February 5 (*Figure 4*). Its peak brightness was equivalent to an absolute magnitude of  $-7.0 \pm 1.0$ . The bolide was included in our meteor database with the code SWEMN20250205\_042454.

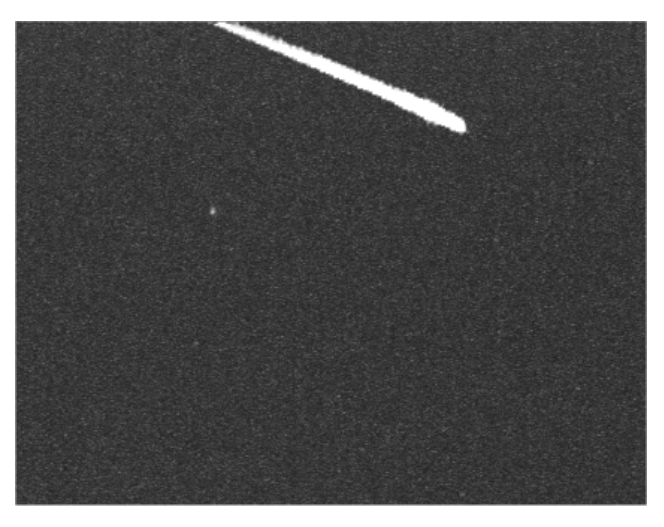


Figure 4 – Stacked image of the SWEMN20250205\_042454 "Cartaojal" fireball.

#### Atmospheric path, radiant and orbit

Following the analysis the path in the atmosphere of the event it was concluded that this meteor overflew the

provinces of Málaga and Córdoba (southern Spain). Its initial altitude was  $H_b = 111.6 \pm 0.5$  km. The event penetrated the atmosphere till a final height  $H_e = 84.0 \pm 0.5$  km. The apparent radiant was located at the equatorial coordinates  $\alpha = 210.30^{\circ}$ ,  $\delta = -19.68^{\circ}$ . Besides, we inferred that the meteoroid hit the atmosphere with a velocity  $v_{\infty} = 71.9 \pm 0.4$  km/s. *Figure 5* shows the calculated luminous path of the fireball. The heliocentric orbit of the meteoroid is drawn in *Figure 6*.



Figure 5 – Atmospheric path of the SWEMN20250205\_042454 "Cartaojal" event, and its projection on the ground.

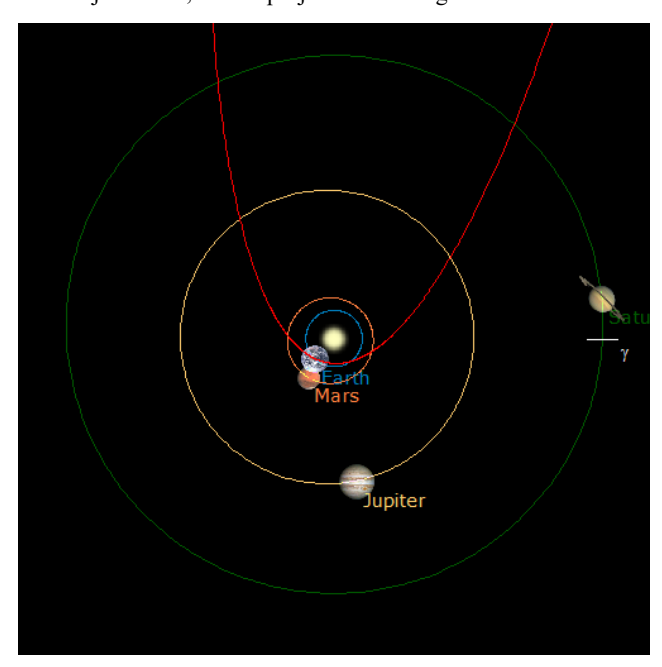


Figure 6 – Projection on the ecliptic plane of the orbit of the progenitor meteoroid of the SWEMN20250205\_042454 "Cartaojal" meteor.

The meteor was named "Cartaojal", since the event passed near the zenith of this locality during its initial phase. The parameters of the heliocentric orbit of the progenitor meteoroid before its encounter with our planet have been listed in *Table 2*, and the geocentric velocity yields  $v_g = 71.0 \pm 0.4$  km/s. From the value obtained for the Tisserand parameter with respect to Jupiter ( $T_J = -1.00$ ), we found that the meteoroid followed a cometary (HTC) orbit

before colliding with our atmosphere. These parameters and the calculated radiant location confirm that the event was associated with the  $\pi$ -Hydrids (IAU code PIH#0101).

*Table 2* – Orbital data (J2000) of the progenitor meteoroid before its encounter with our planet.

a (AU)	$43.5 \pm 71.$	ω (°)	$39.3 \pm 00.8$
e	$0.97 \pm 0.03$	Ω (°)	$136.281675 \pm \pm 10^{\text{-}5}$
q(AU)	$0.875\pm0.002$	i (°)	$166.78\pm0.06$

#### 5 Analysis of the 2025 February 7 event

This event was recorded by our meteor stations at  $5^{\rm h}58^{\rm m}50.0 \pm 0.1^{\rm s}$  UT on 2025 February 7 (*Figure 7*). The fireball had a peak absolute magnitude of  $-6.0 \pm 1.0$ . The unique identifier assigned to the bright meteor in the SWEMN meteor database is SWEMN20250207\_055850.

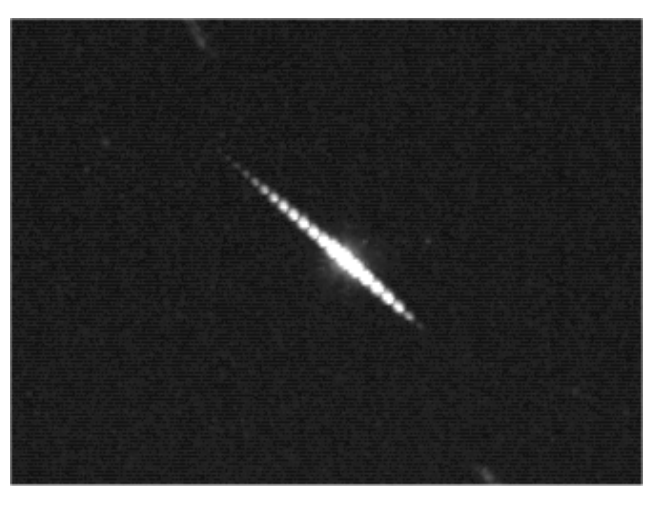


Figure 7 – Stacked image of the SWEMN20250207\_055850 fireball.



Figure 8 – Atmospheric path of the SWEMN20250207\_055850 event, and its projection on the ground.

#### Atmospheric path, radiant and orbit

It was concluded as a result of the analysis of the atmospheric trajectory of the event that this bolide overflew the Mediterranean Sea. Its initial altitude was  $H_b = 112.4 \pm 0.5$  km. The fireball penetrated the atmosphere till a final height  $H_e = 86.8 \pm 0.5$  km. The

equatorial coordinates deduced for the apparent radiant are  $\alpha = 277.68^{\circ}$ ,  $\delta = 28.96^{\circ}$ . The meteoroid impacted the atmosphere with an initial velocity  $v_{\infty} = 21.5 \pm 0.3$  km/s. The obtained trajectory in our atmosphere of the event is shown in *Figure 8*. The orbit in the Solar System of the progenitor meteoroid is shown in *Figure 9*.

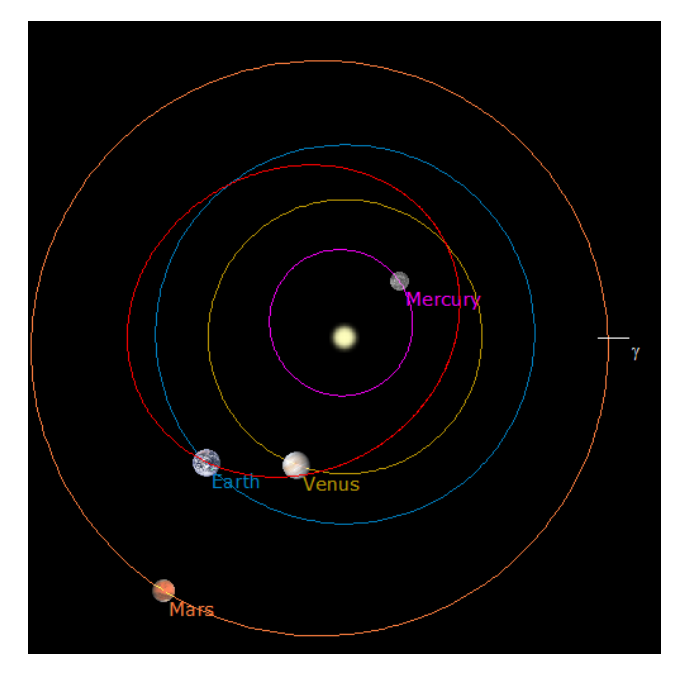


Figure 9 – Projection on the ecliptic plane of the orbit of the progenitor meteoroid of the SWEMN20250207 055850 fireball.

The parameters of the orbit in the Solar System of the parent meteoroid before its encounter with our planet are listed in *Table 3*, and the geocentric velocity derived in this case was  $v_g = 18.1 \pm 0.4$  km/s. The Tisserand parameter with respect to Jupiter ( $T_J = 6.22$ ) suggests that before impacting our atmosphere the particle was moving on an asteroidal orbit. These values and the derived radiant coordinates point to the sporadic nature of this bright meteor.

*Table 3* – Orbital data (J2000) of the progenitor meteoroid before its encounter with our planet.

a (AU)	$0.940\pm0.004$	ω (°)	$62.7 \pm 00.6$
e	$0.336 \pm 0.003$	Ω (°)	$318.368645 \pm 10^{\text{-}5}$
q (AU)	$0.6245 \pm 0.0008$	i (°)	$30.5\pm0.6$

#### 6 Analysis of the 2025 February 9 fireball

On 2025 February 9, at  $5^h15^m58.0 \pm 0.1^s$  UT, our meteor stations recorded this bright meteor. The peak luminosity of the fireball was equivalent to an absolute magnitude of  $-9.0 \pm 1.0$  (*Figure 10*). It was included in the SWEMN meteor database with the unique identifier SWEMN20250209\_051558. The event can be viewed on this YouTube video<sup>26</sup>.



Figure 10 – Stacked image of the SWEMN20250209\_051558 "Tornadizos de Arévalo" meteor.

#### Atmospheric path, radiant and orbit

The calculation of the trajectory in our atmosphere of the bolide allowed to deduce that this bright meteor overflew Portugal and Spain. The meteoroid ablation process began at a height  $H_b = 101.7 \pm 0.5$  km, and the fireball penetrated the atmosphere till a final height  $H_e = 54.2 \pm 0.5$  km. The equatorial coordinates found for the apparent radiant are  $\alpha = 150.68^{\circ}$ ,  $\delta = -11.82^{\circ}$ . The entry velocity in the atmosphere concluded for the parent meteoroid was  $v_{\infty} = 34.5 \pm 0.2$  km/s. The obtained trajectory in the Earth's atmosphere of the event is shown in *Figure 11*. The heliocentric orbit of the meteoroid is drawn in Figure 12.



Figure 11 – Atmospheric path of the SWEMN20250209\_051558 "Tornadizos de Arévalo" event, and its projection on the ground.

We named this bolide "Tornadizos de Arévalo", because the meteor was located over this locality in Spain during its final phase. The orbital parameters of the progenitor meteoroid before its encounter with our planet have been listed in *Table 4*. The geocentric velocity of the meteoroid was  $v_g = 33.0 \pm 0.2$  km/s. The Tisserand parameter with respect to Jupiter ( $T_J = 2.28$ ) indicates that the meteoroid followed a cometary (JFC) orbit before colliding with the Earth's atmosphere. By taking into account this orbit and

<sup>&</sup>lt;sup>26</sup> https://youtu.be/VdkvLQu8cd4

the radiant position, the bright meteor was associated with the sporadic background.

 $Table\ 4$  – Orbital data (J2000) of the progenitor meteoroid before its encounter with our planet.

a (AU)	$3.2 \pm 0.1$	ω (°)	$104.7\pm00.3$
e	$0.872\pm0.005$	Ω (°)	$140.356848{\pm}10^{\text{-}5}$
q (AU)	$0.409\pm0.002$	i (°)	$31.5 \pm 0.2$

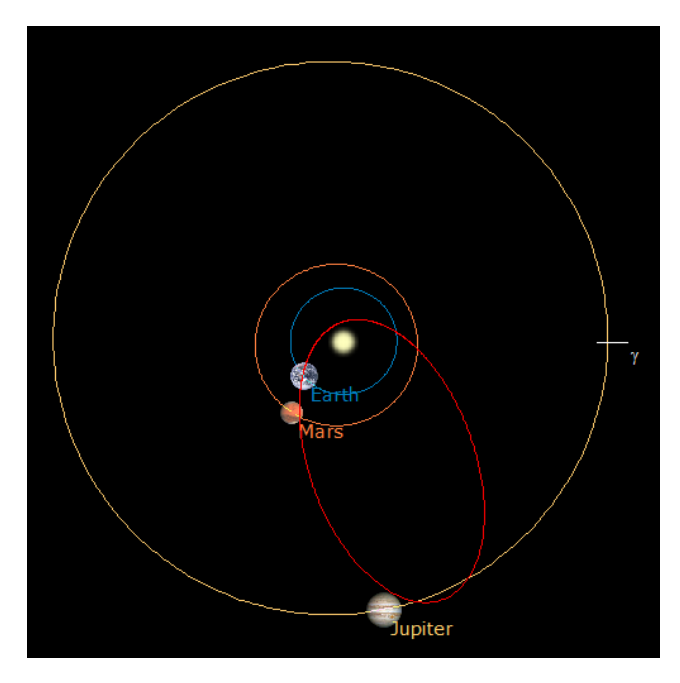


Figure 12 – Projection on the ecliptic plane of the orbit of the progenitor meteoroid of the SWEMN20250209\_051558 "Tornadizos de Arévalo" event.

#### 7 The 2025 March 15 bolide

This bright bolide was recorded on 2025 March 15, at  $23^{\rm h}14^{\rm m}10.0\pm0.1^{\rm s}$  UT. The peak luminosity of the fireball, which showed a series of flares along its atmospheric trajectory, was equivalent to an absolute magnitude of  $-9.0\pm1.0$  (Figure 13). These flares took place as a consequence of the sudden disruption of the meteoroid. The bolide was listed in our meteor database with the code SWEMN20250315\_231410.



Figure 13 – Stacked image of the SWEMN20250315\_231410 "Valsequillo" event.

#### Atmospheric path, radiant and orbit

It was concluded from the analysis of the atmospheric trajectory of the fireball that this bright meteor overflew the province of Córdoba (southern Spain). The luminous event began at an altitude  $H_b = 74.0 \pm 0.5$  km. The bolide penetrated the atmosphere till a final height  $H_e = 29.1 \pm 0.5$  km. From the analysis of the atmospheric path we also obtained that the apparent radiant was located at the position  $\alpha = 106.87^{\circ}$ ,  $\delta = +42.70^{\circ}$ . The meteoroid hit the atmosphere with an initial velocity  $v_{\infty} = 14.1 \pm 0.2$  km/s. The obtained luminous path of the event is shown in *Figure 14*. The orbit in the Solar System of the meteoroid is shown in *Figure 15*.



Figure 14 – Atmospheric path of the SWEMN20250315\_231410 "Valsequillo" event, and its projection on the ground.

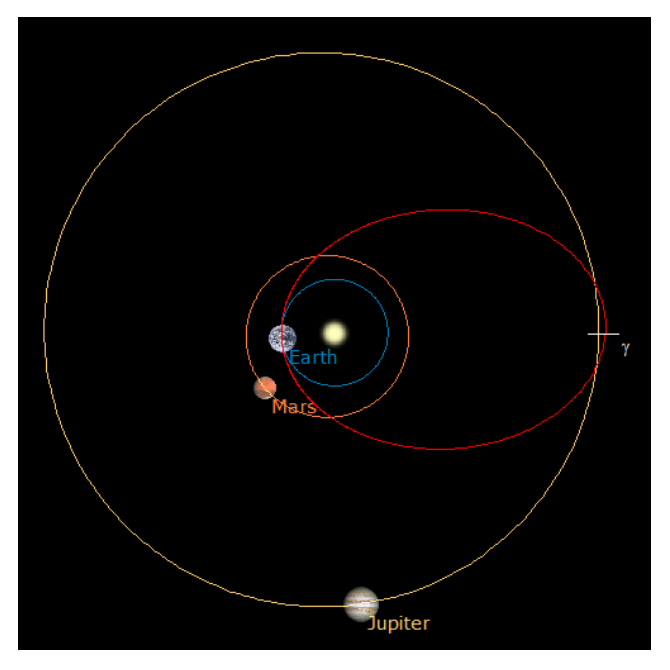


Figure 15 – Projection on the ecliptic plane of the orbit of the progenitor meteoroid of the SWEMN20250315\_231410 "Valsequillo" event.

This event was named "Valsequillo", since the fireball was located near the zenith of this locality during its initial

phase. The parameters of the heliocentric orbit of the progenitor meteoroid before its encounter with our planet have been listed in *Table 5*. The geocentric velocity obtained for the particle yields  $v_g = 9.0 \pm 0.3$  km/s. The value calculated for the Tisserand parameter referred to Jupiter ( $T_J = 2.84$ ) indicates that the meteoroid was moving on a cometary (JFC) orbit before entering the atmosphere. These parameters and the calculated radiant coordinates do not correspond with any of the streams contained in the IAU meteor database. Consequently, it was concluded that the fireball was linked to the sporadic background.

*Table 5* – Orbital data (J2000) of the progenitor meteoroid before its encounter with our planet.

a (AU)	$3.0 \pm 0.2$	ω (°)	$182.2\pm00.2$
e	$0.67 \pm 0.02$	Ω (°)	$355.279495 \pm 10^{\text{-}5}$
q (AU)	$0.99435 \pm 0.00009$	i (°)	$3.6 \pm 0.1$

#### 8 The 2025 March 28 event

This bright meteor was recorded by our cameras at  $4^h32^m38.0 \pm 0.1^s$  UT on 2025 March 28 (*Figure 16*). Its maximum brightness was equivalent to an absolute magnitude of  $-8.0 \pm 1.0$ . The code given to the event in the SWEMN meteor database is SWEMN20250328\_043238.



Figure 16 – Stacked image of the SWEMN20250328\_043238 event.

#### Atmospheric path, radiant and orbit

This bolide overflew the Gulf of Cádiz. The luminous event began at an altitude  $H_b = 99.1 \pm 0.5$  km. The event penetrated the atmosphere till a final height  $H_e = 47.2 \pm 0.5$  km. The equatorial coordinates of the apparent radiant yield  $\alpha = 279.57^{\circ}$ ,  $\delta = +60.89^{\circ}$ . Besides, we concluded that the meteoroid entered the atmosphere with a velocity  $v_{\infty} = 17.7 \pm 0.2$  km/s. The calculated atmospheric trajectory of the fireball is shown in *Figure 17*. The orbit in the Solar System of the meteoroid is shown in *Figure 18*.

The parameters of the heliocentric orbit of the progenitor meteoroid before its encounter with our planet have been included in *Table 6*. The geocentric velocity obtained for the particle yields  $v_g = 13.7 \pm 0.3$  km/s. According to the value calculated for the Tisserand parameter referred to Jupiter ( $T_J = 5.19$ ), the particle followed an asteroidal orbit before hitting our atmosphere. By taking into account these orbital data and the radiant position, it was concluded that the bright meteor was generated by a sporadic meteoroid.

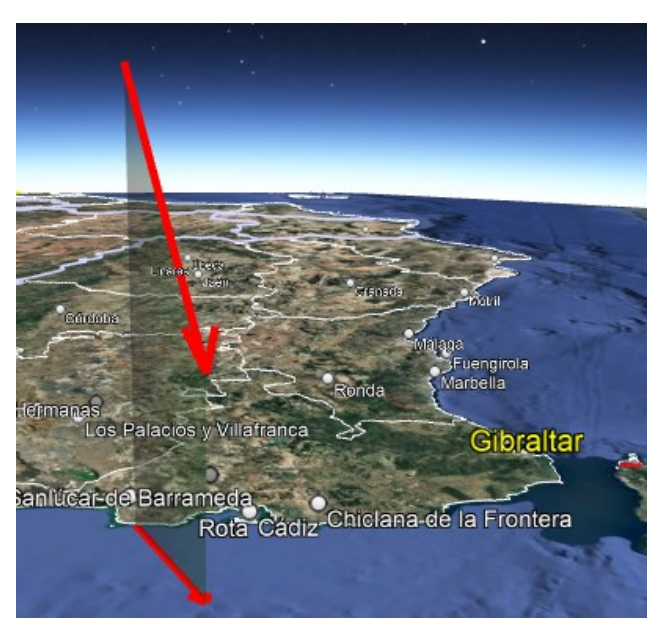


Figure 17 – Atmospheric path of the SWEMN20250328\_043238 event, and its projection on the ground.

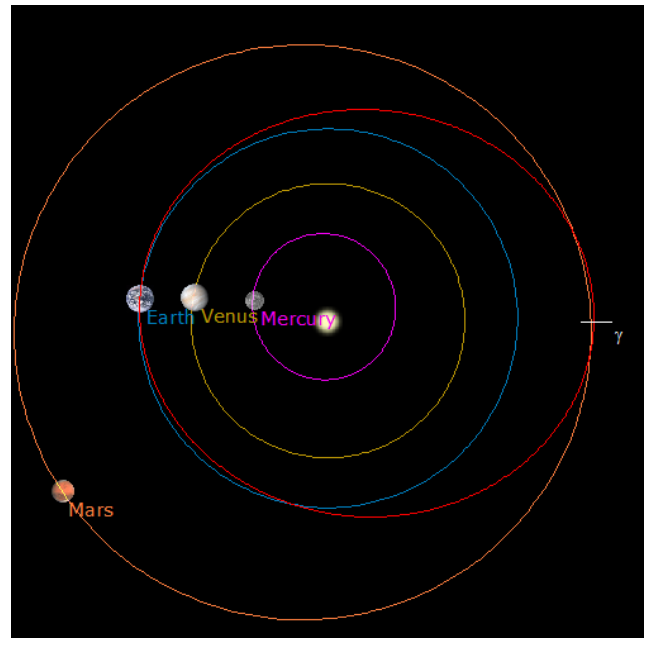


Figure 18 – Projection on the ecliptic plane of the orbit of the progenitor meteoroid of the SWEMN20250328 043238 meteor.

*Table 6* – Orbital data (J2000) of the progenitor meteoroid before its encounter with our planet.

a (AU)	$1.202 \pm 0.008$	ω (°)	$158.6 \pm 00.5$
e	$0.178\pm0.005$	Ω (°)	$7.406006 \pm 10^{\text{-}5}$
q (AU)	$0.9876 \pm 0.0003$	i (°)	$25.0 \pm 0.4$

#### 9 Analysis of the 2025 April 15 event

This bright bolide was recorded by SWEMN cameras at  $20^h05^m00.0 \pm 0.1^s$  UT on 2025 April 15. The bright meteor had a peak absolute magnitude of  $-10.0 \pm 1.0$  (*Figure 19*). It was added to the SWEMN meteor database with the unique identifier SWEMN20250415\_200500. The fireball was witnessed by a wide number of casual observers from the Iberian Peninsula.



Figure 19 – Stacked image of the SWEMN20250415\_200500 "Puebla de Don Rodrigo" event.

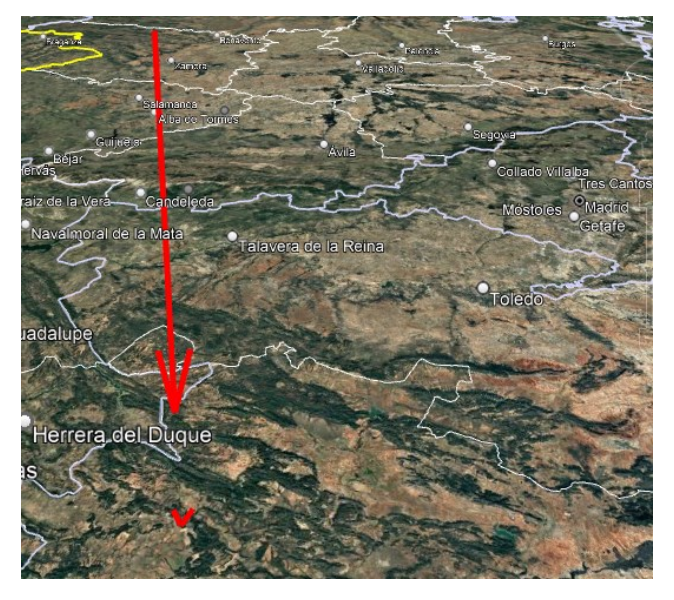


Figure 20 – Atmospheric path of the SWEMN20250415\_200500 "Puebla de Don Rodrigo" meteor, and its projection on the ground.

#### Atmospheric path, radiant and orbit

From the analysis of the trajectory in the Earth's atmosphere of the event it was concluded that this fireball overflew the province of Toledo (central Spain). Its initial altitude was  $H_b = 84.6 \pm 0.5$  km. The event penetrated the atmosphere till a final height  $H_e = 25.8 \pm 0.5$  km. From the analysis of the atmospheric path we also concluded that the apparent radiant was located at the position  $\alpha = 140.85^\circ$ ,  $\delta = +40.13^\circ$ . The entry velocity in the atmosphere inferred for the parent meteoroid was  $v_\infty = 14.8 \pm 0.2$  km/s. *Figure 20* shows the calculated path in the atmosphere of the bolide. The orbit in the Solar System of the progenitor

meteoroid is shown in *Figure 21*. A non-zero terminal mass was derived from the analysis of the trajectory of this deeppenetrating event. However, that mass was very small (below 10 g).

*Table 7* – Orbital data (J2000) of the progenitor meteoroid before its encounter with our planet.

a (AU)	$3.2 \pm 0.2$	ω (°)	$185.18 \pm 00.07$
e	$0.69 \pm 0.02$	Ω(°)	$25.741288 \pm 10^{-5}$
q (AU)	$1.00174 \pm 0.00009$	i (°)	$5.7 \pm 0.1$

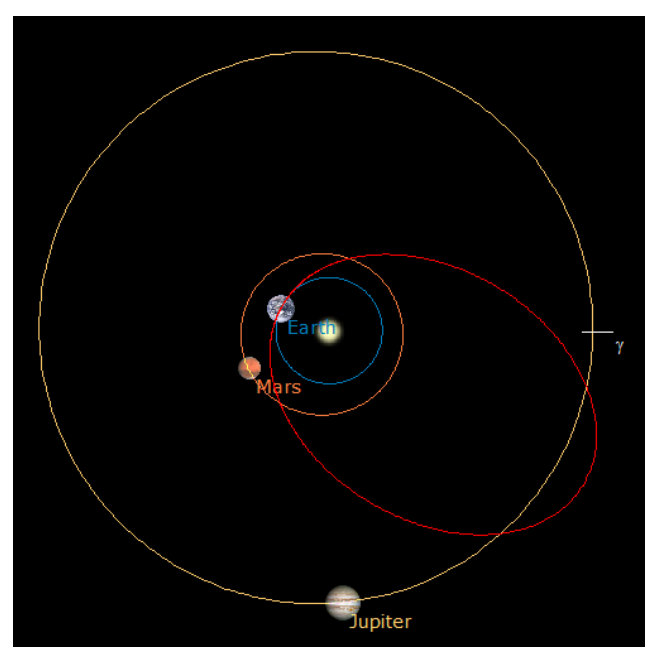


Figure 21 – Projection on the ecliptic plane of the orbit of the progenitor meteoroid of the SWEMN20250415\_200500 "Puebla de Don Rodrigo" meteor.

The bright meteor was named "Puebla de Don Rodrigo", because the fireball was located near the zenith of this locality during its initial phase. *Table 7* contains the orbital parameters of the progenitor meteoroid before its encounter with our planet. The geocentric velocity obtained for the particle yields  $v_g = 9.8 \pm 0.3$  km/s. The Tisserand parameter referred to Jupiter ( $T_J = 2.72$ ) suggests that before entering the Earth's atmosphere the particle was moving on a cometary (JFC) orbit. Radiant and orbital data do not match any of the meteoroid streams in the IAU meteor database. So, we concluded that this was produced by the sporadic background.

#### 10 Analysis of the 2025 April 23 meteor

On 2025 April 23, at  $3^h53^m02.0 \pm 0.1^s$  UT, the systems operated by the SWEMN network spotted this gorgeous bolide (*Figure 22*). The fireball, that showed a bright flare at the terminal stage of its path in the atmosphere, had a peak absolute magnitude of  $-12.0 \pm 1.0$ . This flare appeared as a consequence of the sudden break-up of the meteoroid. Its unique identifier in the SWEMN meteor database is

SWEMN20250423\_035302. The event can be viewed on this YouTube video<sup>27</sup>.



Figure 22 – Stacked image of the SWEMN20250423\_035302 "Morax" event.



Figure 23 – Atmospheric path of the SWEMN20250423\_035302 "Morax" bolide, and its projection on the ground.

*Table 8* – Orbital data (J2000) of the progenitor meteoroid before its encounter with our planet.

a (AU)	$19.3 \pm 8.4$	ω (°)	$214.8 \pm 00.3$
e	$0.95 \pm 0.02$	Ω (°)	$32.910371 \pm 10^{\text{-5}}$
q (AU)	$0.9175 \pm 0.0008$	i (°)	$79.9 \pm 0.2$

#### Atmospheric path, radiant and orbit

The analysis of the luminous path of the bolide led to the conclusion that this fireball overflew the province of Granada (southern Spain). The meteoroid ablation process began at a height  $H_b = 132.2 \pm 0.5$  km, and ended at a height  $H_e = 72.3 \pm 0.5$  km. From the analysis of the atmospheric path we also concluded that the apparent radiant was located at the position  $\alpha = 273.43^{\circ}$ ,  $\delta = +33.00^{\circ}$ . The meteoroid stroke the atmosphere with an initial velocity  $v_{\infty} = 48.2 \pm 0.3$  km/s. *Figure 23* shows the obtained trajectory in the atmosphere of the bright meteor. The orbit

in the Solar System of the progenitor meteoroid is shown in *Figure 24*.

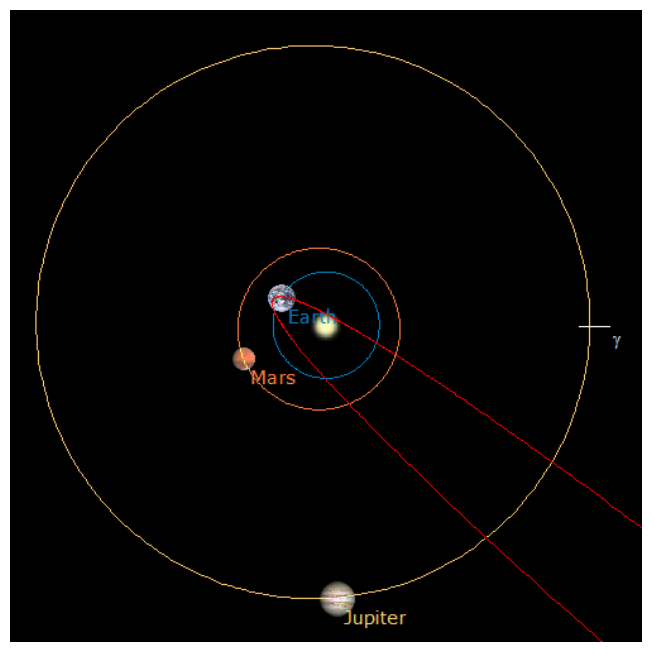


Figure 24 – Projection on the ecliptic plane of the orbit of the parent meteoroid of the SWEMN20250423\_035302 "Morax" event.

This event was named "Morax", because the bolide overflew this locality during its initial phase. The parameters of the heliocentric orbit of the parent meteoroid before its encounter with our planet are listed in *Table 8*. The value calculated for the geocentric velocity was  $v_g = 46.9 \pm 0.3$  km/s. The Tisserand parameter referred to Jupiter ( $T_J = 0.47$ ) suggests that the meteoroid followed a cometary (HTC) orbit before hitting the Earth's atmosphere. By taking into account this orbit and the radiant coordinates, the bolide was generated by the April Lyrids (IAU code LYR#0006). Since the April Lyrids reach their peak on April 22, this event was recorded near this activity peak. C/1861 G1 (Thatcher) is the proposed parent body of this meteor shower (Jenniskens et al., 2016.).

#### 11 Conclusions

We have discussed in this paper some of the most notable bolides recorded by our meteor-observing stations from February to April 2025. Their absolute magnitude ranges from –6 to –12.

The "Serrato"" bright meteor was recorded on February 3. It reached a peak absolute magnitude of -7.0, and belonged to the  $\pi$ -Hydrids (PIH#0101). This meteor event overflew the Mediterranean Sea and the province of Málaga (southern Spain). The parent meteoroid was moving on a cometary (HTC) orbit before entering our planet's atmosphere.

The second event analyzed here was the "Cartaojal" fireball, that was recorded on February 5. It belonged also

<sup>&</sup>lt;sup>27</sup> https://youtu.be/gwiZS-pyAc4

to the  $\pi$ -Hydrids (PIH#0101). Its peak magnitude was -7.0 and overflew the provinces of Málaga and Córdoba (southern Spain). The meteoroid was moving on a cometary (HTC) orbit before hitting the atmosphere.

The next bolide described here was recorded on February 7. Its peak magnitude was -6.0. The meteor event was produced by a sporadic meteoroid and overflew the Mediterranean Sea. The particle followed an asteroidal orbit before impacting the Earth's atmosphere.

Next, we have analyzed the "Tornadizos de Arévalo" event. This was recorded on February 9. It reached a peak absolute magnitude of –9.0, and belonged to the sporadic component. This meteor overflew Portugal and Spain. The progenitor particle was moving on a cometary (JFC) orbit before hitting the atmosphere.

The fifth bolide presented here was an event recorded on March 15 that was named "Valsequillo". It was associated with the sporadic background. Its peak magnitude was –9.0 and overflew the province of Córdoba (southern Spain). The meteoroid followed a cometary (JFC) orbit before colliding with our atmosphere. The final height of this deeppenetrating meteor event was of about 29 km.

We have also discussed a fireball recorded on March 28. It reached a peak absolute magnitude of -8.0, and was associated with the sporadic meteoroid background. This bolide overflew the Gulf of Cádiz. The meteoroid followed an asteroidal orbit before impacting our atmosphere. At the ending stage of its luminous phase this deep-penetrating fireball was located at an altitude of about 47 km.

The next fireball analyzed here was a bolide that was recorded on April 15 named "Puebla de Don Rodrigo". Its peak magnitude was -10.0. The meteor event was produced by a sporadic meteoroid and overflew the province of Toledo (central Spain). The progenitor meteoroid followed a cometary (JFC) orbit before entering the atmosphere. This deep-penetrating fireball reached an ending height of about 25 km. The analysis of the terminal point of the luminous path shows that the meteoroid was not completely ablated in the atmosphere. So, this meteor was a likely meteorite-dropper, but with a very small surviving mass (below 10 g).

The last event presented here was the "Morax" meteor. It was recorded on April 23. The peak magnitude of this April Lyrid (LYR#0006), which overflew the province of Granada (southern Spain), was -12.0.

#### Acknowledgment

Authors from Institute of Astrophysics of Andalusia (IAA-CSIC) acknowledge financial support from the Severo Ochoa grant CEX2021-001131-S, funded by MCIN/AEI/10.13039/501100011033.

#### References

- Ceplecha Z. (1987). "Geometric, dynamic, orbital and photometric data on meteoroids from photographic fireball networks" *Bull. Astron. Inst. Cz.*, **38**, 222–234.
- Jenniskens P., Nénon Q., Albers J., Gural P. S., Haberman B., Holman D., Morales R., Grigsby B. J., Samuels D. and Johannink C. (2016). "The established meteor showers as observed by CAMS". *Icarus*, 266, 331–354.
- Madiedo J. M. (2014). "Robotic systems for the determination of the composition of solar system materials by means of fireball spectroscopy". *Earth, Planets & Space*, **66**, 70.
- Madiedo J. M. (2017). "Automated systems for the analysis of meteor spectra: The SMART Project". *Planetary and Space Science*, **143**, 238–244.
- Madiedo J. M. (2015a). "Spectroscopy of a κ-Cygnid fireball afterglow". *Planetary and Space Science*, **118**, 90–94.
- Madiedo J. M. (2015b). "The ρ-Geminid meteoroid stream: orbits, spectroscopic data and implications for its parent body". *Monthly Notices of the Royal Astronomical Society*, **448**, 2135–2140.
- Madiedo J. M., Ortiz J. L., Organero F., Ana-Hernández L., Fonseca F., Morales N. and Cabrera-Caño J. (2015). "Analysis of Moon impact flashes detected during the 2012 and 2013 Perseids". *A&A*, **577**, A118.
- Madiedo J. M., Ortiz J. L. and Morales N. (2018). "The first observations to determine the temperature of a lunar impact flash and its evolution". *Monthly Notices of the Royal Astronomical Society*, **480**, 5010–5016.
- Madiedo J. M., Ortiz J. L., Morales N. and Santos-Sanz P. (2019). "Multiwavelength observations of a bright impact flash during the 2019 January total lunar eclipse". *Monthly Notices of the Royal Astronomical Society*, **486**, 3380–3387.
- Madiedo J. M., Ortiz J. L., Izquierdo J., Santos-Sanz P., Aceituno J., de Guindos E., Yanguas P., Palacian J., San Segundo A., and Avila D. (2021). "The Southwestern Europe Meteor Network: recent advances and analysis of bright fireballs recorded along April 2021". *eMetN Meteor Journal*, **6**, 397–406.
- Madiedo J. M., Ortiz J. L., Izquierdo J., Santos-Sanz P., Aceituno J., de Guindos E., Yanguas P., Palacian J., San Segundo A., Avila D., Tosar B., Gómez-Hernández A., Gómez-Martínez J., and García A. (2022). "The Southwestern Europe Meteor Network: development of new artificial intelligence tools and remarkable fireballs observed from

January to February 2022". *eMetN Meteor Journal*, 7, 199–208.

Molau S., Rendtel J. (2009). "A Comprehensive List of Meteor Showers Obtained from 10 Years of Observations with the IMO Video Meteor Network". WGN, Journal of the International Meteor Organization, 37, 98–121.

Ortiz J. L., Madiedo J. M., Morales N., Santos-Sanz P. and Aceituno F. J. (2015). "Lunar impact flashes from Geminids: analysis of luminous efficiencies and the flux of large meteoroids on Earth". *Monthly Notices of the Royal Astronomical Society*, **454**, 344–352.



Since 2016 the mission of eMetN Meteor Journal is to offer meteor news to a global audience and to provide a swift exchange of information in all fields of active amateur meteor work. eMetN Meteor Journal is freely available without any fees. eMetN Meteor Journal is independent from any country, society, observatory or institute. Articles are abstracted and archived with ADS Abstract Service: <a href="https://ui.adsabs.harvard.edu/search/q=eMetN">https://ui.adsabs.harvard.edu/search/q=eMetN</a>

You are welcome to contribute to eMetN Meteor Journal on a regular or casual basis, if you wish to. Anyone can become an author or editor, for more info read: <a href="https://www.emeteornews.net/writing-content-for-emeteornews/">https://www.emeteornews.net/writing-content-for-emeteornews/</a>

Articles for eMetN Meteor Journal should be submitted to: <a href="mailto:paul.roggemans@gmail.com">paul.roggemans@gmail.com</a>

eMetN Meteor Journal webmaster: Radim Stano < <a href="mailto:radim.stano@outlook.com">radim.stano@outlook.com</a> >.

Advisory board: Peter Campbell-Burns, Masahiro Koseki, Bob Lunsford, José Madiedo, Mark McIntyre, Koen Miskotte, Damir Šegon, Denis Vida and Jeff Wood.

Contact: <u>info@emeteornews.net</u>

#### **Contributors:**

Aceituno F.
 Gómez-Hernández A.
 Scott J.M.

Aceituno J.Gómez-Martínez J.Šegon D.

■ Aimee A.I. ■ Gorelli R. ■ Shiba Y.

Ávila D.Madiedo J.M.Verbelen F.

■ Barbieri L. ■ Maglione M. ■ Vida D.

■ Campbell-Burns P. ■ Ortiz J.L. ■ Wood J.

de Guindos E.
Penna M.

García A. Roggemans P.

Online publication <a href="https://www.emeteornews.net">https://www.emetn.net</a> and <a href="https://www.emetn.net">https://www.emetn.net</a> ISSN 3041-4261, publisher: Paul Roggemans, Pijnboomstraat 25, 2800 Mechelen, Belgium

Copyright notices © 2025: copyright of all articles submitted to eMetN Meteor Journal remain with the authors.